Generalization of the Haldane conjecture to SU(n) chains

by

Kyle Patrick Wamer

B.Sc., The University of Toronto, 2016
M.Sc., The University of British Columbia, 2018

A THESIS SUBMITTED IN PARTIAL FULFILLMENT OF
THE REQUIREMENTS FOR THE DEGREE OF

DOCTOR OF PHILOSOPHY

in

The Faculty of Graduate and Postdoctoral Studies

(Physics)

THE UNIVERSITY OF BRITISH COLUMBIA

(Vancouver)

April 2021

The following individuals certify that they have read, and recommend to the Faculty of Graduate and Postdoctoral Studies for acceptance, the thesis entitled:

Generalization of the Haldane conjecture to SU(n) chains

submitted by **Kyle Patrick Wamer** in partial fulfillment of the requirements for the degree of Doctor of Philosophy in Physics.

Examining Committee:

Ian Affleck, Physics and Astronomy, UBC
Supervisor

Sven Bachmann, Mathematics, UBC
University Examiner

Mona Berciu, Physics and Astronomy, UBC
University Examiner

Fei Zhou, Physics and Astronomy, UBC
Supervisory Committee Member

Philippe Lecheminant, Université de Cergy-Pontoise
External Examiner

Additional Supervisory Committee Members:

Marcel Franz, Physics and Astronomy, UBC
Supervisory Committee Member

Kirk Madison, Physics and Astronomy, UBC
Supervisory Committee Member

Abstract

In this thesis, we study the low energy properties of $SU(n)$ chains in various representations. We are motivated by Haldane's conjecture about antiferromagnets, namely that integer spin chains exhibit a finite energy gap, while half-odd integer spin chains have gapless excitations. Haldane was led to this conclusion by deriving a sigma model description of the antiferromagnet, and this is what we generalize here to $SU(n)$. We find that most representations of $SU(n)$ admit a mapping to a sigma model with target space equal to the complete flag manifold of $SU(n)$. These theories are not automatically relativistic, but we show that at low energies, their renormalization group flow leads to Lorentz invariance. We also show explicitly in $SU(3)$ that the theory is asymptotically free, and contains a novel two-form operator that is relevant at low energies.

For all n, these sigma models are equipped with $n - 1$ topological angles which depend on the $SU(n)$ representation at each site of the chain. For the rank-p symmetric representations, which generalize the spin representations of the antiferromagnet, these angles are all nontrivial only when $\gcd(n, p) = 1$. This observation, together with recent 't Hooft anomaly matching conditions, and various exact results known about $SU(n)$ chains, allow us to formulate the following generalization of Haldane's conjecture to $SU(n)$ chains in the rank-p symmetric representation: When p is coprime with n, a gapless phase occurs at weak coupling; for all other values of p, there is a finite energy gap with ground state degeneracy equal to $n/\gcd(n, p)$. We offer an intuitive explanation of this behaviour in terms of fractional topological excitations.

We also predict a similar gapless phase for two-row representations with even n. The topological content of these chains is the same as the symmetric ones, with p now equal to the sum of row lengths of the representation. Finally, we show that the most generic representation of $SU(n)$ will admit a sigma model with both linear and quadratic dispersion; such theories requires further understanding before their low energy spectra can be characterized.

Lay Summary

This thesis classifies new types of magnetic materials. Magnets are made up of atoms that, in addition to having a mass and electric charge, also have a property called spin. The spin of a magnet can be thought of as a microscopic arrow: it has a fixed length, and points in a particular direction. In familiar fridge magnets, all of these spins point along the same direction, and this is what causes them to be attracted to metallic surfaces. In this thesis, we consider magnetic materials that are different in two ways: 1) instead of a microscopic arrow, the spin is now a more complicated shape, 2) instead of aligning in the same direction, the spins now point in opposite directions, and do not stick to metals. For these new types of magnets, we classify for the first time how different spin shapes lead to different phases of matter.

Preface

The contents of this thesis were published in the following five articles:

- [1] Miklós Lajkó, Kyle Wamer, Frédéric Mila, and Ian Affleck. Generalization of the Haldane conjecture to SU(3) chains. *Nuclear Physics B*, 924:508 – 577, 2017

- [2] Kyle Wamer, Francisco H. Kim, Miklós Lajkó, Frédéric Mila, and Ian Affleck. Self-conjugate representation SU(3) chains. *Phys. Rev. B*, 100:115114, 2019

- [3] Kyle Wamer, Miklós Lajkó, Frédéric Mila, and Ian Affleck. Generalization of the Haldane conjecture to SU(n) chains. *Nuclear Physics B*, 952:114932, 2020

- [4] Kyle Wamer and Ian Affleck. Mass generation by fractional instantons in SU(n) chains. *Phys. Rev. B.*, 101:245143, 2020

- [5] Kyle Wamer and Ian Affleck. Flag manifold sigma models from SU(n) chains. *Nuclear Physics B*, 959:115156, 2020

The first three articles were cowritten with the Mila group at École Polytechnique Fédérale de Lausanne, and all five articles were written with my supervisor, Ian Affleck. The first publication, [1], constitutes most of Chapter 4, and is the only article from the above list in which I was not the primary writer. My main contribution to [1] was the renormalization group calculations appearing in Section 4.5. The flavour-wave calculations in Section 4.2 were carried out by my collaborators before I joined the project. And while the original sigma model derivation in [1] was worked out by Affleck, Lajkó and Mila, the derivation appearing in Section 4.3 is my own, and takes the different approach of varying the matrix degrees of freedom at each site of the chain, instead of over the 3-site unit cell. The advantage of this method is that the topological terms do not receive contributions from the uniform fluctuation fields, $L_{\alpha\beta}$, as in [1], which is important when one extends to more general representations of SU(n). I also used this approach to present an original derivation of the $\mathbb{CP}^1$ sigma model from an antiferromagnet in Chapter 2

The contents of [2] appear at the end of Chapter 4. Excluding the flavour-wave calculations, which were done by the Mila group, everything else presented in Section 4.7 was led and written by me.

The third publication, [3], was written entirely by me, with the exception of the strong coupling analysis appearing in Section 5.5.1. Indeed, the SU(n) flavour-wave theory (Section 5.2), the derivation of the flag manifold sigma model (Section 5.3), and the renormalization group analysis

(5.4) were all my calculations. The final two articles listed above, [4] and [5], constitute Chapter 3, Chapter 6 and Chapter 7. I wrote these two articles in their entirety, and carried out all of the calculations.

Finally, the content of these five publications can also be found in the review article [6], which I cowrote with Ian Affleck and Dmitri Bykov. The general discussions appearing in Chapter 1 and Chapter 8 are also included in this review.

Table of Contents

List of Tables

List of Figures

Acknowledgements

"It was rejected by multiple journals, and was labelled a "conjecture" even though it was, in my mind, a clear prediction. ... Of course, my predictions were later vindicated both by numerical studies and experiments."

F.D.M. Haldane
2016 Nobel Laureate

Chapter 1

Introduction

The Haldane conjecture is a statement about quantum spin systems in one spatial dimension. Such systems are described by the Heisenberg model, and are either ferromagnetic or antiferromagnetic, depending on the sign of the interaction term between neighbouring spins on the chain [7]. While the ferromagnet's ground state is the same for both classical and quantum chains (it is the state with all spins aligned along a common direction), this is not true for the antiferromagnet. Classically, the ground state is the so-called Néel state, with spins alternating between being aligned and anti-aligned along a common direction, but quantum mechanically the Néel state is no longer an eigenstate of the Heisenberg Hamiltonian [7]. This fact can be understood from Coleman's theorem, which forbids the spontaneous ordering of a continuous symmetry in one spatial dimension [8].[1]

The absence of an ordered ground state in the antiferromagnet has long been of interest to the physics community. Indeed, shortly after Heisenberg introduced his model of a ferromagnet in 1921 [11], Bethe discovered an exact solution of the antiferromagnetic chain with spin $s = \frac{1}{2}$ at each site [12].[2] However, despite this initial progress, spin chains with $s > \frac{1}{2}$ were not amenable to such techniques, and fifty years would pass before their low energy properties could be characterized. In 1981, Duncan Haldane proposed a radical classification of antiferromagnetic chains: Those with integer spin have a finite energy gap above their quantum ground states, and exponentially decaying correlation functions. Meanwhile, those chains with half-odd integer spin have gapless excitations, with algebraically decaying correlation functions [13, 14].[3]

Despite being consistent with Bethe's 1931 solution, Haldane's "conjecture" as it came to be known, was met with widespread skepticism [16]. This was likely due to the fact that spin-wave theory, a method that allows one to calculate the energy spectrum of antiferromagnets in higher dimensions, largely agreed with Bethe's one-dimensional results. We now know this to be a coincidence, but at the time, this suggested to the community that spin-wave results might be reliable in one dimension for all values of s. This would imply that all antiferromagnets would exhibit gapless excitations at low energies [7, 17]. Of course, this was in direct contradiction with Coleman's theorem, that invalidated spin-wave theory in one dimension, but nonetheless, by the 1980s it was

---

[1]Coleman's theorem is often confounded with the Mermin-Wagner-Hohenberg theorem, which forbids an ordered ground state in two spatial dimensions at finite temperature, and applies equally well to both ferromagnets and antiferromagnets [9, 10]. In Section 2.1.1, we review this subject further, and explain why Coleman's theorem breaks down for the ferromagnet.

[2]Unless otherwise specified, it is assumed that the spin value at each site of the chain is identical, so that an antiferromagnetic spin chain is uniquely defined by a positive half integer s.

[3]Haldane's original preprint, which was rejected from publication in 1981, has since been made available online [15].

widely accepted that gapless excitations were universal among one dimensional antiferromagnets.

In fact, Haldane's conjecture was met with surprise in other research areas of physics as well. As will be reviewed in great detail later, Haldane's conjecture hinges on a correspondence between antiferromagnets and the O(3) nonlinear sigma model, a quantum field theory that was being used as a toy model for quantum chromodynamics at the time [18]. The role of the spin, s, manifests as a topological angle θ in the sigma model, so that integer s translates to $\theta = 0$ and half-odd integer s translates to $\theta = \pi$. Thus, Haldane's claim about antiferromagnets was also a claim about mass gaps in the O(3) nonlinear sigma model. At that time, it was widely believed that a finite gap would exist for all values of θ. This was known exactly for $\theta = 0$ [19], and suggested numerically for small values of θ [20, 21].

Over the next few years, Haldane's conjecture would defy these skeptics, thanks to verification from multiple areas of research. Experimentally, neutron scattering on the organic nickel compound NENP, which is a quasi-one dimensional $s = 1$ chain, detected a finite energy gap above the ground state [22, 23]. Numerically, studies using exact diagonalization, Monte Carlo, and density matrix renormalization group methods were able to detect a finite gap in $s = 1, 2$ and 3 [24–29]. Very recently this has been extended to $s = 4$, where a tiny gap of $7.99(5) \times 10^{-4}$ was measured [30]. Meanwhile, in the O(3) nonlinear sigma model picture, Monte Carlo methods were used to numerically verify the absence of a mass gap when $\theta = \pi$ [31–36], and a related integrable model was eventually discovered by the Zamolodchikov brothers [37].

In many cases, the studies carried out in order to verify Haldane's claims were scientific breakthroughs in their own right. Indeed, the fields of density matrix renormalization group [38–40], and more generally tensor networks [41–43], as well as symmetry protected topological matter [44–47] all originated, in part, due to Haldane's conjecture. It is thus not a leap to claim that any generalization of Haldane's conjecture would be an impactful result to the physics community. And indeed, this is what led physicists, including Affleck, Read, Sachdev and others to extend Haldane's work to SU(n) generalizations of spin chains in the late 1980s [48–51]. At the time, these were purely hypothetical models with no experimental realization, but thanks to the correspondence between spin chains and sigma models, they were still interesting in their own right. Another motivation was a proposed relation between nonlinear sigma models and the localization transition in the quantum Hall effect [48, 52, 53]. And while this unsolved problem remains a motivator to study such models, recent developments from the cold atom community have revealed that SU(n) chains are now experimentally realizable, offering a much more physical motivation [54–66]. These proposals have led to a renewed theoretical interest in the field of SU(n) physics [61, 67–77]. Moreover, generalizations of the O(3) nonlinear sigma model, called flag manifold sigma models, have also garnered recent attention, as they realize so-called 't Hooft anomalies, which are interesting to high energy physicists [71, 72, 78, 79]. This calls for not only a generalization of Haldane's prediction of gapped vs. gapless behaviour (driven by topological terms), but also for developing a more general understanding of the spin-chain/sigma model paradigm, so as to understand which families of SU(n) chains correspond to a particular quantum field theory.

In this thesis, we study SU(n) Heisenberg models on one-dimensional chains in various representations. Unlike the familiar spin chains with SU(2) symmetry, for $n > 2$, multiple non-negative

integers are required in order to completely specify the representation. Ultimately, our goal is to establish a generalization of the Haldane conjecture for these models. That is, we seek to determine which families of $SU(n)$ representations give rise to chains with gapless ground states, and which families give rise to chains with unique, gapped ground states. Essential to Haldane's argument is a low energy equivalence between the antiferromagnet and the O(3) nonlinear sigma model, and so in extending Haldane's conjecture, we also generalize this equivalence. That is, we determine which $SU(n)$ representations correspond to chains that admit mappings to flag manifold sigma models, which are the $SU(n)$ generalization of the O(3) nonlinear sigma model.

We begin in Chapter 2 of this thesis with a review of the various arguments that, collectively, provide a modern proof of Haldane's conjecture. A large part of this chapter is dedicated to the derivation of the O(3) nonlinear sigma model description of the spin chain, in an equivalent $\mathbb{CP}^1$ language, as this will serve as our starting point in later chapters. The notion of topological angle, and how it arises from the spin chain as a Berry curvature term is explained. We also introduce spin-wave theory and explain how, despite Coleman's theorem, it is a useful tool in analyzing quantum spin chains in one spatial dimension. In Chapter 3, we promote the symmetry group of the antiferromagnet from $SU(2)$ to $SU(n)$, and discuss these so-called $SU(n)$ chains in full generality. This requires a detailed discussion of the irreducible representations and Casimir operators of $SU(n)$, which we provide. We also explain the issue of local degeneracies in $SU(n)$ chains, and how this requires the addition of longer-range terms in the Heisenberg Hamiltonians. Experimental realization of $SU(n)$ chains is also mentioned. Finally, we finish Chapter 3 by reviewing various exact results that are known for $SU(n)$ chain systems, including the LSMA theorem [80, 81], generalized AKLT models [67, 82, 83], and integrable $SU(n)$ chains [12, 84–89]. Next, in Chapter 4, we focus our attention on the simplest $SU(n)$ chains: the $SU(3)$ chains in the totally symmetric representations. We extend much of the analysis from Chapter 2 to these chains: we introduce 'flavour-wave' theory, which generalizes spin-wave theory, and derive the corresponding low energy quantum field theory description of the $SU(3)$ chain. In this case, the O(3) nonlinear sigma model is replaced with the $SU(3)/[U(1)]^2$ flag manifold sigma model, equipped with two topological angles. We perform extensive renormalization group calculations in this field theory, and combine these with results from a Monte Carlo simulation and a strong coupling analysis to obtain a phase diagram for the $SU(3)$ chain. We discuss the 't Hooft anomalies present in this model, and present an $SU(3)$ version of Haldane's conjecture. We complete this chapter with a discussion of other representations of $SU(3)$, including the self-conjugate ones. Next, in Chapter 5, we consider the symmetric representation $SU(n)$ chains, thus extending the calculations from Chapter 4 from 3 to n. The low energy physics of these chains is captured by the $SU(n)/[U(1)]^{n-1}$ flag manifold sigma model with $n-1$ topological angles. Here, new difficulties arise, perhaps most importantly the absence of Lorentz invariance in the corresponding sigma model. We present extensive calculations that establish that under renormalization, Lorentz invariance is restored. We also extend the strong coupling analysis and 't Hooft anomaly conditions from $SU(3)$ to $SU(n)$. This leads to a version of Haldane's conjecture for $SU(n)$ chains in symmetric representations. Having identified the $SU(n)$ sigma models of interest, we turn in Chapter 6 to the task of reverse engineering the correspondence between $SU(n)$ chains and sigma models. That is, given the $SU(n)/[U(1)]^{n-1}$ flag manifold, we classify all possible

representations of SU(n) chains that admit a mapping from chain to sigma model with this target space. We identify the key property that ensures the presence of an 't Hooft anomaly, namely a transitive $\mathbb{Z}_n$ action on the field content, which is a manifestation of n-site translation invariance in the SU(n) chain. We also discuss the emergence of quadratic Goldstone bosons, and the subtle correspondence between non-Lorentz invariance, Goldstone's theorem, and spontaneous symmetry breaking in general SU(n) chains. This leads to detailed classification tables of dispersion relations for each SU(n) representation. Finally, in the last major chapter of this thesis, Chapter 7, we provide a physical picture of the mass-generating mechanism in SU(n) chains. That is, we explain how topological excitations with fractional charge produce a finite energy gap in the flag manifold sigma model, akin to the vortex-generated gap in the Kosterlitz-Thouless transition [90, 91].[4] This is first done in the absence of topological angles; upon restoring the angles, we show how interference effects inhibit this mass-generating mechanism, and lead to a gapless ground state, for certain SU(n) representations. Remarkably, these are precisely the representations that our generalized Haldane conjecture predicts will have a gapless phase, and can be understood as a consequence of the transitive $\mathbb{Z}_n$ action, which ensures $n-1$ distinct topological angles. In Chapter 8, we summarize our results and provide an outlook towards the rapidly developing field of SU(n) physics.

---

[4]Throughout, we will refer to the Kosterlitz-Thouless transition, but perhaps a more apt name is the Berezinskii-Kosterlitz-Thouless transition.

Chapter 2

A Review of the Haldane Conjecture

2.1 Introduction

Antiferromagnetic chains are described by the Heisenberg model,

$$H = J \sum_j \vec{S}(j) \cdot \vec{S}(j+1). \tag{2.1}$$

Here, the sum runs overs all lattice sites j of the chain, and the interaction strength J is positive. The vectors $\vec{S}$ are 3-tuples of spin operators,

$$\vec{S} = \begin{pmatrix} S_x & S_y & S_z \end{pmatrix}^{\mathrm{T}} \tag{2.2}$$

and satisfy the $\mathfrak{su}(2)$ Lie algebra:[5]

$$[S_a, S_b] = i\epsilon_{abc} S_c. \tag{2.3}$$

These chains are defined by their spin s, which corresponds to the irreducible representation of SU(2) under which the spin operators S_a transform.[6] The spin can be read off from the quadratic Casimir operator,

$$\vec{S} \cdot \vec{S} = s(s+1)\mathbb{I}. \tag{2.4}$$

On the right hand side of this expression, $\mathbb{I}$ is the identity operator, whose dimension is equal to $2s+1$, the dimension of the spin-s representation of SU(2).

Before Haldane, most physicists based their understanding of antiferromagnetic chains on spin-wave theory, which corresponds to taking the limit $s \to \infty$ [17]. This amounts to a semi-classical limit, as can be seen by inserting (2.4) into the Heisenberg uncertainty relation:

$$\Delta S_a \Delta S_b \geq \frac{1}{2} |\langle [S_a, S_b] \rangle| \qquad \Delta S_a := \sqrt{\langle S_a^2 \rangle - \langle S_a \rangle^2}. \tag{2.5}$$

For large values of s, relative fluctuations of the spin operator, $\Delta S_a / |S_a|$ are order $O(s^{-1})$. Thus in the limit $s \to \infty$, the spin operators can be simply treated as three-dimensional vectors constrained to have length $\sqrt{s(s+1)}$, and the Hamiltonian (2.1) resembles that of a classical antiferromagnet. Spin-wave theory proceeds from here, seeking to describe low energy fluctuations about the classical ground state, which has its spins adjacently antiparallel (the so-called Néel state). As we will

---

[5]Here and throughout, we set Planck's constant $\hbar = 1$.

[6]A formal treatment of the representation theory of SU(n) will be provided in Section 3.2.1.

demonstrate shortly, this leads to the prediction of gapless excitations, regardless of the value of s, and largely agrees with Bethe's $s = \frac{1}{2}$ exact solution [12]. This agreement was sufficient evidence for many, and as a consequence, the physics community largely accepted the spin-wave theory prediction of gapless excitations as a universal property of antiferromagnetic chains [7, 16].

However, what most physicists were forgetting, or at least choosing to ignore, was the fact that spin-wave theory inherently assumes an ordered quantum ground state. This is perfectly reasonable in higher-dimensional systems, but is in direct contradiction with Coleman's theorem for one-dimensional chains [8]. In order to demonstrate this fact, we now present a brief review of spin-wave theory, and discuss the Goldstone modes that lead to infrared divergences. Despite its general invalidity, it has been appreciated rather recently that spin-wave theory can still be a useful tool in one dimensional systems [92]. As such, this review will also set the stage for flavour-wave theory, a generalization of spin-wave theory to larger symmetry groups, that we will introduce in later chapters.

2.1.1   Spin-wave theory

To proceed with spin-wave theory, we begin by rewriting the Hamiltonian (2.1) in terms of boson operators that satisfy canonical commutation relations. Since the classical ground state of the antiferromagnet is the Néel state, which has a two-site unit cell, we introduce two bosons b_1 and b_2, each via a Holstein-Primakoff transformation [93]. For example, on the even sites, we may write,

$$S_z = s - b_1^\dagger b_1 \qquad\qquad S_x - iS_y = \sqrt{2s}\, b_1^\dagger \sqrt{1 - \frac{b_1^\dagger b_1}{2s}}, \qquad\qquad (2.6)$$

which preserves the algebra (2.3). For the odd sites, we use a similar expansion, except now the presence of bosons should correspond to deviations of S_z from $-s$: $S_z = -s + b_2^\dagger b_2$. Now, under the assumption of large s, we may expand the square root in powers of s^{-1}, and substitute this expression into (2.1). After performing a Bogoliubov transformation, we obtain a diagonal quadratic Hamiltonian, with dispersion relation[7]

$$E(k) = 2Js|\sin(k)|. \qquad\qquad (2.7)$$

In other words, spin-wave theory predicts gapless excitations that disperse linearly, with a velocity of $v = 2Js$. In this context, these linear modes are referred to as Goldstone modes, since they arise as a consequence of the spontaneous breaking of the spin symmetry, a result known as Goldstone's theorem [94].

It is these Goldstone modes that are the foundation of Coleman's argument for the absence of spontaneous symmetry breaking in one spatial dimension. To see this, note that the evaluation of any physical expectation value, such as the staggered magnetization, necessarily involves a sum

---

[7]Throughout, we set the lattice spacing $a = 1$.

over these modes. Indeed, inverting the Bogoliubov transformation that led to (2.7), we find

$$\langle S_z(x) \rangle = s - \langle b_1^\dagger(x) b_1(x) \rangle \rightarrow s - \frac{1}{2} \int \frac{dk}{2\pi} \frac{1 - |\sin(k)|}{|\sin(k)|} \tag{2.8}$$

in the continuum limit (here x is the continuous coordinate along the chain). For small values of k, the integrand behaves like $\frac{1}{k}$, indicating that $\langle S_z(x) \rangle$ suffers from an infrared divergence. Such divergences are a clear sign of an ill-defined theory, and are ubiquitous in one-dimensional systems whenever one assumes the spontaneous breaking of a continuous symmetry. As an exception, the ferromagnet evades this problem, which is related to the fact that its Goldstone bosons disperse quadratically instead of linearly. The mechanism behind this quadratic dispersion has been completely understood only recently [95–97], and we will have more to say on this subject in Chapter 6.

As we've highlighted above, the fact that spin-wave theory leads to infrared divergences, and is thus an inconsistent theory, did not deter researchers in the field from accepting its predictions. And as it turns out, information can still be gleaned from this formalism, so long as the right calculations are performed. By this, we mean that if one restricts to the calculation of quantities that preserve the symmetry that is being spontaneously broken, then infrared divergences will be absent. This was recently demonstrated explicitly for spin chains for spins up to $s = \frac{5}{2}$, and is expected to be true for all spins [92]. However, for spin-wave theory to be valid when doing numerical simulations, it is important that the system size is much smaller than the correlation length $\xi \sim s^{-1} e^{\pi s}$.

And so, perhaps it is not surprising that the spin-wave prediction at $s = \frac{1}{2}$ roughly reproduces Bethe's exact solution. However, the explanation for why spin-wave theory was fundamentally wrong for $s = 1$ could not have been anticipated at the time. This is because it had to do with a topological distinction between integer and half-odd integer spin chains, and such concepts were foreign to condensed matter physicists in the early 1980s. As we will now detail, Haldane's simple approach of maintaining the large-s limit, while weakening the assumption of a Néel ground state, leads directly to this exciting new field of theoretical physics.

2.2 Sigma Model Derivation

In this section, we derive a low energy mapping between the spin-s antiferromagnetic chain and a particular sigma model. By sigma model, we mean a quantum field theory whose fields define a map from (Euclidean) space time to some curved manifold. Recall that in the large-s limit, we may replace the 3-tuple of operators $\vec{S}$ with a classical vector in $\mathbb{R}^3$, constrained to have length $\sqrt{s(s+1)}$ by the quadratic Casimir. In this case, we are eventually led to a quantum field theory whose field $\vec{n}$ is constrained to live on the sphere S^2, a so-called S^2-sigma model. This was the approach originally taken by Haldane, although he followed the widespread convention of referring to the model as the O(3) nonlinear sigma model, even though O(3) is not isomorphic to S^2 as a group. Instead, what holds is

$$S^2 = O(3)/O(2), \tag{2.9}$$

where the quotient by O(2) corresponds to the gauge symmetry of choosing a particular direction for S_z [98].

A slightly different approach is to make use of a true isomorphism between the groups S^2 and $\mathbb{C}P^1$, and instead work with a complex field $\varphi \in \mathbb{C}^2$ that satisfies $|\varphi| = 1$. This is the approach that we will follow. Our reasoning for this choice will become clear in Chapter 3, when we promote the on-site symmetry of the chain from SU(2) to SU(n). In this more general case, it is much more natural to work with complex vectors $\varphi \in \mathbb{C}^n$ than their real-vector equivalents.

To this end, let us introduce the following matrices of spin operators,

$$S = \begin{pmatrix} S_z & S_x - iS_y \\ S_x + iS_y & -S_z \end{pmatrix}. \tag{2.10}$$

The $\mathfrak{su}(2)$ Lie algebra (2.3) manifests itself in the following commutation relations:

$$[S_{\alpha\beta}, S_{\mu\nu}] = \delta_{\alpha\nu}S_{\mu\beta} - \delta_{\mu\beta}S_{\alpha\nu}. \tag{2.11}$$

In terms of these matrices, the Heisenberg interaction can be rewritten according to

$$\vec{S}(i) \cdot \vec{S}(j) = \frac{1}{2}\text{tr}[S(i)S(j)]. \tag{2.12}$$

As before, in the limit of large s, quantum fluctuations tend to zero and we can treat these matrices as classical objects. The quadratic Casimir constraint (2.4) restricts the eigenvalues of these matrices to be $\pm s$.

The main strategy behind Haldane's derivation, which still carries over here to the complex formalism, is to begin as in spin-wave theory with a classical ground state ansatz, but then promote the matrices S to objects that can vary in space and in time. Therefore, we must first establish a convenient way of representing the Néel state in the complex formalism, before proceeding. Since the eigenvalues of S are constrained in the limit $s \rightarrow \infty$, we may write

$$S = V^{\dagger}\begin{pmatrix} s & 0 \\ 0 & -s \end{pmatrix}V, \tag{2.13}$$

with V a 2×2 unitary matrix. We may shift S by the constant matrix $s\mathbb{I}$, since this only alters the Hamiltonian by a fixed amount. This allows for a convenient representation in terms of the first row of V, $\boldsymbol{\phi} \in \mathbb{C}^2$:

$$S_{\alpha\beta} = s\phi_{\alpha}^*\phi_{\beta}, \tag{2.14}$$

Since V is unitary, we have that $|\boldsymbol{\phi}|^2 = 1$. Inserting this into the Heisenberg interaction, we find

$$\text{tr}[S(j)S(j+1)] = s^2|\boldsymbol{\phi}^*(j) \cdot \boldsymbol{\phi}(j+1)|^2. \tag{2.15}$$

In words, this equation demonstrates that the Heisenberg interaction is minimized when neighbouring complex vectors $\boldsymbol{\phi}$ are orthogonal. Thus, the classical Néel state in this formalism corresponds to a pattern of alternating, orthogonal vectors: At even sites we have $\boldsymbol{\phi} = \boldsymbol{\varphi}^1$, and at odd sites, we

have $\boldsymbol{\phi} = \boldsymbol{\varphi}^2$, which satisfy $\boldsymbol{\varphi}^{1,*} \cdot \boldsymbol{\varphi}^2 = 0$. Pictorially, we may represent this ground state using two coloured nodes $\bullet := \boldsymbol{\varphi}^1$ and $\bullet := \boldsymbol{\varphi}^2$:

$$\cdots \quad \bullet \quad \bullet \quad \bullet \quad \bullet \quad \bullet \quad \bullet \quad \bullet \quad \bullet \quad \cdots \tag{2.16}$$

This diagram can be compared with the typical Néel pattern $\cdots \uparrow\downarrow\uparrow\downarrow \cdots$, in which neighbouring objects are *antiparallel* instead of *orthogonal* – this is a distinguishing feature between the two formalisms.

Now that the ground state ansatz has been established, we introduce fluctuations about the $\boldsymbol{\varphi}^\alpha$, for $\alpha = 1, 2$. In terms of the original $\boldsymbol{\phi}^\alpha$ appearing in (2.13), we write[8]

$$\boldsymbol{\phi}^1 = \frac{1}{s}L_{12}\boldsymbol{\varphi}^2 + \sqrt{1 - \frac{|L_{21}|^2}{s^2}}\boldsymbol{\varphi}^1 \qquad \boldsymbol{\phi}^2 = \frac{1}{s}L_{21}\boldsymbol{\varphi}^1 + \sqrt{1 - \frac{|L_{12}|^2}{s^2}}\boldsymbol{\varphi}^2. \tag{2.17}$$

This somewhat cumbersome notation has been chosen in order to be consistent with similar derivations in later chapters of this thesis. The coefficients $L_{12} = L_{21}^*$ correspond to fluctuations within the two-site unit cell of the Néel state, and are functions of space and time, as are the basis vectors $\boldsymbol{\varphi}^\alpha$. The remaining terms in (2.17), proportional to the radical, correspond to uniform rotations of the entire two-site cell. We have chosen, by convention, to include a factor of $\frac{1}{s}$ in front of the L_{12} and L_{21} coefficients.

In passing, we note that the expansion (2.17) can be related to the more familiar real-space derivation of the spin chain/sigma model correspondence,

$$\vec{n} = \frac{1}{s}\vec{l} \pm \sqrt{1 - \frac{l^2}{s^2}}\vec{m}, \tag{2.18}$$

using the equivalences

$$\vec{m} \cdot \vec{\sigma}^* = U^\dagger \sigma_z U \qquad \vec{l} \cdot \vec{\sigma}^* = 2U^\dagger L U, \tag{2.19}$$

where we've defined a unitary matrix U whose rows corresponds to $\boldsymbol{\varphi}^\alpha$ (i.e. $U_{\alpha\beta} = \varphi_\beta^\alpha$) and set $L_{11} = L_{22} = 0$. Here $\vec{l}, \vec{m}$ and $\vec{n}$ are all vectors in $\mathbb{R}^3$, and the Pauli matrices $\vec{\sigma}$ are defined according to

$$\sigma_1 = \begin{pmatrix} 0 & 1 \\ 1 & 0 \end{pmatrix} \qquad \sigma_2 = \begin{pmatrix} 0 & -i \\ i & 0 \end{pmatrix} \qquad \sigma_3 = \begin{pmatrix} 1 & 0 \\ 0 & -1 \end{pmatrix}. \tag{2.20}$$

In order to derive a sigma model, we now express the matrices S in terms of these new basis vectors, $\boldsymbol{\varphi}^\alpha$, according to

$$S_{\alpha\beta}(2j) = s\phi_\alpha^{*,1}\phi_\beta^1 \qquad S_{\alpha\beta}(2j+1) = s\phi_\alpha^{*,2}\phi_\beta^2. \tag{2.21}$$

---

[8]It is not necessary to work with both $\boldsymbol{\phi}^1$ and $\boldsymbol{\phi}^2$, since they are linearly dependent. We do so for convenience only.

We expand this expression in powers of s^{-1}, and insert it into the Heisenberg Hamiltonian in order to obtain a low energy description of the antiferromagnetic chain. Using

$$S_{\alpha\beta}(2j) \quad = 2s\varphi^{*,1}\varphi^1 + U^\dagger L U + \frac{1}{s}U^\dagger \begin{pmatrix} -|L_{12}|^2 & 0 \\ 0 & |L_{12}|^2 \end{pmatrix} U + O(s^{-2}), \tag{2.22}$$

$$S_{\alpha\beta}(2j+1) \quad = 2s\varphi^{*,2}\varphi^2 + U^\dagger L U + \frac{1}{s}U^\dagger \begin{pmatrix} |L_{12}|^2 & 0 \\ 0 & -|L_{12}|^2 \end{pmatrix} U + O(s^{-2}), \tag{2.23}$$

and Taylor expanding the terms that occur on different sites, the Heisenberg interactions become

$$\text{tr}[S(2j)S(2j+1)] = \tag{2.24}$$
$$4s^2\text{tr}[U\partial_x U^\dagger \Lambda_1 \partial_x U U^\dagger \Lambda_2] + 4|L_{21}|^2$$
$$+4s(L_{21}[\partial_x U U^\dagger]_{12} + L_{12}[U\partial_x U^\dagger]_{21}),$$

$$\text{tr}[S(2j+1)S(2j+2)] = \tag{2.25}$$
$$4s^2\text{tr}[U\partial_x U^\dagger \Lambda_2 \partial_x U U^\dagger \Lambda_1] + 4|L_{12}|^2$$
$$-4s(L_{12}[\partial_x U U^\dagger]_{21} + L_{21}[U\partial_x U^\dagger]_{12}),$$

where we have defined[9]

$$\Lambda_1 := \begin{pmatrix} 1 & 0 \\ 0 & 0 \end{pmatrix} \qquad \Lambda_2 := \begin{pmatrix} 0 & 0 \\ 0 & 1 \end{pmatrix}. \tag{2.26}$$

Above, we have suppressed terms that are at least $O(s^{-2})$. At this point, we are tasked with averaging over the L_{12} fluctuations in order to obtain a theory written in terms of U only. Haldane achieved this by turning from the Hamiltonian formalism to the Lagrangian formalism, and this will be our approach as well.

2.2.1 Coherent state path integral

In order to derive the Lagrangian description of the antiferromagnetic chain, we introduce a complete set of coherent states. Starting with $\phi \in \mathbb{C}^2$, we define

$$|\phi\rangle := \frac{1}{\sqrt{(2s)!}}(\phi \cdot a)^{2s}|0\rangle \tag{2.27}$$

where a is a 2-tuple of boson creation operators (known as Schwinger bosons) [99, 100]. With these objects, we may construct a path integral by inserting them between thin time slices of width $\delta\tau$ of the partition function:

$$\mathcal{Z} = \int \mathcal{D}[\phi] \prod_{k=0}^{N-1} \langle\phi(\tau_k)|e^{-H\delta\tau}|\phi(\tau_k + \delta\tau)\rangle. \tag{2.28}$$

---

[9]Throughout, we will denote by Λ_α the matrix with a single nonzero entry (equalling 1), at row and column α. As an abuse of notation, we will not specify the dimensions of Λ, which will change from 2 to n as we switch from SU(2) to SU(n) in later chapters.

Here $|\phi(\tau_k)\rangle$ is actually a direct product of coherent states, one for each site of the chain,

$$|\phi(\tau_k)\rangle = \otimes_{j=1}^{L}|\phi(j,\tau_k)\rangle, \tag{2.29}$$

and the integration measure is defined to be

$$\mathcal{D}[\phi] := \int \prod_k \prod_j d\Omega_{\phi(j,\tau_k)}, \tag{2.30}$$

where $d\Omega_\phi$ is the normalized Haar measure of the coherent state [98]. To linear order in $\delta\tau$, we may expand

$$\langle\phi(\tau_k)|e^{-H\delta\tau}|\phi(\tau_k + \delta\tau)\rangle \approx \langle\phi(\tau_k)|\phi(\tau_k + \delta\tau)\rangle - \delta\tau\langle\phi(\tau_k)|H|\phi(\tau_k)\rangle. \tag{2.31}$$

The second term will generate the Hamiltonian contribution to the Lagrangian. Meanwhile, the overlap term can be approximated using

$$\langle\phi(\tau_k)|\phi(\tau_k + \delta\tau)\rangle \approx (1 + \boldsymbol{\phi}^* \cdot \partial_\tau\boldsymbol{\phi})^{2s}. \tag{2.32}$$

By taking the product over all time slices τ_k, we can then reexponentiate according to

$$\prod_k \langle\phi(\tau_k)|\phi(\tau_k + \delta\tau)\rangle = \exp\sum_k \log\langle\phi(\tau_k)|\phi(\tau_k + \delta\tau)\rangle \approx \exp\sum_k 2s\boldsymbol{\phi}^* \cdot \partial_\tau\boldsymbol{\phi}. \tag{2.33}$$

This is the so-called "Berry phase contribution" to the path integral. It is a geometric quantity, and mathematically speaking, corresponds to the symplectic form on the coherent state manifold [71, 72]. Adding to it the Hamiltonian term $\delta\tau\langle\phi|H|\phi\rangle$, and taking the number of time slices $N \to \infty$, we obtain a path integral description of the partition function, $\mathcal{Z}$, with Lagrangian density

$$\mathcal{L} = \mathcal{L}_{\text{Berry}} - \langle\phi(\tau)|\mathcal{H}|\phi(\tau)\rangle. \tag{2.34}$$

In the previous subsection, we were able to express H in terms of the matrices U and L. Using (2.17), we also do this for $\mathcal{L}_{\text{Berry}}$. First note that

$$\mathcal{L}_{\text{Berry}} = s\sum_{j=0}^{1} \boldsymbol{\phi}(j)^* \cdot \partial_\tau\boldsymbol{\phi}(j) \tag{2.35}$$

$$\approx s\left[\boldsymbol{\phi}^{1,*} \cdot \partial_\tau\boldsymbol{\phi}^1 + \boldsymbol{\phi}^{2,*} \cdot \partial_\tau\boldsymbol{\phi}^2 + \partial_x\boldsymbol{\phi}^{2,*} \cdot \partial_\tau\boldsymbol{\phi}^2 + \boldsymbol{\phi}^{2,*} \cdot \partial_x\partial_\tau\boldsymbol{\phi}^2\right].$$

To see this, note that the $\mathcal{L}_{\text{Berry}}$ is a Lagrangian density, obtained by summing over both sites of the unit cell, and dividing by the unit cell size, which is 2. It is not important which unit cell we choose, so we have taken sites 0 and 1 of the chain. We have also made use of the Néel ansatz (as reflected in (2.22), to identify $\boldsymbol{\phi}(j = 0) = \boldsymbol{\phi}^1$ and $\boldsymbol{\phi}(j = 1) = \boldsymbol{\phi}^2$. The approximation follows from Taylor expanding all terms about site $j = 1$, to linear order. Using (2.17), we find

$$\mathcal{L}_{\text{Berry}} = -s\epsilon_{\mu\nu}\text{tr}[\partial_\mu U^\dagger \Lambda_2 \partial_\nu U] - 2\text{tr}[L\partial_\tau U U^\dagger], \tag{2.36}$$

where we have made use of the identity $\text{tr}[U^\dagger \partial U] = 0$. This identity will be used repeatedly throughout this thesis, and is proven for $n \times n$ unitary matrices in Appendix A. Combining this result with (2.24) and (2.25), we arrive at the following Lagrangian description of the antiferromagnetic chain:

$$\mathcal{L} = 4s^2 J \text{tr}[U\partial_x U^\dagger \Lambda_1 \partial_x U U^\dagger \Lambda_2] + 4J|L_1^2|^2 + s\epsilon_{\mu\nu}\text{tr}[\partial_\mu U^\dagger \Lambda_2 \partial_\nu U] - 2\text{tr}[L\partial_\tau U U^\dagger]. \tag{2.37}$$

Again, we have divided the Hamiltonian terms by 2, which is the size of the unit cell, to obtain the Hamiltonian density. As a final step, we now integrate over the fluctuations L_{12}, using the identity

$$dz\,dz^* e^{-z^* \omega z + uz + vz^*} = \frac{\pi}{\omega} e^{uv/\omega}. \tag{2.38}$$

This results in a Lagrangian in terms of U only:

$$\mathcal{L} = \frac{1}{4J}\text{tr}[\Lambda_1 U \partial_\tau U^\dagger \Lambda_2 \partial_\tau U U^\dagger] + 4s^2\text{tr}[\Lambda_1 U \partial_x U^\dagger \Lambda_2 \partial_x U U^\dagger] + s\epsilon_{\mu\nu}\text{tr}[\partial_\mu U^\dagger \Lambda_2 \partial_\nu U]. \tag{2.39}$$

There are two names for this quantum field theory. As it is written, it resembles a sigma model in terms of matrices $U \in \text{U}(2)$. However, U can actually be restricted to a smaller manifold, due to the invariance of the theory under diagonal transformations:

$$U \to \begin{pmatrix} e^{i\vartheta_1} & 0 \\ 0 & e^{i\vartheta_2} \end{pmatrix} U. \tag{2.40}$$

These transformations correspond to the group $\text{U}(1) \times \text{U}(1)$, and result in the restriction

$$\text{U}(2) \to \frac{\text{U}(2)}{\text{U}(1) \times \text{U}(1)} = \frac{\text{SU}(2)}{\text{U}(1)}, \tag{2.41}$$

which is an example of a flag manifold. Thus, the above field theory can be referred to as the SU(2)/U(1) flag manifold sigma model.

However, this naming convention is somewhat recent, and is related to extensions of Haldane's work to SU(n) chains, which is the subject of later chapters of this thesis. More commonly, physicists choose to write the theory in terms of the first row of U, that is, in terms of $\boldsymbol{\varphi} := \boldsymbol{\varphi}^1 \in \mathbb{C}^2$ [7]. In this formulation, (2.39) reads

$$\mathcal{L} = 4s^2 \left(|\partial_x \boldsymbol{\varphi}|^2 - |\boldsymbol{\varphi}^* \cdot \partial_x \boldsymbol{\varphi}|^2 \right) + \frac{1}{4J}\left(|\partial_\tau \boldsymbol{\varphi}|^2 - |\boldsymbol{\varphi}^* \cdot \partial_\tau \boldsymbol{\varphi}|^2 \right) - s\epsilon_{\mu\nu}\partial_\mu \boldsymbol{\varphi}^* \cdot \partial_\nu \boldsymbol{\varphi}. \tag{2.42}$$

Since $\boldsymbol{\varphi} \in \mathbb{C}^2$ and is constrained by $|\boldsymbol{\varphi}| = 1$, this is known as the $\mathbb{C}\text{P}^1$ sigma model. It should be emphasized that these two models are not just equivalent: they are identical. We are merely distinguishing between two names for the same manifold, and thus the same sigma model. This should be contrasted with the O(3) nonlinear sigma model originally obtained by Haldane. This theory is equivalent, but distinct from the quantum field theory derived here.

This completes the derivation of Haldane's low energy mapping between antiferromagnet and sigma model. As mentioned previously, these calculations will serve as a template when we consider chain systems with larger symmetry groups in the remaining chapters of this thesis. But before embarking on this generalization program, it is necessary to review additional arguments that led Haldane to his famed conjecture.

2.3 Properties of the Sigma Model

We begin with arguably the most distinguishing property of the quantum field theory derived above; namely, its topological angle.

2.3.1 Topological angle

Perhaps the most surprising aspect of Haldane's conjecture is its discreteness; that is, how it distinguishes between chains with spin $2s$ and $2s + 1$. In many aspects, our above derivation resembles spin-wave theory, which is a large-s expansion and parallels a typical semiclassical perturbative expansion with $s^{-1} \sim \hbar$. But if this were the case, and our calculations were purely perturbative, then it would be impossible to detect a difference between even and odd s, in the limit $s \to \infty$. This paradox is resolved by the final term in (2.39),[10]

$$\mathcal{L}_{\text{top}} = s\epsilon_{\mu\nu}\text{tr}[\partial_\mu U^\dagger \Lambda_2 \partial_\nu U]. \tag{2.43}$$

The subscript 'top' stands for 'topological', and refers to the fact that it is left unaffected by continuous transformations of U. In other words, a topological quantity cannot be detected by continuously varying a small parameter, such as s^{-1}. To see that this explicitly holds for (2.43), note that it is a total derivative:

$$\int d^2x \mathcal{L}_{\text{top}} = s \int d^2x \partial_\mu \left(\epsilon_{\mu\nu}\varphi^* \cdot \partial_\nu\varphi \right) \in 2\pi si\mathbb{Z}. \tag{2.44}$$

Therefore, $\mathcal{L}_{\text{top}}$ is affected only by the behaviour of φ on the boundary of $\mathbb{R}^2$, and will be unchanged by transformations that alter φ in the bulk of $\mathbb{R}^2$ only. Since any field configuration that contributes to the overall partition function $\mathcal{Z}$ must have finite action, we may assume that φ attains a constant value at some radius R away the origin. This allows us to identify $\mathbb{R}^2$ with the sphere S^2, so that φ can be viewed as the following mapping:

$$\varphi : S^2 \mapsto \frac{\text{SU}(2)}{\text{U}(1)}. \tag{2.45}$$

The topological properties of such maps from S^2 to the flag manifold SU(2)/U(1) are classified by the second homotopy group, $\pi_2(\mathbb{CP}^1)$,

$$\pi_2(\mathbb{CP}^1) = \mathbb{Z}. \tag{2.46}$$

---

[10]We have used $\Lambda_2 = \mathbb{I} - \Lambda_1$ and $\text{tr}[U^\dagger \partial U] = 0$ to rewrite $\mathcal{L}_{\text{top}}$ in terms of $\varphi = \varphi^1$ instead.

This is the formal justification for the appearance of $\mathbb{Z}$ on the right hand side of (2.44). Actually, $\mathcal{L}_{\text{top}}$ is usually identified with an element of $H^2(\mathbb{CP}^1, \mathbb{Z})$, the second cohomology group of $\mathbb{CP}^1$. However, for all of the theories that we study, the groups H^2 and π_2 coincide, and so we will not have to worry further about this distinction [71, 72]. And as is becoming a repeated phrase in this chapter, this machinery may seem unnecessarily complicated but will prove to be incredibly useful when we consider more general symmetry groups later on.

The prefactor occurring in (2.44) motivates the following definition:

$$\theta := 2\pi s. \tag{2.47}$$

This is the so-called *topological angle* of the sigma model. This nomenclature can be understood by realizing that $\mathcal{L}_{\text{top}}$ leads to the following prefactor in the path integral of the partition function:

$$e^{-\int d^2 x \mathcal{L}_{\text{top}}} = e^{i\theta k} \qquad k \in \mathbb{Z}. \tag{2.48}$$

In other words $\mathcal{L}_{\text{top}}$ contributes a U(1) phase to particular field configurations, with phase angle θ. Much later, in Chapter 7 of this thesis, we will explain how the energy gap predicted by Haldane is related to this U(1) phase. In short, a nontrivial θ leads to interference effects among fractional topological excitations, resulting in the closing of the energy gap.

At this point, the distinction between half-odd integer s and integer s becomes clear: In the former case, the corresponding sigma model has a topological angle of $\theta = \pi$, while in the latter case, the topological angle is trivial. And while little was understood of the $\mathbb{CP}^1$ sigma model with nonzero θ, it was known that at $\theta = 0$, the model exhibited a finite mass gap [19]. This result, when compared with Bethe's proof that the $s = \frac{1}{2}$ chain is gapless [12], led Haldane to argue that this topological angle, which is ultimately determined by the parity of $2s$, drives a phase transition in the $\mathbb{CP}^1$ sigma model [13, 14]. That is, when $\theta = \pi$, a gapless phase is possible, while when $\theta = 0$, the model should exhibit a finite gap in all cases.[11] And thus, we arrive at the famous Haldane conjecture for spin chains: Integer spin chains are gapped, while half-odd integer spin chains are gapless. In the following subsection, we review additional studies that help elucidate the general phase diagram of these chains.

2.3.2 Renormalization group flow

We may rewrite the sigma model in (2.39) as

$$\mathcal{L} = \frac{1}{g}\text{tr}[U\partial_\mu U^\dagger \Lambda_1 \partial_\mu U U^\dagger \Lambda_2] + \frac{1}{2\pi}\theta \epsilon_{\mu\nu}\text{tr}[\partial_\mu U^\dagger \Lambda_2 \partial_\nu U], \tag{2.49}$$

where we've defined

$$g = \frac{1}{s} \qquad v = 2Js, \tag{2.50}$$

---

[11]The condensed matter community tends to use the phrase "energy gap", while the high energy community tends to instead use "mass gap". This reflects the fact that historically, the $\mathbb{CP}^1$ sigma model was used by particle physicists as a toy model for quantum chromodynamics.

and rescaled $\tau \to v\tau$. With this notation, it is clear that the Lagrangian is invariant under the exchange of spatial and temporal coordinates. In other words, Lorentz invariance has emerged in the low energy theory of the antiferromagnet. This feature will prove to be essential when generalizing Haldane's conjecture to larger symmetry groups, as we will demonstrate in great detail in later chapters of this thesis. Note that if one repeats this field theory derivation for the ferromagnet, such Lorentz invariance is not achieved. This is deeply related to the fact that the corresponding Goldstone bosons of the ferromagnet have quadratic dispersion relations [95–97].

The sigma model (2.49) at $\theta = 0$ exhibits another interesting property, which is known as asymptotic freedom [18, 92]. This means that as we increase the energy scale of our theory, the coupling constant g tends to zero. This is a statement about renormalization group flow, a subject that will be reviewed in detail in Section 4.5, and so we will not prove this result here. As a consequence of asymptotic freedom, perturbatively massless excitations will become massive, which explains the finite mass gap when $\theta = 0$. Moreover, recent work suggests that asymptotic freedom may render spin-wave theory applicable to chains after all, so long as the physical quantities considered preserve the spin symmetry [92]. This fact motivates our consideration of generalized spin-wave theory in later chapters.

Since Haldane's original papers, there has been a large research effort on broadening our understanding of the $\mathbb{C}P^1$ sigma model phase diagram. In [86], it is established that for bare coupling g less than some critical g_c, and for $\theta = \pi$, the model flows to another sigma model which is conformally invariant: the $SU(2)_1$ Wess-Zumino-Witten (WZW) model [101, 102].[12] While it is natural to expect a flow to some $SU(2)$-invariant conformal field theory at the critical point, this particular model is singled out due to the fact that all other theories (which are $SU(2)_k$ WZW models for $k > 1$) are unstabilized due to relevant operators [86]. This flow behaviour is shown in Figure 2.1. Note that for $g > g_c$, the model goes into a gapped phase with a spontaneously broken $\mathbb{Z}_2$ symmetry, which is a manifestation of the underlying translation symmetry in the spin chain.[13] In [86], it is explained how all regions of the phase diagram in Figure 2.1 can be reached: the bare coupling g can be increased by adding antiferromagnetic next-nearest-neighbour interactions, and θ can be changed by adding alternating exchange interactions, which explicitly break translation symmetry. In both cases, the scaling of the mass gap has been calculated using the $SU(2)_1$ WZW model. Finally, the right hand edge of the diagram, corresponding to the strong coupling limit $g \to \infty$, has also been considered [104, 105].

2.4 Exact Results

In addition to the exact result of Bethe for the $s = \frac{1}{2}$ chain [12], which predicts a gapless ground state with no broken symmetries, there are two additional pieces of rigorous evidence for the antiferromagnet phase diagram, Figure 2.1. They are both in agreement with Haldane's conjecture,

---

[12]Another name for these models is WZNW, after Sergei Novikov [103].

[13]If a translationally invariant chain with a d-site unit cell maps onto a sigma model, translation symmetry will manifest as a $\mathbb{Z}_d$ action.
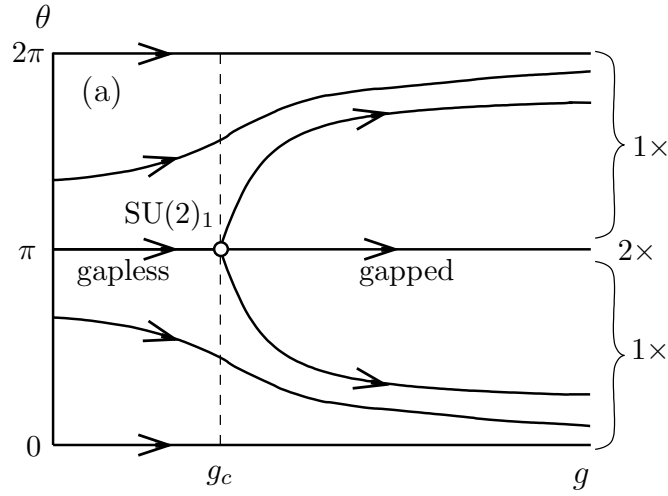
Figure 2.1: Phase diagram of the antiferromagnetic chain.

and are worth mentioning now, since their generalizations will appear later in the text.

2.4.1 The Lieb-Schultz-Mattis Theorem

The Lieb-Schultz-Mattis (LSM) theorem is a rigorous statement about ground states in translationally invariant Hamiltonians [80]. Applied to the spin-s antiferromagnet, this theorem requires that if s is not an integer, then either the ground state is unique with gapless excitations, or there is a ground state degeneracy. This is consistent with the $\theta = \pi$ line in Figure 2.1. In Section 3.5.2, we prove a more general result (an extension of the LSM-A theorem, where A stands for Affleck [81]), from which a proof of the LSM theorem follows automatically.

2.4.2 The Affleck-Kennedy-Lieb-Tasaki model

One of the most important theoretical results to follow Haldane's conjecture and support its conclusion was the Affleck-Kennedy-Lieb-Tasaki (AKLT) construction [82]. By forming singlet bonds between adjacent spin-$\frac{1}{2}$'s of a spin-1 chain, the AKLT Hamiltonian was able to exhibit a unique, translationally invariant ground state with a finite excitation gap. This result compliments the LSM theorem, and corresponds to the $\theta = 0$ line in Figure 2.1. In Figure 2.2, we provide a pictorial representation of this construction, which also serves to introduce notation that we will use later on to draw generalized AKLT states.
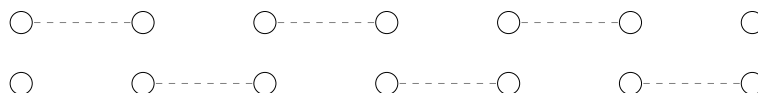
Figure 2.2: The AKLT ground state in an SU(2) antiferromagnetic chain. Each node corresponds to a spin-$\frac{1}{2}$ representation. Two nodes arranged vertically in single column are symmetrized, and correspond to a spin-1 representation. A dashed edge denotes a singlet bond. Notice that this state is translationally invariant.

2.5 Conclusion

In this chapter, we reviewed the various arguments that support Haldane's conjecture about antiferromagnetic spin chains. Our primary focus was the derivation of the correspondence between spin chain and sigma model, which becomes exact in the limit $s \to \infty$. As we proceed to generalize the Haldane conjecture to larger symmetry groups in the following chapters, we will follow the same structure of argument as was presented in this chapter. For clarity, we repeat the steps followed here:

1. Identify the classical ground states of the Hamiltonian, and the target space manifold of the sigma model.

2. Perform a low energy expansion of the Hamiltonian, taking into account fluctuations that both preserve and destroy the classical ground state structure.

3. Generate a Lagrangian from the path integral formalism, using coherent states.

4. Identify the (set of) topological angle(s) of the sigma model.

5. Determine the renormalization group flow of the sigma model, and make use of existing exact solutions.[14]

6. Consult (and generalize) exact results for the original Hamiltonian, such as the LSMA theorem and the AKLT construction.

7. Combine the results of Steps 5 and 6, and formulate a conjecture about the ground state behaviour of the Hamiltonian.

In later chapters, we will attempt to follow this agenda for a variety of quantum chain systems. In doing so, we will run into a variety of technical challenges, and in overcoming these challenges, we will be led to exciting new physical phenomena.

---

[14]A large class of results pertaining to the sigma models that we encounter go by the name of 't Hooft anomaly matching conditions [106, 107]. Such results also exist for the $\mathbb{C}P^1$ sigma model, and offer a modern interpretation of Haldane's conjecture. We will discuss 't Hooft anomalies extensively in Section 4.6.4.

Chapter 3

SU(n) Chain Hamiltonians

3.1 Introduction

The defining symmetry of an antiferromagnet is the Lie group SU(2), the set of special unitary 2×2 matrices. The two complex dimensions of these matrices can be thought of as corresponding to two species of particle: a 'spin-up' particle and a 'spin-down' particle. The fact that the dimensions are complex follows from quantum mechanics, and is related to the invariance of the wave function under U(1) phase transformations. These two particles correspond to the $s = \frac{1}{2}$ representation of SU(2). Larger spin representations are constructed by taking tensor products of these 2-dimensional spaces. For example, a spin-1 particle corresponds to the (symmetric) tensor product of two 2-dimensional spaces, or 2 spin-$\frac{1}{2}$ particles. Adding more spin-$\frac{1}{2}$'s will increase the representation (and thus the total spin), but the underlying symmetry group will remain SU(2).

In order to modify the group SU(2) itself, we must change the number of "species" of particle. For example in quantum chromodynamics, the theory of strong interactions, the presence of three species of quark (red, blue, and green) leads to an internal SU(3) symmetry [108]. However, quarks are confined within hadrons, and do not form long chains like an SU(2) antiferromagnet. In fact, we do not know of any naturally occurring chain systems with an on-site SU(n) symmetry, for $n > 2$. This statement holds true not just for exact symmetries, but also for approximate symmetries, like the SU(3) 'flavour' symmetry that relates the up, down and strange quark [108].

Nonetheless, shortly after Haldane's conjecture was presented, work began on extending his calculations from SU(2) to SU(n) chains [48–51]. Initially, this was a purely theoretical exercise, with hopes of understanding the correspondence between sigma model and chain system on more general grounds. It had been predicted that a certain family of sigma models could be used to characterize the localization transition in the quantum Hall effect, and so there was promise that a generalized Haldane conjecture could shed light onto this problem [48, 52, 53].

After this initial wave in the 1980s, interest in SU(n) chains diminished, likely due to their disconnect from physically realizable systems. However, this all changed in the early 2000s, when advances in cold atom experimentation suggested that chains with larger symmetry groups might be possible to construct using optical traps [54–66]. In the past decade, these ideas have come to fruition, and have resulted in a resurgence in theoretical interest in SU(n) chains.

The idea behind engineering SU(n) chains using cold atoms is the following. Alkaline Earth atoms have vanishing electronic angular momenta. As a result, their nuclear spin Zeeman states are all degenerate, and serve the roll of 'species of particle', in the sense mentioned above. If a collection of these atoms are trapped in a chain-like formation, the interatomic potential between

sites will not distinguish between these Zeeman states, and an $SU(2I+1)$ symmetry will emerge, where I is the atom's nuclear spin [57, 64]. So far, the largest symmetry group that has been realized in this way is $SU(10)$, using Strontium, which has $I = \frac{9}{2}$ [63].

One might ask why is it that alkaline Earth atoms are necessary in order to construct such $SU(n)$ chains. After all, doesn't a spin-s $SU(2)$ chain have $2s+1$ 'species of particle' at each site? The issue is that while spin chains may have the correct number of states at each site, their Hamiltonians are not invariant under larger symmetry groups except at fine-tuned points.[15] This is because the vector $\vec{S}$ of spin operators does not transform nicely under the larger $SU(2s+1)$ symmetry group. On the other hand, when one writes down the Hamiltonian for a chain of alkaline Earth atoms, the interactions are approximated by a pseudopotential that transforms trivially under the $SU(2I+1)$ group [64].

Of course, the symmetry group is only half of the story. A more significant experimental challenge is how to realize different representations of the $SU(n)$ chain, which requires multiple atoms trapped at the same site. There has been some progress is realizing 2-atom representations (the analogue of spin-1) by making use of an additional degeneracy between the so-called s and f states [57]. However, realizing the most general representations of $SU(n)$ remains an outstanding experimental problem. Even so, theoretical physicists have forged ahead, attempting to characterize $SU(n)$ chains in a variety of different representations.

In this chapter, we will introduce our systematic approach to studying $SU(n)$ chain Hamiltonians in the most general representation. Our work builds off the seminal contributions of Affleck [48–50] and Bykov [71, 72], and offers a modern perspective on how $SU(n)$ representations ultimately determine the target space manifold of the sigma model describing the chain's low energy physics. In Section 3.2, we introduce the $SU(n)$ Heisenberg Hamiltonian, and review elements of the representation theory of $SU(n)$, including Casimir operators and Young tableaux, that we will require later on. Then, in Section 3.3, we discuss the classical ground states of these Hamiltonians. We explain how longer-range interaction terms are necessary in order to stabilize these ground states, and how the notion of flag manifolds arise from $SU(n)$ representations. We also introduce graphical notation that will be used throughout this thesis when discussing the structure of $SU(n)$ chains. Next, in Section 3.4, we classify all $SU(n)$ chains that lead to an $SU(n)/[U(1)]^{n-1}$ sigma model at low energies. Finally, in Section 3.5, we review various exact results that exist for $SU(n)$ chains, including the Bethe ansatz models [12, 84, 85], the AKLT models [67, 82], and the Lieb-Schultz-Mattis-Affleck theorem [80, 81]. We will make frequent reference to this section later on, when we formulate our $SU(n)$ versions of Haldane's conjecture.

3.2 SU(n) Hamiltonians

In the previous chapter, we introduced 2×2 matrices in (2.10) that contained the 3 generators of $\mathfrak{su}(2)$. We now repeat these steps for general n. We define a traceless $n \times n$ matrix $S_{\alpha\beta}$ whose

---

[15]For an example of this fine-tuning, it is well known that the spin-1 bilinear-biquadratic chain has two points where $SU(3)$ symmetry emerges [48].

entries correspond to the $n^2 - 1$ $\mathfrak{su}(n)$ generators. The entries of $S_{\alpha\beta}$ satisfy the same commutation relations as in SU(2), (2.11), which we repeat here for convenience:

$$[S_{\alpha\beta}, S_{\mu\nu}] = \delta_{\alpha\nu} S_{\mu\beta} - \delta_{\mu\beta} S_{\alpha\nu}. \tag{3.1}$$

Using these matrices, the Heisenberg interaction takes the same form as the right hand side of (2.12), which is

$$J\text{tr}[S(i)S(j)]. \tag{3.2}$$

As before, we take $J > 0$, which corresponds to an antiferromagnetic-like interaction. Thus, we arrive at the SU(n) Heisenberg model:

$$H = J \sum_j \text{tr}[S(j)S(j+1)]. \tag{3.3}$$

As it will turn out, this Hamiltonian will often be insufficient for our analysis. Instead, we will have to consider a modified Hamiltonian which includes longer-range interaction terms. This is forced on us by the representation theory of SU(n), which we now review.

3.2.1 Representation theory

Unlike SU(2), a representation of SU(n) is not labeled by a single number (the 'spin'). Instead, it is specified by $n - 1$ integers, which are related to so-called Casimir constraints:

$$\text{tr}[S^m] = C_m \mathbb{I} \qquad m = 2, 3, \ldots, n. \tag{3.4}$$

In SU(2), the only constraint is the quadratic Casimir, $\text{tr}[S^2] = \frac{s}{2}(s+1)\mathbb{I}$, which uniquely defines the spin, s. For $n > 2$, a representation's defining integers are conveniently expressed in terms of row lengths of a standard Young tableau. Indeed, the most general representation $[p_1, p_2, \ldots, p_{n-1}]$ of SU(n) corresponds to a unique diagram of boxes arranged in $n - 1$ rows, of lengths $p_1, p_2, \ldots, p_{n-1}$ respectively. The row lengths must satisfy $p_1 \geq p_2 \geq \cdots \geq p_{n-1} \geq 0$. See Fig. 3.1 for some examples. This choice of labelling is related to the limit of large representation: in the limit $p_1 \to \infty$, the matrix of operators S is again replaced with a classical matrix, whose eigenvalues are completely determined by the row lengths p_α [50]:

$$\lambda_\alpha = p_\alpha - p \qquad p := \frac{1}{n} \sum_{\alpha=1}^{n} p_\alpha. \tag{3.5}$$

Here we've defined $p_n := 0$. Note that since the quadratic Casimir $\text{tr}[S^2] \to \infty$ when $p_1 \to \infty$, it is sufficient to only consider large p_1 to obtain the classical limit, as reflected in (2.5); it is not necessary to also require $p_\alpha \to \infty$ for $\alpha > 1$.

It now becomes apparent how different representations of SU(n) may lead to different types of sigma models. Indeed, the matrix S is constrained to live on the manifold U(n)/H, where

$$H = \text{U}(m_1) \times \text{U}(m_2) \times \cdots \times \text{U}(m_k) \tag{3.6}$$
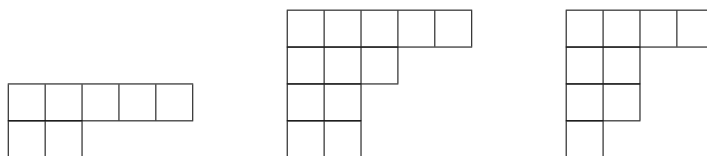
Figure 3.1: Examples of Young tableaux in SU(n). A diagram with k nonzero rows corresponds to a representation in SU(n) with $n \geq k + 1$.

is a product of k unitary groups, one for each distinct value of λ_α, and m_α is the degeneracy of each λ_α. These spaces are known as flag manifolds, and can be thought of as generalizations of Grassmannian manifolds, which correspond to $m_1 = m$ and $m_2 = n - m$ (i.e. $k = 2$). Complex projective space $\mathbb{C}\mathrm{P}^{n-1}$ is the Grassmannian with $m_1 = 1$. Flag manifolds are very interesting mathematical objects, and possess a variety of rich geometric structures, including symplectic and Kähler forms. For an in-depth account of this structure, we encourage the reader to consult the recent review [6].

According to (3.6), it is possible to fix the target space manifold of the matrices S by choosing the appropriate representation of SU(n) on each site. This leads to a very important question that we should ask as we embark on a program to generalize Haldane's conjecture: *what is the appropriate generalization of the spin chain/sigma model correspondence beyond SU(2)?* Recall that in the previous chapter, we established two equivalent mappings for the antiferromagnet: one in terms of the SU(2)/U(1) sigma model (which equals $\mathbb{C}\mathrm{P}^1$), and one in terms of the S^2 sigma model. Critically, when $n > 2$ these two descriptions are not equivalent. Moreover, the manifolds SU(2)/U(1) and $\mathbb{C}\mathrm{P}^1$ are no longer isomorphic when $n > 2$! This leads to at least three candidate families of sigma model as we increase n.

One may protest that our above inquiry about the 'appropriate' generalization of Haldane's conjecture is misguided. After all, we have just established that the target space manifold of S is uniquely determined by its representation, and so wherein lies our freedom to choose how to generalize Haldane's conjecture? In our defense, we stress a distinction that must be made between the target space manifold of S, and the target space manifold of the corresponding sigma model. In SU(2), these two spaces coincided but this is not a requirement for $n > 2$. Indeed, as we will show in the following section, it is possible to work with matrices S that lie in smaller manifolds, and then combine these degrees of freedom over consecutive sites of a unit cell to produce a larger manifold. For example, our focus in Chapter 4 is the SU(3)/[U(1)]^2 sigma model. One may arrive at this sigma model by considering representations of SU(3) that restrict S to SU(3)/[U(1)]^2 directly – these are so-called self-conjugate representations of SU(3). However, a second approach is to consider representations that restrict S to $\mathbb{C}\mathrm{P}^2$, and combine these degrees of freedom over a three-site unit cell using orthogonality conditions to arrive at the same flag manifold. See Figure 3.2

for examples of Young tableau in either case.
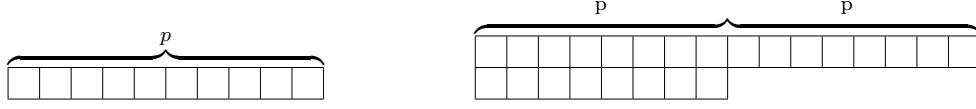
Figure 3.2: Examples of Young tableaux that correspond to representations of SU(3) that lead to the SU(3)/[U(1)]$^{3-1}$ flag manifold sigma model. These representations will be studied in Chapter 4.

This second approach turns out to be a rich source of new physics, as was first emphasized by Bykov [71, 72]. As such, we repeat this construction in Chapter 5 for general n: we choose representations that restrict S to $\mathbb{CP}^{n-1}$, and then combine n such fields across an n-site unit cell to obtain the SU(n)/[U(1)]$^{n-1}$ sigma model. The flag manifold SU(n)/[U(1)]$^{n-1}$ corresponds to $m_\alpha = 1$, for $\alpha = 1, ..., n$ in (3.6), and is referred to as the 'complete' flag manifold associated with U(n). By construction, these sigma models will also have a $\mathbb{Z}_n$ translation symmetry, which is a manifestation of the n-site unit cell. These combined symmetries will lead to a rich classification based on 't Hooft anomaly matching [106, 107], among other exact results. However, various technical hurdles must be cleared along the way.

In passing, it is worth mentioning that the initial studies of SU(n) chains did not consider such multi-site constructions. Instead, those authors focused on sigma models whose target spaces coincided with the target space of the S matrices themselves [49]. In particular, this approach was used to obtain $\mathbb{CP}^{n-1}$ sigma models and their Grassmannian generalizations, with symmetry groups U(n)/[U(m) × U($n-m$)] [48, 50, 51]. In these papers, the desired sigma model was generated by identifying the representation $\mathcal{R}$ that directly restricts S to the sigma model's full manifold, and then placing $\mathcal{R}$ and its conjugate $\overline{\mathcal{R}}$ on even and odd sites of the chain, respectively. For representations satisfying $\mathcal{R} = \overline{\mathcal{R}}$, this construction reduces to the on-site method mentioned previously for SU(3) self-conjugate chains.

3.3 Classical Ground States

In the limit of large representation, we replace S with $V^\dagger \text{diag}(\lambda_1, \ldots, \lambda_n)V$, where V is a unitary matrix, and the eigenvalues λ_α are given in (3.5). Again, this structure of S follows from the $n-1$ Casimir constraints. The Heisenberg interaction then reads

$$\text{tr}[S(i)S(j)] \rightarrow \sum_{\alpha,\beta,\gamma,\delta} \lambda_\alpha \lambda_\beta |\boldsymbol{\phi}^{\alpha,*}(i) \cdot \boldsymbol{\phi}^\beta(j)|^2, \qquad (3.7)$$

where we've defined $V_{\alpha\beta}(i) = \phi_\beta^\alpha(i)$. Since the $\boldsymbol{\phi}^\alpha$ are rows of a unitary matrix, they must be mutually orthonormal on the same site. Implicit in this expression is our assumption that the same representation occurs at each site of the chain, which we will always take to be true. Since $\lambda_\alpha = p_\alpha - p$ for the representation with Young tableau row lengths p_α, we opt to shift S by $p\mathbb{I}$ to simplify our calculations (this merely shifts the interaction term (3.7) by an overall constant).

Having done this, the simplest SU(n) chain Hamiltonian, namely the nearest-neighbour model, becomes

$$H = J \sum_j \sum_{\alpha,\beta=1}^{n-1} p_\alpha p_\beta |\boldsymbol{\phi}^{\alpha,*}(j) \cdot \boldsymbol{\phi}^\beta(j+1)|^2, \qquad J > 0. \tag{3.8}$$

Note that the sums over α and β stop at $n-1$, since $p_n = 0$ by definition. This nearest-neighbour model is the logical starting point for any SU(n) generalization of the antiferromagnetic spin chain. However, in most cases, we will be required to consider Hamiltonians with longer-range interactions. For instance, if one considers an SU(n) chain in the totally symmetric representation, with $p_\alpha = 0$ for $\alpha > 1$, then S is restricted to the manifold $\text{SU}(n)/\text{U}(n-1) = \mathbb{CP}^{n-1}$, meaning it is entirely specified by a single complex unit vector $\boldsymbol{\phi} \in \mathbb{C}^n$. Now, in the nearest-neighbour model (3.8), a Néel-like state that alternates between two orthogonal directions in $\mathbb{C}^n$, such as $\boldsymbol{\phi}(2j) = \boldsymbol{\varphi}^1$ and $\boldsymbol{\phi}(2j+1) = \boldsymbol{\varphi}^2$, would be a classical ground state. For $n = 2$ this is the end of the story, and led us to an appropriate flag manifold description in Chapter 2. But for $n > 2$, there is a nontrivial subspace, namely $\mathbb{C}^{n-2}$, that is spanned by vectors orthogonal to the Néel vectors $\boldsymbol{\varphi}^1$ and $\boldsymbol{\varphi}^2$. As a consequence, any field theory derivation will be plagued with local zero modes – zero energy excitations above the ground state - that correspond to transformations into this unused subspace.

In order to resolve this obstruction in deriving a field theory, we are forced to modify the Hamiltonian (3.8) by adding longer-range interactions. This will couple more lattice sites together, and result in a classical ground state that is made up of vectors that span all of $\mathbb{C}^n$. For the totally symmetric representations, this will require up to $n-1$-neighbour interactions, and will result in an n-site unit cell structure for those chains. This is consistent with the exact Bethe ansatz solutions (reviewed below in Section 3.5) that exhibit such n-site structure.[16] Moreover, it has been shown in SU(3) that zero point fluctuations are minimal in the 3-site state when $p \to \infty$, and this is expected to hold for all n [109]. Accordingly, we believe that the first effect of quantum fluctuations in the symmetric chains will be to select the n-sublattice state by an 'order-by-disorder' mechanism that generates effective additional couplings of order $1/p$ that lift the classical degeneracy. It should be kept in mind however that all the properties discussed for these longer-range Hamiltonians are expected to apply to nearest-neighbour Hamiltonians, and that the longer-range couplings have been introduced as a first effect of quantum fluctuations in those models. This sentiment applies not only to the symmetric chains, but to all of the SU(n) chains that we consider.

In the following section, we explain how this construction generalizes as we increase the number of nonzero p_α. Loosely speaking, the number of nonzero rows k in the representation will correspond to the number of fields $\boldsymbol{\varphi} \in \mathbb{C}^n$ that exist at each site of the chain. We will then take $\lambda \sim \frac{n}{k}$ consecutive sites together to produce a mapping from the chain to the flag manifold sigma model, $\text{SU}(n-1)/[\text{U}(1)]^{n-1}$. As we will show, any attempt to derive a sigma model with a different target space manifold will ultimately fail; again, this will be due to spurious zero modes. Before we embark on this classification task, it will be useful to introduce some graphical notation that

---

[16]By n-site structure, we are referring to the presence of an order-n discrete symmetry $\mathbb{Z}_n$ in the low energy theory. It is not the case that the ground state has n-site order, which would correspond to the spontaneous breaking of this symmetry.

will aid us in our calculations.

3.3.1 Pictorial representation of classical ground states

According to (3.7), to each site of the chain we should assign a set of orthonormalized vectors $\boldsymbol{\varphi}^\alpha$. We may use the same basis on each site of the chain, since any local change of basis transformation leaves the Hamiltonian invariant (and fortunately, no superpositions of states arise). Further, we will use coloured circles to represent the first few elements of this basis, in an effort to visually aid the reader. This generalizes what we originally did for the Néel state in the previous chapter (see (2.16). Our colour dictionary, for the first eight basis elements, can be found in Figure 3.3.

$$\varphi^1 = \bullet \qquad \varphi^2 = \bullet \qquad \varphi^3 = \bullet \qquad \varphi^4 = \circ$$

$$\varphi^5 = \circ \qquad \varphi^6 = \bullet \qquad \varphi^7 = \bullet \qquad \varphi^8 = \bullet$$

Figure 3.3: Colour dictionary for the first eight basis elements in $\mathbb{C}^n$. These coloured circles will be used to pictorially represent ground states throughout.

When drawing a classical ground state, we will arrange the same-site vectors into a single column, and use a white space to separate neighbouring chain sites. For example, the Néel state of the SU(2) antiferromagnet is

$$\cdots \quad \bullet \ \bullet \ \bullet \ \bullet \ \bullet \ \bullet \ \bullet \ \bullet \quad \cdots \ , \tag{3.9}$$

while a classical ground state of the adjoint SU(3) chain is

$$\cdots \quad \bullet \ \bullet \ \bullet \ \bullet \ \bullet \ \bullet \ \bullet \quad \cdots \tag{3.10}$$
$$\cdots \quad \bullet \ \bullet \ \bullet \ \bullet \ \bullet \ \bullet \ \bullet \quad \cdots \ . \tag{3.11}$$

That this is the ground state of the SU(3) adjoint chain will be demonstrated below.

The benefit of these ground state pictures is that it makes it easy to read off the energy cost of a term $\mathrm{tr}[S(i)S(j)]$. Indeed, in a classical ground state, each colour corresponds to a standard unit vector $\boldsymbol{\varphi}^\alpha$, and we have according to (3.8),

$$\mathrm{tr}[S(i)S(j)] = \sum_{\alpha,\beta} p_\alpha p_\beta |\boldsymbol{\varphi}^{\alpha,*}(i) \cdot \boldsymbol{\varphi}^\beta(j)|^2. \tag{3.12}$$

The right hand side of this expression vanishes unless one of the complex unit vectors (i.e. one of the colours) at site i equals one of the complex unit vectors at site j. In this case, the right hand

side equals $p_{\alpha_0} p_{\beta_0}$, where α_0 and β_0 are the respective positions of the unit vector/colour in column i and column j. To visualize this, it is useful to imagine bonds between all of the circles of the two columns, as in Figure 3.4. These bonds are inactive (meaning zero energy cost), unless two nodes are the same colour. For example, the Néel state in (3.9) has an energy cost of zero per site (recall we have shifted the $S_{\alpha\beta}$ matrices by a constant), while the classical ground state of the adjoint chain, (3.10), has an energy cost of p_2^2 per site.
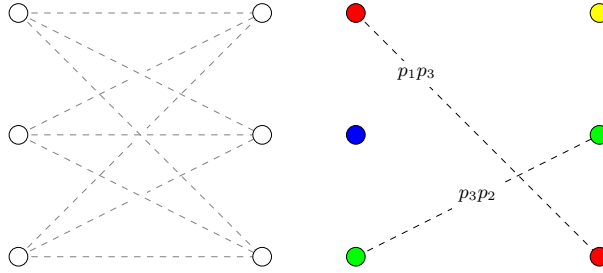
Figure 3.4: Left: Imaginary bonds between two sets of vectors $\boldsymbol{\varphi}^\alpha$ and $\boldsymbol{\varphi}^\beta$ at sites i and j of the chain. Right: The energy cost of each bond is $p_{\alpha_0} p_{\beta_0}$ whenever two nodes have the same colour; α_0 and β_0 are the column positions of these nodes.

3.4   Classification of SU(n) Chains

As a warm-up to the more complicated representations below, we begin with the totally symmetric representations that have Young tableaux with a single row of length p_1. According to (3.12), any configuration that has no energy cost per bond will be a classical ground state of the nearest-neighbour SU(n) Hamiltonian. Since only one node is present at each site, the Néel state is such an example. However, as mentioned above, the basis at each site is larger than 2 for $n > 2$ (i.e. there are more than 2 colours available), and this leads to an infinite number of ground states. Indeed, the ground state

$$\cdots \quad \bullet \quad \bullet \quad \bullet \quad \bullet \quad \bullet \quad \bullet \quad \bullet \quad \cdots \, , \tag{3.13}$$

which exists for $n > 2$, is related by a zero-energy transformation to the Néel state. This local degree of freedom is an example of a zero-energy mode, and destabilizes any candidate ground state above which we would like to derive a quantum field theory. As a result, the nearest-neighbour Hamiltonian must be modified if we would like to proceed. Since it is believed that longer-range interactions may be dynamically generated from the nearest-neighbour model [109], we add further-neighbour interactions to realize a stable ground state. Since there are n possible colours, we require up to $(n-1)$-neighbour interactions, all of which are taken to be antiferromagnetic, in order

to remove the zero modes.[17] For example, in SU(5), with interactions up to 4th-neighbour, one such ground state is

$$\cdots \quad \bullet \ \bullet \ \bullet \ \bullet \ \bullet \ \bullet \ \bullet \ \bullet \ \bullet \ \bullet \quad \cdots \ . \tag{3.14}$$

While this large number of interaction terms may seem contrived, there is a second reason why one should consider adding them. Arguably, it is the simplest way to restrict to classical ground states that have a $\mathbb{Z}_n$ symmetry, which is to be expected for the symmetric chains, since this is a feature of the integrable SU(n) chains, that correspond to $p = 1$ (see Section 3.5). Moreover, in the following two chapters, we will explicitly demonstrate how the SU(n)/[U(1)]$^{n-1}$ sigma model arises as the low energy description of this longer-range Hamiltonian. In short, while the on-site matrix S lines in $\mathbb{C}P^{n-1}$, by coupling n neighbouring sites, our underlying degrees of freedom are actually n orthogonally coupled $\mathbb{C}P^{n-1}$ fields, which is equivalent to SU(n)/[U(1)]$^{n-1}$.

In the more general representations with more than one Young tableau row, we will see a similar pattern: collections of $\mathbb{C}P^{n-1}$ fields from neighbouring sites will become orthogonally coupled, ultimately leading to the flag manifold SU(n)/[U(1)]$^{n-1}$. Actually, the fields at each site will correspond to a Grassmannian manifold in this more general case. If the following discussion seems too abstract, we encourage the reader to first turn to Chapter 4, where the symmetric representation SU(3) chains are considered in great detail.

Loosely speaking, the number of nonzero rows k in the representation will correspond to the number of fields $\boldsymbol{\varphi}$ that exist at each site of the chain. We can think of these k fields as living in the product space $P_{k,n} := [\mathbb{C}P^{n-1}]^k$ of k copies of $\mathbb{C}P^{n-1}$. We will then take $\lambda := \frac{n}{k}$ consecutive sites together to produce a mapping to the complete flag manifold SU(n)/[U(1)]$^{n-1}$. In other words, we construct an embedding,

$$\mathrm{SU}(n)/[\mathrm{U}(1)]^{n-1} \hookrightarrow P_{k,n} \times \cdots \times P_{k,n}, \tag{3.15}$$

into the λ-fold product of $P_{k,n}$s. However, this isn't the whole story, since the k fields on each site (those within $P_{k,n}$) can still be locally rotated amongst one another, leading to additional zero modes. This is resolved by adding a λ-neighbour interaction that freezes out these additional degrees of freedom, which is essentially mimicking what happens when a representation $\mathcal{R}$ is coupled to its conjugate representation $\overline{\mathcal{R}}$. It corresponds to the embedding $G_{k,n} \hookrightarrow P_{k,n}$, where $G_{k,n} := \mathrm{U}(n)/[\mathrm{U}(k) \times \mathrm{U}(n-k)]$ is a Grassmannian manifold. In other words, by adding a sufficient number of interaction terms to our Hamiltonian, we end up with the following embedding of a flag manifold into a λ-fold product of Grassmannians:

$$\mathrm{SU}(n)/[\mathrm{U}(1)]^{n-1} \hookrightarrow G_{k,n} \times \cdots \times G_{k,n}. \tag{3.16}$$

The argument that we have just sketched assumes that it is always possible to derive a complete flag manifold sigma model description of an SU(n) chain. However, this is not entirely true: there is a large family of representations that do not admit such a mapping, namely those representations that satisfy $p_\alpha = p_\beta \neq 0$ for at least two rows of the Young tableau. For such representations, this

---

[17]This is consistent with [109], which found that the energetically favoured state should have n colours.

produces a factor of U(2) in the quotient group H in (3.6). While this also occurs when we have two rows of zero length, as in the symmetric representations of SU(4), the result is fundamentally different. In both cases, there are spurious local degrees of freedom on each site (corresponding to rotating the φ fields into each other); however, the trick of adding a λ-range interaction does not freeze this additional symmetry in the case of $p_\alpha = p_\beta \neq 0$. This should become apparent below. As a result, for the most general representation of SU(n), we do not expect that a well-defined mapping to the SU(n)/[U(1)]$^{n-1}$ sigma model exists, and so henceforth we restrict to the representations that satisfy $p_\alpha \neq p_\beta$ for all nonzero row lengths. Our justification for this restriction should be clear in Chapter 5, and it has to do with the classification of 't Hooft anomalies in these theories. As we will explain later, any generalization of Haldane's conjecture is greatly bolstered by the presence of an 't Hooft anomaly, and at this time, only the SU(n)/[U(1)]$^{n-1}$ sigma models have been show to have this property. A second justification follows from Chapter 7, where we interpret the Haldane gap as being generated by fractional instantons.

3.4.1 Representations with $n-1$ rows

We now consider representations of SU(n) whose Young tableau have $n-1$ nonzero rows. As previously stated, we will assume throughout that no two rows have the same length. Arguably, these representations are simpler than the symmetric ones considered above. Since the on-site representation of the S matrix already corresponds to the manifold SU(n)/[U(1)]$^{n-1}$, a nearest-neighbour Heisenberg interaction is sufficient to derive the associated sigma model. Let us first demonstrate this in SU(3). The interaction term for a classical ground state,

$$\text{tr}[S(j)S(j+1)] = \sum_{\alpha,\beta=1}^{2} p_\alpha p_\beta |\varphi^{\alpha,*}(j) \cdot \varphi^\beta(j+1)|^2, \tag{3.17}$$

is never zero for two adjacent sites, which requires choosing the colour for four nodes. Since $p_1 > p_2$, the minimum is p_2^2, which is achieved when the two same-colour nodes are in the second position of the column. Thus, a typical ground state in SU(3) looks like

which is precisely what we drew above for the adjoint SU(3) chain (which corresponds to the case $p_1 = 2, p_2 = 1$). Note that no local transformations exist that cost zero energy: all of the p_2 nodes must stay the same colour in order to minimize the tr[$S(j)S(j+1)$] term, and the remaining two colours behave just like the Néel state of SU(2). We will return to these chains near the end of Chapter 4.

In SU(4), the term tr[$S(j)S(j+1)$] requires the introduction of six coloured nodes. Using the

inequality $p_2^2 + p_3^2 \geq 2p_2p_3$, we see that the ground states have the following form:
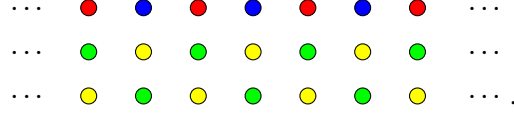
This pattern extends to general n: the first row of nodes establishes a Néel-like state, while the remaining $n-2$ rows have a "reverse-ordered" pattern: the colour ordering along a column switches direction between even and odd sites. Let us explain how this works. For general n, our task is to minimize (3.12). Using orthonormality, this reduces to

$$\text{tr}[S(j)S(j+1)] = \sum_{\alpha,\beta=1}^{n} p_\alpha p_\beta |\varphi_\alpha^\beta(j+1)|, \tag{3.18}$$

where we've defined $p_n := 0$. Since $\varphi^\beta(j+1) = \varphi^{\alpha'}$ for some α' (and all of the α' are distinct), we may introduce a permutation operator on the set of n elements, $\sigma : \{1, 2, \ldots, n\} \to \{1, 2, \ldots, n\}$ that obeys

$$\varphi^\beta(i+1) = \varphi^{\sigma(\beta)}$$

and rewrite (3.18) as

$$\text{tr}[S(j)S(j+1)] = \sum_{\alpha=1}^{n} p_\alpha p_{\sigma(\alpha)}. \tag{3.19}$$

Thus, our task amounts to finding the permutation σ that minimizes (3.19). By defining a vector $\vec{x} := (p_1, p_2, \ldots, p_n)$, we can think of σ as specifying a second vector $\vec{y}$; (3.19) is then their dot product. Since the entries of both $\vec{x}$ and $\vec{y}$ are nonnegative and nondegenerate, it is clear how to choose σ so that $\vec{y}$ is as orthogonal to $\vec{x}$ as possible:

- Since p_1 is the largest component of $\vec{x}$, we assign to $\sigma(1)$ the smallest possible component of $\vec{y}$, which is p_n.
- Next, assign to $\sigma(2)$ the second smallest possible component of $\vec{y}$, which is p_{n-1}.
- Repeating this procedure, we see that indeed the classical Hamiltonian is minimized by the reverse-ordered ground state, corresponding to a permutation operator

$$\sigma : i \mapsto k + 1 - i.$$

The basis states at site $j + 1$ are $\varphi^\beta(j+1) = \varphi^{\sigma(\beta)}$.

The above procedure will work for all n. For another example, here is a ground state in SU(5):
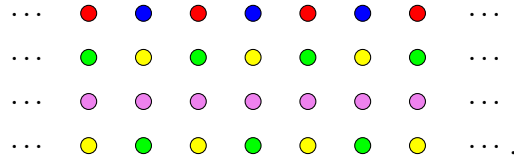
For these representations, the unit cell is always 2 sites in length, which leads to a $\mathbb{Z}_2$ translation symmetry in the sigma model.

3.4.2 Representations with row number dividing *n*

Let k be the number of nonzero rows in the Young tableau, and write $n = k\lambda$. In this case, the matrix S at each site of the chain lies neither in $\mathbb{C}P^{n-1}$ nor $SU(n)/[U(1)]^{n-1}$. While it would be straightforward to derive other families of flag manifold sigma models from these representations, we are only interested in those with target space $SU(n)/[U(1)]^{n-1}$, as these models have been shown to exhibit an 't Hooft anomaly in certain cases. Thus, some care must be taken in order to realize the appropriate degrees of freedom. As before, we begin with an example, this time with $k = 2$ in $SU(4)$. This requires choosing four colours for four nodes in order to minimize the $\text{tr}[S(j)S(j+1)]$ term, which is easily done. For example:

However, such a configuration does not lead to the manifold $SU(n)/[U(1)]^{n-1}$, because the four colours do not behave like four orthogonal $\mathbb{C}P^3$ fields. Indeed, at each site, we may additionally rotate the two colours into each other at no energy cost, which corresponds to another type of zero mode. In order to achieve the correct flag manifold, we "freeze out" these additional degrees of freedom by adding a weaker second-neighbour interaction, $\text{tr}[S(j)S(j+2)]$. The effect of this term is to invoke a "reverse-ordering" pattern between sites and their second-neighbours. The new ground state is

The fact that this ground state minimizes the combined $J_1\text{tr}[S(j)S(j+1)]+J_2\text{tr}[S(j+1)S(j+2)]$ term (for antiferromagnetic couplings $J_1 \gg J_2$) follows from the identity $p_1^2 + p_2^2 \geq 2p_1p_2$. In a sense, this second-neighbour interaction generates the same behaviour that we saw in the previous case of $k = n - 1$: The nearest-neighbour term partitions the colours into subsets, and the second-neighbour term reverse-orders these subsets, effectively breaking the additional on-site rotation symmetry between colours. In the $k = n - 1$ case, both of these steps are achieved by the same interaction term: first the colours are partitioned into 3 sets: e.g. {●}, {●}, {●, ○, ○}, and then each set is reverse-ordered compared to the previous time it occurred. It will turn out that this reverse-ordering is a generic feature of all the representations that we consider.

As a next step, we extend from 4 to general even n, and consider $k = \frac{n}{2}$. A nearest-neighbour interaction will again serve to partition the colours into two sets, leaving a local rotation symmetry among the k colours on each site. In order to freeze out these degrees of freedom, we again add a second-neighbour interaction, which reverse-orders each set. For example, in $SU(6)$ we have

Clearly, the ground state will always have a 4-site unit cell for $k = \frac{n}{2}$.

Now, when $k < \frac{n}{2}$, the full set of colours is no longer used up when the nodes on two neighbouring sites are filled. As a result, additional zero modes are present that cannot be removed by reverse-ordering the colours within a set. To resolve this, we first add up to $(\lambda - 1)$-neighbour interactions (always with antiferromagnetic couplings), to properly partition the full set of n colours into λ sets of k elements ($\lambda := \frac{n}{k}$). Then, we add a weaker λ-neighbour interaction which serves to reverse-order within each set of the partition. For example, in SU(6) with $k = 2$, the Hamiltonian we should consider is

$$H = \sum_j \left(J_1 \text{tr}[S(j)S(j+1)] + J_2 \text{tr}[S(j)S(j+2)] + J_3 \text{tr}[S(j)S(j+3)] \right), \qquad (3.20)$$

with $J_1 > J_2 \gg J_3 > 0$, which has, for example, the following ground state:
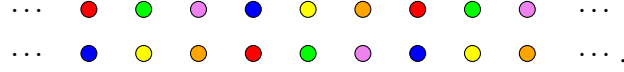
The J_1 and J_2 terms serve to partition the colours into three sets: $\{●,●\}, \{●,○\}, \{○,○\}$, and the J_3 terms serve to reverse-order within each of these three sets. Based off of this example, we can see that the unit cell has size 2λ for these representations.

3.4.3 Remaining representations

Finally, we consider all remaining values of k (the number of nonzero rows in the Young tableau). Let $c = n \bmod k$, so that $n = \lambda k + c$ for some $\lambda \in \mathbb{Z}$. As in the previous case of $n = k\lambda$, local zero modes will be present unless sufficiently long-range interactions are included to use up all of the available colours. We add up to λ-neighbour terms, which partitions the colours into λ sets of k elements, and one set of c elements. Briefly, we return to the notation $\boldsymbol{\varphi}^\alpha$ for the basis vectors instead of coloured nodes. Then, a possible partitioning of the colours is:

$$\{\boldsymbol{\varphi}^1, \ldots, \boldsymbol{\varphi}^k\}, \{\boldsymbol{\varphi}^{k+1}, \ldots, \boldsymbol{\varphi}^{2k}\}, \ldots, \{\boldsymbol{\varphi}^{(\lambda-1)k+1}, \ldots, \boldsymbol{\varphi}^{\lambda k}\}, \{\boldsymbol{\varphi}^{\lambda k+1}, \ldots, \boldsymbol{\varphi}^{\lambda k+c}\}. \qquad (3.21)$$

Now, in order to minimize the interaction term $\text{tr}[S(j)S(j+\lambda)]$, the remaining nodes on the $(\lambda+1)$th site will be the reverse-ordered set $\{\boldsymbol{\varphi}^k, \boldsymbol{\varphi}^{k-1}, \ldots, \boldsymbol{\varphi}^{c+1}\}$. For example, in SU(7) with $k = 3$, three consecutive sites may look like
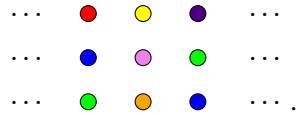
The nodes of the next site (which is a $(\lambda + 1)$th neighbour), will then begin to be filled with the remaining $\{\boldsymbol{\varphi}^1, \ldots, \boldsymbol{\varphi}^c\}$ colours from the first site. In our present SU(7) example, this looks like:

$$\cdots \quad \bullet \quad \circ \quad \bullet \quad \bullet \quad \circ \quad \bullet \quad \cdots \tag{3.22}$$

Since $c = 1$ in this example, the drawn ground state is stable. However for $c > 1$, there will still be zero modes associated with rotating among the set $\{\boldsymbol{\varphi}^1, \ldots, \boldsymbol{\varphi}^k\}$. Thus, an additional $(\lambda + 1)$-neighbour interaction must also be added! The following ground state for SU(5) with $k = 3$ demonstrates this:

$$\cdots \quad \bullet \quad \circ \quad \bullet \quad \circ \quad \cdots \tag{3.23}$$

Thus, we are led to the following conclusion for this class of representations: If $c = 1$, our Hamiltonians should contain up to λ-neighbour interactions, and if $c > 1$, we should also add an additional $(\lambda + 1)$-neighbour interaction term.

Using the emerging patterns in the previous examples as a guide, we may now determine the unit cell size for the most general representation. This quantity is very important, as it determines the translation group symmetry that is present in the flag manifold sigma model. Note that in both (3.22) and (3.23), there are two competing types of order among the coloured nodes. The first c rows exhibit one type of order, which has periodicity $\lambda + 1$ when $c = 1$, and $2(\lambda + 1)$ otherwise. Meanwhile, the remaining $k - c$ rows have a periodicity 2λ for all c except $c = k - 1$, in which case the periodicity is λ. In order to determine the overall unit cell length, we must find the least common multiple of these two periodicities. For example, in our SU(7) example, we see that the unit cell will have length 12, leading to a $\mathbb{Z}_{12}$ symmetry in the field theory. This can be seen in Figure 3.5.

3.4.4 Summary of classification

In Table 3.1, we summarize our results from the previous subsections. In the first column, we specify the number of nonzero rows in the Young tableau, k, and the integer $c := n \bmod k$. In the second column, we write down the longest-range interaction that must be included in the Hamiltonian in order to eliminate any local zero modes. As always, it is understood that each interaction term is $J_r \mathrm{tr}[S(j)S(j + r)]$ for some coupling $J_r > 0$, and that $J_r > J_s$ for $r < s$. Finally, in the third column, we specify the order d of the translation group $\mathbb{Z}_d$ that acts on the corresponding flag manifold sigma model. This order equals the size of the unit cell in the classical ground states of the Hamiltonian. In the final column of the table, the following identities are useful:

$$\mathrm{lcm}[2\lambda, (\lambda + 1)] = \begin{cases} \lambda(\lambda + 1) & \lambda \text{ is odd} \\ 2\lambda(\lambda + 1) & \lambda \text{ is even} \end{cases} \tag{3.24}$$

31
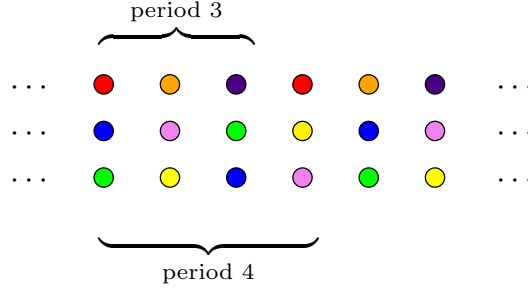
Figure 3.5: Potential ground state of an SU(7) chain. Since the first row has 3-site periodicity, and the remaining rows have 4-site periodicity, the unit cell is 12 sites in length.

$$\text{lcm}[\lambda, 2(\lambda + 1)] = \begin{cases} 2\lambda(\lambda + 1) & \lambda \text{ is odd} \\ \lambda(\lambda + 1) & \lambda \text{ is even} \end{cases} \tag{3.25}$$

Representation		Longest Interaction	Translation Group Order
$k = 1$		$J_{n-1}\text{tr}[S(j)S(j + n - 1)]$	n
$k = n - 1$		$J_1\text{tr}[S(j)S(j + 1)]$	2
$k = \frac{n}{\lambda},$	$\lambda < n$	$J_\lambda\text{tr}[S(j)S(j + \lambda)]$	2λ
$n = 2\lambda + 1,$	$k = 2$	$J_\lambda\text{tr}[S(j)S(j + \lambda)]$	$\lambda(\lambda + 1)$
$n = k\lambda + 1,$	$\lambda > 1, k > 2$	$J_\lambda\text{tr}[S(j)S(j + \lambda)]$	$\text{lcm}[2\lambda, (\lambda + 1)]$
$n = k\lambda + c,$	$c \neq 1, k - 1$	$J_{\lambda+1}\text{tr}[S(j)S(j + \lambda + 1)]$	$2\lambda(\lambda + 1)$
$n = k\lambda + (k - 1)$		$J_{\lambda+1}\text{tr}[S(j)S(j + \lambda + 1)]$	$\text{lcm}[\lambda, 2(\lambda + 1)]$

Table 3.1: Classification results of all SU(n) representations satisfying $p_\alpha \neq p_\beta$ for all nonzero p_α. We use the notation $\text{lcm}[a, b]$ to denote the least common multiple of a and b.

3.5 Exact Results for SU(n) Chains

In this final section, we now review various exact results that are known for the SU(n) Hamiltonians considered above. These exact results will prove to be especially useful when we attempt to generalize the Haldane conjecture to certain SU(n) chains in later chapters.

3.5.1 Integrable SU(n) chains and SU(n)$_k$ critical points

Let us begin our discussion with the simplest representation of SU(n): the fundamental representation whose Young tableau consists of a single box. While this is a special case of the symmetric models discussed above, we do not need to consider longer-range interactions, since in this case, the model is exactly solvable. This was first realized by Sutherland [84], who used the Bethe ansatz to find the exact spectrum of the $p = 1$ SU(n) chain, and show that it was gapless. Later, it was discovered that the low energy degrees of freedom of this chain correspond to the SU(n)$_1$ WZW model [50, 85, 110]. This generalizes the SU(2) result of Bethe that was mentioned in Chapter 2: The low energy spectrum is gapless, with $n - 1$ relativistic bosons propagating with velocity $v = 2\pi J/n$ [83, 84].

In order to understand this result, we may rewrite the nearest-neighbour SU(n) Hamiltonian in terms of fermion operators. To this end, we introduce n flavours of fermion ψ_α and rewrite the matrices S of SU(n) generators according to

$$S_{\alpha\beta}(j) = \psi_\beta^\dagger(j)\psi_\alpha(j). \tag{3.26}$$

There is only one independent Casimir constraint for the $p = 1$ model, $\text{tr}[S^2]$, which in the fermion language, corresponds to the condition of 1 particle on each site:

$$\psi_\alpha^\dagger(j)\psi_\alpha(j) = 1. \tag{3.27}$$

The nearest-neighbour Hamiltonian becomes a simple exchange term:

$$\mathcal{H} = J \sum_j \psi_\beta^\dagger(j)\psi_\alpha(j)\psi_\alpha^\dagger(j+1)\psi_\beta(j+1). \tag{3.28}$$

As in SU(2), we may obtain this model from an SU(n) Hubbard model,

$$H = \sum_j \left(-t[\psi_\alpha^\dagger(j)\psi_\alpha(j+1) + h.c.] + U[\psi_\alpha^\dagger(j)\psi_\alpha(j) - 1]^2 \right) \tag{3.29}$$

, in the limit $U/t \gg 1$. Starting at small U, we may take the continuum limit, giving n flavours of relativistic Dirac fermion. Next, by using non-abelian bosonization, we obtain a charge boson plus the SU(n)$_1$ WZW model. The Hubbard interactions can be seen to gap the charge boson without affecting the low energy behaviour in the spin sector, yielding the SU(n)$_1$ WZW model as the low energy effective theory [86].

It is worth mentioning that without any additional symmetries, the SU(n)$_1$ model is actual unstable, due to the relevant operator tr[g], for WZW field $g \in$ U(n). However, for the SU(n) chains presently discussed, at low energies there is an additional discrete symmetry, $\mathbb{Z}_n$, whose action on g is

$$g \mapsto e^{\frac{2\pi i}{n}} g, \tag{3.30}$$

and forbids the term tr[g]. In our longer-range models, a similar symmetry also emerges, as we will see in the following chapters. There, it will be a manifestation of the underlying translation

symmetry on the chain. Thus, the results in Table 3.1 should be quite suggestive of how Haldane's conjecture should be extended to SU(n).

For larger p, there exist integrable SU(n) models that can also be solved exactly [87–89]. These models have more complicated nearest-neighbour interactions, and have been shown to correspond to the SU(n)$_p$ WZW models at low energies [50, 68, 111]. Again, we can understand this from non-abelian bosonization. In this case we must introduce fermions with p colours as well as n flavours, and write a generalized Hubbard model. Non-abelian bosonization now gives the SU(n)$_p$ WZW model in the flavour sector, together with a charge boson and an SU(p)$_n$ WZW model for the colour degrees of freedom. However it is now seen that the Hubbard interactions will generally gap the flavour sector as well as the charge and colour sector, unless the interactions are fine-tuned. This can be understood from the fact that the SU(n)$_p$ WZW models contain relevant operators allowed by symmetry for all $p > 1$, which are expected to appear in the Hamiltonian and destabilize the critical theory. We understand the fine-tuned nature of the Bethe ansatz integrable models as, remarkably, corresponding to fine-tuning of the field theory to eliminate all relevant operators.

In Section 2.3.2, we explained how the gapless phase predicted by Haldane in half-odd integer spin chains is characterized by the SU(n)$_1$ WZW model. We can now better explain why this is the case. For arbitrary s, the spin chain may be mapped to the SU(2)$_k$ WZW model, with level $k = 2s$ [112, 113]. As mentioned above, these models will generically contain relevant operators (unless they are fine-tuned, corresponding to the integrable models). Thus, under renormalization, we expect the SU(2) chain to be described by some other, *stable* critical theory. With the added $\mathbb{Z}_2$ symmetry arising from a 2-site unit cell, the only candidate theory is SU(2)$_1$. Thus, if a gapless phase is to occur in the spin chain, we predict it will be characterized by this 'attractor' theory. This is consistent with the Zamolodchikov c-theorem, which requires that k be a nonincreasing function of energy scale [114].

Now, the obvious question is how to generalize this mechanism to SU(n). As hinted above, when the $\mathbb{Z}_n$ symmetry (3.30) is present, the SU(n)$_1$ WZW model is stable. In fact, it is the only stable WZW model with SU(n) symmetry [78, 79]. For instance, the primary operator transforming under the adjoint representation of $\mathfrak{su}(n)$ is a relevant operator in all levels $k > 1$. Therefore, one might reasonably conclude that whenever an SU(n) chain can be mapped to an SU(n)$_k$ critical theory, it will flow to SU(n)$_1$ at low energies. Unfortunately, the flow from $k \mapsto k' < k$ is actually quite subtle for general n, and is related to the concept of 't Hooft anomaly matching [115, 116]. We will return to this issue in the following two chapters.

Let us conclude this subsection by making a distinction between the low energy sigma models that we seek in this thesis, and the Bethe ansatz integrable models mentioned above. Like Haldane, our motivation is to predict gapless phases only at weak coupling, which lies outside the strong-coupling regime of the integrable models. Thus, it is not appropriate to view our models as a perturbation of the integrable ones, if we want to make any weak coupling predictions. However, this is not to say that we aren't interested in what happens when we add relevant operators to SU(n)$_k$ for $k > 1$. For example, the operator $|\text{tr}[g]|^2$ is a relevant perturbation for $k > 1$ and may lead to a symmetry broken phase. However, we believe that this mechanism relies crucially on the sign of the coupling constant in front of this term, and the gapped broken symmetry phase only occurs

when this constant is negative. When it is positive, we instead expect a massless RG flow to $SU(n)_1$ (so long as the other constraints on the flow of k do not apply). Note that both of these scenarios are consistent with the LSMA theorem (reviewed below), and are present in the SU(2) phase diagram Figure 2.1. This issue is discussed in detail by Affleck and Haldane in [86].

3.5.2   The Lieb-Schultz-Mattis-Affleck theorem

The Lieb-Schultz-Mattis-Affleck theorem (LSMA) is a rigorous statement about ground states in translationally invariant SU(n) Hamiltonians [80, 81]. It claims that if the number of boxes p in a Young tableau is not a multiple of n, then either the ground state is unique with gapless excitations, or there is a ground state degeneracy. Recently, it was claimed in [67] that the LSMA theorem is not applicable to models with longer-range interactions than nearest-neighbour. Here, we dispute this claim by extending the original proof in [81] to models with further-range interactions. Explicitly, we consider the following Hamiltonian on a ring of L sites:

$$H = \sum_{r=1}^{R} H_r \qquad H_r := \sum_{j=1}^{L} J_r \mathrm{tr}[S(j)S(j+r)] \tag{3.31}$$

where S is defined as above. We assume that $|\psi\rangle$ is the unique ground state of H, and is translationally invariant: $T|\psi\rangle = |\psi\rangle$. We then define a twist operator

$$U = e^A \qquad A := \frac{2\pi i}{nL} \sum_{j=1}^{L} jQ(j) \tag{3.32}$$

with

$$Q = \sum_{\alpha=1}^{n-1} S_{\alpha\alpha} - (n-1)S_{nn} = \mathrm{tr}S - nS_{nn} = p - nS_{nn}. \tag{3.33}$$

Note that A is a Hermitian operator. Here $p = \sum_\alpha p_\alpha$ is the total number of boxes occurring in the Young tableau. Using the commutation relations (3.1), it is easy to verify that

$$\left[\mathrm{tr}[S(j)S(j+r)], Q(j) + Q(j+r)\right] = 0, \tag{3.34}$$

which then implies

$$U^\dagger \mathrm{tr}[S(j)S(j+r)]U = e^{-\frac{r\pi i}{nL}(Q(j+r)-Q(j))} \mathrm{tr}[S(j)S(j+r)] e^{\frac{r\pi i}{nL}(Q(j+r)-Q(j))}. \tag{3.35}$$

Using this, one can show that

$$U^\dagger HU - U = [H, A] - H + O(L^{-1}) \tag{3.36}$$

so that $U|\psi\rangle$ has energy $O(L^{-1})$. Now, using the translational invariance of $|\psi\rangle$, we find

$$\langle\psi|U|\psi\rangle = \langle\psi|T^{-t}UT|\psi\rangle = \langle\psi|Ue^{\frac{2\pi i}{n}Q(1)}e^{-\frac{2\pi i}{nL}\sum_{j=1}^{L}Q(j)}|\psi\rangle. \tag{3.37}$$

Since $|\psi\rangle$ is a ground state of H, it is an SU(n) singlet, and so must be left unchanged by the global SU(n) transformation $e^{-\frac{2\pi i}{nL}\sum_{j=1}^{L} Q(j)}$. Moreover, using (3.33), we have

$$\langle\psi|U|\psi\rangle = e^{\frac{2\pi i p}{n}} \langle\psi|U e^{2\pi i S_{nn}}|\psi\rangle. \tag{3.38}$$

In Chapter 2, we saw that the matrices S could be written in terms of Schwinger bosons. This is true for all n, as we will see in Chapters 4 and 5 when we discuss flavour-wave theory. The diagonal elements S_{nn} always correspond to number operators for these bosons. Thus, S_{nn} acting on $|\psi\rangle$ will always return an integer, and $e^{2\pi i S_{nn}}$ can be dropped. Thus, we find that so long as p is not a multiple of n,

$$\langle\psi|U|\psi\rangle = 0, \tag{3.39}$$

implying that $U|\psi\rangle$ is a distinct, low-lying state above $|\psi\rangle$. This completes the proof. Finally, we may also comment on the ground state degeneracy in the event that a gap exists above the ground state. Through the repeated application of (3.38), we have

$$\langle\psi|U^k|\psi\rangle = e^{\frac{2\pi i p k}{n}} \langle\psi|U|\psi\rangle. \tag{3.40}$$

So long as $k < r := n/\gcd(n, p)$, the family $\{U^k|\psi\rangle\}$ is an orthogonal set of low-lying states. If an energy gap is present, this suggests that the ground state is at least r-fold degenerate. In the following subsection, we introduce valence bond solids that exhibit translation invariance when p is a multiple of n. It is easy to see that when $1 < \gcd(n, p) < n$, these constructions lead to explicit r-fold degeneracies, consistent with our findings here. For example, the symmetric representation of SU(4) with $p = 2$ leads to 2 distinct valence bond solids that are both invariant under translation by 2 sites.

3.5.3 Affleck-Kennedy-Lieb-Tasaki models

In Chapter 2, we introduced the AKLT model as an important theoretical result that served to bolster Haldane's conjecture in its infancy. This is because it exhibits a unique, translationally invariant ground state with a finite excitation gap for a spin-1 chain. Note that this does not violate the LSMA theorem since a spin-1 chain has a corresponding Young tableau with $2 = n$ boxes. Recently, the AKLT construction has been generalized by various research groups to SU(n) chains [61, 67, 69, 74–76, 83, 117]. In particular, symmetric representation AKLT Hamiltonians have been constructed whenever p is a multiple of n [67]. Again, this is precisely when the LSMA theorem does not apply. These Hamiltonians exhibit a unique, translationally invariant ground state, and are constructed by forming SU(n) singlets from n fundamental representations on adjacent sites. Since p is a multiple of n, this may be done in a translationally invariant manner, by shifting the left-most site of the singlet along the chain as one cycles through the p (symmetrized) fundamentals at each site of the chain. See Figure 3.6 for the case of $n = p = 3$. This picture can be understood as follows. If we denote by α_j^a a fundamental representation of SU(3) at site j, then at each site we have

$$|\alpha_j^1, \alpha_j^2, \alpha_j^3\rangle, \tag{3.41}$$

which is symmetric under permutation of its entries (by definition). By considering three adjacent sites, we may construct an SU(3) singlet out of three of these entries:

$$\epsilon_{\alpha_j^1 \alpha_{j+1}^2} \alpha_{j+2}^3 |\alpha_j^1, \alpha_j^a, \alpha_j^b\rangle |\alpha_{j+1}^2, \alpha_{j+1}^c, \alpha_{j+1}^d\rangle |\alpha_{j+2}^3, \alpha_{j+2}^e, \alpha_{j+2}^f\rangle. \tag{3.42}$$

Here ϵ_{ab} is the antisymmetric unit tensor with $\epsilon_{01} = -\epsilon_{10} = 1$. The remaining free representations $\alpha_j^a, \ldots, \alpha_{j+2}^e$ are similarly combined with adjacent sites, eventually creating an SU(3) singlet out of the entire chain.
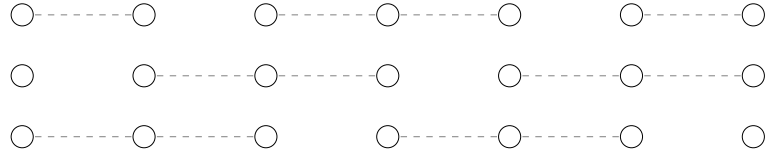
Figure 3.6: AKLT state for an SU(3) chain in the symmetric representation with $p = 3$. Singlets are formed from three consecutive sites.

Note that when n is not prime, similar valence bond solids may be constructed that are consistent with a nontrivial result from the LSMA theorem. That is, for p not a multiple of n, with $r := n/\gcd(n, p)$, Hamiltonians may be constructed with r-fold degenerate ground states that are invariant under translations by r sites. In Figure 3.7, we provide an example of two-fold degenerate ground states in SU(4). All of these models have short range correlations, and are expected to have gapped ground states, based on arguments of spinon confinement [67].
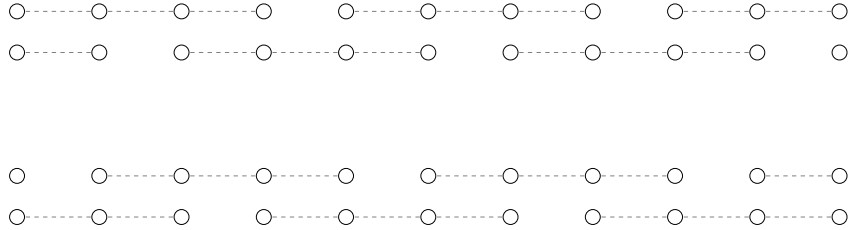
Figure 3.7: Two-fold degenerate AKLT states for an SU(4) chain in the symmetric representation with $p = 2$.

Another generalization of AKLT models is possible for self-conjugate representations of SU(n). We will make use of this fact explicitly in Section 4.7, when we discuss self-conjugate SU(3) chains. Recall that such representations are labeled by a single integer $p > 0$, and have a Young

tableau of the form

$$\tag{3.43}$$

For all p, we may write down a translationally invariant valence bond state. This is done by forming SU(3) singlets at each site, by pairing each fundamental representation with an adjacent antifundamental representation. For example, in the adjoint representation of SU(3) with $p = 1$, at each site we have

$$|\alpha_j^1, \alpha_j^2; \alpha_j^3\rangle \tag{3.44}$$

which is antisymmetric across the ';' symbol. Then a singlet bond between sites j and $j + 1$ is constructed as follows:

$$\epsilon_{\alpha_j^1, \alpha_{j+1}^2, \alpha_{j+1}^3} |\alpha_j^1, \alpha_j^a; \alpha_j^b\rangle |\alpha_{j+1}^c, \alpha_{j+1}^2; \alpha_{j+1}^3\rangle. \tag{3.45}$$

This is shown in Figure 3.8. Here and throughout, objects appearing within the same column are symmetrized, and two nodes that appear close together in the same row are antisymmetrized. Dashed lines denote singlet bonds, as before.

Figure 3.8: AKLT state for an SU(3) chain in the self-conjugate representation with $p = 1$. This state spontanesouly breaks parity symmetry.

However, only when p is even is this ground state also invariant under a $\mathbb{Z}_2$ parity symmetry, which corresponds to a mirror reflection about the center of a bond between two sites of the chain. This is demonstrated in Figure 3.9 for the case of $p = 2$. Similar constructions exist for all n.

Figure 3.9: AKLT state for an SU(3) chain in the self-conjugate representation with $p = 2$. This state is invariant under parity symmetry.

Finally, there is one more version of AKLT model that we will discuss in this thesis. In Chapter 6, we will be led to SU(n) representations whose Young tableaux have two rows, with lengths

p_1, p_2 satisfying $p_1 \neq p_2 \neq 0$. We note here that when $p_1 + p_2 = n$, it is straightforward to write down a translationally invariant AKLT state. Indeed, we may construct a singlet over p_1 consecutive sites using $(p_1 - p_2)$ fundamentals and p_2 antisymmetric doublets. Since each site has p_1 representations (either fundamentals or doublets), we may shift the singlet by one site as we move down the rows of the valence bond solid. Note that the self-conjugate SU(3) AKLT model is a special case of this more general construction.

As a new example, let us explain this construction in greater detail for the case of SU(4), with $p_1 = 3$ and $p_2 = 1$. We denote by α_j^a a fundamental representation of SU(4) at site j. Then on each site of the chain, we have the representation

$$|\alpha_j^1, \alpha_j^2, \alpha_j^3; \alpha_j^4\rangle, \tag{3.46}$$

which is symmetric under permutations of the first three entries, and antisymmetric under exchanges with the fourth entry. For instance,

$$|\alpha_j^1, \alpha_j^2, \alpha_j^3; \alpha_j^4\rangle = |\alpha_j^2, \alpha_j^1, \alpha_j^3; \alpha_j^4\rangle = |\alpha_j^2, \alpha_j^3, \alpha_j^1; \alpha_j^4\rangle,$$
$$|\alpha_j^1, \alpha_j^2, \alpha_j^4; \alpha_j^3\rangle = -|\alpha_j^1, \alpha_j^2, \alpha_j^3; \alpha_j^4\rangle = -|\alpha_j^1, \alpha_j^4, \alpha_j^3; \alpha_j^2\rangle.$$

Using two fundamental representations α_j^a, and one antisymmetric doublet representation
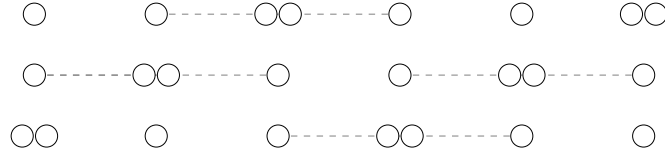
Figure 3.10: AKLT state for an SU(4) chain with $p_1 = 3$ and $p_2 = 1$. Singlets are formed from three consecutive sites, using two fundamentals and one antisymmetric doublet.

$|\alpha_j^a; \alpha_j^b\rangle = -|\alpha_j^b; \alpha_j^a\rangle$, we may contract indices to form a singlet across three sites according to

$$\epsilon_{\alpha_j^1 \alpha_{j+1}^2 \alpha_{j+1}^3 \alpha_{j+2}^4} |\alpha_j^a, \alpha_j^1, \alpha_j^b; \alpha_j^c\rangle |\alpha_{j+1}^d, \alpha_{j+1}^e, \alpha_{j+1}^2; \alpha_{j+1}^3\rangle |\alpha_{j+2}^4, \alpha_{j+2}^f, \alpha_{j+2}^g; \alpha_{j+2}^h\rangle. \tag{3.47}$$

The remaining free representations $\alpha_j^a, \ldots, \alpha_{j+2}^h$ are then contracted into different singlet bonds, over different sets of three sites. By using the pattern shown in Figure 3.10, a translationally invariant valence bond solid can be constructed, that is also parity symmetric. In fact, for general even n, we may always choose a p_1-site singlet bond that is symmetric under parity, leading to a parity-symmetric AKLT state. See Figure 3.11a and Figure 3.11b for two additional examples in SU(6).
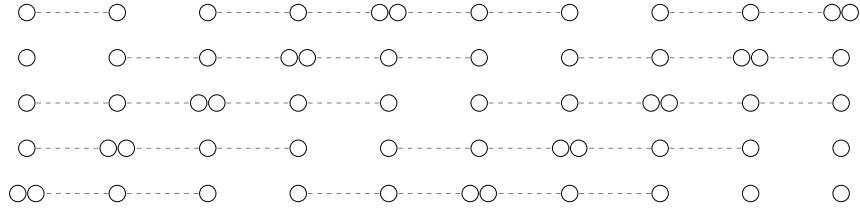
(a) AKLT state for an SU(6) chain with $p_1 = 5$ and $p_2 = 1$. Singlets are formed from five consecutive sites, using four fundamentals and one antisymmetric doublet.
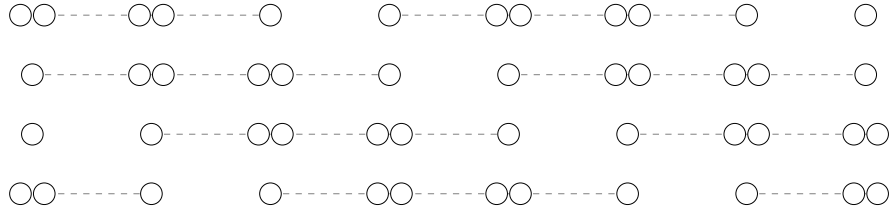
(b) AKLT state for an SU(6) chain with $p_1 = 4$ and $p_2 = 2$. Singlets are formed from four consecutive sites, using two fundamentals (single circles), and two antisymmetric doublet (double circle).

3.6 Conclusion

We began this chapter by motivating the study of SU(n) chains as a natural extension to the familiar Heisenberg model. Thanks to recent advances in cold atom experimentation, what started out as a purely theoretical study has since developed into an exciting cross-disciplinary effort. Indeed, SU(n) chains now garner interest from condensed matter physicists, cold atom physicists, and even theoretical high energy physicists.

We first introduced the SU(n) Hamiltonian, and the $n \times n$ matrices of operators, S. Then, by reviewing the representation theory of SU(n), we were able to relate Young tableaux to the eigenvalues of S, and ultimately to a classical Hamiltonian. Then, in exhaustive detail, we considered all of the possible ways of realizing a particular quantum field theory, the SU(n)/[U(1)]$^{n-1}$ flag manifold sigma model, by adding sufficiently long-range interactions to the Hamiltonian in order to stabilize zero mode fluctuations. The results of this classification are presented in Table 3.1. Then, in Section 3.5, we proceeded to review various exact results that exist for SU(n) Hamiltonians, namely the LSMA theorem, the AKLT construction, and the Bethe-ansatz integrable SU(n) models. We also hinted at the renormalization flow of these SU(n) theories; this subject will treated more thoroughly later on.

With this groundwork in place, we would now like to focus in more detail on particular representations of SU(n). Admittedly, this chapter has been quite abstract, and quite removed from our

ultimate goal of obtaining an SU(n)-version of the Haldane conjecture. In the following chapter, we turn to SU(3) chains, and connect back to this overarching goal. The results of this chapter will prove to be useful here, so that the appropriate Hamiltonian can be used, depending on which SU(3) chain we consider. However, we will also draw on ideas from Chapter 2; in particular, we will attempt to follow the prescription outlined in Section 2.5. This will lead to unexpected challenges, including the absence of Lorentz invariance, and also the presence of pure-imaginary, yet non-topological terms in the sigma model.

Chapter 4

SU(3) Chains

4.1 Introduction

In the previous chapter, we introduced SU(n) chains in full generality, and discussed how their classical ground states, and consequently their underlying symmetries, depended on the chosen SU(n) representation at each site. An important realization was that longer-range interaction terms are necessary to include in the SU(n) Heisenberg Hamiltonian in order to stabilize local zero modes that are present due to the larger symmetry available.

At this point, we are now prepared to derive our first mapping between SU(n) chain and quantum field theory, and ultimately arrive at a generalization of Haldane's conjecture. As will become clear quite shortly, this is by no means a trivial task, and will require us to develop substantial renormalization group results in order to arrive at any meaningful conclusion. As such, we restrict in this chapter to the simplest extension possible; namely, we consider SU(3) chains in the totally symmetric representations. According to the classification in Table 3.1, these chains require both first and second-neighbour interactions in their Hamiltonian. Therefore, the model that we consider in this chapter is

$$H = \sum_j (J_1 \text{tr}[S(j)S(j+1)] + J_2 \text{tr}[S(j)S(j+1)]). \tag{4.1}$$

As always, we take $J_1, J_2 > 0$. Each matrix S transforms under the symmetric representation, labeled by p, which corresponds to the length of the single row in a Young tableau:

$$\tag{4.2}$$

Later on, we will comment on the remaining representations of SU(3), and explain how our results can be extended to the self-conjugate representations of SU(3), with two-row Young tableaux.

For the most part, this chapter will follow the outline presented in Section 2.5. We will begin with extending the familiar theory of spin-waves to SU(3), and derive the predicted velocities of such low-lying excitations. As mentioned in Chapter 2, despite the lack of spontaneous symmetry breaking in one spatial dimension, this perturbative treatment still serves its purpose; in particular, we will use this so-called flavour-wave theory to verify the absence of zero-mode excitations when second-neighbour interactions are added to the SU(3) Heisenberg Hamiltonian. Next, in Section 4.3, we derive the SU(3)/[U(1)]^2 sigma model description of the symmetric SU(3) chain in great detail. Our approach will be generalized in Chapter 5 to all $n > 3$, and so we make sure to be

very explicit in our calculations. Following this, we turn to our renormalization group (RG) calculations in Section 4.5. Since this is the first appearance of RG technology in this thesis, we offer a brief introduction to the subject, before turning to the flag manifold sigma model in particular. In Section 4.6, we discuss the implications of these RG results, and present a phase diagram of the SU(3) chain, which generalizes the SU(2) story in Figure 2.1. This phase diagram is supported by the various exact results that we mentioned in the previous chapter, and we recall them here. The phase diagram is also supported by a strong coupling analysis, and some Monte Carlo simulations, which we review. At this stage, we are able to formulate our SU(3) version of Haldane's conjecture for symmetric chains. Finally, we finish this chapter by turning to the remaining representations of SU(3) in Section 4.7.

The above work on symmetric SU(3) chains was published in 2017 in [1]. Section 4.7 was published in [2]. Preceding our papers, Greiter and Rachel considered symmetric SU(n) chains in [67], which was published in 2007. By constructing valence bond solids, à la AKLT, they predicted a finite energy gap for those representations whose row length p is a multiple of 3. The result that we obtain will be consistent with this prediction. Similar results followed [61, 69, 74]. Furthermore, in 2012, Bykov established in two separate papers the first correspondence between the symmetric SU(3) chains and the SU(3)/[U(1)]^2 flag manifold sigma model [71, 72]. We were not aware of Bykov's contribution at the time of our research, and as such there is a large overlap between his calculations and our derivation in Section 4.3. However, the remaining sections of this chapter, including the extensive renormalization group calculations in Section 4.5, are entirely novel. Finally, it is worth noting that various numerical studies have been carried out on the symmetric SU(3) chains, with contradicting predictions [70, 118–120]. However, these results were recently surveyed in [77], and these contradictions are now better understood. This publication also presented the most convincing results to date, using the density matrix renormalization group to study the symmetric SU(3) chain with $p = 3$. Their findings are in complete accord with our generalized Haldane conjecture, namely that a finite energy gap exists in this representation.

4.2 Flavour-Wave Theory

According to Coleman's theorem [8], we do not expect spontaneous symmetry breaking of the SU(3) symmetry in the exact ground state of our Hamiltonian. Nonetheless, we may still expand about the classical (symmetry broken) ground state to predict the Goldstone mode velocities. If the theory is asymptotically free (as in SU(2)), then at sufficiently high energies the excitations may propagate with these velocities. In the familiar antiferromagnet, this procedure is known as spin-wave theory; in SU(n) it is called flavour-wave theory [121, 122].

To begin, we rewrite the Hamiltonian (4.1) in terms of Schwinger bosons with three flavours. The generators at site j can be written as

$$S_{\alpha\beta}(j) = b_\beta^\dagger(j)b_\alpha(j) \tag{4.3}$$

and the local Hilbert spaces are defined by putting p bosons at each site, i.e. by the Casimir

constraint

$$\sum_\alpha b_\alpha^\dagger(j)b_\alpha(j) = p. \tag{4.4}$$

The resulting Hamiltonian is quartic in bosonic operators:

$$H = \sum_j \left(J_1 b_\beta^\dagger(j)b_\alpha(j)b_\alpha^\dagger(j+1)b_\beta(j+1) + J_2 b_\beta^\dagger(j)b_\alpha(j)b_\alpha^\dagger(j+2)b_\beta(j+2) \right). \tag{4.5}$$

As in SU(2), we proceed by identifying a classical ground state which corresponds to a true ground state of (4.1) in the limit $p \to \infty$. It is a product wave function in which, at each site, all bosons are in the same state. Note that if J_2 were zero, there would be an infinite degeneracy of potential states, and it would not be clear around which state the quantum fluctuations should be introduced. Moreover, this degeneracy would lead to local zero modes with vanishing velocity.

The introduction of J_2 resolves these issues and imposes a 3-site structure for the reference state.[18] As mentioned previously, this 3-site structure is consistent with the $p = 1$ Bethe ansatz solution [12, 84, 85], and has been shown to be the state with minimal zero point fluctuations for large p [109]. We view J_2 as originating from quantum fluctuations in the nearest-neighbour model, and accordingly, we will apply our conclusions about (4.1) to the nearest-neighbour model without hesitation. Unfortunately, the exact mechanism by which J_2 is generated is not yet understood, and we cannot express J_2 as a function of J_1; however, on general grounds we at least know that it should be suppressed by a factor of p^{-1}.

Since we have 3 bosons for each of the 3 sites, we have actually introduced 9 bosonic operators. To emphasize this, we introduce the following notation:

$$j_\alpha := 3j + (\alpha - 1). \tag{4.6}$$

The classical ground state involves only 'diagonal' bosons of the type $b_\gamma(j_\gamma)$ and $b_\gamma^\dagger(j_\gamma)$. The 'off-diagonal' bosons are Holstein-Primakoff bosons, like those defined in (2.6). Flavour-wave theory allows for a small number of Holstein-Primakoff bosons at each site, captured by

$$\nu(j_\gamma) = \sum_{\alpha \neq \gamma} b_\alpha^\dagger(j_\gamma)b_\alpha(j_\gamma), \tag{4.7}$$

and writes the Hamiltonian in terms of these 6 bosons. In the large-p limit, we have $p \gg \nu(j_\gamma)$, and we can expand

$$S_{\gamma\gamma} = p - \nu(j_\gamma),$$
$$S_{\alpha\gamma}(j_\gamma) \approx \sqrt{p}\, b_\alpha^\dagger(j_\gamma),$$
$$S_{\gamma\alpha}(j_\gamma) \approx \sqrt{p}\, b_\alpha(j_\gamma),$$

---

[18]Another coupling that works is a ferromagnetic third-neighbour interaction. This was considered in [1].

to find

$$\text{tr}[S(j_\gamma)S(j_\eta)] = p\left[b_\gamma^\dagger(j_\eta)b_\gamma(j_\eta) + b_\gamma^\dagger(j_\eta)b_\eta(j_\gamma) + b_\eta^\dagger(j_\gamma)b_\gamma^\dagger(j_\eta) + b_\eta(j_\gamma)b_\gamma(j_\eta)\right] + O(p^0). \quad (4.8)$$

In terms of these degrees of freedom, the Hamiltonian (4.1) decomposes into a sum

$$H = H_{12} + H_{13} + H_{23}, \quad (4.9)$$

where $H_{\gamma\eta}$ is a Hamiltonian involving only the two boson flavours $b_\gamma(j_\eta)$ and $b_\eta(j_\gamma)$. In momentum space, this gives 3 different 2×2 matrices, each of which can be diagonalized by the same Bogoliubov transformation:

$$H_{\gamma,\gamma+1} = \text{const.} + \sum_k \omega(k) \sum_{j=1}^{2}\left(d_j^\dagger(k)d_j(k) + \frac{1}{2}\right) \quad (4.10)$$

where

$$\omega_t(k) = 2p\sqrt{J_1 J_2}\left|\sin\frac{3ka}{2}\right|. \quad (4.11)$$

Therefore, the corresponding flavour-wave velocity is

$$v = 3p\sqrt{J_1 J_2}, \quad (4.12)$$

which is equal for each of the six Goldstone bosons. Later, when we consider $\text{SU}(n)$ chains with $n > 3$, we will learn that different branches of boson will generically propagate with different velocities. This will inhibit the automatic emergence of Lorentz invariance in the corresponding flag manifold sigma models.

4.3 Derivation of the Flag Manifold Sigma Model

Having verified that a unique, nonzero Goldstone velocity exists for the $J_1 - J_2$ Heisenberg Hamiltonian in (4.1), we now derive a low energy quantum field theory description of the chain. Since the classical ground state has 3-site sublattice order, with unit vectors $\varphi^\alpha \in \mathbb{C}^n$ defined on each site (as per Chapter 3), we may define a unitary matrix U, by

$$U_{\alpha\beta} = \varphi_\beta^\alpha. \quad (4.13)$$

Throughout, a superscript index labels the vector, and a subscript index labels the component of the vector. Applying the pictorial notation from Chapter 3, we may represent the classical ground state at hand by

$$\cdots \quad \bullet \; \bullet \; \bullet \; \bullet \; \bullet \; \bullet \; \bullet \; \bullet \; \bullet \quad \cdots . \quad (4.14)$$

Since the Hamiltonian is invariant under changing the overall phase of each of the three vectors φ^α, (see (3.12)), we see that the ground state manifold is isomorphic to $\text{SU}(3)/[\text{U}(1)]^2$. Two phases

can be changed independently, later referred to as gauge symmetries, while the third phase is fixed by setting the determinant of U to 1. This manifold has 6 generators, namely the six off-diagonal Gell-Mann matrices of SU(3), which corresponds to the same amount of Goldstone bosons found in the previous flavour-wave calculations.

To describe fluctuations about the φ^α, and thus about the ground state manifold, we write:

$$\phi^\alpha = \sum_\beta \frac{1}{p} L_{\alpha\beta} \varphi^\beta + \sqrt{1 - \mu(\alpha)} \varphi^\alpha. \tag{4.15}$$

Here $L_{\alpha\alpha} = 0$ (no sum) and

$$p^2 \mu(\alpha) := \sum_\beta |L_{\alpha\beta}|^2. \tag{4.16}$$

These complex coefficients $L_{\alpha\beta}$ describe general fluctuations about the φ^α. The vectors ϕ^α are those that appear in the formula for the SU(n) matrices S in the limit of large p:

$$S_{\alpha\beta}(j_\gamma) = \phi_\alpha^{*,\gamma}(j_\gamma) \phi_\beta^\gamma(j_\gamma). \tag{4.17}$$

This is the generalization to SU(3) of (2.21). By redefining the unitary matrix U, we may take L to be Hermitian.[19] Now, by letting U and L vary uniformly from site to site, we write

$$S_{\alpha\beta}(j_\gamma) = p\phi_\alpha^{*,\gamma}(j_\gamma) \phi_\beta^\gamma(j_\gamma) = p \sum_{\delta,\sigma} \tilde{L}_{\delta\gamma}(j_\gamma) U_{\alpha\delta}^\dagger(j_\gamma) \tilde{L}_{\gamma\sigma}(j_\gamma) U_{\sigma\beta}(j_\gamma), \tag{4.18}$$

where we've defined $\tilde{L}_{\alpha\beta} = \frac{1}{p} L_{\alpha\beta}$ when $\alpha \neq \beta$, and $\tilde{L}_{\alpha\alpha} = \sqrt{1 - \mu(\alpha)}$. Explicitly, the $\tilde{L}$ matrix is

$$\tilde{L} = \frac{1}{p} \begin{pmatrix} p\sqrt{1 - \frac{1}{p^2}(|L_{12}|^2 - |L_{13}|^2)} & L_{12} & L_{13} \\ L_{12}^* & p\sqrt{1 - \frac{1}{p^2}(|L_{12}|^2 + |L_{23}|^2)} & L_3^2 \\ L_{13}^* & L_{23}^* & p\sqrt{1 - \frac{1}{p^2}(|L_{13}|^2 + |L_{23}|^2)} \end{pmatrix}. \tag{4.19}$$

The expression (4.18) can be rewritten as

$$S_{\alpha\beta}(j_\gamma) = p\tilde{L}_{\gamma\gamma}(j_\gamma) \sum_{\delta \neq \gamma} \left(\tilde{L}_{\delta\gamma}(j_\gamma) U_{\alpha\delta}^\dagger(j_\gamma) U_{\gamma\beta}(j_\gamma) + U_{\alpha\gamma}^\dagger(j_\gamma) \tilde{L}_{\gamma\delta}(j_\gamma) U_{\delta\beta}(j_\gamma) \right) \tag{4.20}$$

$$+ p\left[\tilde{L}_{\gamma\gamma}(j_\gamma)\right]^2 U_{\alpha\gamma}^\dagger(j_\gamma) U_{\gamma\beta}(j_\gamma) + p \sum_{\delta,\sigma \neq \gamma} \tilde{L}_{\delta\gamma}(j_\gamma) U_{\alpha\delta}^\dagger(j_\gamma) \tilde{L}_{\gamma\sigma}(j_\gamma) U_{\sigma\beta}(j_\gamma).$$

Using

$$\tilde{L}_{\gamma\gamma} \tilde{L}_{\delta\gamma} = \tilde{L}_{\delta\gamma} + O(p^{-2}) \tag{4.21}$$

_____

[19]The skew components of L generate unitary transformations, and can be recombined with the matrix U.

we have

$$S_{\alpha\beta}(j_\gamma) = \sum_{\delta \neq \gamma} \left(L_{\delta\gamma}(j_\gamma) U^\dagger_{\alpha\delta}(j_\gamma) U_{\gamma\beta}(j_\gamma) + U^\dagger_{\alpha\gamma}(j_\gamma) L_{\gamma\delta}(j_\gamma) U_{\delta\beta}(j_\gamma) \right) \tag{4.22}$$

$$+p(1 - \mu(\gamma)) U^\dagger_{\alpha\gamma}(j_\gamma) U_{\gamma\beta}(j_\gamma) + p^{-1} \sum_{\delta,\sigma \neq \gamma} L_{\delta\gamma}(j_\gamma) U^\dagger_{\alpha\delta}(j_\gamma) L_{\gamma\sigma}(j_\gamma) U_{\sigma\beta}(j_\gamma).$$

In matrix form, this is

$$S(j_\gamma) = pU^\dagger \Lambda_\gamma U + U^\dagger \{L, \Lambda_\gamma\} U + p^{-1} U^\dagger \mathcal{L}^\gamma U, \tag{4.23}$$

where Λ_γ is zero except at entry (γ, γ) where it equals 1:

$$\Lambda_1 = \begin{pmatrix} 1 & 0 & 0 \\ 0 & 0 & 0 \\ 0 & 0 & 0 \end{pmatrix}, \quad \Lambda_2 = \begin{pmatrix} 0 & 0 & 0 \\ 0 & 1 & 0 \\ 0 & 0 & 0 \end{pmatrix}, \quad \Lambda_3 = \begin{pmatrix} 0 & 0 & 0 \\ 0 & 0 & 0 \\ 0 & 0 & 1 \end{pmatrix}. \tag{4.24}$$

We've also defined

$$\mathcal{L}_{\alpha\beta}(j_\gamma) = L_{\alpha\gamma}(j_\gamma) L_{\gamma\beta}(j_\gamma) - p^2 \mu(\gamma) [\Lambda_\gamma]_{\alpha\beta}. \tag{4.25}$$

Let us pause for a moment and reflect on our calculations. Note that at no stage did we explicitly use the fact that U, L and Λ_γ are 3×3 matrices. Indeed, the above calculations carry over directly to SU(n) when we promote the objects φ^α to lie in $\mathbb{C}^n$ instead of $\mathbb{C}^3$. This observation will allow us in Chapter 5 to immediately use the result (4.23) without further proof.

Using (4.23), we now evaluate the trace terms appearing in (4.1). Again, this derivation will hold for general $n \times n$ matrices, and we will refer to these calculations in Chapter 5. Since the matrices U and L are evaluated at different sites, we Taylor expand which introduces spatial derivatives. For example

$$U(j_\gamma) = U(nj + (\gamma - 1)) = U(j_\eta) + (\eta - \gamma)\partial_x U(j_\eta) + \frac{1}{2}(\eta - \gamma)^2 \partial_x^2 U(j_\eta) + \cdots, \tag{4.26}$$

where we've assumed the derivative is uniform: $\partial_x U(j_\eta) = \partial_x U(j'_\lambda)$. Expanding in powers of L and p^{-1}, we find after some tedious algebra,

$$\text{tr}[S(j_\gamma)S(j_\eta)] = p^2(\eta - \gamma)^2 \text{tr}[U\partial_x U^\dagger \Lambda_\gamma \partial_x U U^\dagger \Lambda_\eta] \tag{4.27}$$

$$+2(\eta - \gamma)p \left(L_{\eta\gamma}[\partial_x U U^\dagger]_{\gamma\eta} + L_{\gamma\eta}[U\partial_x U^\dagger]_{\eta\gamma} \right) + 4|L_{\eta\gamma}|^2 + \text{const.}$$

For the complete derivation of this result, see Appendix B. This completes the second item on the recipe presented in Section 2.5.

4.3.1 Coherent state path integral

Having rewritten the Hamiltonian in terms of U and L, we now derive the Lagrangian by using a coherent state path integral approach [99, 100, 123]. Our approach mimics the procedure outlined in Section 2.2.1. As a complete set of states, we introduce

$$|\phi\rangle = (\boldsymbol{\phi} \cdot \boldsymbol{a})^p|0\rangle, \qquad (4.28)$$

with $\boldsymbol{\phi} \in \mathbb{C}^n$. As in SU(2), the $\boldsymbol{a}$ are bosonic operators, known as Schwinger bosons. Again, we promote all of the fields to n-complex dimensional objects, so that we may make use of this derivation again in Chapter 5. These states correspond to an element of the rank-p symmetric representation of SU(n), $[\boldsymbol{\phi}]_p$, acting on a highest-weight state in the Hilbert space:

$$|\phi\rangle = [\boldsymbol{\phi}]_p|\text{highest weight}\rangle. \qquad (4.29)$$

The resolution of the identity is then the integration over all of SU(n) of the projection $|\boldsymbol{\phi}\rangle\langle\boldsymbol{\phi}|$:

$$1 = \int \mathcal{D}\phi|\phi\rangle\langle\phi|. \qquad (4.30)$$

Inserting this between each time slice τ_i of the partition function, we obtain terms of the form

$$\langle\phi(\tau_i)|e^{-H\delta\tau}|\phi(\tau_{i+1})\rangle = \langle\phi(\tau)|\phi_{\tau+\delta\tau}\rangle e^{-H\delta\tau}. \qquad (4.31)$$

Exponentiating these terms, we find the following contribution to the action:

$$\prod_i \langle\phi(\tau_i)|\phi(\tau_{i+1})\rangle \propto (1 + \boldsymbol{\phi}^*(\tau_i)\cdot\partial_\tau\boldsymbol{\phi}(\tau_i))^p = \exp p \log \sum_i (1 + \boldsymbol{\phi}^*(\tau_i)\cdot\partial_\tau\boldsymbol{\phi}(\tau_i)) \approx \exp p \int d\tau \boldsymbol{\phi}^* \cdot \partial_\tau\boldsymbol{\phi}, \qquad (4.32)$$

where we've used $\langle\phi|\phi'\rangle = (\boldsymbol{\phi}^* \cdot \boldsymbol{\phi}')^p$. Now, using (4.15), we have

$$\partial_\tau\phi_\beta^\alpha = \sum_\gamma \partial_\tau\tilde{L}_{\alpha\gamma}U_{\gamma\beta} + \tilde{L}_{\alpha\gamma}\partial_\tau U_{\gamma\beta}, \qquad (4.33)$$

where $\tilde{L}$ is defined below (4.18). We neglect time derivatives of $\tilde{L}$, which are already small fluctuations. Then we have

$$\boldsymbol{\phi}^{*,\alpha} \cdot \partial_\tau\boldsymbol{\phi}^\alpha = \sum_{\delta,\gamma,\beta} \tilde{L}_{\delta\alpha}U_{\beta\delta}^\dagger\tilde{L}_{\alpha\gamma}\partial_\tau U_{\gamma\beta} \qquad (4.34)$$

$$= \sum_{\delta\neq\alpha}\sum_\beta \left[L_{\delta\alpha}U_{\beta\delta}^\dagger\partial_\tau U_{\alpha\beta} + U_{\beta\alpha}^\dagger\tilde{L}_{\alpha\delta}\partial_\tau U_{\delta\beta} + (1 - \mu(\alpha))U_{\beta\alpha}^\dagger\partial_\tau U_{\alpha\beta} \right] + O(p^{-2})$$

$$= \text{tr}[\Lambda_\alpha\partial_\tau UU^\dagger] + p^{-1}\text{tr}[\{\Lambda_\alpha, L\}\partial_\tau UU^\dagger] + O(p^{-2}). \qquad (4.35)$$

Therefore, we see that the Lagrangian receives the following Berry contribution for each of the n sites of the unit cell:

$$\mathcal{L}_B = -\frac{1}{n}\Big(p\text{tr}[\Lambda_\alpha \partial_\tau U U^\dagger] + \text{tr}[\{\Lambda_\alpha, L\}\partial_\tau U U^\dagger]\Big) + O(p^{-1}). \tag{4.36}$$

We have divided by n, the size of the unit cell, since $\mathcal{L}_B$ is technically a Lagrangian density that will be integrated against the two-dimensional measure $dxd\tau$. In SU(3), the explicit contribution from a sum over 3 sites is, to $O(p^{-1})$,

$$\mathcal{L}_B = -\frac{p}{3}\text{tr}[\Lambda_1 \partial_\tau U(x) U^\dagger(x) + \Lambda_2 \partial_\tau U(x+1) U^\dagger(x+1) + \Lambda_3 \partial_\tau U(x+2) U^\dagger(x+2)] \tag{4.37}$$

$$-\frac{1}{3}\text{tr}[\{\Lambda_1, L(x)\}\partial_\tau U(x) U^\dagger(x) + \{\Lambda_2, L(x+1)\}\partial_\tau U(x+1) U^\dagger(x+1) + \{\Lambda_3, L(x+1)\}\partial_\tau U(x+2) U^\dagger(x+2)].$$

In SU(2), such an expression led directly to the topological term (2.44) upon Taylor expansion and integrating out the L matrices. Here, we will find that such a procedure will lead to additional terms that are purely imaginary in imaginary time (like a topological term), yet are not quantized. These so-called 'λ-terms', which are absent in SU(2), can be interpreted as torsion terms in the flag manifold metric tensor. In Section 4.5, we will devote considerable effort to analyzing the λ-term in SU(3) using the renormalization group.

4.3.2 Complete field theory

We now are in a position to derive the complete field theory of the SU(3) chain in the symmetric representation. First, we Taylor expand the result (4.37). Note that since the L matrices are already subleading, this Taylor expansion is only nontrivial for the first line in (4.37). We find

$$\mathcal{L}_B = -\frac{p}{3}\epsilon_{\mu\nu}\text{tr}[(\Lambda_2 + 2\Lambda_3)\partial_\mu U \partial_\nu U^\dagger] - \frac{2}{3}\text{tr}[L\partial_\tau U U^\dagger], \tag{4.38}$$

where we again made use of the identity $\text{tr}[\partial U U^\dagger] = 0$, which is proven in Appendix A. Now, let us determine the Lagrangian contribution from the Hamiltonian. Using the formula (2.34), we have

$$\mathcal{L} - \mathcal{L}_B = -\frac{J_1}{3}\Big(\text{tr}[S(x)S(x+1)] + \text{tr}[S(x+1)S(x+2)] + \text{tr}[S(x+2)S(x)]\Big) \tag{4.39}$$

$$-\frac{J_2}{3}\Big(\text{tr}[S(x)S(x+2)] + \text{tr}[S(x+2)S(x)]\Big).$$

Note that we have remembered to divide by 3, the size of the unit cell, when adding (4.27) into this expression. We have also made use of the 3-site order to make the identification $x \sim x + 3$. Inserting (4.27), we then have

$$\mathcal{L} - \mathcal{L}_B = -\frac{J_1}{3}\Big[\sum_{\alpha=1}^{3} p^2 \text{tr}[U\partial_x U^\dagger \Lambda_\alpha \partial_x U U^\dagger \Lambda_{\alpha+1}] + 2p\text{tr}[\{L, \Lambda_\alpha\}\partial_x U U^\dagger \Lambda_{\alpha+1}] + 4|L_{\alpha,\alpha+1}|^2\Big] \tag{4.40}$$

$$-\frac{J_2}{3}\Big[4p^2\sum_{\alpha=1}^{3}\text{tr}[U\partial_x U^\dagger\Lambda_\alpha\partial_x UU^\dagger\Lambda_{\alpha+2}] + 4p\text{tr}[\{L,\Lambda_\alpha\}\partial_x UU^\dagger\Lambda_{\alpha+2}] + 4|L_{\alpha,\alpha+2}|^2\Big],$$

where all indices are defined modulo 3. Now, the L matrices can be integrated out using the same Gaussian identity we used in Chapter 2, (2.38), as well as the result (4.38). For example, integrating out L_{12} and L_{12}^* leads to

$$\int dL_{12}dL_{12}^* \exp\left[-\frac{4}{3}(J_1 + J_2)|L_{12}|^2 - 2L_{12}\left([\partial_\tau UU^\dagger]_{21} + 2(2J_2 - J_1)[\partial_x UU^\dagger]_{21}\right)\right] \quad (4.41)$$

$$\times \exp\left[-2L_{21}\left([\partial_\tau UU^\dagger]_{12} - 2((2J_2 - J_1)[\partial_x UU^\dagger]_{12}\right)\right]$$

$$= \exp\left[-\frac{1}{3(J_1 + J_2)}\text{tr}[\Lambda_1 U\partial_\tau U^\dagger\Lambda_2\partial_\tau UU^\dagger] + p^2\frac{(2J_2 - J_1)^2}{3(J_1 + J_2)}\text{tr}[\Lambda_1 U\partial_x U^\dagger\Lambda_2\partial_x UU^\dagger]\right]$$

$$\times \exp\left[p\frac{2J_2 - J_1}{3(J_1 + J_2)}\epsilon_{\mu\nu}\text{tr}[\partial_\mu UU^\dagger\Lambda_2\partial_\tau UU^\dagger\Lambda_1]\right].$$

Similar integrals can be done for the L_{23} and L_{13} terms as well. In the end, we arrive at the following action:

$$S[U] = \int dxd\tau\Big(\sum_{\alpha=1}^{3}\frac{1}{g}\Big[v\text{tr}[\Lambda_{\alpha-1}U\partial_x U^\dagger\Lambda_\alpha\partial_x UU^\dagger] + \frac{1}{v}\text{tr}[\Lambda_{\alpha-1}U\partial_\tau U^\dagger\Lambda_\alpha\partial_\tau UU^\dagger]\Big] \quad (4.42)$$

$$+i\frac{\theta}{2\pi i}\epsilon_{\mu\nu}\text{tr}\Big[(\Lambda_1 - \Lambda_3)\partial_\mu U\partial_\nu U^\dagger\Big] + i\frac{\lambda}{2\pi i}\epsilon_{\mu\nu}\sum_{\alpha=1}^{3}\text{tr}[\Lambda_{\alpha-1}U\partial_\mu U^\dagger\Lambda_\alpha\partial_\nu UU^\dagger]\Big).$$

Let us define the various parameters introduced above. The coupling constants g and λ obey

$$\frac{1}{g} = p\frac{\sqrt{J_1 J_2}}{J_1 + J_2} \qquad\qquad \lambda = \frac{2\pi p}{3}\frac{2J_2 - J_1}{J_1 + J_2}, \quad (4.43)$$

the velocity satisfies

$$v = 3p\sqrt{J_1 J_2}, \quad (4.44)$$

and the topological angle is defined by

$$\theta = \frac{2\pi p}{3}. \quad (4.45)$$

This action defines a sigma model quantum field theory. That is, a theory whose fields, (in this case the matrices U), are restricted to lie in a particular smooth manifold. For us, this space is the flag manifold $SU(3)/[U(1)]^2$: the space of special unitary 3x3 matrices that are invariant under two $U(1)$ gauge transformations. The terms proportional to $\frac{1}{g}$ correspond to a symmetric metric tensor on this manifold, and the λ-term corresponds to an antisymmetric metric torsion. For more details on the mathematical structure of both sigma models, as well as flag manifolds in general, we refer

the reader to the papers of Bykov [71, 72], as well as the recent review [6].[20] In the following section, where we list the various properties of this model, these gauge transformations will be verified explicitly.

But before moving on, we make an additional useful observation. Since our quantum field theory was derived to capture small fluctuations about a classical ground state, we may treat U as a matrix close to the identity operator, and write

$$U = e^{i \sum_A \omega_A T_A}, \tag{4.46}$$

for small real fields ω_A, and $\mathfrak{su}(3)$ Lie algebra generators T_A. Indeed, this is a defining property of any Lie group, including SU(3) in which U belongs. Now, in Appendix C, we prove a factorization property of SU(3) matrices. Namely, any matrix U can actually be written as

$$U = e^{i(\omega_3 T_3 + \omega_8 T_8)} e^{i \sum_{A \neq 3,8} \omega_A T_A}, \tag{4.47}$$

where T_3 and T_8 are diagonal matrices, and the remaining generators are off-diagonal. Inserting this factorization into (4.42), the gauge invariance cited above will ensure that the fields ω_3 and ω_8 do not appear in the action. In other words, the flag manifold sigma model action is described by only 6 fields, which agrees with the real dimension of SU(3)/[U(1)]^2. This number of degrees of freedom is consistent with the fact that we found 6 Goldstone bosons in our flavour-wave theory calculations. Moreover the ω_A fields propagate with precisely the same velocity, v. This is to be expected, since it was flavour-wave theory that provided our reference state for deriving the quantum field theory in the first place!

4.4 Properties of the Field Theory

The first symmetry to notice in (4.42) is the invariance under exchanging the spatial and temporal coordinates, $x \leftrightarrow \tau$; i.e. the theory is Lorentz invariant just as in SU(2). This can be made more obvious by rescaling $\tau \mapsto v\tau$.

Next, we comment on the coupling constants. The first, g, is a direct analogue of the $\mathbb{CP}^1$ coupling (2.50), and as in that theory, it tends to zero in the limit of large representation, $p \to \infty$. We will make use of this fact in the following section when we perform perturbation theory to determine various renormalization group flows in the sigma model. Meanwhile, the coupling constant λ is novel, and arises due to a mismatch between the first and second-neighbour interactions in the Heisenberg Hamiltonian. Only for the fine-tuned choice of $J_1 = 2J_2$ does this term vanish. Unfortunately, we are unable to identify a physical symmetry of the SU(3) chain that would rule out such a term, and so we are forced to analyze its consequences. Interestingly, this λ-term is a pure-imaginary term in imaginary time, and contributes only a phase to the underlying SU(3) partition function, much like the topological term analyzed in Section 2.3.1. However, unlike a topological term, it is not related to an invariant, and so is not quantized in any way.

---

[20]The 'flag' structure is more obvious when we recall the isomorphism U(3) $\equiv$ SU(3) $\times$ U(1), so that the manifold is U(3)/[U(1)]^3. In [6], additional equivalent definitions of flag manifolds can be found.

Finally, let us direct our attention to the terms involving θ. As our notation suggests, these *are* topological invariants, and correspond to the second cohomology group of the manifold $\text{SU}(3)/[\text{U}(1)]^2$:

$$H^2(\text{SU}(3)/[\text{U}(1)]^2) = \mathbb{Z} \times \mathbb{Z}. \tag{4.48}$$

Recall that this group is equivalent to the second homotopy group for flag manifolds, which classifies topologically distinct maps from S^2 to the target space. As we explained in Chapter 2, since any finite-action field configuration must attain a constant value at some radius R away from the origin in spacetime, we may identify $\mathbb{R}^2$ with the sphere S^2, and view any field $\boldsymbol{\varphi} \in \text{SU}(3)/[\text{U}(1)]^2$ as a map from S^2 to the flag manifold. Explicitly, the topological invariant is

$$Q_\alpha := \frac{1}{2\pi i}\epsilon_{\mu\nu}\int dx d\tau \text{tr}[\Lambda_\alpha \partial_\mu U \partial_\nu U] \in \mathbb{Z}, \tag{4.49}$$

so that topological action arising from (4.42) reads

$$S_{\text{top}} = i\sum_{\alpha=1}^{3}\theta_\alpha Q_\alpha, \tag{4.50}$$

with $\theta_1 = -\theta_3 = \theta = \frac{2\pi p}{3}$, and $\theta_2 = 0$. Actually, we have some freedom in our definition of the θ_α, since it is easily verified using $\text{tr}[U\partial U^\dagger] = 0$ that the topological charges Q_α satisfy

$$Q_1 + Q_2 + Q_3 = 0. \tag{4.51}$$

In fact, not only do the topological charges sum to zero, but so do their densities, $q_\alpha := \text{tr}[\Lambda_\alpha \partial_\mu U \partial_\nu U^\dagger]$.

4.4.1   The flag manifold as coupled $\mathbb{C}\text{P}^2$ sigma models

In Section 3.3, we explained how longer-range interactions in the Heisenberg Hamiltonian served to couple degrees of freedom together across sites of the chain. According to (4.18), in the symmetric representations we presently consider, to each site of the chain we may assign a field $\boldsymbol{\varphi}^\alpha$, which corresponds to a $\mathbb{C}\text{P}^2$ degree of freedom. In a nearest-neighbour model, the unit cell would involve only two such $\mathbb{C}\text{P}^2$ fields, and local zero modes would persist. But as we have seen, by adding a J_2 term in (4.1), we couple three sites together, and obtain a field theory involving three separate $\mathbb{C}\text{P}^2$ fields. We now rewrite our sigma model in a manner that makes this threefold $\mathbb{C}\text{P}^2$ structure explicit. Using the identity

$$\sum_{\alpha=1}^{3}|\boldsymbol{\varphi}^{*,\alpha-1}\cdot\partial_\mu\boldsymbol{\varphi}^\alpha|^2 = \frac{1}{2}\sum_{\alpha=1}^{3}\left(|\partial_\mu\boldsymbol{\varphi}^\alpha|^2 - |\boldsymbol{\varphi}^{*,\alpha}\cdot\partial_\mu\boldsymbol{\varphi}^\alpha|^2\right), \tag{4.52}$$

we see that the flag manifold sigma model resembles that of three $\mathbb{C}\text{P}^2$ fields, coupled via orthogonality and the λ-term. Indeed, after some algebra we find

$$S = \frac{1}{2g}\sum_{\alpha=1}^{3}\left(|\partial_\mu\boldsymbol{\varphi}^\alpha|^2 - |\boldsymbol{\varphi}^{*,\alpha}\cdot\partial_\mu\boldsymbol{\varphi}^\alpha|^2\right) + \frac{\epsilon_{\mu\nu}}{2\pi i}\sum_{\alpha=1}^{3}\left[i\lambda(\boldsymbol{\varphi}^{*,\alpha+1}\cdot\partial_\mu\boldsymbol{\varphi}^\alpha)(\boldsymbol{\varphi}^{\alpha+1}\cdot\partial_\nu\boldsymbol{\varphi}^{*,\alpha}) + i\theta_\alpha\partial_\mu\boldsymbol{\varphi}^\alpha\cdot\partial_\nu\boldsymbol{\varphi}^{*,\alpha}\right], \tag{4.53}$$

where we have rescaled τ by setting $v = 1$. The first term occurring above is precisely the action for a $\mathbb{CP}^2$ field. This expression makes explicit the embedding of the flag manifold $SU(3)/[U(1)]^2$ into three copies of $\mathbb{CP}^2$:

$$\frac{U(3)}{U(1) \times U(1) \times U(1)} \hookrightarrow \mathbb{CP}^2 \times \mathbb{CP}^2 \times \mathbb{CP}^2. \tag{4.54}$$

Since $\mathbb{CP}^2$ is the Grassmannian $G_{1,n}$, this embedding is a special case of (3.16).

4.4.2 Gauge symmetry

We now turn to the $U(1) \times U(1)$ gauge structure of the sigma model. In (4.42), this manifests as invariance of the action under the transformation $U'(x, \tau) = D(x, \tau)U(x, \tau)$, where

$$D(x, \tau) = \begin{pmatrix} e^{i\vartheta_1(x,\tau)} & 0 & 0 \\ 0 & e^{i\vartheta_2(x,\tau)} & 0 \\ 0 & 0 & e^{i\vartheta_3(x,\tau)} \end{pmatrix} \tag{4.55}$$

with $\vartheta_3 = -\vartheta_1 - \vartheta_2$. It is actually easier to verify the gauge symmetry in terms of the φ^α. In terms of these fields, this transformation corresponds to $\varphi'^\alpha = e^{i\vartheta_\alpha}\varphi^\alpha$. Let us verify each term in (4.53) separately. Since

$$|\varphi'^{*,\alpha\pm1} \cdot \partial_\mu\varphi'^\alpha|^2 = |\varphi^{*,\alpha\pm1}e^{-i\vartheta_{\alpha\pm1}} \cdot (\partial_\mu\varphi^\alpha e^{i\vartheta_\alpha} + \varphi^\alpha\partial_\mu e^{i\vartheta_\alpha})|^2 = |\varphi^{*,\alpha\pm1} \cdot \partial_\mu\varphi^\alpha|^2 \tag{4.56}$$

because the φ^α are mutually orthogonal, we can use (4.52) to verify that the real terms in (4.53) are gauge invariant. The λ-term can be similarly shown to be invariant since the phase factors cancel out. Finally, the topological charges transform as

$$\epsilon_{\mu\nu}(\partial_\mu\varphi'^\alpha \cdot \partial_\nu\varphi'^{*,\alpha}) = \epsilon_{\mu\nu}(\partial_\mu\varphi^\alpha \cdot \partial_\nu\varphi^{*,\alpha}) + \epsilon_{\mu\nu}(\partial_\mu(i\vartheta_\alpha)\partial_\nu(-i\vartheta_\alpha)) \tag{4.57}$$

$$+\epsilon_{\mu\nu}(\partial_\mu\varphi^\alpha \cdot \varphi^{*,\alpha}\partial_\nu(-i\vartheta_\alpha)) + \epsilon_{\mu\nu}(\partial_\mu(i\vartheta_\alpha)\varphi^\alpha \cdot \partial_\nu\varphi^{*,\alpha}).$$

The second term on the right hand side vanishes by symmetry: $\epsilon_{\mu\nu}$ is antisymmetric while $(\partial_\mu\vartheta_\alpha\partial_\nu\vartheta_\alpha)$ is symmetric. Meanwhile, the third and fourth terms cancel due to the identity

$$\partial(\varphi^\alpha \cdot \varphi^{*,\alpha}) = 0. \tag{4.58}$$

Thus, the topological term is invariant, and (4.42) possesses the gauge symmetry (4.55) as claimed.

It is perhaps useful to relate these gauge symmetries to the familiar $U(1)$ gauge symmetry of the $\mathbb{CP}^2$ sigma model. To this end, we introduce three fields $A_\mu^\alpha \in \mathbb{R}^2$, which satisfy

$$A_\mu^1(x) + A_\mu^2(x) + A_\mu^3(x) = 0 \tag{4.59}$$

for all x and μ. This constraint is equivalent to the condition that $\vartheta_3 = -\vartheta_1 - \vartheta_2$ in (4.55). In terms of these A_μ^α, there exists yet another rewriting of (4.42), which is

$$S = \int dx d\tau \left(\sum_{\alpha=1}^{3} \left[\frac{1}{2g} \left| (\partial_\mu + iA_\mu^\alpha)\boldsymbol{\varphi}_\alpha \right|^2 + \frac{i\theta_\alpha}{2\pi i} \epsilon_{\mu\nu} A_\nu^\alpha + \frac{\epsilon_{\mu\nu}}{2\pi i} \lambda (\boldsymbol{\varphi}^{*,\alpha+1} \cdot \partial_\mu \boldsymbol{\varphi}^\alpha)(\boldsymbol{\varphi}^{\alpha+1} \cdot \partial_\nu \boldsymbol{\varphi}^{*,\alpha}) \right] \right). \quad (4.60)$$

To prove this, we first expand the real term in (4.60):

$$\left| (\partial_\mu + iA_\mu^\alpha)\boldsymbol{\varphi}^\alpha \right|^2 = \left| \partial_\mu \boldsymbol{\varphi}^\alpha \right|^2 + (A_\mu^\alpha)^2 - 2iA_\mu^\alpha \boldsymbol{\varphi}^{*,\alpha} \cdot \partial_\mu \boldsymbol{\varphi}^\alpha \quad (4.61)$$

$$= \left| \partial_\mu \boldsymbol{\varphi}^\alpha \right|^2 - \left| \boldsymbol{\varphi}^{*,\alpha} \cdot \partial_\mu \boldsymbol{\varphi}^\alpha \right|^2 + (A_\mu^\alpha - i\boldsymbol{\varphi}^{*,\alpha} \cdot \partial_\mu \boldsymbol{\varphi}^\alpha)^2.$$

This form suggests we shift A_μ^α by $i\boldsymbol{\varphi}^{*,\alpha} \cdot \partial_\mu \boldsymbol{\varphi}^\alpha$. In doing so, this changes the topological term in (4.60) according to

$$\epsilon_{\mu\nu} \partial_\mu A_\nu^\alpha \mapsto \epsilon_{\mu\nu} \partial_\mu A_\nu^\alpha + i\epsilon_{\mu\nu} \partial_\mu \boldsymbol{\varphi}^{*,\alpha} \cdot \partial_\nu \boldsymbol{\varphi}^\alpha. \quad (4.62)$$

Since the A_μ^α are decoupled from the $\boldsymbol{\varphi}^\alpha$, we may now integrate out the gauge fields completely, and obtain the desired theory (4.53). Note that shifting the gauge fields does not disturb the constraint (4.59), since

$$A_\mu^1(x) + A_\mu^2(x) + A_\mu^3(x) \mapsto A_\mu^1(x) + A_\mu^2(x) + A_\mu^3(x) + \sum_{\alpha=1}^{3} \boldsymbol{\varphi}^{*,\alpha} \cdot \partial_\mu \boldsymbol{\varphi}^\alpha, \quad (4.63)$$

and the second term vanishes since it is of the form $\mathrm{tr}[U\partial U^\dagger]$.

4.4.3 $\mathbb{Z}_3$ symmetry

Translation symmetry in the underlying SU(3) chain is realized in the sigma model as a global $\mathbb{Z}_3$ symmetry: $U \mapsto U' = RU$, with

$$R = \begin{pmatrix} 0 & 1 & 0 \\ 0 & 0 & 1 \\ 1 & 0 & 0 \end{pmatrix}. \quad (4.64)$$

This cyclically permutes the three $\boldsymbol{\varphi}^\alpha$ fields, which can be represented pictorially as

$$\textcolor{red}{\bullet} \mapsto^R \textcolor{blue}{\bullet} \mapsto^R \textcolor{green}{\bullet} \mapsto^R \textcolor{red}{\bullet}. \quad (4.65)$$

Note that $R^3 = 1$, as it must. Using the form of the action (4.53), the only nontrivial calculation we must do to verify symmetry under R has to do with the topological term. Note that

$$\frac{2\pi}{3}(Q_1 - Q_3) \mapsto \frac{2\pi}{3}(Q_2 - Q_1) = \frac{2\pi}{3}(Q_1 - Q_3) + \frac{2\pi}{3}(Q_1 + Q_2 + Q_3) - 3\frac{2\pi}{3}Q_1. \quad (4.66)$$

Since $Q_1 + Q_2 + Q_3 = 0$, the second term vanishes. Now recall that the topological term enters the partition function as a pure phase. Since $Q_1 \in \mathbb{Z}$, we have

$$e^{\frac{2\pi ip}{3}(Q_1 - Q_3)} \mapsto e^{\frac{2\pi ip}{3}(Q_1 - Q_3)} e^{2\pi ip Q_1} = e^{\frac{2\pi ip}{3}(Q_1 - Q_3)}, \quad (4.67)$$

which proves the symmetry. We will have more to say on this symmetry later on, when we discuss the concept of 't Hooft anomaly matching.

4.4.4 Other discrete symmetries

Another discrete global symmetry of the sigma model is parity symmetry, which corresponds to a mirror symmetry in the SU(3) chain. In fact, there are three non-equivalent mirror symmetries, which lead to three non-equivalent parity symmetries. For example, a reflection about the line separating ● and ● sites in the chain corresponds to

$$\boldsymbol{\varphi}^1(x, \tau) \mapsto \boldsymbol{\varphi}^3(-x, \tau) \qquad \boldsymbol{\varphi}^2(x, \tau) \mapsto \boldsymbol{\varphi}^2(-x, \tau) \qquad \boldsymbol{\varphi}^3(x, \tau) \mapsto \boldsymbol{\varphi}^1(-x, \tau). \qquad (4.68)$$

It is easily verified that such a transformation leaves (4.53) invariant. Note for instance that the topological term is unchanged: Q_1 and Q_3 change sign, but so does the partial derivative, ∂_x, and these two changes cancel out. This parity symmetry will not be related to any 't Hooft anomalies, but will become important in Section 4.7 when we discuss other SU(3) representations.

Finally, the sigma model is also unchanged under the symmetry $\boldsymbol{\varphi}^\alpha(x, \tau) \to \boldsymbol{\varphi}^\alpha(x, -\tau)$, as well as $i \mapsto -i$. This corresponds to time-reversal symmetry in the SU(3) chain.

4.5 Renormalization Group Calculations

In Chapter 2, once we derived the corresponding sigma model of the antiferromagnet, we were immediately able to draw conclusions about its phase diagram. This was because a great deal of theoretical investigation had already been carried out for the $\mathbb{CP}^1$ sigma model. In particular, it was well established that the theory is asymptotically free, meaning that the coupling constant g flows to small values at high enough energies [18].

Having derived the flag manifold sigma model description of the SU(3) chain in this chapter, we would now like to proceed in a similar fashion. Ultimately, we hope to establish a phase diagram for the chain that depends on the representation p, and uncover an SU(3) version of Haldane's conjecture. Unfortunately, we have more work to do first. Since these flag manifolds are relatively novel theories, they have not been studied to the same extend as in SU(2). Therefore, in this section, we are forced to do the necessary renormalization group (RG) calculations ourselves, in order to establish asymptotic freedom in the SU(3) chain. We will also investigate the relevance of the λ-term, as it is an operator that is not often considered in standard quantum field theories.

4.5.1 A primer on renormalization group theory

Since the notion of renormalization group flow will be central to the results of this thesis, we offer here a brief reminder of its theoretical foundation.[21] The fundamental idea behind the renormalization group is that coupling constants change as we change the length scale of our theory. In the context of spin chains, this notion of different length scales is very natural: the atomic spacing of spins along the chain is a much smaller distance than the observable lengths defined by macroscopic phenomena. This motivates the search for so-called *relevant operators* – those operators

---

[21]The content of this subsection is partially transcribed from the author's MSc thesis [124].

whose coupling constants increase as we increase length scales. In contrast, *irrelevant operators*, those whose couplings decrease as we increase length scales, are less interesting to us as physicists who seek to model and identify macroscopic phenomena.[22] When we apply this thinking to our flag manifold sigma model, what we hope to understand is which of the couplings g and λ are associated with relevant operators.

In order to achieve this understanding, we must determine the functions governing the evolution of g and λ as a function of length scale. These are known as beta functions, and can be defined as follows. Given a family of length scales $b\Lambda$ parametrized by b, the beta function of coupling constant X is defined according to

$$\beta_X := \frac{dX}{d\log b}.$$ (4.69)

Here Λ can be thought of as an underlying ultraviolet (i.e. high energy) cutoff in the theory, determined in part by the inverse lattice spacing, a^{-1}.[23] Since increasing b corresponds to increasing length, relevant operators have positive beta functions. Now, there are various ways of calculating β_X; we choose to follow Ken Wilson's approach, who is credited for much of our modern understanding of the renormalization group [125]. According to Wilson, one reduces the length scale of the quantum field theory by integrating out those fields whose momentum modes are restricted to lie in a thin shell in momentum space. This shell consists of all momenta with magnitude lying within $(b^{-1}\Lambda, \Lambda)$.[24]

Let us explain how this integration is carried out for the case of a single scalar field, ϕ. Then we will turn to the flag manifold sigma model in the following subsection. The Lagrangian density is taken to be

$$\mathcal{L}_\varphi = \frac{1}{2}(\partial\varphi)^2 + \sum_i X_i O_i[\varphi],$$ (4.70)

where $O_i[\varphi]$ is a generic operator involving the field φ and its derivatives. We begin by separating the field into slow and fast components,

$$\varphi = \varphi_s + \varphi_f,$$ (4.71)

where φ_s contains the momentum modes of φ with magnitude less than $b^{-1}\Lambda$, and φ_f contains the modes that lie within the shell. In terms of these new variables, the Lagrangian density can be reorganized as follows:

$$\mathcal{L}_\varphi = \mathcal{L}_s + \mathcal{L}_f^0 + \mathcal{L}_{sf}.$$ (4.72)

The first term, $\mathcal{L}_s$, equals the original Lagrangian density, but with φ replaced with φ_s. The second term, $\mathcal{L}_f^0$, equals the free fast Lagrangian density, $\frac{1}{2}(\partial\varphi_f)^2$. The remaining term contains all

---

[22]For completeness, we note that operators that are neither relevant nor irrelevant are referred to as *marginal*.

[23]In practice, Λ is a reduced cutoff, which is less than the bare cutoff $\Lambda_0 := a^{-1}$. This is because we typically work with a Lagrangian that already corresponds to some lower energy description of the system than the original underlying Hamiltonian.

[24]Note that since b is a length scale, $b^{-1}\Lambda$ corresponds to an energy scale less than Λ.

operators that mix slow and fast components. The partition function can then be rewritten as

$$Z = \int \mathcal{D}\varphi_s \varphi_f e^{-\int d^d x (\mathcal{L}_s + \mathcal{L}_f^0 + \mathcal{L}_{sf})} = Z_{0,f} \int \mathcal{D}\varphi_s e^{-\int d^d x (\mathcal{L}_s + \delta \mathcal{L})}, \tag{4.73}$$

where

$$Z_{0,f} := \int \mathcal{D}\varphi_f e^{-\int d^d x \mathcal{L}_f} \qquad \langle \cdots \rangle_f := Z_{0,f}^{-1} \int \mathcal{D}\varphi_f \cdots e^{-\int d^d x \mathcal{L}_f} \tag{4.74}$$

and

$$e^{-\int d^d x \delta \mathcal{L}} := \langle e^{-\int d^d x \mathcal{L}_{sf}} \rangle_f. \tag{4.75}$$

In other words, integrating out the fast modes has generated new terms in the Lagrangian. Since the operators appearing in (4.70) were generic, we can write

$$\delta \mathcal{L} = \frac{1}{2} \delta Z_\varphi (\partial \varphi_s)^2 + \sum_i \delta Z_i O_i[\varphi_s] \tag{4.76}$$

in terms of *renormalization constants* δZ_φ and δZ_i. To compare $\mathcal{L}_s + \delta \mathcal{L}$ to the original theory, we rescale coordinates

$$x \rightarrow b^{-1} x \tag{4.77}$$

so that the new UV cutoff is once again Λ, and rescale the field

$$\varphi_s \rightarrow \varphi_s \sqrt{(1 + \delta Z_\varphi) b^{d-2}} \tag{4.78}$$

so that the new kinetic term is once again $\frac{1}{2}(\partial \varphi)^2$. Defining d_i and n_i to be the mass dimension and number of factors of φ, respectively, of O_i, we find that the coupling constants of the reduced theory, $X_i(b)$, satisfy

$$X_i(b) = X_i \left(1 + \frac{\delta Z_i}{X_i} \right) (1 + \delta Z_\varphi)^{-n_i} b^{d_i}. \tag{4.79}$$

This expression can now be differentiated with respect to $\log b$, yielding the beta functions of the theory, β_{X_i}. Often, we use flow diagrams that capture the information provided by these beta functions.

4.5.2 Renormalization of the SU(3) chain

According to the steps outlined above, we begin by deriving a perturbative expansion of the sigma model, (4.42). This is achieved by rewriting the matrices U in terms of the 8 generators T_A of SU(3), according to

$$U = e^{i \sum_{A=1}^8 \omega_A T_A}. \tag{4.80}$$

These matrices are defined explicitly in (E.1), and can be thought of as generalized Pauli matrices. They satisfy the $\mathfrak{su}(3)$ algebra

$$[T_A, T_B] = 2i f_{ABC} T_C, \tag{4.81}$$

where the f_{ABC} structure constants are fully antisymmetric. Due to the factorization property of SU(3) matrices (4.47), and the gauge symmetry (4.55), we can replace (4.80) with the simpler relation

$$U = e^{i\omega_a T_a}.\tag{4.82}$$

Here and throughout, lowercase Latin letters index the off-diagonal Gell-Mann matrices, lowercase Greek letters index the diagonal ones, uppercase Latin letters index all eight Gell-Mann matrices, and repeated indices are summed over. Now following Wilson, we rewrite the fields U in terms of 'slow' (U_s) and 'fast' (U_f) fields, as

$$U = U_f U_s\tag{4.83}$$

and make use of (4.82) for each factor. These fast fields have momentum modes restricted to a Wilson shell $[b^{-1}\Lambda, \Lambda)$, where Λ is an energy cutoff (less than the inverse lattice spacing), and $b \gtrsim 1$. The RG step of integrating over this shell is then equivalent to integrating out the fields U_f from the theory. This factorization of U is motivated by Polyakov's work on the O(3) nonlinear sigma model, which found the model's RG equations by a quadratic expansion of the 'fast fields' [126]. In Appendix D, we review this calculation, and also demonstrate the equivalence between Polyakov's decomposition and (4.83) for the SU(2) case.

We are now ready to insert (4.83) into our Lagrangian. But since we will be forced to make use of many identities involving the structure factors f_{ABC}, we choose to rewrite the Lagrangian in an equivalent form, which is derived in Appendix E.2. Neglecting the topological term, as it does not contribute to perturbative RG equations, this equivalent form reads

$$\mathcal{L} = \frac{1}{8g}\text{tr}[\partial_\mu(U^\dagger T_\gamma U)\partial_\mu(U^\dagger T_\gamma U)] + \lambda\frac{\sqrt{3}}{2}\epsilon_{\mu\nu}\text{tr}[\partial_\mu U U^\dagger T_8 \partial_\nu U U^\dagger T_3].\tag{4.84}$$

For convenience, we define the composite objects

$$M_A = U_s^\dagger T_A U_s \qquad N_\mu = \partial_\mu U_s U_s^\dagger\tag{4.85}$$

which will simplify our notation greatly. We now derive a perturbative Lagrangian by focusing on each term in (4.84) separately.

First term of (4.84)

We start by inserting $U = U_f U_s$ into the first term of (4.84), and expanding $U_f = \mathbb{I} + i\omega_a T_a - \frac{1}{2}\omega_a\omega_b T_a T_b + O(\omega^3)$. Then to leading order

$$U_f^\dagger T_\gamma U_f = T_\gamma - i\omega_a[T_a, T_\gamma] + \omega_a\omega_b T_a T_\gamma T_b - \frac{1}{2}\omega_a\omega_b\{T_a T_b, T_\gamma\}.\tag{4.86}$$

The quadratic term can be simplified by noting that since $\omega_a\omega_b$ is symmetric in a and b,

$$\omega_a\omega_b\left(T_a T_\gamma T_b - \frac{1}{2}\{T_a T_b, T_\gamma\}\right) = \frac{1}{4}\omega_a\omega_b\left([T_a, [T_\gamma, T_b]] + [T_b, [T_\gamma, T_a]]\right).\tag{4.87}$$

Now using the $\mathfrak{su}(3)$ algebra, and defining

$$h_{ab\gamma D} = \left(f_{acD} f_{\gamma bc} + f_{bcD} f_{\gamma ac} \right), \tag{4.88}$$

we obtain

$$U^\dagger T_\gamma U = M_\gamma + 2 f_{a\gamma b} \omega_a M_b - \omega_a \omega_b h_{ab\gamma D} M_D. \tag{4.89}$$

Derivatives and traces are now taken, resulting in

$$\text{tr}[(\partial_\mu (U^\dagger T_\gamma U))^2] = \tag{4.90}$$

$$\text{tr}[(\partial_\mu M_\gamma)^2] + 4 f_{a\gamma c} f_{b\gamma d} \partial_\mu \omega_a \partial_\mu \omega_b \text{tr}[M_c M_d] + 4 f_{a\gamma c} f_{b\gamma d} \omega_a \omega_b \text{tr}[\partial_\mu M_c \partial_\mu M_d]$$

$$+ 4 f_{a\gamma b} \partial_\mu \omega_a \text{tr}[\partial_\mu M_\gamma M_b] + 4 f_{a\gamma b} \omega_a \text{tr}[\partial_\mu M_\gamma \partial_\mu M_b]$$

$$+ 8 f_{a\gamma c} f_{b\gamma d} \partial_\mu \omega_a \omega_b \text{tr}[M_c \partial_\mu M_d] - 4 \partial_\mu \omega_a \omega_b h_{ab\gamma D} \text{tr}[\partial_\mu M_\gamma M_D]$$

$$- 2 \omega_a \omega_b h_{ab\gamma D} \text{tr}[\partial_\mu M_\gamma \partial_\mu M_D] + O(\omega^3).$$

We can simplify some terms. Using (E.4), we have

$$\text{tr}[M_c M_d] = \text{tr}[U_s^\dagger T_c U_s U_s^\dagger T_d U_s] = \text{tr}[T_c T_d] = 2\delta_{cd}. \tag{4.91}$$

Additionally,

$$\text{tr}[M_A \partial_\mu M_B] = \text{tr}[U_s \partial_\mu U_s^\dagger T_B T_A] + \text{tr}[\partial_\mu U_s U_s^\dagger T_A T_B] \tag{4.92}$$

$$= \text{tr}[\partial_\mu U_s U_s^\dagger [T_A, T_B]] \tag{4.93}$$

$$= 2i f_{ABC} \text{tr}[\partial_\mu U_s U_s^\dagger T_C] \tag{4.94}$$

and

$$h_{ab\gamma D} f_{D\gamma C} = -f_{DaE} f_{b\gamma E} f_{D\gamma C} - f_{DbE} f_{a\gamma E} f_{D\gamma C} = 0 \tag{4.95}$$

imply that the term proportional to $\partial_\mu \omega_a \omega_b h_{ab\gamma D}$ vanishes. The result is

$$\text{tr}[(\partial_\mu (U^\dagger T_\gamma U))^2] = \text{tr}[(\partial_\mu M_\gamma)^2] + 8(\partial_\mu \omega_a)^2 + 4 f_{a\gamma c} f_{b\gamma d} \omega_a \omega_b \text{tr}[\partial_\mu M_c \partial_\mu M_d]$$

$$+ 8i f_{abe} \partial_\mu \omega_a \omega_b \text{tr}[\partial_\mu U_s U_s^\dagger T_e] + 16i f_{ab\rho} \partial_\mu \omega_a \omega_b \text{tr}[\partial_\mu U_s U_s^\dagger T_\rho]$$

$$- 2 \omega_a \omega_b h_{ab\gamma D} \text{tr}[\partial_\mu M_\gamma \partial_\mu M_D]$$

plus linear terms in ω_a and higher-order corrections. For now, we neglect the linear terms: this will be justified shortly. Then, to quadratic order in ω_a, the first term of (4.84) can be written as

$$\frac{1}{8g} \text{tr}[(\partial_\mu (U^\dagger T_\gamma U))^2] = \tag{4.96}$$

$$\frac{1}{8g} \text{tr}(\partial_\mu M_\gamma)^2 + \frac{1}{8g}\Bigg[8(\partial_\mu \omega_a)^2 + 4 f_{a\gamma C} f_{b\gamma D} \omega_a \omega_b \text{tr}[\partial_\mu M_C \partial_\mu M_D]$$

$$+ 8i f_{abe} \partial_\mu \omega_a \omega_b \text{tr}[\partial_\mu U_s U_s^\dagger T_e] + 16i f_{ab\rho} \partial_\mu \omega_a \omega_b \text{tr}[\partial_\mu U_s U_s^\dagger T_\rho]$$

$$- 2 \omega_a \omega_b h_{ab\gamma D} \text{tr}[\partial_\mu M_\gamma \partial_\mu M_D]\Bigg].$$

Second term of (4.84)

We now perform the same expansion of U_f to simplify the second term of (4.84). Define

$$\mathcal{L}_q := \epsilon_{\mu\nu}\mathrm{tr}[\partial_\mu U U^\dagger T_8 \partial_\nu U U^\dagger T_3], \qquad N_\mu := \partial_\mu U_s U_s^\dagger. \qquad (4.97)$$

Then we have

$$\mathcal{L}_q = \quad \epsilon_{\mu\nu}\mathrm{tr}[\partial_\mu U_f U_f^\dagger T_8 \partial_\nu U_f U_f^\dagger T_3] + \epsilon_{\mu\nu}\mathrm{tr}[\partial_\mu U_f U_f^\dagger T_8 U_f N_\nu U_f^\dagger T_3] \qquad (4.98)$$
$$+ \epsilon_{\mu\nu}\mathrm{tr}[N_\mu U_f^\dagger T_8 \partial_\nu U_f U_f^\dagger T_3 U_f] + \epsilon_{\mu\nu}\mathrm{tr}[N_\mu U_f^\dagger T_8 U_f N_\nu U_f^\dagger T_3 U_f].$$

Using (4.89), this is

$$\mathcal{L}_q = \; + \epsilon_{\mu\nu}\mathrm{tr}[\partial_\mu U_f U_f^\dagger T_8 \partial_\nu U_f U_f^\dagger T_3] \qquad (4.99)$$
$$+ \epsilon_{\mu\nu}\mathrm{tr}[\partial_\mu U_f \left(T_8 + 2f_{a8b}\omega_a T_b - \omega_a\omega_b h_{ab8D} T_D\right) N_\nu U_f^\dagger T_3]$$
$$+ \epsilon_{\mu\nu}\mathrm{tr}[N_\mu U_f^\dagger T_8 \partial_\nu U_f \left(T_3 + 2f_{a3b}\omega_a T_b - \omega_a\omega_b h_{ab3D} T_D\right)]$$
$$+ \epsilon_{\mu\nu}\mathrm{tr}[N_\mu \left(T_8 + 2f_{a8b}\omega_a T_b - \omega_a\omega_b h_{ab8D} T_D\right) N_\nu \left(T_3 + 2f_{a3b}\omega_a T_b - \omega_a\omega_b h_{ab3D} T_D\right)].$$

Expanding the remaining U_f, and dropping a term proportional to $\partial_\mu\omega_a\partial_\nu\omega_b\epsilon_{\mu\nu}$ which vanishes after Fourier transforming, we find

$$\lambda\mathcal{L}_q = \epsilon_{\mu\nu}\lambda\frac{\sqrt{3}}{2}\Bigg[\mathrm{tr}[N_\mu T_8 N_\nu T_3] + \partial_\mu\omega_a\omega_b\mathrm{tr}[N_\nu T_b \left(T_3 T_a T_8 - T_8 T_a T_3\right)] \qquad (4.100)$$
$$+ \frac{1}{2}\partial_\mu(\omega_a\omega_b)\mathrm{tr}[N_\nu(T_8 T_a T_b T_3 - T_3 T_a T_b T_8)])]$$
$$+ \omega_a\omega_b(4f_{b3d}f_{a8c}\mathrm{tr}[N_\mu T_c N_\nu T_d] + \mathrm{tr}[N_\nu T_D N_\mu \left(h_{ab8D} T_3 - h_{ab3D} T_8\right)])$$
$$+ 2i\partial_\mu\omega_a\omega_b\mathrm{tr}[T_a T_c N_\nu \left(f_{b8c} T_3 - f_{b3c} T_8\right)],\Bigg]$$

where again we have omitted the terms linear in ω_a.

Discussion of linear terms

In both parts of (4.84), we have refrained from writing the terms linear in ω_a explicitly. We now justify this choice. After integrating by parts, all such terms are of the form

$$\omega_a F_a(\vec{x}) \qquad (4.101)$$

where $F_a(\vec{x})$ is a function of the slow matrices U_s, and involves two derivatives. Naively, we may argue that $\int d^2x \omega_a F_a(\vec{x}) = 0$, since ω_a only contains fast modes, while F_a is made of slow functions. However, since F_a contains *products* of slow modes, it will generically have some fast

modes; thus a different argument is required to justify neglecting these terms. We present two such arguments:

First, upon integrating out the fast fields, the contribution to the effective Lagrangian is

$$\delta\mathcal{L} = \frac{1}{2} \int d^2\vec{x} d^2\vec{y} F_a(\vec{x}) G_{ab}(\vec{x} - \vec{y}) F_b(\vec{y}), \tag{4.102}$$

where $G_{ab}(\vec{x})$ is the Green's function of the ω fields. In $\vec{k}$-space, this is

$$\delta\mathcal{L}(\vec{k}) = \frac{1}{2} \int_{b^{-1}\Lambda < |\vec{k}| < \Lambda} \frac{d^2\vec{k}}{(2\pi)^2} \frac{1}{k^2} F_a(\vec{k}) F_a(-\vec{k}) \tag{4.103}$$

because the ω fields only have momentum modes in the Wilson shell. Since $F(\vec{k})$ involves no more than four slow fields, k is restricted to $|k| < 4\tilde{\Lambda}$, where $\tilde{\Lambda} := b^{-1}\Lambda$. Following [126], we will take the limit $\tilde{\Lambda} \to 0$, and argue that $|\delta\mathcal{L}(\vec{k})| \to 0$. Indeed, since $F_a(\vec{k})$ contains two derivatives of slow modes,

$$|F(\vec{k})| < \tilde{\Lambda}^2 |\tilde{F}(\vec{k})| \tag{4.104}$$

for some operator $\tilde{F}(\vec{k})$ involving up to four slow fields, without derivatives. Therefore,

$$|\delta\mathcal{L}| < \frac{3}{2} \tilde{\Lambda}^3 \max_{\tilde{\Lambda} < |k| < 4\tilde{\Lambda}} |\tilde{F}(\vec{k})||\tilde{F}(-\vec{k})|. \tag{4.105}$$

Since $\tilde{F}(\vec{k})$ just involves products of slow fields, this maximum should be bounded by some $\tilde{\Lambda}$ independent constant as $\tilde{\Lambda} \to 0$, say $\max_{0 < |k| < \Lambda} |F(\vec{k})||\tilde{F}(-\vec{k})|$. Therefore $|\delta\mathcal{L}|$ vanishes as $\tilde{\Lambda}^3$. This is to be compared with the marginal kinetic term, $(\partial_\mu \omega_a)^2$, which only vanishes as $\tilde{\Lambda}^2$. This agrees with our naive intuition, that since $F_a(\vec{x})$ involves two derivatives, $\delta\mathcal{L}$ should consist of irrelevant operators; however, we are more careful here, since the momenta of $G_{ab}(\vec{x} - \vec{y})$ in (4.102) is restricted to the Wilson shell.

An alternative argument for neglecting linear terms is as follows. In the perturbative Lagrangian, the leading term that arises from $\omega_a(x)F_a(x)$ will correspond to a Feynman diagram with a single internal line. Since the leading g-dependent interaction is a four-point vertex, the simplest $O(\lambda)$ diagram arising from $\omega_a(x)F_a(x)$ will serve to renormalize a five-point or six-point interaction. Such diagrams can be excluded from a first-order perturbative calculation of $\beta(g)$ and $\beta(\lambda)$, which consider the four-point and three-point interactions, respectively.

4.5.3 Integration over a Wilson shell

Having justified the dropping of linear terms, we now Fourier transform the sum of (4.96) and (4.100) and perform Gaussian integrals over the ω_a. We use the general formula

$$\int \mathcal{D}[\phi] e^{-\int d^2x (\mathcal{L} - \mathcal{L}_0)} = N e^{-\frac{1}{2} \text{tr}[\log \int O]} \tag{4.106}$$

where O is a formal expression involving the Green's functions of ω_a. Following Polyakov's approach (reviewed in Appendix D), we expand the tr[log] to second order, since higher-order terms will involve more than two derivatives acting on the U_s, and correspond to irrelevant operators. The slow functions appearing in the linear term of this expansion can be replaced by their averages, as in (D.7). Meanwhile, the quadratic terms of the tr[log] can be approximated using (D.11). Notice that terms proportional to $\partial_\mu\omega_a\omega_b$ do not contribute to linear order, according to (D.8). The result is

$$\text{tr}[\log O] = \tag{4.107}$$

$$\int d^2x \bigg(\int \frac{d^2k}{(2\pi)^2} \Big(\frac{1}{2k^2} f_{a\gamma C} f_{a\gamma D} \text{tr}[\partial_\mu M_C \partial_\mu M_D] - \frac{1}{4k^2} h_{aa\gamma D} \text{tr}[\partial_\mu M_\gamma \partial_\mu M_D] \Big)$$

$$- \frac{1}{2} \int \frac{d^2k}{(2\pi)^2} \frac{k_\mu k_\nu}{k^4} \Big(f_{abE} \text{tr}[N_\mu T_E] + f_{ab\rho} \text{tr}[N_\mu T_\rho] \Big)^2$$

$$+ \sqrt{3} \int \frac{d^2k}{(2\pi)^2} \Big(\frac{2}{gk^2} \lambda f_{a3d} f_{a8c} \epsilon_{\mu\nu} \text{tr}[N_\mu T_c N_\nu T_d] + \frac{g}{2k^2} \lambda \epsilon_{\mu\nu} \text{tr}[N_\nu T_D N_\mu (h_{aa8d} T_3 - h_{aa3D} T_8)] \Big)$$

$$+ \sqrt{3} \lambda g \int \frac{d^2k}{(2\pi)^2} \frac{k_\mu k_\rho \epsilon_{\rho\nu}}{k^4} \Big(f_{abE} \text{tr}[N_\mu T_E] + f_{ab\gamma} \text{tr}[N_\mu T_\gamma] \Big)$$

$$\times \Big(+ \frac{i}{2} (\text{tr}[T_b T_8 N_\nu T_a T_3] - \text{tr}[N_\nu T_a T_8 T_b T_3]) - \text{tr}[N_\nu (f_{a8c} T_3 T_b T_c - f_{a3c} T_8 T_b T_c)]$$

$$+ \frac{i}{4} \text{tr}[N_\nu (T_8 \{T_a, T_b\} T_3 - T_3 \{T_a, T_b\} T_8)] \Big) \bigg) + \text{higher-order corrections.}$$

Here the integration over k is restricted to the Wilson shell. The *first line* can be simplified using $h_{aa\gamma D} = 6\delta_{\gamma D}$, and (E.7). The *second line* can be simplified using

$$\Big(f_{abE} \text{tr}[N_\mu T_E] + f_{ab\rho} \text{tr}[N_\mu T_\rho] \Big)^2 = -12(\text{tr}[N_\mu T_\gamma])^2 - (\text{tr}[N_\mu T_a])^2. \tag{4.108}$$

The *third line* can be simplified too. Since $f_{a8c} f_{a3d}$ vanishes unless $c = d$, the first term is proportional to $\epsilon_{\mu\nu} \text{tr}[N_\mu T_c N_\nu T_c] = 0$. Using $h_{aa\gamma D} = 6\delta_{\gamma D}$, the whole third line is

$$6\sqrt{3} g \lambda \epsilon_{\mu\nu} \int \frac{d^2k}{(2\pi)^2} \frac{1}{k^2} \text{tr}[N_\nu T_8 N_\mu T_3]. \tag{4.109}$$

The *last line* can be dropped, since it is symmetric in a, b and multiplies terms proportional to $f_{ab\gamma}$. Finally, we use the momentum-shell integrals

$$\int_{b^{-1}\Lambda < k < \Lambda} \frac{d^2k}{(2\pi)^2} \frac{1}{k^2} = \frac{1}{2\pi} \log b \qquad \int d^2k \frac{k_\mu k_\nu}{k^4} g(k^2) = \int d^2k \frac{1}{2k^2} g(k^2) \tag{4.110}$$

for a general function $g(k^2)$. At last, we arrive at

$$\text{tr}[\log O] \approx \int d^2x \left(\frac{\log b}{4\pi} \left(\text{tr}[(\partial_\mu M_c)^2] - 3\text{tr}[(\partial_\mu M_\gamma)^2] \right) + \frac{\log b}{8\pi} \left(12(\text{tr}[N_\mu T_A])^2 - 11(\text{tr}[N_\mu T_a])^2 \right) \right.$$

(4.111)

$$+ 3\sqrt{3}(\log b)g\lambda\epsilon_{\mu\nu}\text{tr}[N_\nu T_8 N_\mu T_3] + i\sqrt{3}\frac{\epsilon_{\mu\nu}\lambda g \log b}{8\pi}\left(f_{abE}\text{tr}[N_\mu T_E] + f_{ab\gamma}\text{tr}[N_\mu T_\gamma] \right)$$

$$\left. \times \left((\text{tr}[N_\nu T_a T_3 T_b T_8] - \text{tr}[N_\nu T_a T_8 T_b T_3]) + 2i\text{tr}[N_\nu(f_{a8c}T_3 T_b T_c - f_{a3c}T_8 T_b T_c)] \right) \right).$$

Now, we make use of various identities proven in Appendix E. The identities (E.16) and (E.21) let us rewrite the first line as

$$-\frac{5\log b}{16\pi}\text{tr}[(\partial_\mu M_\gamma)^2].$$

(4.112)

Now consider the last term:

$$A := i\sqrt{3}\frac{\epsilon_{\mu\nu}\lambda g \log b}{8\pi}\left(f_{abE}\text{tr}[N_\mu T_E] + f_{ab\gamma}\text{tr}[N_\mu T_\gamma] \right)$$

(4.113)

$$\times \left((\text{tr}[N_\nu T_a T_3 T_b T_8] - \text{tr}[N_\nu T_a T_8 T_b T_3]) + 2i\text{tr}[N_\nu(f_{a8c}T_3 T_b T_c - f_{a3c}T_8 T_b T_c)] \right).$$

The first term of the second line is simplified using (E.26). Then antisymmetry in a and b imply

$$A = -\sqrt{3}\frac{\epsilon_{\mu\nu}\lambda g \log b}{8\pi}\left(f_{abE}\text{tr}[N_\mu T_E] + f_{ab\gamma}\text{tr}[N_\mu T_\gamma] \right)$$

(4.114)

$$\times \left(f_{3bc}\text{tr}[N_\nu(T_a T_c T_8 - T_8 T_a T_c)] + f_{8bc}\text{tr}[N_\nu(T_3 T_a T_c - T_a T_c T_3)] \right.$$

$$\left. + f_{3ac}\text{tr}[N_\nu(T_8 T_b T_c - T_b T_c T_8)] + f_{8ac}\text{tr}[N_\nu(T_b T_c T_3 - T_3 T_b T_c)] \right).$$

Now we use (E.28) to simplify this to:

$$A = -2\sqrt{3}i\frac{\epsilon_{\mu\nu}\lambda g \log b}{8\pi}\left(f_{abE}\text{tr}[N_\mu T_E] + f_{ab\gamma}\text{tr}[N_\mu T_\gamma] \right)\text{tr}[N_\nu T_d T_c]\left(f_{3bc}f_{a8d} + f_{8bc}f_{3ad} + f_{3ac}f_{8bd} + f_{8ac}f_{b3d} \right).$$

(4.115)

Recognizing the antisymmetry, this is

$$A = -\sqrt{3}4i\frac{\epsilon_{\mu\nu}\lambda g \log b}{4\pi}\text{tr}[N_\nu T_d T_c]\left(f_{abE}\text{tr}[N_\mu T_E] + f_{ab\gamma}\text{tr}[N_\mu T_\gamma] \right)\left(f_{8bc}f_{3ad} + f_{3ac}f_{8bd} \right). \quad (4.116)$$

Now we use (E.33). The result is

$$A = \sqrt{3}i\frac{\epsilon_{\mu\nu}\sqrt{3}\lambda g \log b}{2\pi}\left(\text{tr}[N_\mu T_1 \text{tr} N_\nu T_2] - \text{tr}[N_\mu T_4 \text{tr} N_\nu T_5] + \text{tr}[N_\mu T_6 \text{tr} N_\nu T_7] \right). \quad (4.117)$$

Now we need to prove that the operator appear here is proportional to $\mathcal{L}_0^q$. This is (E.41):

$$\epsilon_{\mu\nu}\Big(\text{tr}[N_\mu T_1 \text{tr} N_\nu T_2] - \text{tr}[N_\mu T_4 \text{tr} N_\nu T_5] + \text{tr}[N_\mu T_6 \text{tr} N_\nu T_7]\Big) = -i\sqrt{3}\text{tr}[N_\mu T_8 N_\nu T_3]. \tag{4.118}$$

Therefore,

$$A = \lambda \frac{\sqrt{3}}{2} \frac{3g \log b}{4\pi} \epsilon_{\mu\nu} \text{tr}[N_\mu T_8 N_\nu T_3]. \tag{4.119}$$

Now we return to the Lagrangian, which requires dividing (4.111) by 2. Using (4.119) and (4.112), this is

$$\mathcal{L} = \frac{1}{8g}\left(1 - g\frac{5\log b}{16\pi}\right)\text{tr}[\partial_\mu M_\gamma \partial_\mu M_\gamma] + \frac{\sqrt{3}}{2}\lambda\epsilon_{\mu\nu}\text{tr}[N_\mu T_8 N_\nu T_3]\Big(1 - 2\frac{3g}{2\pi}\log b + 2\frac{g\log b}{4\pi}3\Big). \tag{4.120}$$

This allows for the identification of

$$\lambda_{\text{eff}} = \lambda\left(1 - \frac{3g}{2\pi}\log b\right) \qquad g_{\text{eff}} = g\left(1 - \frac{5g\log b}{4\pi}\right)^{-1} \tag{4.121}$$

from which we can read off the β functions:

$$\beta_g(\lambda, g) = \frac{5g^2}{4\pi} \qquad \beta_\lambda(\lambda, g) = -\frac{3g\lambda}{2\pi}. \tag{4.122}$$

4.5.4 Results of the RG calculations

Let us consider each beta function in turn. First off, we conclude that g is a relevant parameter: Since it has a positive beta function, it flows to large values at large length scales. Such behaviour is referred to as asymptotic freedom, since the opposite flow towards short length scales, or equivalently high energies, renders the theory 'free' (i.e. $g \to 0$). This is precisely the behaviour that occurs in the $\mathbb{CP}^1$ sigma model considered in Chapter 2. In fact, asymptotic freedom is known to occur in $\mathbb{CP}^{n-1}$ for all $n > 2$, and so our result should not be that surprising, since we have demonstrated in (4.53) that the flag manifold can be viewed as three coupled $\mathbb{CP}^2$ fields.[25] A fact that we will use repeatedly throughout this thesis is that in the absence of topological angles, asymptotic freedom indicates the presence of a finite energy scale in the theory. In other words, when θ is trivial (corresponding to p being a multiple of 3), we expect our sigma model, and thus our underlying SU(3) chain, to exhibit a finite energy gap. This is our first result that will lead us to an SU(3) generalization of Haldane's conjecture.

Now let us turn to the beta function for λ. At first glance, it appears that the λ-term is irrelevant: at large length scales λ will flow to zero and we may drop it from our analysis. Unfortunately, this is not the complete story. Recall that we are doing RG calculations for a perturbative Lagrangian,

---

[25]However, a critical difference between the theories $\mathbb{CP}^1$ and $\mathbb{CP}^{n-1}$ for $n > 2$ is that the latter is known to exhibit a finite mass gap even in the presence of topological angle. This is where the intuition of a flag manifold as being coupled $\mathbb{CP}^{n-1}$ sigma models dramatically breaks down.

obtained by replacing U with $e^{i\omega_a T_a}$ in (4.42). The kinetic term that results upon this replacement is

$$\mathcal{L}_0 = \frac{1}{g}\partial_\mu\omega_a\partial_\mu\omega_a. \tag{4.123}$$

In order to obtain the more familiar kinetic term of free bosons, we must rescale the fields according to $\omega_a \to \sqrt{\frac{g}{2}}\omega_a$. As a result, the perturbative Lagrangian we obtain has the following structure

$$\mathcal{L} = \frac{1}{2}\partial_\mu\omega_a\partial_\mu\omega_a + i\lambda g^{\frac{3}{2}}\epsilon_{\mu\nu}R_{abc}\omega_a\partial_\mu\omega_b\partial_\nu\omega_c + gP_{abcd}\omega_a\omega_b\partial_\mu\omega_c\partial_\mu\omega_d + O(\lambda g^2) + O(g^2) \tag{4.124}$$

where R_{abc} and P_{abcd} are tensors of real coefficients that can be expressed in terms of the SU(3) structure factors. At this order in perturbation theory, the imaginary term does not have coupling constant λ. Instead, its coupling constant is $\tilde{\lambda} = \lambda g^{3/2}$. Therefore, in order to accurately assess the relevance of the imaginary term, we must calculate the beta function of $\tilde{\lambda}$, and determine its sign. Since

$$\beta_{\tilde{\lambda}}(\lambda, g) = g^{\frac{3}{2}}\beta_\lambda + \frac{3}{2}g^{\frac{1}{2}}\lambda\beta_g = \frac{3g}{8\pi}\tilde{\lambda} > 0 \tag{4.125}$$

we conclude that the imaginary term in (4.124) is also relevant. Therefore, any comprehensive phase diagram of the symmetric SU(3) must include axes for both λ and g. Despite this fact, a novel interpretation of RG flows based on 't Hooft anomalies suggests that it may be safe to neglect the λ-term in many cases. This will be explained shortly. As a consequence, in some of the arguments that follow, we will make the simplifying assumption that $\lambda = 0$.

4.6 Phase Diagram of the Symmetric SU(3) Chain

At this stage, let us reflect on our findings. Given an SU(3) chain in the rank-p symmetric representation, we have obtained a mapping to an SU(3)/[U(1)]^2 flag manifold sigma model, with topological angles $\theta = \pm\frac{2\pi p}{3}$. In the absence of these angles, i.e. when $p = 3k$ for some $k \in \mathbb{Z}_+$, we expect this sigma model, and thus the underlying chain, to exhibit a finite mass gap.

Meanwhile, we have learned from the exact results of Chapter 3 that when the angles are nontrivial ($p \neq 3k$), the LSMA theorem forbids such a finite mass gap in the SU(3) chain, unless translation symmetry is spontaneously broken (see Section 3.5.2). This is consistent with the fact that the spectrum of the chain with $p = 1$ is known exactly, and it does not exhibit a finite energy gap (see Section 3.5.1). When $p = 3k$, the LSMA theorem breaks down, which is consistent with our sigma model conclusions, and also the SU(3) AKLT model, which explicitly constructs a translationally invariant SU(3) chain with a finite energy gap, as shown in Figure 3.6.

Together, these facts suggest that there should exist a gapless phase in the SU(3) chain driven by topological effects. In other words, there should exist a critical coupling g_c, below which the model exhibits gapless excitations. Above g_c, translation symmetry will be spontaneously broken with 3-fold ground state degeneracy. Indeed, this is consistent with the findings of Corboz et. al. [109], who found a trimerized phase in the $J_1 - J_2$ SU(3) Heisenberg model. According to our expression

for the coupling constant (4.43), g is an increasing function of J_2, and so we expect that for J_2 sufficiently large, the system will correspond to $g > g_c$, and will be gapped with a spontaneous breakdown of the $\mathbb{Z}_3$ symmetry.

See Figure 4.1 for our proposed phase diagram. So far, we haven't discussed the model at $\theta = \pi$, which corresponds to a model that explicitly breaks the $\mathbb{Z}_3$ symmetry, and thus breaks translation symmetry in the chain model. This aspect of the phase diagram, as well as the other ground state degeneracy predictions, will be justified in the following subsections.
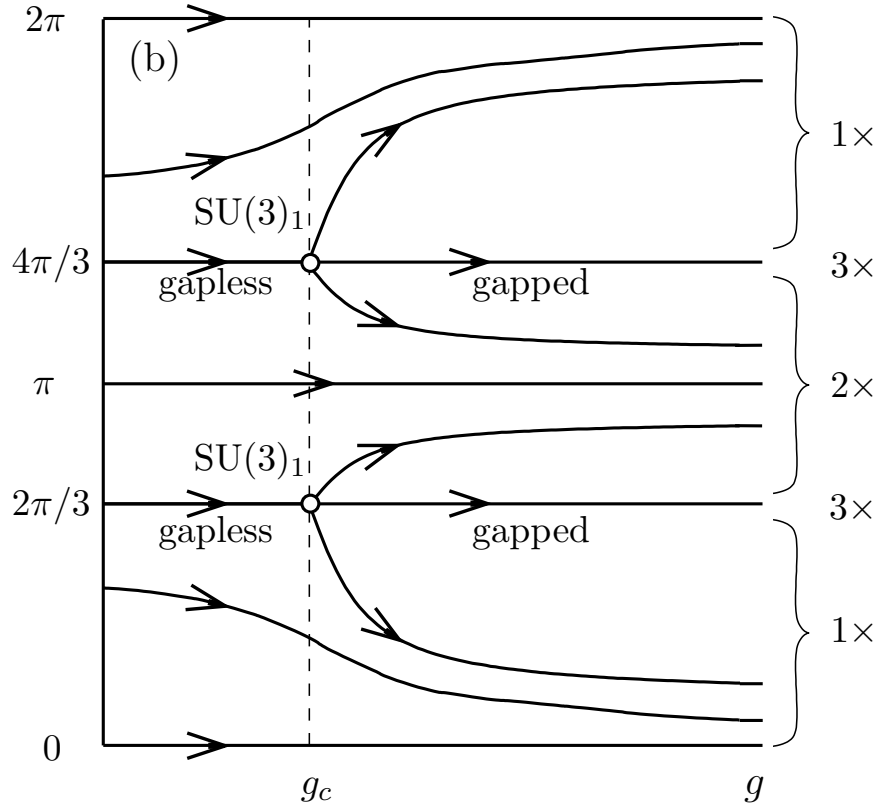
Figure 4.1: Phase diagram of the SU(3) chain in the rank-p symmetric representation. The angle, $\theta = \frac{2\pi p}{3}$, vanishes when p is a multiple of 3.

Let us compare our phase diagram to what occurs in the $\mathbb{CP}^1$ sigma model of the SU(2) chain (see Figure 2.1). Both include gapless phases that are characterized by SU$(n)_1$ Wess-Zumino-Witten CFTs, and occur when $\theta = \frac{2\pi}{n}$. Indeed, this will be a general trait of symmetric SU(n) chains – a fact that we will prove in following chapter, after a great deal of work. Both also include gapped phases at $\theta = 0$; it is here that the AKLT-like models reside. What is unique to SU(3) is the

2-fold degeneracy at $\theta = \pi$, which can only be realized by explicitly breaking translation symmetry, and will be shown below.

As it stands, our arguments are very similar to those initially put forward by Haldane, and so perhaps one is also tempted to caveat our prediction as a 'conjecture'. However, just as modern developments have bolstered Haldane's original arguments, there exist additional results in SU(3) which support our findings. We now review each of these in turn.

4.6.1 Monte Carlo simulations

In order to verify the effect of topological angle on mass gap in the SU(3) chain, classical Monte Carlo simulations were carried out by Lajkó in [1]. Typically, such a calculation is not possible due to the sign-problem related to the pure-imaginary nature of the topological term. However, this issue was resolved using a clever method of Allés and Papa, which first carries out the simulations for imaginary topological angles $\vartheta = -i\theta$, and then extrapolates to real angles [33, 36]. This procedure works only if we exclude the λ-term from our analysis (which is also a pure-imaginary term, and contributes to the sign problem). Explicitly, the topological pat of the action was discretized by splitting each square plaquette (in 2d Euclidean space) into two triangles [127], and defining a local topological charge density q_α according to

$$e^{i2\pi q_\alpha(\Delta_{ijk})} = \frac{(\boldsymbol{\varphi}^{*,\alpha}(\vec{r}_i) \cdot \boldsymbol{\varphi}^\alpha(\vec{r}_j))(\boldsymbol{\varphi}^{*,\alpha}(\vec{r}_j) \cdot \boldsymbol{\varphi}^\alpha(\vec{r}_k))(\boldsymbol{\varphi}^{*,\alpha}(\vec{r}_k) \cdot \boldsymbol{\varphi}^\alpha(\vec{r}_i))}{|\boldsymbol{\varphi}^{*,\alpha}(\vec{r}_i) \cdot \boldsymbol{\varphi}^\alpha(\vec{r}_j)||\boldsymbol{\varphi}^{*,\alpha}(\vec{r}_j) \cdot \boldsymbol{\varphi}^\alpha(\vec{r}_k)||\boldsymbol{\varphi}^{*,\alpha}(\vec{r}_k) \cdot \boldsymbol{\varphi}^\alpha(\vec{r}_i)|}. \tag{4.126}$$

Here Δ_{ijk} is the triangle with nodes i, j and k defined in clockwise order. Combining these topological charge densities with the discretized real action,

$$-\frac{1}{2g} \sum_{\alpha=1}^{2} \sum_{\mu=x,\tau} \left|\boldsymbol{\varphi}^{*,\alpha}(\vec{r}_j) \cdot \boldsymbol{\varphi}^\alpha(\vec{r}_j + \vec{\delta}_\mu)\right|^2, \tag{4.127}$$

the algorithm proceeds by sampling the time averaged correlation functions,

$$C(x) = \frac{1}{L} \sum_{\tau} \left\langle (\boldsymbol{\varphi}^1(0,0) \cdot \boldsymbol{\varphi}^{*,1}(x,\tau))(\boldsymbol{\varphi}^{*,1}(0,0) \cdot \boldsymbol{\varphi}^1(x,\tau)) \right\rangle. \tag{4.128}$$

Note that the λ-term is neglected in these simulations. The correlation length can then be extracted by fitting $C(x)$ with an exponential; its inverse defines the mass gap above the ground state that we seek. The mass gap is extracted from imaginary to real angles using the fitting function $(c_1 + c_2\theta^2)/(1 + c_3\theta^2)$ [33, 36].

In Figure 4.2, the results of these Monte Carlo simulations for the SU(3) chain can be found. For completeness, we also include similar results for the SU(2) chain in Figure 4.3. As expected, when $\theta = 0$ a finite mass gap exists for all values of g, in both SU(3) and SU(2). However, for sufficiently small g, this mass gap closes for particular values of θ^2: in SU(3), this occurs at $\theta = \pm\frac{2\pi}{3}$, and in SU(2), this occurs at $\theta = \pm\pi$. These are precisely the topological angles that occur
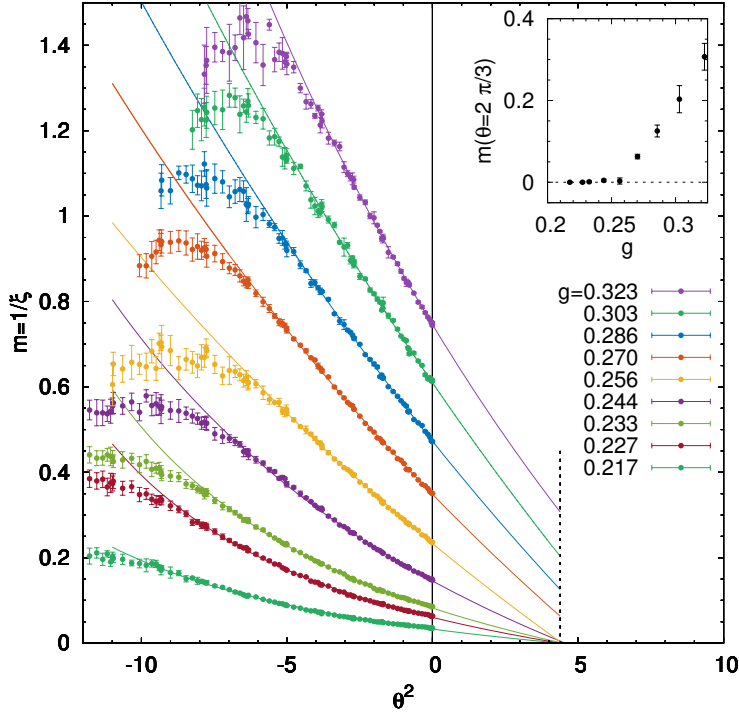
Figure 4.2: Monte Carlo simulations in the $SU(3)/[U(1)]^2$ sigma model, with $\lambda = 0$. By extrapolating from imaginary topological angles, we see that below a critical coupling, the mass gap closes at $\theta = \pm 2\pi/3$.

in our flag manifold sigma models when p is not a multiple of n, for $n = 2, 3$. We believe the finite mass gap that persists beyond some critical coupling g_c, which is approximately 2.55 in SU(3), corresponds to a phase transition from a gapless phase into a gapped phase with spontaneously broken translation symmetry, in accordance with the LSMA theorem. Therefore, these Monte Carlo simulations present strong evidence in favour of our proposed phase diagram in Figure 4.1.

4.6.2 Strong coupling analysis

A second calculation, also led by Lajkó in [1], was to consider the $g \to \infty$ limit of the flag manifold sigma model, with λ set to zero. In this limit, the action consists only of a topological term, and can be used to extract information about ground state degeneracies. Indeed, a similar calculation was originally carried out by Seiberg in [104] and Plefka and Samuel in [105] for $\mathbb{CP}^{n-1}$ sigma models, and their findings were in agreement with the far-right side of the SU(2) phase diagram in Figure 2.1. In particular, the presence of a finite gap for all values of θ follows from the fact
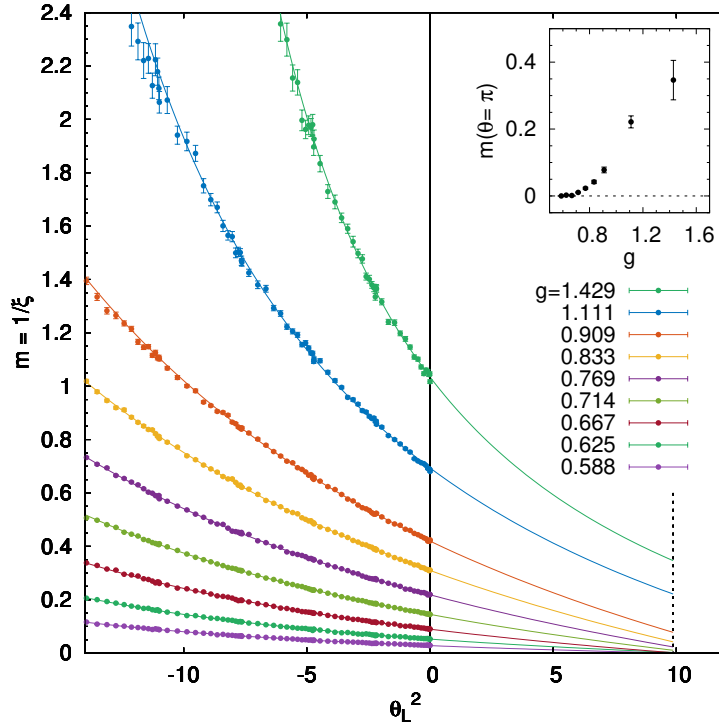
Figure 4.3: Monte Carlo simulations in the $\mathbb{CP}^1$ sigma model (corresponding to the SU(2) chain). Below a critical coupling, we see that the mass gap closes at $\theta = \pm\pi$.

that when the action is purely topological, the field φ^α become correlation free. Thus, we may also conclude that in SU(3), a finite gap will be universal in the limit $g \to \infty$.

In short, the strong coupling analysis of the sigma model involves obtaining the free energy density, by first developing a lattice version of the gauge-field formulation of the action, (4.60). It is found that in the limit $g \to \infty$, this density is given by

$$f(\theta_1, \theta_3) = -\log\left(\max_{m,n} z(\theta_1 + 2\pi m, \theta_3 + 2\pi n)\right), \tag{4.129}$$

where

$$\frac{1}{2}z(\theta_1, \theta_3) = \frac{(\theta_1 - \theta_3)\cos\left(\frac{\theta_1 - \theta_3}{2}\right) - \theta_1 \cos\left(\frac{\theta_1}{2}\right) + \theta_3 \cos\left(\frac{\theta_3}{2}\right)}{\theta_1 \theta_3 (\theta_1 - \theta_3)}. \tag{4.130}$$

Since (4.64) ensures that $\theta_1 = -\theta_3$ in our theories, we plot $f(\theta_1, \theta_3)$ along this line in Figure 4.4.

The cusp in the free-energy at $2\pi/3$ (the blue line) is indicative of a phase transition, and will be what we consider in this section. The behaviour at $\theta = \pi$ (the red line) corresponds to a model
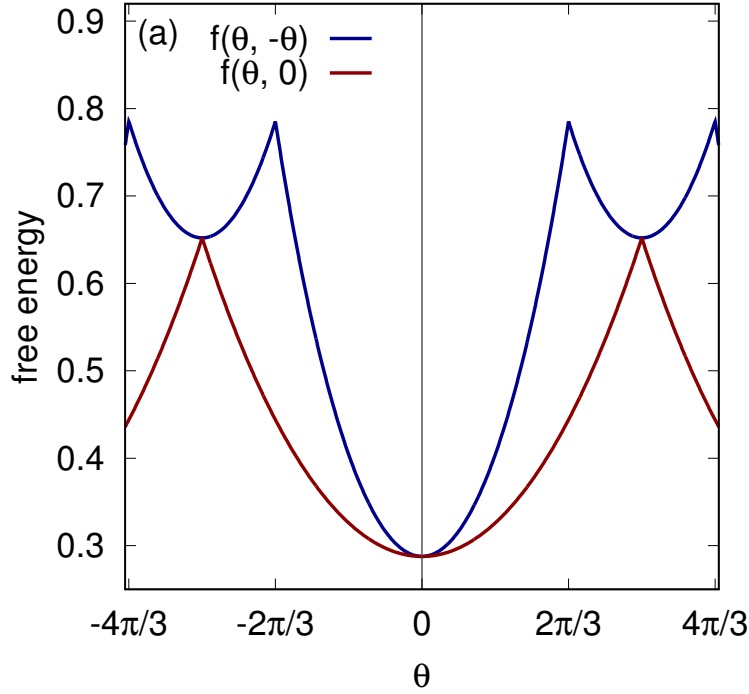
Figure 4.4: Free energy of the SU(3)/[U(1)]^2 sigma model at strong coupling. The blue line, corresponding to our model with two topological angles, exhibits a cusp at $\theta = \pm 2\pi/3$. The red line, corresponding to a single topological angle, exhibits a cusp at $\theta = \pm \pi$. This corresponds to the self-conjugate SU(3) chains, discussed in Section 4.7.

with explicitly broken $\mathbb{Z}_3$ symmetry, but possessing a $\mathbb{Z}_2$ parity symmetry. We will consider such a model in Section 4.7.

Since a finite mass gap is present for all values of θ in the strong coupling limit, it should be that the $\mathbb{Z}_3$ symmetry is spontaneously broken. We verify this explicitly by calculating the expectation value of the topological charge densities,

$$\langle q_1 \rangle = -i \frac{\partial f(\theta_1, \theta_3, g \to \infty)}{\partial \theta_1} \qquad \langle q_3 \rangle = -i \frac{\partial f(\theta_1, \theta_3, g \to \infty)}{\partial \theta_3} \qquad (4.131)$$

depending on from which sector $\mathcal{R}_{m,n}$ we approach the point $\theta_1 = -\theta_3 = 2\pi/3$. By sector, we mean

which values of m, n that maximize the free energy in (4.129). We find

$$
\begin{array}{c|ccc}
\begin{matrix}\theta_1 \to 2\pi/3 \\ \theta_3 \to -2\pi/3\end{matrix} & \langle q_1 \rangle & \langle q_2 \rangle & \langle q_3 \rangle \\
\hline
\text{from } \mathcal{R}_{0,0} & -i\frac{3}{2\pi} + i\frac{\sqrt{3}}{8} & 0 & i\frac{3}{2\pi} - i\frac{\sqrt{3}}{8} \\
\text{from } \mathcal{R}_{-1,0} & i\frac{3}{2\pi} - i\frac{\sqrt{3}}{8} & -i\frac{3}{2\pi} + i\frac{\sqrt{3}}{8} & 0 \\
\text{from } \mathcal{R}_{0,-1} & 0 & i\frac{3}{2\pi} - i\frac{\sqrt{3}}{8} & -i\frac{3}{2\pi} + i\frac{\sqrt{3}}{8}.
\end{array}
\tag{4.132}
$$

where $\langle q_2 \rangle$ was calculated using $q_2 = -(q_1 + q_3)$. These cases are connected by the $\mathbb{Z}_3$ transformation, clearly showing the spontaneous breaking of the symmetry.

4.6.3 Wess-Zumino-Witten models and the explicit breaking of $\mathbb{Z}_3$

The final two arguments that we mention here are related to the renormalization group flow of the SU(3) chain. As discussed in Section 3.5, we expect that any gapless critical point that occurs in our SU(3)/[U(1)]^2 flag manifold sigma model will be described by a particular CFT, the SU(3)$_1$ Wess-Zumino-Witten model. This relies crucially on the fact that the model possesses an additional $\mathbb{Z}_3$ symmetry; otherwise the relevant operator tr[g] will destabilize the theory, where g is a fundamental WZW field.[26] We comment in passing that SU(3)$_1$ has a marginal operator whose coupling constant will change sign at the phase transitions identified in Figure 4.1. That is to say, at strong enough coupling g in the sigma model, a marginal operator becomes marginally relevant, and drives a phase transition to a gapped phase with 3 ground states that spontaneously break translation symmetry. This is discussed further in Chapter 5.

Now, we consider what happens when the $\mathbb{Z}_3$ is explicitly broken, in order to predict the phase structure of the sigma model at topological angles other than $\theta = 0, \pm\frac{2\pi}{3}$.

Let us break the $\mathbb{Z}_3$ explicitly, but preserve a $\mathbb{Z}_2$ symmetry that exchanges g and $g^\dagger$. Then the following relevant operator is permitted:

$$
V = \rho(\text{tr}[g] + \text{tr}[g^\dagger]).
\tag{4.133}
$$

Here ρ is an undetermined coupling constant. This is what occurs, for example, when we preserve the parity symmetry (4.68) that interchanges $\boldsymbol{\varphi}^1$ and $\boldsymbol{\varphi}^3$. Such an explicit breaking could be achieved by altering the nearest-neighbour bonds between the 1 and 3 sites from J_1 to $J_1(1 + \delta)$. As a consequence of this, the topological angle θ is altered accordingly:

$$
\theta \to \frac{2\pi p}{3}\left(1 + \frac{J_2}{J_1 + J_2} - \frac{J_2}{J_1(1 + \delta) + J_2}\right).
\tag{4.134}
$$

We now consider two possible scenarios, distinguished by the sign of δ:

---

[26]Despite the confusing notation, we insist on using the standard variable g for our WZW fields, despite the fact that it has nothing to do with the sigma model's coupling constant, g.

- Case 1: $\delta > 0$ In this case, the bond is weakened, so that the underlying chain exhibits the following pattern

$$\cdots \text{W S S W S S W S S W S S} \cdots \tag{4.135}$$

where 'W' refers to a weaker bond, and 'S' to a stronger bond. Such a chain will form SU(3) singlets from the three sites adjacent to two 'S' bonds, resulting in a unique ground state. Since θ is shifted below $\frac{2\pi}{3}$, we predict a unique ground state for all values of θ until the critical value of $\theta = 0$.

- Case 2: $\delta < 0$ In this case, the bond is strengthened, and the chain's pattern becomes

$$\cdots \text{S W W S W W S W W S W W S} \cdots \tag{4.136}$$

Instead of forming singlets, now the chain will form $\bar{3}$ representations out of the two sites adjacent to a single 'S' bond.[27] Such '$3\bar{3}$ chains' are known to spontaneously dimerize and exhibit a finite energy gap [128, 129]. Since θ is shifted above $\frac{2\pi}{3}$, we predict a 2-fold degenerate ground state for angles in the interval $(\frac{2\pi}{3}, \frac{4\pi}{3})$, including the angle $\theta = \pi$.

The previous discussion justifies the right edge of Figure 4.1. Now let us return to the WZW operator V, defined in (4.133). We claim that ρ should have the following dependance on θ:

$$\rho \propto \left(\theta - \frac{2\pi}{3} \right). \tag{4.137}$$

Then, if we write the diagonal elements of the WZW fundamental g as $e^{i\vartheta}$, V becomes

$$V \propto \left(\theta - \frac{2\pi}{3} \right) \sum_{\alpha} \cos \vartheta_{\alpha}. \tag{4.138}$$

For values of θ less than $\frac{2\pi}{3}$, this term has a unique minimum with $\vartheta_{\alpha} = 0$, and corresponds to a unique ground state. On the other hand, for $\theta > \frac{2\pi}{3}$, V is minimized by the two values $\vartheta_{\alpha} = \pm\frac{2\pi}{3}$. Thus, with the form (4.137), we obtain the desired degeneracies.

4.6.4 't Hooft anomaly matching

Finally, we discuss the notion of 't Hooft anomaly matching [106, 107]. In short, the presence of an 't Hooft anomaly signifies nontrivial low energy physics. In one spatial dimension this necessitates a gapless phase so long as the symmetries of the model are not spontaneously broken. Often, this consequence is described as a field-theoretic version of the LSMA theorem. In this subsection, we first review the theory of 't Hooft anomalies, and then cite results that apply to our SU(3) chains.

In order to understand 't Hooft anomalies, we must first define anomalies themselves. Consider a quantum theory which has a symmetry group G that leaves the classical action invariant. We say

---

[27]The $\bar{3}$ representation of SU(3) has a Young tableau with $p_1 = p_2 = 1$, that is, ⊟.

that G is anomalous if G is violated in the full quantum theory. Thus anomalous symmetries are symmetries of classical theories which do not survive the transition to quantum mechanics. For instance, if G is a continuous global symmetry, then it has a conserved current j_μ^A with A labeling the generators of G. If this symmetry is anomalous, then there are quantum corrections which makes the divergence of j_μ^A nonzero:

$$\partial^\mu j_\mu^A = \mathcal{A}^A. \tag{4.139}$$

The quantity $\mathcal{A}^a$ on the right hand side of this equation is what is referred to as the anomaly. The chiral anomaly in quantum electrodynamics is the prototypical example of this behaviour [130].

So far, what we have said applies to global symmetries. If instead G is a gauge symmetry, then anomalies indicate a fundamental inconsistency of the theory and must vanish. Recall that gauge symmetries are not conventional symmetries that act on the configuration space and lead to identical physics. Rather, they are redundancies in our description of the physics when we work in the space of gauge fields rather than its quotient by gauge transformations. While these gauge anomalies tell us our theory is sick, they can be used as a field theoretical tool, as was first shown by 't Hooft [106]. Given a theory with an exact global symmetry G (no anomaly), we can imagine 'gauge-ing' the symmetry by introducing gauge bosons B_μ^A, minimally coupled to the theory according to the prescription

$$\partial_\mu \mapsto \partial_\mu - igB_\mu^A T^A \tag{4.140}$$

for generators T^A of G. If this G-gauge theory is anomalous, we say that the original theory has an 't Hoot anomaly. Thus, 't Hooft anomalies do not invalidate the global symmetry, but they lead to powerful constraints on the phases of the theory.

The utility of 't Hooft anomalies stems from their nonrenormalization property: the anomaly is independent of energy scale. This implies that it can be calculated exactly using the low energy degrees of freedom, which is precisely what we access when we derive field theory descriptions of condensed matter systems. In one spatial dimension, if a symmetry with an 't Hooft anomaly is not spontaneously broken, we therefore may conclude that there exist low-lying excitations in the theory.[28] Otherwise, there would be no degrees of freedom to couple to the gauge fields and generate the anomaly.

Let us now turn to the $\mathbb{CP}^1$ sigma model of the spin chain, which will prepare us for our discussion of 't Hooft anomalies in SU(3) chains below. While there are no pure 't Hooft anomalies as we've defined them above, there are so-called mixed t' Hooft anomalies in $\mathbb{CP}^1$. By this we mean that if we gauge a continuous global symmetry, a second, independent symmetry becomes anomalous. For $\mathbb{CP}^1$, this mixed anomaly is between the continuous group PSU(2), and the discrete group of translations $\mathbb{Z}_2$. Here it is essential that we properly identify the continuous global symmetry of the model as PSU(2) = SU(2)/$\mathbb{Z}_2$, and not SU(2), since otherwise no anomaly would be detectable [78, 79, 132].[29] This is because SU(2) gauge fields have integer quantized topological

---

[28]In higher spatial dimensions there is another possibility: the system is gapped with some topological quantum field theory [131].

[29]This quotient by $\mathbb{Z}_2$ follows from the fact that the center of SU(2) acts trivially on the spin chain.

charge, while PSU(2) gauge fields can correspond to nontrivial sections of a PSU(2) bundle with half-integer quantized charge. Now, it is found that if one tries to gauge PSU(2), the $\mathbb{Z}_2$ group of translations is violated whenever $\theta = \pi$: the corresponding counterterm added to the Lagrangian to account for half-quantized PSU(2) gauge fields is not invariant under $\mathbb{Z}_2$. This is the 't Hooft anomaly, and implies that half-odd integer spin chains either have spontaneously broken translation symmetry, or gapless excitations. These possibilities reaffirm Haldane's conjecture, and are consistent with the phase diagram in Figure 2.1.

In the $SU(3)/[U(1)]^2$ sigma model, a similar 't Hooft anomaly result holds [78, 79]. When $\theta = \frac{2\pi}{3}$, there is a mixed anomaly between the continuous group $PSU(3) = SU(3)/\mathbb{Z}_3$ and $\mathbb{Z}_3$, the latter of which corresponds to translations in the SU(3) chain. Thus, when p is not a multiple of 3, we may conclude that either a gapless phase exists, or translation symmetry is spontaneously broken. This is entirely consistent with the phase diagram presented in Figure 4.1.

In fact, the nonrenormalizaiton of 't Hooft anomalies provides further evidence that the critical point characterizing these gapless phases indeed corresponds to the $SU(3)_1$ universality class. In [78, 79], the anomalies for both our flag manifold sigma model and the $SU(3)_1$ WZW model were calculated, and were shown to agree. Thus, a renormalization group flow from one to the other is completely plausible. We will have more to say on how 't Hooft anomalies constrain renormalization group flow of these flag manifold sigma models in the following chapter.

4.7 Other SU(3) Chains

Before concluding this chapter, we turn to the remaining representations of SU(3): those which have Young tableaux with row lengths p_1 and $p_2 \neq 0$. According to the discussion in Section 3.4, so long as $p_1 \neq p_2$, it suffices to consider a nearest-neighbour Heisenberg Hamiltonian (i.e. $J_2 = 0$). The edge case $p_1 = p_2$ corresponds to a representation that is conjugate to a symmetric model with $p = p_1$, and leads to the same sigma model as the symmetric chains presented above. In the following, we attempt to generalize our symmetric SU(3) calculations to this more general setting of $p_1 \neq p_2 \neq 0$.

4.7.1 Classical ground states and mixed order parameters

In Section 3.4, we already established the classical ground states of these more general SU(3) chains. Using the pictorial notation from that chapter, a typical ground state is

$$\cdots \quad \bullet \ \bullet \ \bullet \ \bullet \ \bullet \ \bullet \ \bullet \quad \cdots \tag{4.141}$$

$$\cdots \quad \bullet \ \bullet \ \bullet \ \bullet \ \bullet \ \bullet \ \bullet \quad \cdots . \tag{4.142}$$

Unlike the symmetric ones, these representations correspond to states with 2-site order. Another novel property is the existence of both ferromagnetic and antiferromagnetic order parameters. Indeed, we have that

$$\langle S_{\alpha\beta}(2j) \pm S_{\alpha\beta}(2j+1) \rangle \neq 0 \tag{4.143}$$

for both the choices of '+' and '-', which follows from the equation

$$\langle S_{\alpha\beta}(\cdot)\rangle = \begin{cases} p_1\phi_\alpha^{*,1}\phi_\beta^1 + p_2\phi_\alpha^{*,3}\phi_\beta^3 & \cdot = 2j \\ p_1\phi_\alpha^{*,3}\phi_\beta^2 + p_2\phi_\alpha^{*,3}\phi_\beta^3 & \cdot = 2j+1 \end{cases} \tag{4.144}$$

The expectation values taken in (4.144) are with respect to SU(3) coherent states, which are a direct generalization of those in (4.28). We assume a lowest-order expansion, so that each ϕ^α is evaluated at the same site. Explicitly, the positive sign corresponds to a ferromagnetic order parameter, F,

$$F_{\alpha\beta} = \frac{1}{2}\langle S_{\alpha\beta}(2j) + S_{\alpha\beta}(2j+1)\rangle = \frac{2p_2 - p_1}{2}\phi_\alpha^{*,3}\phi_\beta^3, \tag{4.145}$$

and the negative sign corresponds to an antiferromagnetic order parameter, A,

$$A_{\alpha\beta} = \frac{1}{2}\langle S_{\alpha\beta}(2j) - S_{\alpha\beta}(2j+1)\rangle = \frac{p_1}{2}(\phi_\alpha^{*,1}\phi_\beta^1 - \phi_\alpha^{*,2}\phi_\beta^2). \tag{4.146}$$

If we recall our discussion of Coleman's theorem and spontaneous symmetry breaking in one spatial dimension, the presence of both F and A is rather interesting. On the one hand, we have an antiferromagnetic order parameter, which leads to linearly dispersing Goldstone bosons which are the source of infrared divergences when the symmetry is spontaneously broken. On the other hand, we have a ferromagnetic order parameter, which leads to quadratically dispersing Goldstone bosons.[30] Such bosons are not ruled out by infrared divergence considerations. Thus, in this general setting, it may be possible for the SU(3) symmetry to be partially broken spontaneously, so that quadratic Goldstone bosons persist, while the remaining degrees of freedom correspond to a true symmetry of the ground state [95–97]. In Chapter 6, we will further discuss these possibilities, and speculate on an entire flag manifold sigma model hierarchy that may arise in generic SU(n) chains. But for now, we turn to flavour-wave theory, and explicitly check that both linear and quadratic modes are indeed present in the spectrum.

4.7.2 Flavour-wave theory

Following Mathur and Sen [123], we write the matrix of generators, S, in terms of two 3-component commuting boson operators b_α^1 and b_α^2:

$$S_{\alpha\beta} = (p_1 - p_2)b_\alpha^{\dagger,1}b_\beta^1 - p_2 b_\beta^{\dagger,2}b_\alpha^2. \tag{4.147}$$

---

[30]That quadratically dispersing modes arise from a ferromagnetic order parameter can be understood as follows. When one derives an effective Lagrangian for Goldstone bosons corresponding to broken symmetry generators Q_α, there is a term linear in ∂_τ that is proportional to $\langle[Q_\alpha, Q_\beta]\rangle$ [95]. In the case of spin chains, these broken symmetry generators are $\hat{S}_x$ and $\hat{S}_y$, so that the linear time-derivative term depends on $\langle\hat{S}_z\rangle$. For ferromagnets, this is nonzero and quadratic dispersion results; for antiferromagnets it vanishes so that the leading time-derivative term in the Lagrangian is proportional to ∂_τ^2, and results in linear dispersion. These results extend in a straightforward way to the SU(n) order parameters discussed in the present section.

The classical ground state corresponds to $(p_1 - p_2)$ bosons of type b^1, and p_2 bosons of type b^2. Now, following the same steps as laid out in Section 4.2, including Holstein-Primakoff and Bogoliubov transformations, we obtain a diagonalized Hamiltonian involving 6 Goldstone bosons.[31] The dispersion relations of the bosons at small energies are as follows:

$$\omega_{1,2}(k) = 2J_1 p_1 |k| \qquad \omega_{3,4}(k) = \omega_{5,6}(k) = \begin{cases} \frac{2J_1(p_1-p_2)p_2|k|^2}{p_1-2p_2} & p_1 \neq 2p_2 \\ Jp_1|k| & p_1 = 2p_2 \end{cases} \qquad (4.148)$$

As expected, we find both linear and quadratic dispersion relations. However, for the special case of $p_1 = 2p_2$, only linear modes exist. This is consistent with the fact that the ferromagnetic order parameter (4.145) vanishes in this case. These representations are the so-called self-conjugate representations of SU(3), with Young tableaux

$$(4.149)$$

In the mathematical language of Bykov, we say that the self-conjugate representations correspond to a Lagrangian embedding, in which the total Berry phase of the unit cell vanishes [6, 71, 72].

Ultimately, we are interested in low energy theories that only possess linearly dispersing modes. This is so that the emergence of Lorentz invariance can be facilitated, which would lead to a flag manifold sigma model like the ones considered earlier in this chapter. Accordingly, we now restrict to the self-conjugate SU(3) chains, and derive a low energy description.

4.7.3 Low energy field theory and the absence of Lorentz invariance

The field theory derivation for self-conjugate SU(3) chains (i.e. those with $p_1 = 2p_2$) is very similar to that of Section 4.3 for the symmetric chains. Indeed, the only modification has to do with the coherent states that we use. Defining p according to $p = p_2 = p_1/2$, these coherent states are

$$|\phi^1, \phi^2\rangle = (\boldsymbol{\phi}^1 \cdot \boldsymbol{a}^{\dagger,1})^p (\boldsymbol{\phi}^2 \cdot \boldsymbol{a}^{\dagger,2})^p |0\rangle, \qquad (4.150)$$

with $\boldsymbol{\phi}^{*,1} \cdot \boldsymbol{\phi}^2 = 0$ and $|\boldsymbol{\phi}^\alpha|^2 = 1$. The $\boldsymbol{a}^\alpha$ are Schwinger bosons. After a series of lengthy calculations, we obtain the following action

$$S = \int dx d\tau \left(p^2 J_1 \left[4|\boldsymbol{\varphi}^{*,2} \cdot \partial_x \boldsymbol{\varphi}^1|^2 + |\boldsymbol{\varphi}^{*,3} \cdot \partial_x \boldsymbol{\varphi}^2|^2 + |\boldsymbol{\varphi}^{*,1} \cdot \partial_x \boldsymbol{\varphi}^3|^2 \right] \right. \qquad (4.151)$$

$$\left. + \frac{1}{4J} \left[4|\boldsymbol{\varphi}^{*,2} \cdot \partial_\tau \boldsymbol{\varphi}^1|^2 + |\boldsymbol{\varphi}^{*,2} \cdot \partial_\tau \boldsymbol{\varphi}^2|^2 + |\boldsymbol{\varphi}^{*,1} \cdot \partial_\tau \boldsymbol{\varphi}^3|^2 \right] \right) + S_{\text{top}}.$$

---

[31]Actually, flavour-wave theory also produces two spurious 'flat modes', with momentum-independent dispersion relations $\omega_{7,8}(k) = 4(p_1 - p_2)$. However, these modes do not lie entirely in the representation, and should be removed from the analysis. Indeed, they do not appear in the field theory.

Here

$$S_{\text{top}} = i\pi p(Q_1 - Q_2), \tag{4.152}$$

where Q_α is defined in (4.49), with $Q_\alpha \in \mathbb{Z}$. Note that the topological angle is now $\theta = \pi p$, instead of the value $\pm \frac{2\pi p}{3}$ found previously. Therefore, in the strong coupling limit the free energy of this model coincides with the red line in Figure 4.4.

Moreover, we observe that while this theory involves three complex fields $\boldsymbol{\varphi}^\alpha$, it does not possess the same symmetries of the symmetric chain's sigma model derived above. Most notably, there are now two distinct velocities, which prevents the theory from being invariant under Lorentz transformations. In a perturbative expansion, in which we replace the matrix $U_{\alpha\beta} = \varphi_\beta^\alpha$ with $e^{i\omega_a T_a}$, we find that four of the ω_a propagate with one velocity v, while the remaining two fields propagate with $v/2$. These velocities, as well as the counting of these modes, are in agreement with the flavour-wave findings of the previous subsection.

A further point of interest is that while this theory lacks Lorentz invariance, it does possess a symmetry that rules out the possibility of a λ-term. Indeed, the $\mathbb{Z}_2$ translation symmetry, which acts as

$$\boldsymbol{\varphi}^1 \mapsto \boldsymbol{\varphi}^2 \qquad \boldsymbol{\varphi}^3 \to -\boldsymbol{\varphi}^3, \tag{4.153}$$

or

🔴 ↔ 🔵 　　 🟢 → 🟢,

changes the sign of each term proportional to λ in (4.42). This symmetry is also responsible for restricting the number of velocities to 2, down from the most general possibility of 3. It also leads to the 2-fold degeneracy at strong coupling that we see at $\theta = \pi$ in the phase diagram, Figure 4.1.

4.7.4 Phase diagram

Let us consider how the phase diagram of these self-conjugate SU(3) chains should differ from that of the symmetric chains, Figure 4.1. Unfortunately, the LSMA theorem does not apply to these models, as can be seen by examining the proof in Section 3.5.2. The so-called twist operator that served to generate a distinct low-lying state acts trivially on the self-conjugate representations of SU(3), so that no conclusions may be drawn.

In fact, none of the arguments in favour of a gapless phase carry over to these SU(3) chains. There is no self-conjugate analogue of the Bethe-ansatz solvable model discussed in Section 3.5.1. Moreover, Monte Carlo analysis indicate a finite gap for all values of p [2]. And finally, the 't Hooft anomaly was related to the $\mathbb{Z}_3$ manifestation of translation invariance, and does not occur for the $\mathbb{Z}_2$ symmetry of a chain with a 2-site unit cell. These facts lead us to predict that there is no gapless phase in the self-conjugate SU(3) chain: there is a finite energy gap for every value of p.

That being said, there is still a way to distinguish between the cases of even and odd p. When p is even, we may write down a translationally invariant valence bond state, which is a self-conjugate generalization of the SU(3) AKLT state. This state is also invariant under the $\mathbb{Z}_2$ parity symmetry, (4.153). When p is odd, any translationally invariant AKLT-like state we attempt to write down necessarily breaks this parity symmetry. These states are shown in Figures 3.8 and 3.9. This leads

us to conclude that self-conjugate SU(3) chains with p odd will exhibit spontaneously broken parity symmetry. This is also supported by a strong coupling analysis, which finds broken parity when $\theta = \pi$, but not when $\theta = 0$.

4.8 Conclusion

In this chapter, we have generalized Haldane's conjecture to SU(3) chains in various representations. First, we considered the rank-p symmetric SU(3) chains, whose Young tableaux have a single row of p boxes. Such chains admit a low energy mapping to the SU(3)/[U(1)]^2 flag manifold sigma model, with topological angles $\theta = \pm 2\pi p/3$. By combining extensive renormalization group calculations with a collection of supporting arguments, including Monte Carlo simulations, a strong coupling analysis, 't Hooft anomaly matching conditions and known exact results for SU(3) chains, we proposed the phase diagram in Figure 4.1. In particular, we argued that when p is a multiple of 3, the SU(3) chain will exhibit a unique, gapped ground state, in a fashion similar to the integer-spin SU(2) chains. For all remaining values of p, we argued that gapless excitations would exist for small enough interaction strengths, with a transition to a phase with spontaneously broken translation symmetry at larger strengths.

Next, we considered SU(3) chains with 2-row Young tableaux. We demonstrated that in this more general setting, the spectrum is no longer purely linearly dispersing. Instead, there are both linear and quadratic low energy modes, which can be understood as arising from the mixed ferro- and antiferromagnetic order parameters that exist simultaneously in these models. This led us to focus on the self-conjugate representations, with $p_1 = 2p_2$, since these are the only other SU(3) representations with linear modes only. Again, a flag manifold sigma model description was obtained, but this time it lacks Lorentz invariance due to the presence of two distinct velocities. Consequently, we conclude that a gapless phase does not occur in the self-conjugate chains for any value of $p_1 = 2p_2$. When p_2 is odd, we further predict that parity symmetry is always spontaneously broken.

Our findings are summarized below in Table 4.1 for all SU(3) representations that lead to flag manifold sigma model descriptions.

Representation (p_1, p_2)	Spectrum
$(3k, 0)$	gapped; unique
$(3k \pm 1, 0)$	gapless
$(4k, 2k)$	gapped; unique
$(4k+2, 2k+1)$	gapped; 2-fold

Table 4.1: A generalization of the Haldane conjecture to SU(3) chains. We label representations by the lengths of their Young tableau's rows, p_1 and p_2. Here k is a positive integer.

Chapter 5

Symmetric SU(n) Chains

5.1 Introduction

In the previous chapter, we established a low energy mapping between the symmetric SU(3) chain and the SU(3)/[U(1)]^2 flag manifold sigma model. This model can be visualized as three copies of $\mathbb{C}P^2$ that are coupled via orthogonality. And since each copy of $\mathbb{C}P^2$ has the same velocity and coupling constant, the resulting flag manifold exhibits Lorentz invariance. This fact is not always guaranteed, as we saw when we studied the self-conjugate SU(3) chains, and were led to a sigma model with two distinct velocities.

In this chapter, we again focus on symmetric representations, but promote the symmetry group from SU(3) to SU(n) in general. We will attempt to derive a flag manifold sigma model description of these chains in a similar fashion; namely, by starting with flavour-wave theory and then deriving a path integral using SU(n) coherent states. As expected, the structure of an SU(n)/[U(1)]$^{n-1}$ manifold will emerge, equipped with $n-1$ topological angles that depend on the representation size, p. However, the unique velocity property in SU(3) that ensured Lorentz invariance will not prove to be a general property of SU(n). Instead, we will find that there exist $\lfloor \frac{n}{2} \rfloor$ unique velocities, which at first appears to be a major impediment to any SU(n) generalization of Haldane's conjecture. Indeed, any gapless phase should correspond to some Lorentz invariant conformal field theory, and so, perhaps these distinct velocities prevent such a phase from occurring.

The majority of the calculations in this chapter are devoted to resolving this concern. In particular, we make use of the renormalization group to study the flow of these distinct velocities as we change the energy scale of our theory. Ultimately, we will find that these velocities flow to a single unique value, so that Lorentz invariance emerges after all. At this point, we are then able to extend our SU(3) phase diagram to SU(n), and predict various gapless phases driven by topological terms. Again, we will rely on the presence of 't Hooft anomalies, as well as more general results about the renormalization group flow of conformally invariant field theories with SU(n) symmetry, namely the SU(n)$_k$ WZW models. Our main result is the prediction of gapless excitations above the ground state when p and n have no common divisor greater than 1.

In Section 5.2, we begin by writing down the SU(n) Heisenberg Hamiltonian with interactions up to ($n - 1$)-th neighbour. As explained in Chapter 3, such long-range interactions are necessary in order to stabilize local zero modes. We also present the findings of SU(n) flavour-wave theory in this section. Next, in Section 5.3, we derive the low energy quantum field theory description of the chain, and obtain the same flavour-wave velocities in a perturbative expansion. In Section 5.4, we use the renormalization group to argue that at low energies, these (distinct) velocities flow

to a common value, so that Lorentz invariance emerges and the field theory becomes a Lorentz invariant $SU(n)/[U(1)]^{n-1}$ flag manifold sigma model. The first derivation of the $SU(n)/[U(1)]^{n-1}$ flag manifold sigma model from $SU(n)$ chains was done by Bykov in [71, 72], who elected to fine-tune the various interaction strengths in the Heisenberg Hamiltonian to guarantee Lorentz invariance from the outset. These sigma models were also studied systematically in [78] and [79]. In Section 5.5, we present our proposed phase diagram for the $SU(n)$ chain, incorporating the 't Hooft anomaly matching conditions of [78, 79] and [116], This phase diagram is the source of our $SU(n)$ version of the Haldane conjecture. We also perform a strong coupling analysis. Finally, our conclusions follow in Section 5.6.

5.2   SU(n) Chains and Flavour-Wave Theory

Our starting point is the following $SU(n)$ Heisenberg Hamiltonian, with interactions $J_1, J_2, \ldots, J_{n-1}$, all positive, that couple each site of the chain with up to its $(n-1)$-th neighbours:

$$H = \sum_j \sum_{r=1}^{n-1} J_r \text{tr}[S(j)S(j+r)]. \tag{5.1}$$

In Figure 5.1, we draw the first few interactions in a typical $SU(n)$ chain.
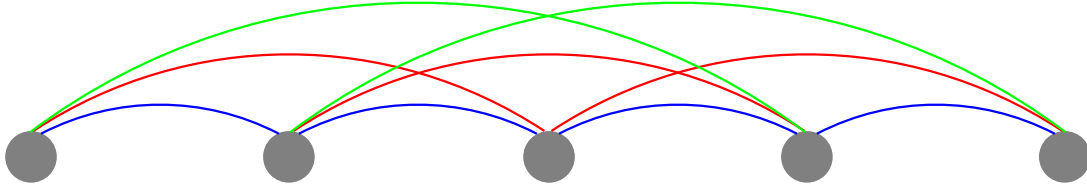
Figure 5.1: Interactions in a typical symmetric $SU(n)$ chain. Explicitly, we have drawn the nearest-neighbour interactions in blue, second-neighbour interactions in red, and third-neighbour interactions in green. For $n > 4$, further interactions must also be included.

As always, $S(j)$ is an $n \times n$ matrix whose entries contain the $n^2 - 1$ generators of $SU(n)$. We consider only symmetric representations in this chapter, meaning that the chain is characterized by a single integer p, according to $\text{tr}[S] = p$. In the large-p limit, we are able to replace S with a matrix of classical numbers. To this order in p, the Casimir constraints of $SU(n)$ completely determine the eigenvalues of S. We have

$$S_{\alpha\beta} = p\phi^{*,\alpha}\phi_\beta \tag{5.2}$$

for $\boldsymbol{\phi} \in \mathbb{C}^n$ with $|\boldsymbol{\phi}|^2 = 1$. The interaction terms appearing in (5.1) reduce to

$$\text{tr}[S(j)S(j+r)] = p^2|\boldsymbol{\phi}(j)^* \cdot \boldsymbol{\phi}(j+r)|^2. \tag{5.3}$$

Since ϕ lives in $\mathbb{C}^n$, a classical ground state will possess local zero modes unless the Hamiltonian gives rise to $n-1$ constraints. This is the justification for our study of the longer-range Hamiltonian above, which removes any local zero modes by including longer-range interactions. These interactions result in an n-site ordered classical ground state which gives rise to a $\mathbb{Z}_n$ symmetry in any low energy field theory description. For example, in SU(5), one such ground state is

$$\cdots \quad \bullet \ \bullet \ \bullet \ \circ \ \circ \ \bullet \ \bullet \ \bullet \ \circ \ \circ \quad \cdots . \tag{5.4}$$

This $\mathbb{Z}_n$ symmetry is also present for the $p = 1$ Bethe ansatz-solvable models, as mentioned in Section 3.5.1 [12, 84, 85]. In fact, it is expected that quantum fluctuations may produce an n-site structure through an order-by-disorder mechanism that generates effective additional couplings of order p^{-1} that lift the local zero modes [109].[32] However, the explicit mechanism for generating these couplings has not yet been worked out, so that we cannot predict the numerical values of these longer-range interactions from a nearest-neighbour model.

Since the classical ground state minimizing (5.1) has n-site order, it is characterized by n normalized vectors that mutually minimize (5.3). That is, the classical ground state gives rise to an orthonormal basis of $\mathbb{C}^n$. Due to this n-fold structure, we rewrite the Hamiltonian as a sum over unit cells (indexed by j):

$$H = \sum_j \sum_{\alpha=1}^{n} \sum_{r=1}^{n-1} J_r \text{tr}[S(j_\alpha)S(j_\alpha + r)] \qquad j_\alpha := nj + (\alpha - 1). \tag{5.5}$$

5.2.1 Flavour-wave theory

As we've mentioned repeatedly above, we do not expect spontaneous symmetry breaking of the SU(n) symmetry in the exact ground state of our Hamiltonian, due to Coleman's theorem [8]. Nonetheless, we may still expand about the classical (symmetry broken) ground state to predict the Goldstone mode velocities. If the theory is asymptotically free, as in SU(2) and SU(3), then at sufficiently high energies (set by the inverse correlation length) the excitations may propagate with these velocities [92].

To this end, we introduce n^2 bosons in each unit cell to reproduce the commutation relations of the S matrices, (3.1):

$$S_{\alpha\beta}(j_\gamma) = b_\alpha^\dagger(j_\gamma)b_\beta(j_\gamma). \tag{5.6}$$

The counting is n flavours of boson for each of the n sites of a unit cell. The condition $\text{tr}[S] = p$ implies there are p bosons at each site. The classical ground state involves only 'diagonal' bosons of the type $b_\gamma(j_\gamma)$ and $b_\gamma^\dagger(j_\gamma)$. The 'off-diagonal' bosons are Holstein-Primakoff bosons. Flavour-wave theory allows for a small number of Holstein-Primakoff bosons at each site, captured by

$$\nu(j_\gamma) = \sum_{\alpha \neq \gamma} b_\alpha^\dagger(j_\gamma)b_\alpha(j_\gamma),$$

---

[32] Again, we emphasize that n-site structure refers to the presence of a $\mathbb{Z}_n$ symmetry, and not of a spontaneously broken quantum ground state.

and writes the Hamiltonian (5.5) in terms of these $n(n-1)$ bosons. In the large-p limit, $p \gg \nu(j_\gamma)$ and we expand

$$S_\gamma^\gamma(j_\gamma) = p - \nu(j_\gamma),$$
$$S_\gamma^\alpha(j_\gamma) \approx \sqrt{p} b_\alpha^\dagger(j_\gamma),$$
$$S_\alpha^\gamma(j_\gamma) \approx \sqrt{p} b_\alpha(j_\gamma),$$

to find

$$\text{tr}[S(j_\gamma)S(j_\eta)] = p \left[b_\gamma^\dagger(j_\eta)b_\gamma(j_\eta) + b_\gamma^\dagger(j_\eta)b_\eta(j_\gamma) + b_\eta^\dagger(j_\gamma)b_\gamma^\dagger(j_\eta) + b_\eta(j_\gamma)b_\gamma(j_\eta) \right] + O(p^0). \quad (5.7)$$

In terms of these degrees of freedom, the Hamiltonian (5.5) decomposes into a sum

$$H = \sum_{\gamma<\eta} H_{\gamma\eta}, \quad (5.8)$$

where $H_{\gamma\eta}$ is a Hamiltonian involving only the two bosons $b_\gamma(j_\eta)$ and $b_\eta(j_\gamma)$. In momentum space, this gives $\frac{n(n-1)}{2}$ different 2×2 matrices, each of which can be diagonalized by a Bogoliubov transformation:

$$H_{\gamma,\gamma+t} = \text{const.} + \sum_k \omega_t(k) \sum_{j=1}^{2} \left(d_{j,t}^\dagger(k)d_{j,t}(k) + \frac{1}{2} \right), \quad (5.9)$$

where

$$\omega_t(k) = 2p \sqrt{J_t J_{n-t}} \left| \sin \frac{nka}{2} \right|, \quad (5.10)$$

and the $d_{j,t}$ are new boson operators. Therefore, the corresponding flavour-wave velocities are

$$v_t = np \sqrt{J_t J_{n-t}} \qquad t = 1, 2, \ldots, n-1. \quad (5.11)$$

When n is odd, there are n modes with each flavour-wave velocity. When n is even, this is true except for the velocity $v_{\frac{n}{2}}$, which has only $\frac{n}{2}$ modes. In each case, the number of modes adds up to $n(n-1)$. We note that for $n > 3$, there is no longer a unique velocity, and the emergence of Lorentz invariance does not occur. Only for a specific fine-tuning of the couplings can Lorentz invariance be restored. These tuned models were the ones considered by Bykov in [71] and [72].

5.3 Derivation of the Flag Manifold Sigma Model

As hinted in Section 4.3, much of our calculations from the symmetric SU(3) chains easily general-ize to SU(n) chains in the same representation. As such, we include only an abbreviated derivation of the sigma model; for further details, we refer the reader to Chapter 4. Since the classical ground

state has n-site order, with unit vectors $\boldsymbol{\phi}^\alpha \in \mathbb{C}^n$ defined on each site, we first introduce a second set of vectors, $\boldsymbol{\varphi}^\alpha \in \mathbb{C}^n$, defined via a unitary matrix, U:

$$U_{\alpha\beta} = \varphi_\beta^\alpha. \tag{5.12}$$

This new basis can be used to describe fluctuations about the $\boldsymbol{\phi}^\alpha$ on each site, as in (4.15):

$$\boldsymbol{\phi}^\alpha = \sum_\beta \frac{1}{p} L_{\alpha\beta} \boldsymbol{\varphi}^\beta + \sqrt{1 - \mu(\alpha)} \boldsymbol{\varphi}^\alpha. \tag{5.13}$$

As before, $L_{\alpha\alpha} = 0$ (no sum), and $p^2\mu(\alpha) = \sum_\beta |L_{\alpha\beta}|^2$. Following Chapter 4 (which in turn follows Chapter 2 for SU(2)), we let U and L vary uniformly from site to site, and write $S(j_\gamma)$ in terms of them. After many simplifications, we find

$$\text{tr}[S(j_\gamma)S(j_\eta)] = p^2(\eta - \gamma)^2 \text{tr}[U\partial_x U^\dagger \Lambda_\gamma \partial_x U U^\dagger \Lambda_\eta] \tag{5.14}$$

$$+2(\eta - \gamma)p(L_{\eta\gamma}[\partial_x U U^\dagger]_{\gamma\eta} + L_{\gamma\eta}[U\partial_x U^\dagger]_{\eta\gamma}) + 4|L_{\gamma\gamma}|^2 + \text{ const.}.$$

The complete derivation of this result can be found in Appendix B. The next step is to construct the coherent state path integral, and derive the Berry phase contribution to the Lagrangian. This procedure was done for general n in Section 4.3.1. We repeat the result here, (4.36), for convenience:

$$\mathcal{L}_B = -\frac{1}{n} \left(p\text{tr}[\Lambda_\alpha \partial_\tau U U^\dagger] + \text{tr}[\{\Lambda_\alpha, L\}\partial_\tau U U^\dagger] \right) + O(p^{-1}). \tag{5.15}$$

5.3.1 The complete field theory

Since our approximated action is only quadratic in the L matrices, we may integrate out these modes to obtain an action in terms of the U matrices only. Combining (5.14) and (5.15), the Lagrangian terms involving a given matrix element $L_{\alpha\beta}$ are:

$$4(J_t + J_{n-t})|L_{\alpha\beta}|^2 - 2L_{\alpha\beta} \left([\partial_\tau U U^\dagger]_{\beta\alpha} + p((n - t)J_{n-t} - tJ_t)[\partial_x U U^\dagger]_{\beta\alpha} \right) \tag{5.16}$$

$$-2L_\alpha^\beta \left([\partial_\tau U U^\dagger]_\beta^\alpha - p((n - t)J_{n-t} - tJ_t)[\partial_x U U^\dagger]_\beta^\alpha \right),$$

where $t := |\alpha - \beta|$. The ∂_τ-dependent terms have come from the Berry phase term (5.15), and the ∂_x-dependent terms have come from

$$J_t\text{tr}[S(j_\alpha)S(j_\beta)] + J_{n-t}\text{tr}[S(j_\beta)S(j_{n+\alpha})] \tag{5.17}$$

in the Hamiltonian. Integrating over $L_{\alpha\beta}$, we are left with a real term,

$$\mathcal{L}_{\alpha\beta}^{\text{real}} = \frac{1}{n(J_t + J_{n-t})} \text{tr}[\Lambda_\alpha U\partial_\tau U^\dagger \Lambda_\beta \partial_\tau U U^\dagger] - p^2 \frac{[(n - t)J_{n-t} - tJ_t]^2}{n(J_t + J_{n-t})} \text{tr}[\Lambda_\alpha U\partial_x U^\dagger \Lambda_\beta \partial_x U U^\dagger], \tag{5.18}$$

as well as an imaginary term

$$\mathcal{L}_{\alpha\beta}^{\text{imag}} = p\frac{((n-t)J_{n-t} - tJ_t)}{n(J_t + J_{n-t})}\left([\partial_x UU^\dagger]_{\alpha\beta}[\partial_\tau UU^\dagger]_{\beta\alpha} - [\partial_\tau UU^\dagger]_{\beta\alpha}[\partial_x UU^\dagger]_{\alpha\beta}\right). \tag{5.19}$$

Above, there is no sum over the repeated α, β indices. The factor of n in the denominator comes from converting the sum over lattice sites within the n-site unit cell to an integral. To these terms, we must add the L-independent terms appearing in (5.14) and (5.15). They modify (5.18) to

$$\mathcal{L}_{\alpha\beta}^{\text{real}} \rightarrow \frac{1}{n(J_t + J_{n-t})}\text{tr}[\Lambda_\alpha U\partial_\tau U^\dagger \Lambda_\beta \partial_\tau UU^\dagger] + p^2\frac{J_{n-t}J_t n}{(J_t + J_{n-t})}\text{tr}[\Lambda_\alpha U\partial_x U^\dagger \Lambda_\beta \partial_x UU^\dagger]. \tag{5.20}$$

Comparing the ratios of the prefactors of the spatial and imaginary temporal terms, we identify the velocities of the theory as

$$v_t^2 = n^2 p^2 J_{n-t} J_t. \tag{5.21}$$

This agrees with the flavour-wave velocities found in Section 5.2. Meanwhile, the terms in (5.15) modify (5.19) to produce the following pure-imaginary contribution to the Lagrangian:

$$\mathcal{L}^{\text{imag}} = -\epsilon_{\mu\nu}\sum_{\alpha<\beta} \lambda_{|\alpha-\beta|}\text{tr}[\partial_\mu UU^\dagger \Lambda_\alpha \partial_\nu UU^\dagger \Lambda_\beta] - \mathcal{S}, \tag{5.22}$$

where

$$\mathcal{S} := \frac{p}{n}\sum_\alpha \text{tr}[\Lambda_\alpha \partial_\tau UU^\dagger] \tag{5.23}$$

and

$$\frac{n\lambda_t}{p} := \frac{(n-t)J_{n-t} - tJ_t}{J_t + J_{n-t}}. \tag{5.24}$$

Using the identity $\text{tr}[\partial UU^\dagger] = 0$, the integral of $\mathcal{S}$ can be shown to be a total derivative:

$$i\mathcal{S} = \frac{2\pi p}{n}\sum_{\alpha=2}^{n}(\alpha-1)Q_\alpha \tag{5.25}$$

where

$$Q_\alpha := \frac{1}{2\pi i}\epsilon_{\mu\nu}\int dx d\tau \text{tr}[\partial_\mu U\partial_\nu U^\dagger \Lambda_\alpha]. \tag{5.26}$$

Relabelling $\mathcal{S} = -S_{\text{top}}$, and combining (5.22) with (5.20), we arrive at the following action:

$$S = \sum_{\alpha<\beta}\int dx d\tau \frac{1}{g_{|\alpha-\beta|}}\left(v_{|\alpha-\beta|}\text{tr}[\Lambda_\alpha U\partial_x U^\dagger \Lambda_\beta \partial_x UU^\dagger] + \frac{1}{v_{|\alpha-\beta|}}\text{tr}[\Lambda_\alpha U\partial_\tau U^\dagger \Lambda_\beta \partial_\tau UU^\dagger]\right) \tag{5.27}$$

$$-\epsilon_{\mu\nu}\sum_{\alpha<\beta}\lambda_{|\alpha-\beta|}\int dx d\tau \text{tr}[\partial_\mu UU^\dagger \Lambda_\alpha \partial_\nu UU^\dagger \Lambda_\beta] + S_{\text{top}},$$

84

with

$$g_t = \frac{n}{v_t}(J_t + J_{n-t}).\tag{5.28}$$

Since the coupling constants and velocities satisfy $g_t = g_{n-t}$ and $v_t = v_{n-t}$, we conclude that there are $\lfloor n \rfloor$ velocities and coupling constants. Moreover, we have that

$$\sum_{\alpha=1}^{n} Q_\alpha = \frac{1}{2\pi i}\epsilon_{\mu\nu}\int dx d\tau \mathrm{tr}[\partial_\mu U \partial_\nu U^\dagger] = \frac{1}{2\pi i}\epsilon_{\mu\nu}\int dx d\tau \partial_\mu \mathrm{tr}[U\partial_\nu U^\dagger] = 0,\tag{5.29}$$

so that there are $n-1$ independent topological charges. We note that the λ-terms appearing in (5.27) are not quantized, despite the fact that they are pure-imaginary in imaginary time. We give an interpretation of these terms below. In [72], these λ-terms were absent as a result of the same fine-tuning that ensured a unique velocity. Indeed, the choice $J_t = \sqrt{\frac{n-t}{t}}$ ensures that $v_t \equiv 1$ for all t, and moreover that $\lambda_t = 0$ for all t. Note that this choice does not, however, equate all of the coupling constants, g_t.

5.3.2 Gauge invariance

The theory (5.27) is invariant under the gauge transformations

$$U(x,\tau) \to D(x,\tau)U(x,\tau),\tag{5.30}$$

where $D(x,\tau)$ is a local, diagonal matrix. Since such matrices are generated by the $n-1$ diagonal SU(n) generators, this corresponds to a $[\mathrm{U}(1)]^{n-1}$ gauge symmetry. Thus, we have obtained the SU(n)/$[\mathrm{U}(1)]^{n-1}$ flag manifold sigma model description of the SU(n) chain, as expected. The topological angle content of this model follows from the second cohomology group, which is

$$H^2(\mathrm{SU}(n)/[\mathrm{U}(1)]^{n-1}) = \overbrace{\mathbb{Z}\times\cdots\times\mathbb{Z}}^{n-1\ \text{times}}.\tag{5.31}$$

So, this model is characterized by $n-1$ topological charges, which is consistent with S_{top} in (5.27). The coupling constants g_t and λ_t correspond to the metric and torsion tensors on this manifold, respectively [79]. However, a unique metric cannot be defined, since the theory (5.27) lacks the Lorentz invariance that is often assumed for sigma models. Thus, we have a non-Lorentz invariant flag manifold sigma model, just as was the case in Section 4.7, where self-conjugate SU(3) chains were considered. In the following section, we will use the renormalization group to show that at low enough energies, these distinct velocities in fact flow to a single value, so that Lorentz invariance emerges after all.

5.3.3 Embedding into complex projective spaces

In Chapter 3, it was explained how the complete flag manifold SU(n)/$[\mathrm{U}(1)]^{n-1}$ can be embedded into an n-fold product of $\mathbb{CP}^{n-1}$ spaces. In (6.7), this was restated explicitly for the case of SU(3).

Here, the situation is no different. The n complex fields $\boldsymbol{\varphi}^\alpha$ may be viewed as each living in its own $\mathbb{C}P^{n-1}$ sector, and we may identify the flag manifold with its image under the following map:

$$\frac{\mathrm{U}(n)}{[\mathrm{U}(1)]^n} \hookrightarrow \overbrace{\mathbb{C}P^{n-1} \times \cdots \times \mathbb{C}P^{n-1}}^{n \text{ copies}}. \tag{5.32}$$

Explicitly, this embedding is determined by the metric parameters g_t, the torsion parameters λ_t, as well as the condition of orthogonality between the fields. In this context, we may view the topological charges Q_α as the pull-backs to the flag manifold of the familiar topological charges defined on $\mathbb{C}P^{n-1}$. In Section 4.4.2, we further made use of this embedding to introduce U(1) gauge fields A_μ^a, to rewrite the action as in (4.60). A similar rewriting proves to be much more difficult in SU(n), since now there are multiple coupling constants g_t. Said differently, the metric is no longer diagonal in the $\boldsymbol{\varphi}^\alpha$.

5.3.4 Translation invariance

Since it will be critical below, we take a moment to observe the action of translation on the flag manifold sigma model. Since translation shifts the chain by one site, it corresponds to the mapping

$$\boldsymbol{\varphi}^\alpha \mapsto \boldsymbol{\varphi}^{\alpha+1}, \tag{5.33}$$

where the index α is defined modulo n. Therefore, translation manifests itself in the sigma model as a $\mathbb{Z}_n$ action, generalizing the $\mathbb{Z}_3$ symmetry present in the symmetric SU(3) chains. We will return to this fact when we discuss 't Hooft anomalies below.

5.4 Renormalization Group Analysis

Recently, the Lorentz invariant versions of the above flag manifold sigma models were studied in great detail in [79]. In particular, the renormalization group flow of both the g_t and λ_t parameters were determined for general n. Moreover, field theoretic versions of the LSMA theorem were formulated, using the methods of 't Hooft anomaly matching. For a review of this subject, see Section 4.6.4. Here, we would like to apply these results to our SU(n) chains which lack Lorentz invariance in general. To do so, we consider the differences of velocities occurring in (5.27), namely

$$\Delta_{tt'} := v_t - v_{t'}, \tag{5.34}$$

and ask how they behave at low energies. More precisely, we calculate the one-loop beta functions of these $\Delta_{tt'}$, to $O(g_t)$ and $O(\lambda_t)$. We will find that each of the $\Delta_{tt'}$ flows to zero under renormalization. Moreover, we will show that this implies Lorentz invariance at our order of approximation. This is consistent with the fundamental SU(n) models with $p = 1$, where it is known by Bethe ansatz that Lorentz invariance is present [12, 84, 85]. Our calculations were motivated by a similar phenomenon in 2+1 dimensional systems, where an interacting theory of bosons and Weyl fermions renormalizes to a Lorentz invariant model [133, 134].

5.4.1 Goldstone mode expansion

In the following, it will be useful to introduce dimensionless velocities, u_t, defined according to

$$u_t := \frac{v_t}{\bar{v}} \qquad \bar{v} = \frac{1}{\lfloor \frac{n}{2} \rfloor} \sum_{t=1}^{\lfloor \frac{n}{2} \rfloor} v_t, \qquad (5.35)$$

and introduce new spacetime coordinates which both have units of $(\text{length} \cdot \text{time})^{1/2}$:

$$x \to \frac{x}{\sqrt{\bar{v}}} \qquad \tau \to \sqrt{\bar{v}}\tau. \qquad (5.36)$$

In these units, $\Delta_{tt'} = u_t - u_{t'}$. The coefficients g_t appearing in (5.27) are dimensionless, and are all proportional to $\frac{1}{p}$. Since we've taken a large-p limit, we will expand all quantities in powers of the g_t. As we will see below, the coefficients λ_t in (5.27) do not enter into our one-loop calculations, and so we will neglect them throughout.

Since we are interested in the low energy dynamics of these quantum field theories, we make the simplifying assumption that the matrices U are close to the identity matrix, and expand them in terms of the SU(n) generators. In Appendix C, we prove that U may factorized according to

$$U = DV \qquad \begin{cases} D = e^{i\omega_\gamma T_\gamma} \\ V = e^{i\omega_a T_a} \end{cases}. \qquad (5.37)$$

Let us explain our notation. Here and throughout, we use Greek letters to index the diagonal SU(n) generators, lowercase Latin letters to index the off-diagonal ones, and uppercase Latin letters to index the complete set. Repeated indices will always be summed over unless otherwise specified. Since D is diagonal, this factorization of U implies that D drops out from the traces occurring in (5.27):

$$\text{tr}[U\partial_\mu U^\dagger \Lambda_\alpha \partial_\mu U U^\dagger \Lambda_\beta] = \text{tr}[V\partial_\mu V^\dagger \Lambda_\alpha \partial_\mu V V^\dagger \Lambda_\beta] \qquad (5.38)$$

Therefore, when deriving the Lagrangian of the ω_a, we may write U in terms of the off-diagonal generators only:

$$U = e^{i\omega_a T_a} = 1 + i\omega_a T_a - \frac{1}{2}\omega_a \omega_b T_a T_b + O(\omega^3). \qquad (5.39)$$

We choose a convenient normalization in which the off-diagonal generators have entries 1 or $\pm i$, and satisfy

$$[T_a, T_b] = 2if_{abC}T_C. \qquad (5.40)$$

These generators are $n \times n$ matrices that have a very specific structure. There are $n - 1$ diagonal ones, and $n(n - 1)$ off-diagonal ones, that come in pairs. For each pair of integers $\{\alpha, \beta\}$ with $\alpha, \beta = 1, \ldots, n$ and $\alpha \neq \beta$, there are exactly two generators with nonzero (α, β) entries. We define $I_{\alpha\beta}$ to be the set of two indices corresponding to the SU(n) generators with nonzero (α, β) entries. For example, in SU(3), the off-diagonal generators (in Gell-Mann's notation) are T_1, T_2 with nonzero

entries in the $(1, 2)$ positions; T_4, T_5 with nonzero entries in the $(1, 3)$ positions; and T_6, T_7 with nonzero entries in the $(2, 3)$ positions. They are provided explicitly in Appendix E. Then,

$$I_{12} = \{1, 2\} \quad I_{13} = \{4, 5\} \quad I_{23} = \{6, 7\}. \tag{5.41}$$

With this notation, we now expand $-\text{tr}[\partial_\mu U U^\dagger \Lambda_\alpha \partial_\mu U U^\dagger \Lambda_\beta]$ to $O(\omega^4)$. We start with

$$\partial_\mu U U^\dagger = i\partial_\mu \omega_a T_a + \left[\partial_\mu \omega_a \omega_b - \frac{1}{2} \partial_\mu(\omega_a \omega_b) \right] T_a T_b \tag{5.42}$$

$$- \frac{i}{2} \left[\partial_\mu \omega_a \omega_b \omega_c - \partial_\mu(\omega_a \omega_b) \omega_c + \frac{1}{3} \partial_\mu(\omega_a \omega_b \omega_c) \right] T_a T_b T_c + O(\omega^4). \tag{5.43}$$

Since

$$\partial_\mu \omega_a \omega_b - \frac{1}{2} \partial_\mu(\omega_a \omega_b) = \frac{1}{2} \left[\partial_\mu \omega_a \omega_b - \omega_a \partial_\mu \omega_b \right], \tag{5.44}$$

we have

$$\left[\partial_\mu \omega_a \omega_b - \frac{1}{2} \partial_\mu(\omega_a \omega_b) \right] T_a T_b = \frac{1}{2} \partial_\mu \omega_a \omega_b [T_a, T_b] = i\partial_\mu \omega_a \omega_b f_{abC} T_C. \tag{5.45}$$

Moreover, since

$$\partial_\mu \omega_a \omega_b \omega_c - \partial_\mu(\omega_a \omega_b) \omega_c + \frac{1}{3} \partial_\mu(\omega_a \omega_b \omega_c) = \frac{1}{3}(\partial_\mu \omega_a \omega_b \omega_c - \omega_a \partial_\mu \omega_b \omega_c) + \frac{1}{3}(\omega_a \omega_b \partial_\mu \omega_c - \omega_a \partial_\mu \omega_b \omega_c), \tag{5.46}$$

we also have

$$\left[\partial_\mu \omega_a \omega_b \omega_c - \partial_\mu(\omega_a \omega_b) \omega_c + \frac{1}{3} \partial_\mu(\omega_a \omega_b \omega_c) \right] T_a T_b T_c \tag{5.47}$$

$$= -\frac{1}{3} \omega_a \partial_\mu \omega_b \omega_c \left([T_a, T_b] T_c + T_a [T_b, T_c] \right)$$

$$= -\frac{2i}{3} \omega_a \partial_\mu \omega_b \omega_c f_{abD} [T_D, T_c]$$

$$= \frac{4}{3} \omega_a \partial_\mu \omega_b \omega_c f_{abD} f_{DcE} T_E.$$

Combining these facts, we have

$$\partial_\mu U U^\dagger = i\partial_\mu \omega_a T_a + i\partial_\mu \omega_a \omega_b f_{abC} T_C - \frac{2i}{3} f_{abD} f_{DcE} \omega_a \partial_\mu \omega_b \omega_c T_E + O(\omega^4). \tag{5.48}$$

This yields

$$-\text{tr}[\partial_\mu U U^\dagger \Lambda_\alpha \partial_\mu U U^\dagger \Lambda_\beta] = \partial_\mu \omega_a \partial_\mu \omega_b \text{tr}[T_a \Lambda_\alpha T_b \Lambda_\beta] \tag{5.49}$$

$$+ \left[f_{bcE} + \frac{2}{3} f_{bcD} f_{DgE} \omega_g \right] \partial_\mu \omega_a \partial_\mu \omega_b \omega_c \left(\text{tr}[T_a \Lambda_\alpha T_E \Lambda_\beta] + \text{tr}[T_E \Lambda_\beta T_a \Lambda_\alpha] \right)$$

$$+\partial_\mu\omega_a\omega_b\partial_\mu\omega_c\omega_d f_{abE}f_{cdG}\mathrm{tr}\Lambda_\alpha T_E\Lambda_\beta T_G.$$

Now we want to simplify this by understanding

$$\mathrm{tr}[T_a\Lambda_\alpha T_b\Lambda_\beta] = [T_a]_{\beta\alpha}[T_b]_{\alpha\beta}. \tag{5.50}$$

Since $\alpha \neq \beta$, the above expression vanishes if either of a or b is a diagonal generator. In fact, we have

$$\mathrm{tr}[T_a\Lambda_\alpha T_b\Lambda_\beta] + \mathrm{tr}[T_b\Lambda_\alpha T_a\Lambda_\beta] = \begin{cases} 2\delta_{ab} & a,b \in I_{\alpha\beta} \\ 0 & \text{else} \end{cases}. \tag{5.51}$$

Returning to our calculation, we now have

$$-\mathrm{tr}[\partial_\mu UU^\dagger\Lambda_\alpha\partial_\mu UU^\dagger\Lambda_\beta] = \sum_{a\in I_{\alpha\beta}}\Big[(\partial_\mu\omega_a^2) + 2f_{bca}\partial_\mu\omega_a\partial_\mu\omega_b\omega_c \tag{5.52}$$

$$+ \frac{4}{3}f_{bcE}f_{Eda}\partial_\mu\omega_a\partial_\mu\omega_b\omega_c\omega_d + \partial_\mu\omega_e\omega_b\partial_\mu\omega_c\omega_d f_{eba}f_{cda}\Big],$$

where all repeated indices are summed over. Now, to obtain the full Lagrangian, we must sum over the possible combinations of α and β. Since

$$\sum_{\alpha<\beta}\sum_{a\in I_{\alpha\beta}} := \sum_{\beta=2}^{n}\sum_{\alpha=1}^{\beta-1}\sum_{a\in I_{\alpha\beta}} = \sum_a, \tag{5.53}$$

where $\sum_a$ again denotes a sum over all the off-diagonal generators of SU(n), the non-interacting Lagrangian has the form

$$\mathcal{L}_0 = \frac{1}{g_a}\left[\frac{1}{u_a}(\partial_\tau\omega_a)^2 + u_a(\partial_x\omega_a)^2\right], \tag{5.54}$$

where

$$g_a := g_{|\alpha-\beta|}\Big|_{I_{\alpha\beta}\ni a} \qquad u_a := u_{|\alpha-\beta|}\Big|_{I_{\alpha\beta}\ni a}. \tag{5.55}$$

and again, all repeated indices are summed over. We rescale the fields according to

$$\omega_a \mapsto \sqrt{\frac{g_a}{2}}\omega_a \tag{5.56}$$

to yield

$$\mathcal{L} = \frac{1}{2}\left[\frac{1}{u_a}(\partial_\tau\omega_a)^2 + u_a(\partial_x\omega_a)^2\right] + \frac{\sqrt{g_ag_bg_c}}{\sqrt{2}}\frac{h_a(\mu)}{g_a}f_{bca}\partial_\mu\omega_a\partial_\mu\omega_b\omega_c \tag{5.57}$$

$$\frac{\sqrt{g_bg_cg_d}}{4}\frac{h_a(\mu)}{g_a}\Big[\sqrt{g_e}\partial_\mu\omega_e\partial_\mu\omega_b\omega_c\omega_d f_{eca}f_{bda} + \frac{4}{3}f_{bcE}f_{Eda}\sqrt{g_a}\partial_\mu\omega_a\partial_\mu\omega_b\omega_c\omega_d\Big] + O(\omega^5),$$

where

$$h_a(\mu) = \begin{cases} \frac{1}{u_a} & \mu = \tau \\ u_a & \mu = x \end{cases}. \tag{5.58}$$

This expression will be the starting point of our renormalization group calculations.

5.4.2 Dimensional regularization

In Chapter 4, we introduced the theory behind the renormalization group and proceeded to use Wilson's formalism in order to calculate the beta functions of g and λ in the symmetric SU(3) chain. In this approach, the length scale of the theory is explicitly changed, and the beta functions are determined by finding the altered values of g and λ at this new scale.

An alternative approach is to use a regularized theory at a fixed energy scale.[33] Consider the following example Lagrangian density of a real scalar field:

$$\mathcal{L}_{\varphi^4} = \frac{1}{2}(\partial\varphi)^2 + m^2\varphi^2 + X\varphi^4. \tag{5.59}$$

This theory is not regularized: a perturbative expansion of its correlation functions will lead to divergences, order by order. To resolve this, we use a procedure known as dimensional regularization, in which we continue the spacetime dimension away from an integer, rendering momentum loop integrals finite. We then subtract off these contributions by introducing *counterterms* into the Lagrangian density, before continuing back to an integer dimension. This is performed at a given energy scale M, which we fix.

For example, at one loop, the φ self energy receives a contribution proportional to

$$\int \frac{d^d p}{(2\pi)^d} \frac{1}{(p^2 + m^2)} \propto \Gamma\left(1 - \frac{d}{2}\right), \tag{5.60}$$

where $\Gamma(x)$ is the gamma function with poles at non-positive integers. For non-integer d, this expression is finite, and can be cancelled by introducing a counterterm

$$\delta Z_\varphi \frac{1}{2}(\partial\varphi)^2 \tag{5.61}$$

into the Lagrangian, with

$$\delta Z_\varphi \propto -\Gamma\left(1 - \frac{d}{2}\right). \tag{5.62}$$

Repeating these steps for all divergences at a given order, we arrive at a *renormalized Lagrangian* density at scale M,

$$\mathcal{L}_{\varphi^4,r} = \frac{1}{2}Z_\varphi(\partial\varphi_r)^2 + Z_m M^2 m_r^2 \varphi_r^2 + Z_X M^{4-d} X_r \varphi_r^4, \tag{5.63}$$

in terms of a renormalized field φ_r and renormalized coupling constants m_r and X_r. The *renormalization constants Z_i* contain the introduced counterterms δZ_i according to

$$Z_i = 1 + \delta Z_i. \tag{5.64}$$

The explicit energy scale M enters to make the renormalized coupling constants dimensionless. Now, to extract the beta functions, we must relate the two Lagrangian densities (5.59) and (5.63). Matching kinetic terms, we find

$$\varphi = \sqrt{Z_\varphi}\varphi_r, \tag{5.65}$$

---

[33]The beginning of this discussion first appeared in [124].

and then rescaling, we find

$$m_r = mM^{-1}Z_\varphi Z_m^{-1}, \tag{5.66}$$

$$X_r = XM^{4-d}Z_\varphi^2 Z_X^{-1}. \tag{5.67}$$

These equations are the dimensional regularized analogues of (4.79) in Chapter 4. Differentiating with respect to $(-\log M)$ generates the desired beta functions. The negative sign enters because an increase in energy M corresponds to a decrease in length scale, b.

Exactly how the counterterms in (5.64) are defined leads to further choice in renormalization scheme. If only the divergent parts of the loop diagram are included in the counterterm, the scheme is known as 'minimal subtraction'. In our calculations, we use the more common 'modified minimal subtraction' scheme, or $\overline{MS}$, which adds to the counterterm the universal constant $\log(e^{\gamma_E}/4\pi)$ that often occurs in Feynman diagrams. This is implemented by rescaling the energy scale $M \to M\frac{e^{\gamma_E}}{4\pi}$ in (5.63) [130, 135].

5.4.3 Renormalization group equations

In order to derive the renormalization group equations for the model (5.57), we introduce a set of renormalization coefficients, Z_a^μ and $Z_{\mu abcd}^e$, as follows. Since (5.57) has divergences at one-loop order, we rewrite the theory in terms of renormalized parameters, as

$$\mathcal{L} = \frac{1}{2}\left[Z_a^\tau \frac{1}{u_a^r}(\partial_\tau \omega_a)^2 + u_a^r Z_a^x(\partial_x \omega_a)^2\right] + Z_{\mu abc}^{(1)}\frac{\sqrt{g_a^r g_b^r g_c^r}}{\sqrt{2}}\frac{h_a^r(\mu)}{g_a^r}f_{bca}\partial_\mu \omega_a \partial_\mu \omega_b \omega_c \tag{5.68}$$

$$+\frac{\sqrt{g_b^r g_c^r g_d^r}}{4}\frac{h_a^r(\mu)}{g_a^r}\left[Z_{\mu abcd}^{(2),e}\sqrt{g_e^r}\partial_\mu \omega_e \partial_\mu \omega_b \omega_c \omega_d f_{eca}f_{bda}+Z_{\mu abcd}^{(3)}\frac{4}{3}f_{bcE}f_{Eda}\sqrt{g_a^r}\partial_\mu \omega_a \partial_\mu \omega_b \omega_c \omega_d\right]+O(\omega^5).$$

The superscripts 'r' emphasize that the coupling constants and velocities appearing in (5.68) are different from those appearing in (5.57) (and are not indices to be summed over). Each of the renormalization coefficients has the form $Z = 1 + \delta Z$, where δZ is a one-loop counterterm regularizing any UV divergence. Below, we use dimensional regularization to calculate the δZ at a fixed energy scale M. Then, by rescaling

$$\omega_a \to \left(\frac{1}{Z_a^x Z_a^\tau}\right)^{1/4} \tag{5.69}$$

in (5.68), and comparing $(\partial_x \omega_a)^2$ terms in (5.57) and (5.68), we obtain the following equation for u_a^r:

$$u_a = u_a^r \sqrt{\frac{Z_a^x}{Z_a^\tau}}. \tag{5.70}$$

The derivative of u_a^r with respect to $-\log M$,

$$\beta_{u_a} := -\frac{du_a^r}{d\log M}, \tag{5.71}$$

is the beta function of u_a, and describes the flow of u_a as the energy scale, M, is changed. The negative sign is present, so as to be consistent with our definition of beta function in Chapter 4, which differentiated with respect to a length scale, $\log(b)$. It is important to note that since this equation only depends on Z_a^τ and Z_a^x, we are only tasked with calculating divergences of two-point functions in our lowest-order regularization scheme.

We use dimensional regularization to evaluate one-loop diagrams in $d = 2 - \epsilon$ dimensions in (5.68). We drop all 'r' superscripts, and introduce the following compact notation:

$$g_{abcd}^{(1)}(\mu) := \frac{M^\epsilon}{4} \sqrt{g_a g_b g_c g_d} h_e(\mu) \frac{f_{ace} f_{bde}}{g_e} \tag{5.72}$$

$$g_{abcd}^{(2)}(\mu) := \frac{M^\epsilon h_a(\mu)}{3} \frac{\sqrt{g_a g_b g_c g_d}}{g_a} f_{bcE} f_{Eda} \tag{5.73}$$

Again, all indices refer to off-diagonal $SU(n)$ generators, except for the uppercase letters, which refer to the complete set. We've introduced the renormalization scale M so that the coupling constants remain dimensionless. Since we are only tasked with calculating the Z_a^μ, the only diverging diagrams we must consider are those that correct the boson self energy. This immediately implies that the cubic interaction term occurring in (5.68) plays no effect at this order. The only contributing diagram $\Pi_{ab}(k)$, shown in Figure 5.2, equals

$$\Pi_{ab}(k) = -2 \int \frac{d^d q}{(2\pi)^d} \langle \omega_c(q)\omega_c(-q) \rangle \left[g_{abcc}(\mu) k_\mu k_\mu + g_{ccab}(\mu) q_\mu q_\mu \right] \tag{5.74}$$

where

$$g_{abcd} = g_{abcd}^{(1)} + g_{abcd}^{(2)}. \tag{5.75}$$

In addition to UV divergences, there are also IR divergences occurring at zero momenta. To remove these, we introduce a small mass m to the boson fields ω_a, and take the limit $m \to 0$ once we've extracted the UV divergence. A convenient mass term with the appropriate dimensions is $m^2 \bar{v}^3 u_a \omega_a^2$. Then, the free propagator is

$$\langle \omega_c(q)\omega_c(-q) \rangle = \frac{u_c}{\omega^2 + u_c^2 \vec{q}^2 + m^2 u_c^2 \bar{v}^3} \qquad q = (\omega, \vec{q}) \tag{5.76}$$

and we have two integrals to consider:

- **Integral 1:**

$$\int \frac{d^d q}{(2\pi)^d} \langle \omega_c(q)\omega_c(-q) \rangle = \frac{1}{2} \int \frac{d^{d-1}q}{(2\pi)^{d-1}} \frac{1}{\sqrt{\vec{q}^2 + m^2 \bar{v}^3}} = \frac{1}{2\pi\epsilon} + O(\epsilon^0) \tag{5.77}$$

- **Integral 2:**

$$\int \frac{d^d q}{(2\pi)^d} \langle \omega_c(q)\omega_c(-q) \rangle q_x q_x = \frac{1}{2} \int \frac{d^{d-1}q}{(2\pi)^{d-1}} \frac{\vec{q}^2}{\sqrt{\vec{q}^2 + m^2 \bar{v}^3}} = \frac{1}{2\pi\epsilon} m^2 \bar{v}^3 + O(\epsilon^0) \tag{5.78}$$

92
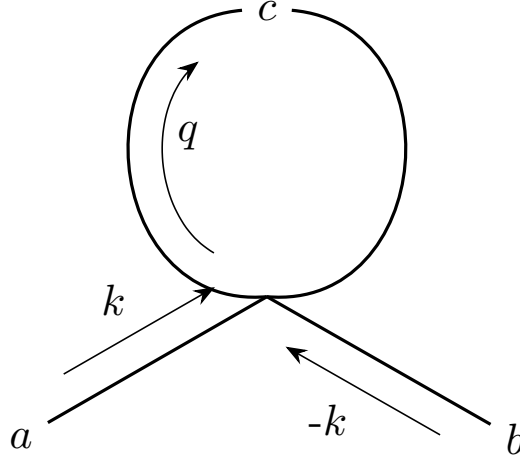
Figure 5.2: The diagram $\Pi_{ab}(k)$, drawn using [136].

In Integral 2, we've taken $\mu = x$ without loss of generality. It appears that such integrals will renormalize the boson masses; however, since these contributions are proportional to the IR cutoff m, when we restore $m \to 0$, these poles will drop out of our calculations. See equation 13.82 of [130] for a similar argument in the O(3) nonlinear sigma model.

Returning to the process (5.74), we find that

$$\Pi_{ab}(k) = -\frac{1}{\pi\epsilon}k_\mu k_\mu g_{abcc}(\mu) = -\frac{M^\epsilon \sqrt{g_a g_b}}{\pi\epsilon}k_\mu k_\mu g_c \left[\frac{1}{4}h_e(\mu)\frac{f_{ace}f_{bce}}{g_e} - \frac{h_a(\mu)}{3g_a}f_{bcE}f_{acE}\right]. \quad (5.79)$$

This result will contribute to the renormalization constants involving ω_a and ω_b.

5.4.4 Beta functions of the Goldstone velocities

In order to simplify (5.79) further, we make use of two identities (F.1) and (F.12), proven in Appendix F. Doing so, we conclude that (5.79) equals

$$\Pi_{ab}(k) = -\frac{M^\epsilon g_a \delta_{ab}}{2\pi\epsilon}k_\mu k_\mu \left(\sum_{\substack{i=1 \\ i\neq t}}^{n-1} \frac{h_i(\mu)}{2g_i}g_{|t-i|} - \frac{h_a(\mu)}{3g_a}[g_a + \frac{1}{2}\sum_c g_c]\right). \quad (5.80)$$

(no sum over a). Since

$$\partial_\mu \omega \partial_\mu \omega \sim -\omega \partial_\mu^2 \omega \sim +k_\mu k_\mu \omega(k)\omega(-k) \quad (5.81)$$

we may read off from $\Pi_{ab}(k)$ the renormalization group constants:

$$Z_a^\tau = 1 + \frac{M^\epsilon g_a u_a}{2\pi\epsilon} \Big(\sum_{\substack{i=1 \\ i\neq t}}^{n-1} \frac{1}{u_i g_i} g_{|t-i|} - \frac{2}{3g_a u_a}[g_a + \frac{1}{2}\sum_c g_c] \Big) \tag{5.82}$$

$$Z_a^x = 1 + \frac{M^\epsilon g_a}{2\pi u_a \epsilon} \Big(\sum_{\substack{i=1 \\ i\neq t}}^{n-1} \frac{u_i}{g_i} g_{|t-i|} - \frac{2u_a}{3g_a}[g_a + \frac{1}{2}\sum_c g_c] \Big) \tag{5.83}$$

(no sum over a). Inserting these expressions into (5.71), and using (5.70), we find that for $t = 1, 2, \ldots, q := \lfloor \frac{n}{2} \rfloor$,

$$\beta_{u_t} = -\frac{u_t g_t}{4\pi} \sum_{\substack{i=1 \\ i\neq t}}^{n-1} \frac{g_{|t-i|}}{g_i} \left[\frac{u_t}{u_i} - \frac{u_i}{u_t} \right]. \tag{5.84}$$

These are the beta functions for the different Goldstone velocities in the flag manifold sigma model. In the following subsection, we use (5.84) to show that these velocities flow to a common value at small energies.

5.4.5 Renormalization of velocity differences

We want to study the renormalization group flow of the velocity differences, $\Delta_{tt'}$ defined in (5.34). As mentioned above, the identity $u_t = u_{n-t}$ reduces the number of independent velocities to $q = \lfloor \frac{n}{2} \rfloor$, and the relation

$$\Delta_{tt'} = \Delta_{t1} + \Delta_{1t'} = \Delta_{1t'} - \Delta_{1t} \tag{5.85}$$

shows that the number of independent velocity differences is $q - 1$. To study their flow collectively, we introduce a $(q - 1)$-component vector, $\boldsymbol{\Delta}$, with components

$$\Delta^i := \Delta_{1,i+1} \qquad i = 1, 2, \ldots, q - 1. \tag{5.86}$$

If we assume that the velocities u_t are initially close together, so that the SU(n) chain is approximately Lorentz invariant, the vector $\boldsymbol{\Delta}$ will obey an equation of the form

$$-\beta_{\boldsymbol{\Delta}} = \frac{d}{d\log M}\boldsymbol{\Delta} = R\boldsymbol{\Delta} \tag{5.87}$$

for a $(q-1) \times (q-1)$ matrix R. The spectrum of R will reveal the low energy behaviour of the $\Delta_{tt'}$: if the spectrum is strictly positive, we may conclude that all velocity differences flow to zero in the IR. Let us now determine R.

Assuming the velocities u_t are initially close together, we rewrite (5.84) to linear order in Δ^t as

$$\beta_{u_t}^{n=2q} = -\frac{g_t}{2\pi} \Big[\sum_{i=1}^{q-1} \frac{\Delta_{ti}}{g_i}(g_{i+t} + g_{|t-i|}) + \frac{g_{|t-q|}}{g_q}\Delta_{tq} \Big] + O(\Delta^2), \tag{5.88}$$

94

$$\beta_{u_t}^{n=2q+1} = -\frac{g_t}{2\pi} \sum_{i=1}^{q} \frac{\Delta_{ti}}{g_i} \left(g_{i+t} + g_{|i-t|}\right) + O(\Delta^2), \tag{5.89}$$

depending on the parity of n. (We've introduced a $g_0 := 0$ for notational convenience). Here we have used the fact that only $q := \lfloor \frac{n}{2} \rfloor$ velocities and coupling constants are unique. The beta function for a component Δ^i of $\mathbf{\Delta}$ is then

$$\beta_{\Delta^t}^{n=2q} = -\frac{1}{2\pi} \sum_{i=1}^{q-1} \frac{\Delta^i}{g_i} \left[g_1 \left(g_{i+1} + g_{|1-i|}\right) - g_t \left(g_{i+t} + g_{|t-i|}\right) \right] \tag{5.90}$$

$$-\frac{g_t \Delta^t}{2\pi} \left[\sum_{i=1}^{q-1} \frac{1}{g_i} \left(g_{i+t} + g_{|t-i|}\right) + \frac{g_{|t-q|}}{g_q} \right] - \frac{\Delta^q}{2\pi g_q} \left[-g_t g_{|t-q|} + g_1 g_{|1-q|} \right] + O(\Delta^2),$$

$$\beta_{\Delta^t}^{n=2q+1} = -\frac{1}{2\pi} \sum_{i=1}^{q} \frac{\Delta^i}{g_i} \left[g_1 \left(g_{i+1} + g_{|i-1|}\right) - g_t \left(g_{i+t} + g_{|i-t|}\right) \right] - \frac{g_t \Delta^t}{2\pi} \sum_{i=1}^{q} \frac{1}{g_i} \left(g_{i+t} + g_{|i-t|}\right) + O(\Delta^2), \tag{5.91}$$

depending on the parity of n. Clearly, finding the eigenvalues of the R matrix in (5.87) is a difficult task. As a first check, we consider the symmetric point where all couplings equal the same value, g (except for the artificial g_0, which is always zero). In this case, we can clearly read off from (5.84) that

$$\beta_{\Delta^t} = -\frac{g\Delta^t}{2\pi}(n-1) \tag{5.92}$$

so that the matrix beta equation is diagonal, with R having positive eigenvalues. Next, we consider small values of n.

- SU(4)
  In this case, there is a single velocity difference, $\beta_{\Delta_{12}}$, with

$$\beta_{\Delta_{12}} = -\frac{\Delta_{12}}{2\pi g_2} \left[g_1^2 + 2g_2^2 \right] < 0. \tag{5.93}$$

- SU(5)
  In this case, there is again a single velocity difference, with

$$\beta_{\Delta_{12}} == \frac{1}{\pi g_2} \Delta_{12}(g_1^2 + g_2^2) < 0. \tag{5.94}$$

- SU(6)
  In this case, there are three velocities, three coupling constants, and two unique velocity differences, Δ_{12} and Δ_{13}. The eigenvalues of the 2×2 matrix R are both positive. Explicitly, they are

$$\{ \frac{1}{2\pi g_1 g_2 g_3} \left(g_1^2 g_2^2 + g_1^3 g_3 + g_1 g_2^2 g_3 + g_1^2 g_3^2 + g_2^2 g_3^2 \right), \frac{1}{2\pi g_1 g_2 g_3} \left(g_1^2 g_2^2 + 2g_1^2 g_3^2 + 2g_2^2 g_3^2 \right) \}. \tag{5.95}$$

Unable to find the eigenvalues of the R matrix explicitly, we resort to a numerical investigation of its spectrum. We verify that the spectrum is positive definite by computing the minimal eigenvalue of R for fixed coupling constants. First, we choose the $\lfloor \frac{n}{2} \rfloor$ coupling constants randomly from the interval $(0, 1)$. In 10 000 trials, we find that the minimal eigenvalue is always strictly positive, for SU(n) with $n = 3, 4, \ldots, 50$. Next, we probe points in parameter space where different coupling constants have a common value, by choosing coupling constants from a discrete lattice on $(0, 1)^{\lfloor \frac{n}{2} \rfloor}$. Since the dimension of the lattice increases with n, we choose a coarser discretization as n increases, to keep the number of lattice points below 100 000. In this case, we find that for $n = 3, 4, \ldots, 16$, the minimal eigenvalue of the R matrix is again strictly positive. This supports the conjecture that the spectrum of R is always positive, so that each velocity difference $\Delta_{tt'}$ flows to zero in the IR.

So far, we have verified that the velocity differences $\Delta_{tt'}$ in these sigma models flow to zero at low energies. However, we now claim that this is sufficient to conclude that the entire theory (5.27) is Lorentz invariant at low energies. We note that we are not required to restore the pure-imaginary λ-terms occurring in (5.27), since they are proportional to $\epsilon_{\mu\nu}\partial_\mu\phi\partial_\nu\phi$, a Lorentz scalar. Indeed, since the interaction vertex receives no $O(g)$ correction, the only spacetime dependence enters through the renormalization of $h_t(\mu)$ and through the renormalization of the fields ω_a themselves. Since the latter are independent of μ (see (5.82) and (5.83)), the Lorentz non-invariance of the interactions is entirely captured by the $h_t(\mu)$. Since $u_t - u'_t \to 0$ implies $u_t^{-1} - u_{t'}^{-1} \to 0$ at $O(g)$, we may use the results of the previous subsection to conclude that the $h_t(\mu)$ all flow to a common value $h(\mu)$, and thus Lorentz invariance of the entire model (5.27) is possible if the velocities are initially close to each other.

5.5 General Phase Diagram

Based on the renormalization group analysis in the previous section, we conclude that at low enough energies, SU(n) chains in the rank-p symmetric representation (without fine-tuning) will be described by a Lorentz invariant flag manifold sigma model

$$\mathcal{L} = \sum_{\alpha<\beta} \frac{1}{g_{|\alpha-\beta|}} \mathrm{tr}[\Lambda_\alpha U\partial_\mu U^\dagger \Lambda_\beta \partial_\mu UU^\dagger] - \epsilon_{\mu\nu}\sum_{\alpha<\beta}\lambda_{|\alpha-\beta|}\mathrm{tr}[\partial_\mu UU^\dagger\Lambda_\alpha\partial_\nu UU^\dagger\Lambda_\beta], \qquad (5.96)$$

with topological term

$$S_{\text{top}} = i\theta\sum_{\alpha=1}^{n-1}\alpha Q_\alpha \qquad \theta := \frac{2\pi p}{n}. \qquad (5.97)$$

In [79], the renormalization group flow of the λ_t and the g_t was determined, and given a geometric interpretation. It was found that for $n > 4$, the g_t flow to a common value in the IR, and that for $n > 6$, the λ_t flow to zero in the IR. Thus we may expect an S_n (permutation group) symmetry to emerge at low enough energies, and for $n > 6$. It is known that in these S_n-symmetric models, the

unique coupling constant g obeys [79]

$$\beta_g = -\frac{dg}{d \log M} = \frac{n+2}{4\pi} g^2 > 0,$$ (5.98)

and the theory is asymptotically free. These facts suggest that a gapless phase, driven by topological terms, may be present in these types of SU(n) chains. In previous chapters, we learned that this occurred whenever the topological angles of the theory were nontrivial, i.e. for p not a multiple of n. Should this phenomenon extend to all values of n?

Before jumping to this conclusion, it is important to realize that SU(2) and SU(3) are special. Since 2 and 3 are prime, any value of p not a multiple of n is necessarily coprime with n, and leads to $n-1$ nontrivial topological angles. And, by the LSMA theorem, this leads to either a gapless phase or an n-fold degenerate ground state. However, for nonprime values of n, that have nontrivial greatest common divisors with p, another scenario is possible. For example, in the $p = 2$ representation of SU(4), the topological angle $\theta_2 = \frac{\pi p}{2}$ becomes trivial; moreover, the LSMA theorem implies only a 2-fold degenerate ground state, instead of an n-fold one. These observations should make one hesitate before extrapolating our results from the previous chapters.

On the other hand, we do expect the prediction of a unique gapped ground state when p is a multiple of n to be robust. This follows directly from the fact that AKLT-like states exist for these representations, as shown in Section 3.5.3.

5.5.1 Strong coupling analysis

By taking the large coupling limit, $g_t \to \infty$, we are able to see that the ground state degeneracy of the flag manifold sigma model does in fact depend on $\gcd(n, p)$. In this limit, only the λ-terms and topological terms survive. We will neglect the λ-terms: for $n > 6$ this is justified by the fact that the λ_t parameters flow to zero under renormalization; for $n \leq 6$, this is an added assumption that is made to simplify our analysis. In this case, with only the topological terms remaining, the partition function is a path integral over the topological charge densities, with the extra constraints that the topological charges take integer values, and that the topological charge densities on each plaquette of the lattice sum to zero. We find

$$Z(\theta_1, \ldots, \theta_n) = \sum_{\{m_1, \ldots, m_n\}} z(\theta_1, \theta_2 + 2\pi m_2, \ldots, \theta_n + 2\pi m_n)^V$$ (5.99)

where V is the spacetime volume, $m_i \in \mathbb{Z}$, and

$$z(\theta_1, \theta_2, \ldots, \theta_n) = \int \frac{dk}{2\pi} \prod_{\alpha=1}^{n} \frac{2 \sin\left(\frac{1}{2}(k - \theta_\alpha)\right)}{(k - \theta_\alpha)}.$$ (5.100)

For our models, we have $\theta_\alpha = \frac{2\pi p}{n}(\alpha - 1)$, so that the denominator of this expression does not diverge. The term(s) with the largest value dominate the sum, so that the free energy density reads

as

$$f(\theta_1, \ldots, \theta_n) = -\log\left(\max_{\{m_2, m_3, \cdots, m_n\}} z(\theta_1, \theta_2 + 2\pi m_2, \ldots, \theta_n + 2\pi m_n)\right). \tag{5.101}$$

Just as in SU(3), we may identify phase transitions in this model by identifying sets of $\{m_\alpha\}$ where multiple terms in the free energy density dominate the logarithm. Indeed, as we pass from one phase to another, we shift from one dominant term to another, resulting in a cusp in f. The number of dominant terms meeting at a given point will give the degeneracy of the phase transition. Thus, we search for distinct sets $\{m_\alpha\}$ and $\{n_\alpha\}$ that obey

$$z(\theta_1, \theta_2 + 2\pi m_2, \ldots, \theta_n + 2\pi m_n) = z(\theta_1, \theta_2 + 2\pi n_2, \ldots, \theta_n + 2\pi n_n), \tag{5.102}$$

which can happen if the angles on the right hand side are a permutation of the ones on the left, up to a constant shift. This fact follows from the explicit expression of z, given in (5.100). So, we look for permutations $\sigma \in S_n$ such that

$$m_{\sigma(\alpha)} = n_\alpha + \Delta, \tag{5.103}$$

where Δ is some constant shift. The solutions of this expression are

$$\sigma^{(k)} : \alpha \mapsto \alpha + k \qquad k = 1, 2, \ldots, n - 1, \tag{5.104}$$

where the right hand side is defined modulo n. The number of distinct solutions equals $n/\gcd(n, p)$. Thus, we find that if n and p are coprime, there are n such solutions, leading to an n-fold ground state degeneracy. Meanwhile, if $\gcd(n, p) = q > 1$, we find an r-fold degeneracy, where $r := n/q$.

5.5.2 't Hooft anomaly matching

Using the notion of 't Hooft anomaly matching, both [79] and [78] were able to formulate a field-theoretic version of the LSMA theorem for SU(n) chains. In short, the presence of an 't Hooft anomaly signifies nontrivial low energy physics; in one dimension, this necessitates a gapless phase so long as the symmetries of the SU(n) chain are not spontaneously broken (see Section 4.6.4 for a review). It was shown that in these models, an 't Hooft anomaly is present so long as p is not a multiple of n. Explicitly, it is a mixed anomaly between the PSU(n) := SU(n)/$\mathbb{Z}_n$ symmetry and the $\mathbb{Z}_n$ translation symmetry of the n-site-ordered classical ground state. It is a PSU(n) symmetry, and not an SU(n) symmetry, because of a $\mathbb{Z}_n$ subgroup of SU(n) that acts trivially on each term in the field theory. This is important because when one tries to gauge PSU(n), it leads to gauge fields with topological charge $\frac{1}{n}$, and forces one to include in the Lagrangian a counterterm that violates the $\mathbb{Z}_n$ symmetry. When this anomaly is present, the gapped phase must have spontaneously broken translation or PSU(n) symmetry; the latter is ruled out by Coleman's theorem. In the gapped phase, the ground state degeneracy is predicted to be $\frac{n}{\gcd(n,p)}$, which is consistent with the strong coupling analysis of the previous subsection, as well as the LSMA theorem.

The authors of [79] then argued that while an anomaly is present whenever $p \mod n \neq 0$, an RG flow to an IR stable WZW fixed point is possible only when p and n have no nontrivial common divisor. In this case, the flow is to SU(n)$_1$. Otherwise, the candidate IR fixed point

is $SU(n)_q$, where $q = \gcd(n, p)$, which is unstable and requires fine-tuning in order for the flag manifold sigma model to flow there. Also, there is no possible flow from this unstable theory to $SU(n)_1$, since this would violate the anomaly matching conditions derived in [116] for generic $SU(n)$ WZW models. There, it was found that the WZW model of level k' can flow to level k only if $k' > k$ and $\gcd(n, k) = \gcd(n, k')$.

5.5.3   A Haldane conjecture for SU(n) chains

Based on these arguments, we conclude that the rank-p symmetric $SU(n)$ chains may flow to an $SU(n)_1$ WZW model if p and n do not have a common divisor. In this case, we expect gapless excitations to appear in the excitation spectrum. For other values of p not a multiple of n, we predict a gapped phase with $n/\gcd(n, p)$-fold ground state degeneracy, in accordance with the LSMA theorem. Finally, when p is a multiple of n, we predict a unique gapped ground state, such as the AKLT-like configuration given in Section 3.5.3. See Figure 5.3 for a simplified phase diagram of the $SU(n)$ chain in the case when p and n are coprime. We can understand this phase transition as being driven by the $SU(n)$-invariant interaction term $\sum_a J_L^a J_R^a$ in the $SU(n)_1$ WZW model, where J_L and J_R are the left and right moving currents, respectively. This operator is marginal: for one sign of its coupling constant, it is marginally irrelevant and flows to zero; for the other sign it flows to large values [115]. Our claim about gapless behaviour translates to a statement about the sign of this coupling constant: at weak flag manifold coupling g, we expect this term to be marginally irrelevant. Then, at larger couplings, the term becomes marginally relevant, and there is an RG flow to a gapped phase with n degenerate ground states that break translation symmetry.

These predictions are a natural extension of our SU(3) Haldane conjecture from the previous chapter. We note that when p and n have a common divisor, at least one of the topological angles occurring in (5.97) is necessarily trivial. In the instanton gas picture of Haldane's conjecture, each type of topological excitation must have a nontrivial topological angle in order to ensure total destructive interference in half-odd integer spin chains [137]. This might lead one to speculate that a similar mechanism is at play here in $SU(n)$ chains. We will prove that this is indeed the case in Chapter 7.
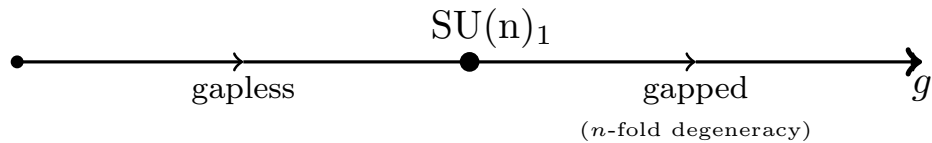
Figure 5.3: A simplified phase diagram of the SU(n) chains we consider, as a function of coupling constant g when p and n are coprime. A more accurate diagram would include $\lfloor \frac{n}{2} \rfloor$ different coupling constants; in this case, we predict a critical point described by $SU(n)_1$ occurring somewhere in this multidimensional space.

Finally, we may speculate on the size of the energy gap when p is not coprime with n. In general this is a difficult task, but in the special case of a theory with a unique coupling constant g, one may identify a characteristic length scale. This follows from the fact that g is described by the beta function (5.98), which has a lowest-order solution of the form

$$g(M) = \frac{g_0}{1 + \frac{n+2}{4\pi} g_0 \log(M)}. \tag{5.105}$$

Here g_0 is the bare value of g, and is a function of the interaction strengths J_t of the underlying SU(n) chain. This equation shows that g becomes order 1 at an energy scale of

$$\Delta = Ce^{-\frac{4\pi}{(n+2)g_0}}, \tag{5.106}$$

for some unknown prefactor C with units of energy. This expression defines a characteristic energy scale that should correspond in magnitude to the finite mass gap in our SU(n) chains. For SU(2) and SU(3) chains, this calculation leads to a direct prediction. In particular, we predict the Haldane gap in SU(3) chains with p a multiple of 3 to be of the order

$$\Delta_{n=3} = Ce^{-\frac{4\pi p \sqrt{J_1 J_2}}{5(J_1 + J_2)}}. \tag{5.107}$$

Of course, if one starts with a nearest-neighbour SU(3) model, then this expression is less predictive because of the difficulty in finding J_2 as a function of J_1. And even still, the prefactor C is unknown. In [77], a numerical estimate of this gap in the nearest-neighbour $p = 3$ model was found to be $\Delta_{n=3}/J \in (0.017, 0.046)$.

For $n > 3$, the presence of multiple coupling constants leads to another complication. While we know that each coupling is inversely proportional to p, the prefactors depends on the interaction strengths J_t of the chain, and we do not have a beta function as simple as (5.98). Nonetheless, if the interaction strengths are chosen so that all of the couplings g_t are of the same magnitude $g_t \sim c/p$, then we may still expect the gap to scale like $e^{-\frac{4\pi cp}{(n+2)}}$. For example, in SU(4) the simultaneous tuning

$$\sqrt{J_1 J_3}/(J_1 + J_3) \sim c \qquad J_2 \sim c \tag{5.108}$$

leads to a Haldane gap prediction of order $\Delta_{n=4} = Ce^{-\frac{2\pi p}{3c}}$. In any case, the prediction of a gap that decreases exponentially in p should hold for all values of n, even without fine-tuning.

5.6 Conclusion

In this chapter, we have extended Haldane's conjecture to SU(n) chains that have a rank-p symmetric representation at each site. Our starting point was SU(n) flavour-wave theory, where we first realized that the property of having a unique excitation velocity, which is present in SU(2) and SU(3) chains, no longer is true for chains with $n > 3$. This fact inhibits the immediate emergence of Lorentz invariance that occurred in those simpler models. In Section 5.4, we came to

the same conclusion by deriving in detail the low energy sigma model description of these $SU(n)$ chains. However, in Section 5.5, after extensive renormalization group calculations, we were able to conclude that these distinct velocities in fact flow to a common value at low enough energies. Because of this, we argued that $SU(n)$ chains in the rank-p symmetric representation do in fact correspond to the (Lorentz-invariant) $SU(n)/[U(1)]^{n-1}$ flag manifold sigma model, equipped with $n-1$ topological angles $\theta_\alpha = \frac{2\pi}{n} p\alpha$. Then, by applying a combination of exact results, including the LSMA theorem, AKLT constructions, and 't Hooft anomaly matching, we were able to formulate the following conjecture:

- **For p and n coprime**, we predict a gapless phase driven by topological angles to exist below some critical interaction strength. This phase is characterized by the $SU(n)_1$ WZW model. Above this critical coupling, we predict spontaneously broken translation symmetry and n-fold degenerate ground states.

- **For $1 < \gcd(n, p) < n$**, we predict that a gapless phase can never occur, so that translation symmetry is always spontaneously broken by the LSMA theorem. The ground states are $n/\gcd(n, p)$-fold degenerate.

- Finally, **for p a multiple of n**, we predict a unique, gapped ground state that is translationally invariant. The AKLT ground states presented in Section 3.5.3 correspond to this scenario.

Our prediction that translation symmetry is necessarily broken when p and n have a nontrivial common divisor other than n is rather interesting. This was not a possibility for the chains with smaller symmetry groups considered in Chapters 2 and 4, because $n = 2$ and $n = 3$ are both prime numbers. When this is the case, we see that *some, but not all* of the topological angles in the sigma model vanish. It appears then, that in order for a phase transition to be driven by topological effects in these $SU(n)$ chains, we require all $n - 1$ angles to be nontrivial. In Chapter 7, we present an elegant argument for why this is the case. In essence, the finite gap in $SU(n)$ chains can be understood as being generated by topological excitations. However, when all $n - 1$ topological angles are nonzero, these excitations destructively interfere with each other, and destroy the mass-generating mechanism.

Chapter 6

Flag Manifold Sigma Models From Other Representations of SU(n)

6.1 Introduction

In the previous chapters, we have clearly seen that much can be learned by establishing a mapping between SU(n) chains and flag manifold sigma models. In this chapter, we seek a more complete understanding of this correspondence. What this entails is addressing the following question: What representations of SU(n) chains give rise to SU(n)/[U(1)]$^{n-1}$ flag manifold sigma models? Once this has been answered, we should then further ask: What representations of SU(n) chains give rise to those flag manifold sigma models that possess 't Hooft anomalies, and lend themselves to a Haldane-like prediction of gapless excitations in certain cases.

In this chapter, we answer these two questions, ultimately classifying all SU(n) chains that admit such a flag manifold sigma model mapping. We have already set the stage in Section 3.4, where we classified the classical ground states for the most general representations of SU(n). In fact, we suggest to the reader that they recall much of Chapter 3 in order to motivate the present discussion. Here, we will begin by summarizing various facts about the flag manifold sigma models in Section 6.2. Then we turn in Section 6.3 to the derivation of the dispersion relations of low energy modes in generic SU(n) chains. In Chapters 2, 4, 5, these were called the dispersion relations of flavour-wave, or Goldstone mode excitations. We will see that generically, both quadratic and linear dispersing modes are present in these models, which is a manifestation of the ferro- and antiferromagnetic order parameters that coexist. This phenomenon was previously observed in Section 4.7 for SU(3) chains; now we learn that it occurs for all n. We also speculate in this section about how such coexisting order parameters may lead to an entire hierarchy of flag manifold sigma models, of different dimension, for a given value of n. Next, in Section 6.3, we restrict our attention to the representations with linear dispersion only, and determine their topological angle content. In Section 4.7, this amounted to considering the self-conjugate SU(3) chains, in addition to the symmetric ones. For $n > 3$, we will see that many other families of representations also possess this property. Then, in Section 6.4, we summarize our calculations and determine which of the representations considered in the previous section also admit a mixed 't Hooft anomaly. This will allow us to extend our SU(n) version of the Haldane conjecture from the previous chapter to new representations of SU(n). Finally, our concluding remarks can be found in Section 6.6.

6.2 Flag Manifold Sigma Models

For concreteness, let us write down the Lagrangian for the $SU(n)/[U(1)]^{n-1}$ flag manifold sigma model, in a manner more formal than that found in previous chapters. We introduce n orthonormalized fields $\varphi^\alpha \in \mathbb{C}^n$, which are each invariant under a separate U(1) symmetry,

$$\varphi^\alpha \mapsto e^{i\theta}\varphi^\alpha. \tag{6.1}$$

If we denote by $g_{\alpha\beta}$ the (symmetric) metric on the flag manifold, and $b_{\alpha\beta}$ the (antisymmetric) torsion, then the Lagrangian (5.97) can be rewritten as

$$\mathcal{L} = \sum_{\alpha,\beta=1}^{n} \left[g_{\alpha\beta}\delta^{\mu\nu} + b_{\alpha\beta}\epsilon^{\mu\nu} \right] (\varphi^\alpha \cdot \partial_\mu\varphi^{*,\beta})(\varphi_\beta \cdot \partial_\nu\varphi^{*,\alpha}) + \mathcal{L}_{\text{top}} \tag{6.2}$$

where $\mathcal{L}_{\text{top}}$ is the topological term

$$\mathcal{L}_{\text{top}} = \sum_{\alpha=1}^{n} \frac{\theta_\alpha}{2\pi}\epsilon^{\mu\nu}\partial_\mu\varphi^\alpha \cdot \partial_\nu\varphi^{*,\alpha}. \tag{6.3}$$

Only $n-1$ of the angles θ_α are independent, since the theory is invariant under shifting all angles by the same amount. This reflects the fact that

$$H^2(SU(n)/[U(1)]^{n-1}) = \mathbb{Z}^{n-1}. \tag{6.4}$$

In fact, all of the topological angles may be removed using the combined shifts

$$\theta_\alpha \to \theta_\alpha + 2\pi b_\alpha \qquad + \qquad b_{\alpha\beta} \mapsto b_{\alpha\beta} - b_\alpha - b_\beta \tag{6.5}$$

but this hides the 2π periodicity of the θ_α [79]. Finally, the shift $g_{\alpha\beta} \to g_{\alpha\beta} - c_\alpha - c_\beta$ introduces the familiar $\mathbb{C}P^{n-1}$ kinetic terms into the Lagrangian:

$$\mathcal{L} \to \mathcal{L} + \sum_{\alpha=1}^{n} c_\alpha \left[|\partial_\mu\varphi^\alpha|^2 - |\varphi^{*,\alpha} \cdot \partial_\mu\varphi^\alpha|^2 \right]. \tag{6.6}$$

Based on this fact, it is useful to use think of the embedding

$$\frac{SU(n)}{[U(1)]^{n-1}} \hookrightarrow \mathbb{C}P^{n-1} \times \cdots \times \mathbb{C}P^{n-1} \tag{6.7}$$

and visualize the field content as a set of orthogonal $\mathbb{C}P^{n-1}$ fields, coupled through the metric and torsion terms. Since $\mathbb{C}P^{n-1} = G_{1,n}$, this embedding is a special case of (3.16).

In most cases, the tensors $g_{\alpha\beta}$ and $b_{\alpha\beta}$ will admit additional, discrete symmetries. For example, a sigma model that arises from an $SU(n)$ chain with a d-site unit cell in its classical ground state will possess a $\mathbb{Z}_d$ symmetry as a manifestation of the translation symmetry on the chain.

However, what is also true is that in most cases, the SU(n) chain will not directly map to the above Lorentz-invariant sigma model. There are two reasons for this. The first is that the fields φ^α are not guaranteed to propagate with the same velocity. Indeed, for the symmetric representation SU(n) chains, it was shown in Chapter 5 that only for a fine-tuned choice of SU(n) chain coupling constants do these velocities become equal. However, we now know that at low enough energies, all of the velocity differences flow to zero under renormalization. In this chapter, we will assume that this mechanism holds more generally, so that we may identify the various velocities of the $\mathbb{CP}^{n-1}$ fields.

The second reason for Lorentz non-invariance is more of a hindrance. It follows from a mismatch of terms arising from the coherent state path integral construction, ultimately leading to some of the φ^α having quadratic dispersion. Mathematically, we say that the embedding SU(n)/[U(1)]$^{n-1} \hookrightarrow [\mathbb{CP}^{n-1}]^n$ is not Lagrangian in this case. Let us speculate a consequence of these quadratic modes. Since Coleman's theorem does not apply in 1+1 dimensions to modes with quadratic dispersion, the generators associated with these modes may spontaneously order, resulting in true Goldstone modes with quadratic dispersion [95–97, 138]. These Goldstone bosons will couple to the remaining linear modes, which themselves form an SU(n')/[U(1)]$^{n'-1}$ sigma model with $n' < n$. If a subgroup of the translation symmetry acts transitively on the n' linear fields, then it becomes possible for a novel 't Hooft anomaly (mixed with the $\mathbb{Z}_{n'}$ subgroup) to exist in such SU(n) chains.[34] However, for now we will avoid these complications by focusing only on theories with purely linearly dispersing modes. In the following section, we determine exactly which representations of SU(n) lead to such theories.

6.3 Dispersion Relations

In Section 3.4, we determined which SU(n) Hamiltonians were required in order to establish a flag manifold sigma model mapping for a given representation, $\mathcal{R}$. In other words, we determined how many longer-range interaction terms had to be included in order to stabilize local zero modes. These results are summarized in Table 3.1, which is repeated here for convenience:

With these results in hand, we now turn to the field theory mapping itself. Of course, a detailed derivation for each Hamiltonian would be a very tedious undertaking, and we do not pursue this here. Instead, we focus on particular features, namely the topological angles and possible dispersion relations that exist in these theories, and refrain from determining the precise coupling constants and velocities as a function of the interaction strengths J_r. Later on, we will explain how these pieces of information, combined with a set of reasonable assumptions, will allow us to make predictions about the ground state behaviour of certain SU(n) chains. But first, let us review the

---

[34]Note that while mixed anomalies between PSU(n) and $\mathbb{Z}_{n'}$ do exist for n and n' sharing a nontrivial common divisor, they will not allow for a renormalization group flow to the stable fixed point SU(n)$_1$ [78].

Representation		Longest Interaction	Translation Group Order
$k = 1$		$J_{n-1}\text{tr}[S(j)S(j + n - 1)]$	n
$k = n - 1$		$J_1\text{tr}[S(j)S(j + 1)]$	2
$k = \frac{n}{\lambda},$	$\lambda < n$	$J_\lambda\text{tr}[S(j)S(j + \lambda)]$	2λ
$n = 2\lambda + 1,$	$k = 2$	$J_\lambda\text{tr}[S(j)S(j + \lambda)]$	$\lambda(\lambda + 1)$
$n = k\lambda + 1,$	$\lambda > 1, k > 2$	$J_\lambda\text{tr}[S(j)S(j + \lambda)]$	$\text{lcm}[2\lambda, (\lambda + 1)]$
$n = k\lambda + c,$	$c \neq 1, k - 1$	$J_{\lambda+1}\text{tr}[S(j)S(j + \lambda + 1)]$	$2\lambda(\lambda + 1)$
$n = k\lambda + (k - 1)$		$J_{\lambda+1}\text{tr}[S(j)S(j + \lambda + 1)]$	$\text{lcm}[\lambda, 2(\lambda + 1)]$

Table 6.1: Classification results of all SU(n) representations satisfying $p_\alpha \neq p_\beta$ for all nonzero p_α.

coherent state path integral construction for an arbitrary representation of SU(n). This generalizes the discussion found in Section 4.3.1.

6.3.1 Generalizing the coherent state path integral construction

In order to construct a mapping from Hamiltonian to sigma model, we use coherent states to generate a path integral of the ground state fluctuations. These coherent states are constructed as follows. For a representation with nonzero Young tableau rows $p_1, \ldots, p_k$, we introduce k orthonormal fields $\boldsymbol{\phi}^\alpha \in \mathbb{C}^n$, and k n-component creation operators $\boldsymbol{a}^{\alpha,\dagger}$. We then define [99, 100]

$$|\Phi\rangle := \sum_{\alpha=1}^{k} [\boldsymbol{\phi}^\alpha \cdot \boldsymbol{a}^\alpha]^{p_\alpha} |0\rangle. \tag{6.8}$$

These are the coherent states of SU(n), and in order to construct a path integral, we insert them between thin time slices of the partition function:

$$\langle \Phi(\tau_i)|e^{-H\delta\tau}|\Phi(\tau_i + \delta\tau)\rangle = \langle \Phi(\tau_i)|\Phi(\tau_i + \delta\tau)\rangle e^{-H\delta\tau}. \tag{6.9}$$

The right hand side can be approximated using

$$\langle \Phi(\tau_i)|\Phi(\tau_i + \delta\tau)\rangle \approx \sum_{\alpha=1}^{k} [1 + \boldsymbol{\phi}^{*,\alpha} \cdot \partial_\tau \boldsymbol{\phi}^\alpha]^{p_\alpha}, \tag{6.10}$$

which follows from

$$\langle \Phi(\tau)|\Phi(\tau')\rangle = \sum_{\alpha=1}^{k} (\boldsymbol{\phi}^{*,\alpha}(\tau) \cdot \boldsymbol{\phi}^\alpha(\tau'))^{p_\alpha}. \tag{6.11}$$

105

By taking the product over all time slices τ_i, we can then reexponentiate according to

$$\prod_i \langle \Phi(\tau_i)|\Phi(\tau_i + \delta\tau)\rangle = \exp \sum_i \log \langle \Phi(\tau_i)|\Phi(\tau_i + \delta\tau)\rangle \approx \exp \sum_i \sum_\alpha p_\alpha \boldsymbol{\phi}^{*,\alpha} \cdot \partial_\tau \boldsymbol{\phi}^\alpha. \qquad (6.12)$$

The Berry phase contribution to the path integral is obtained by adding up this contribution over each site of the unit cell:

$$\mathcal{L}_{\text{Berry}} = -\frac{1}{d} \sum_{j=1}^d \sum_{\alpha=1}^k p_\alpha \boldsymbol{\phi}^{*,\alpha}(j) \cdot \partial_\tau \boldsymbol{\phi}^\alpha(j). \qquad (6.13)$$

Here d is the size of the unit cell, and $\boldsymbol{\phi}^\alpha(j)$ is the field $\boldsymbol{\phi}^\alpha$ evaluate at site j. Since we are deriving a field theory about a classical ground state, to lowest order $\boldsymbol{\phi}^\alpha(j)$ is the colour of node α at site j, which we have been representing using $\boldsymbol{\varphi}^\alpha$.

To obtain the complete quantum field theory, one must add to $\mathcal{L}_{\text{Berry}}$ a gradient expansion of the SU(n) lattice Hamiltonian, and this is where the lengthy calculations lie. However, if one is interested only in time-derivatives, it suffices to restrict attention to $\mathcal{L}_{\text{Berry}}$, since the Hamiltonian is time-independent. The lowest-order expansion of $\mathcal{L}_{\text{Berry}}$, which amounts to replacing the $\boldsymbol{\phi}^\alpha(j)$ with their uniform counterparts $\boldsymbol{\varphi}^\beta$ (where β depends on α and j), will indicate how many of the sigma model's modes have linear dispersion. The next-order expansion, which takes into account the spatial fluctuations of the $\boldsymbol{\varphi}^\alpha$ across the unit cell, will provide the topological angle content of the theory. It turns out that the non-uniform fluctuations of the $\boldsymbol{\phi}^\alpha$, namely $L_{\alpha\beta}$ as defined in (5.13), do not contribute to the topological term, and so in the following, we may safely replace $\boldsymbol{\phi}^\alpha$ with $\boldsymbol{\varphi}^\alpha$ in (6.13) throughout.

Let us explain why this is the case. According to (5.13), in deriving a field theory we should write

$$\boldsymbol{\phi}^\alpha = \sum_\beta L_{\alpha\beta} \boldsymbol{\varphi}^\beta + \sqrt{1 - \mu(\alpha)} \boldsymbol{\varphi}^\alpha, \qquad (6.14)$$

where $L_{\alpha\alpha} = 0$ (no sum), and $\mu(\alpha) = \sum_\beta |L_{\alpha\beta}|^2$. Unlike (5.13), we absorb the 'large representation' parameter p^{-1} into the definition of the $L_{\alpha\beta}$ terms. This is to avoid the notational complication of dealing with multiple nonzero parameters p_α in the expansion of the $\boldsymbol{\phi}^\alpha$.

Now, this expansion formula (6.14) will be inserted both into the Hamiltonian and the Berry phase term (6.13). What we seek to show here is that no term involving the $L_{\alpha\beta}$ will contribute to the topological terms $\epsilon_{\mu\nu} \partial_\mu \boldsymbol{\varphi}^{*,\alpha} \cdot \partial_\nu \boldsymbol{\varphi}^\beta$ upon integrating out the $L_{\alpha\beta}$. Indeed, this follows from the Gaussian integral formula[35]

$$\int dL_{\alpha\beta} dL_{\alpha\beta}^* e^{-L_{12}^* w L_{12} + u L_{12} + v L_{12}^*} = \frac{\pi}{w} e^{uv/w}, \qquad (6.15)$$

which we used explicitly in Chapters 2, 4, and 5. Now, any term involving one time derivative and one space derivative on the right hand side of (6.15) will have come from expressions of the form

$$uL_{12} = aL_{12}[\partial_\tau UU^\dagger]_{12} + bL_{12}[\partial_x UU^\dagger]_{12} \qquad (6.16)$$

$$vL_{12}^* = aL_{12}^*[\partial_\tau UU^\dagger]_{12} - bL_{12}^*[\partial_x UU^\dagger]_{12}, \qquad (6.17)$$

---

[35]In the following, we restrict to the case of $L_{\alpha\beta} = L_{12}$.

for real parameters a and b. This structure arises from the Hermitian requirement of the Hamiltonian, which is the source of the spatial derivative terms. Meanwhile, the time-derivative terms are anti-Hermitian in imaginary time. This is a property generic to any integral over $L_{\alpha\beta}$ appearing in our field theory derivation. From here, it is easy to see that the cross-terms involving ∂_τ and ∂_x will always be of the form

$$\epsilon_{\mu\nu}\text{tr}[\Lambda_\alpha\partial_\mu UU^\dagger\Lambda_\beta\partial_\nu UU^\dagger], \tag{6.18}$$

with $\alpha \neq \beta$. These terms are *not* topological; instead, they are the so-called 'torsion terms', which occur in (6.2) with coefficients $b_{\alpha\beta}$ (in previous chapters, we referred to them as λ-terms). Therefore, we conclude that the $L_{\alpha\beta}$ do not play a role in our discussion of topological angles below, and we will henceforth omit them entirely.

Dispersion Relation Calculations

For each family of representations in Table 6.1, we determine the lowest-order contribution to $\mathcal{L}_\text{Berry}$. For each field φ^α that is present, this indicates the presence of $(n-1)$ quadratically dispersing modes. Only in the case of a vanishing $\mathcal{L}_\text{Berry}$ at this order does linear dispersion occur for each mode of the theory. However, even in this case, Lorentz invariance is not automatic since the fields φ^α will generically propagate with different velocities, as we saw in the previous chapter.

6.3.2 Representations with 1 row

First we consider representations with one row. The ground states are very simple in this case: one row of n nodes, with each colour occurring once. For example, in SU(5) one such ground state is

$$\cdots \quad \bullet \; \bullet \; \bullet \; \circ \; \circ \; \bullet \; \bullet \; \bullet \; \circ \; \circ \quad \cdots . \tag{6.19}$$

Therefore, we have

$$\mathcal{L}_\text{Berry} = -\frac{p_1}{n}\sum_{j=1}^{n}\varphi^{*,\alpha}(j)\cdot\partial_\tau\varphi^\alpha(j) + \text{ H.O.} \tag{6.20}$$

where H.O. includes higher-order terms. Since each colour occurs once in the sum on the right hand side, the sum equals $\text{tr}[U^\dagger\partial_\tau U]$ for a unitary matrix U, which vanishes by Appendix A, and so all modes have linear dispersion in the representations with $k = 1$ row.

6.3.3 Representations with $n - 1$ rows

Next, we consider representations with $k = n - 1$ rows. According to the pattern of ground states, two of the colours occur once (in the first position of the columns), and the remaining $n - 2$ colours

occur twice, with reverse-ordering. For example, in SU(5), the ground state looks like
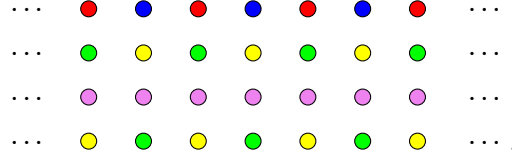
Therefore we have, according to (6.13),

$$\mathcal{L}_{\text{Berry}} = -\frac{p_1}{2}(\varphi^{*,1} \cdot \partial_\tau \varphi^1 + \varphi^{*,2} \cdot \partial_\tau \varphi^2) - \frac{1}{2}\sum_{\alpha=3}^{n}(p_{\alpha-1} + p_{n-\alpha+2})\varphi^{*,\alpha}(j) \cdot \partial_\tau \varphi^\alpha(j). \tag{6.21}$$

Using $\text{tr}[U^\dagger \partial_\tau U] = 0$, this can be rewritten as

$$\mathcal{L}_{\text{Berry}} = -\frac{1}{2}\sum_{\alpha=3}^{n}(p_{\alpha-1} + p_{n-\alpha+2} - p_1)\varphi^{*,\alpha}(j) \cdot \partial_\tau \varphi^\alpha(j). \tag{6.22}$$

Now we have up to $(n-2)$ fields with quadratic dispersion. The exact number will depend on how many of the conditions $p_{\alpha-1} + p_{n-\alpha+2} - p_1 = 0$ are satisfied. Each constraint corresponds to two fields φ^α, except for the constraint $2p_{(n+1)/2} = p_1$ when n is odd, which corresponds to a single field. The representations that satisfy every constraint, and thus give rise to sigma models with purely linear dispersion, correspond to the so-called self-conjugate representations of SU(n) (that don't have equal row lengths in their tableaux). Indeed, in SU(3), the condition is $2p_2 = p_1$, corresponding to the self-conjugate representations considered in Section 4.7. Similarly, in SU(4), the condition for linear dispersion is $p_2 + p_3 = p_1$, which is equivalent to the self-conjugate condition $p_1 - p_2 = p_3$.

6.3.4 Representations with row number dividing n.

Now we consider representations with k rows, with $\frac{n}{k} = \lambda \in \mathbb{Z}$. In this case, the ground states have order of length 2λ, with each colour occurring twice. If $k = \frac{n}{2}$, the pattern looks like
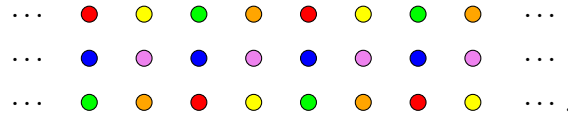
For $k < \frac{n}{2}$, the pattern is modified, which can be seen in (3.20). Introducing the notation

$$A^\alpha := \varphi^{*,\alpha} \cdot \partial_\tau \varphi^\alpha, \tag{6.23}$$

and following these patterns as a guide, we find that

$$\mathcal{L}_{\text{Berry}} = -\frac{1}{2\lambda}\sum_{\alpha=1}^{k}\sum_{j=1}^{\lambda}(p_\alpha + p_{k+1-\alpha})A^{\alpha+(j-1)k}, \tag{6.24}$$

which can be rewritten using $\text{tr}[U^\dagger \partial_\tau U] = 0$ to yield

$$\mathcal{L}_{\text{Berry}} = -\frac{1}{2\lambda} \sum_{\alpha=2}^{k-1} \sum_{j=1}^{\lambda} (p_\alpha + p_{k+1-\alpha} - p_1 - p_k) A^{\alpha+(j-1)k}. \tag{6.25}$$

This suggests that there can be up to $(k-2)\lambda$ fields with quadratic dispersion. In order to remove all of these modes, the representation must satisfy certain constraints. When k is even, they are

$$p_\alpha + p_{k+1-\alpha} = p_1 + p_k \qquad \alpha = 2, \ldots, \frac{k}{2} \tag{6.26}$$

and when k is odd, they are

$$p_\alpha + p_{k+1-\alpha} = p_1 + p_k \qquad \alpha = 2, \ldots, \frac{k-1}{2} \tag{6.27}$$

$$2p_{\frac{k+1}{2}} = p_1 + p_k \tag{6.28}$$

Each of the constraints (6.26), (6.27) corresponds to the dispersion of 2λ fields, and the constraint (6.28) corresponds to the dispersion relation of λ fields. In the special case of $k = 2$, which corresponds to Young tableaux with two rows, we have automatically that $\mathcal{L}_{\text{Berry}} = 0$ for all values of p_1 and p_2. The simplest representation for larger k is shown below, for SU(8):

$$\tag{6.29}$$

This diagram satisfies $p_1 + p_4 = p_2 + p_3$.

6.3.5 Remaining representations

Representations of SU($2\lambda + 1$) with two rows

Let $n = 2\lambda + 1$, and consider representations with 2 rows. In this case the ground states have unit cells of length $\lambda(\lambda + 1)$. For example, in SU(5) with $k = 2$, a candidate ground state is

$$\mathcal{L}_{\text{Berry}} = -\frac{p_1}{(\lambda + 1)} \sum_{\alpha=1}^{\lambda+1} A^\alpha - \frac{p_2}{\lambda} \sum_{\beta=1}^{\lambda} A^\beta, \tag{6.30}$$
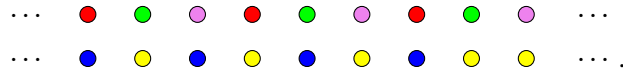
For all of these representations, the first row will have periodicity $\lambda + 1$, and the second row will have periodicity λ. The Berry phase term is then

$$\mathcal{L}_{\text{Berry}} = -\frac{p_1}{(\lambda + 1)} \sum_{\alpha=1}^{\lambda+1} A^\alpha - \frac{p_2}{\lambda} \sum_{\beta=1}^{\lambda} A^\beta, \tag{6.30}$$

which can be rewritten to give

$$\mathcal{L}_{\text{Berry}} = -\frac{1}{\lambda(\lambda+1)}\left[p_2(\lambda+1) - p_1\lambda\right]\sum_{\beta=1}^{\lambda}A^{\beta}. \tag{6.31}$$

For most values of p_1 and p_2, the corresponding sigma model will have λ fields with quadratic dispersion, and $\lambda + 1$ fields with linear dispersion.[36] However, for the special representations satisfying

$$\lambda p_1 = (\lambda+1)p_2 \tag{6.32}$$

a theory with purely linearly dispersing modes is achieved.

Representations of SU($k\lambda + 1$), with $\lambda > 1, k > 2$

Now we let $n = k\lambda + 1$, with $\lambda > 1$ and $k > 2$, and consider representations with k rows. According to Table 6.1, we must further specify the parity of λ:

- λ even:
  The ground state unit cell has length $2\lambda(\lambda + 1)$ in this case. The first row has $(\lambda + 1)$-site order, while the remaining $k - 1$ rows have 2λ-site order, with the coloured nodes exhibiting reverse-ordering. Therefore, the Berry phase term is

$$\mathcal{L}_{\text{Berry}} = -\frac{p_1}{(\lambda+1)}\sum_{\alpha=1}^{\lambda+1}A^{\alpha} - \frac{1}{2\lambda}\sum_{\beta=2}^{k}\sum_{j=1}^{\lambda}(p_{\beta}+p_{k+2-\beta})A^{\beta+j(k-1)}. \tag{6.33}$$

While simpler to rewrite in terms of the A^{α} with $\alpha > \lambda + 1$, we will always choose to rewrite the Berry phase in terms of the least number of fields possible. This leads to

$$\mathcal{L}_{\text{Berry}} = -\frac{1}{2\lambda(\lambda+1)}\sum_{\alpha=1}^{\lambda+1}\left[2\lambda p_1 - (\lambda+1)(p_2+p_k)\right]A^{\alpha} - \frac{1}{2\lambda}\sum_{\beta=3}^{k-1}\sum_{j=1}^{\lambda}(p_{\beta}+p_{k+2-\beta}-p_2-p_k)A^{\beta+j(k-1)}. \tag{6.34}$$

- λ odd:
  In this case, the result found in (6.34) is slightly modified to

$$\mathcal{L}_{\text{Berry}} = -\frac{1}{\lambda(\lambda+1)}\sum_{\alpha=1}^{\lambda+1}\left[\lambda p_1 - (\lambda+1)(p_2+p_k)\right]A^{\alpha} - \frac{1}{\lambda}\sum_{\beta=3}^{k-1}\sum_{j=1}^{\lambda}(p_{\beta}+p_{k+2-\beta}-p_2-p_k)A^{\beta+j(k-1)}. \tag{6.35}$$

---

[36]As mentioned below (6.40), we can rewrite $\mathcal{L}_{\text{Berry}}$ to have $\lambda + 1$ fields with quadratic dispersion, and λ fields with linear dispersion.

Representations of SU($k\lambda + c$) with $c \neq 1, k - 1$

Again, let k be the number of rows. The ground states in the case have unit cell order of length $2\lambda(\lambda + 1)$. The Berry phase contribution is

$$\mathcal{L}_{\text{Berry}} = -\frac{1}{2(\lambda + 1)} \sum_{\alpha=1}^{c} \sum_{j=1}^{\lambda+1} [p_\alpha + p_{c+1-\alpha}] A^{\alpha+(j-1)c} - \frac{1}{2\lambda} \sum_{\beta=c+1}^{k} \sum_{j=1}^{\lambda} [p_\beta + p_{k-\beta+c+1}] A^{c(\lambda+1)+(\beta-c)+(j-1)(k-c)}.$$

(6.36)

Using the $\text{tr}[U^\dagger \partial U] = 0$ identity, we can only remove $2(\lambda + 1)$ fields. We are left with:

$$\mathcal{L}_{\text{Berry}} = -\frac{1}{2(\lambda + 1)} \sum_{\alpha=2}^{c-1} \sum_{j=1}^{\lambda+1} [p_\alpha + p_{c+1-\alpha} - (p_1 + p_c)] A^{\alpha+(j-1)c}$$

(6.37)

$$-\frac{1}{2\lambda(\lambda + 1)} \sum_{\beta=c+1}^{k} \sum_{j=1}^{\lambda} \left[(\lambda + 1)(p_\beta + p_{k-\beta+c+1}) - \lambda(p_1 + p_c)\right] A^{c(\lambda+1)+(\beta-c)+(j-1)(k-c)}.$$

The number of independent constraints that must be satisfied in order to achieve a sigma model with purely linear dispersion is $\lfloor \frac{c}{2} \rfloor + \lfloor \frac{k-c}{2} \rfloor$.

Representations of SU($k\lambda + (k - 1)$)

The remaining representations are for $n = k\lambda + (k - 1)$. In this final case, we must again split into two subcases, based on the parity of λ:

- λ even:
  According to Table 6.1, the ground state has $\lambda(\lambda + 1)$-site order. The first $c - 1$ rows of the ground state have period $2(\lambda + 1)$, while the last row has period λ. The Berry phase term is

$$\mathcal{L}_{\text{Berry}} = -\frac{1}{(\lambda + 1)} \sum_{\alpha=1}^{k-1} \sum_{j=1}^{\lambda+1} [p_\alpha + p_{k-\alpha}] A^{\alpha+(j-1)(k-1)} - \frac{1}{\lambda} \sum_{\beta=1}^{\lambda} p_k A^{(k-1)(\lambda+1)+\beta}$$

(6.38)

$$= -\frac{1}{(\lambda + 1)} \sum_{\alpha=2}^{k-2} \sum_{j=1}^{\lambda+1} [p_\alpha + p_{k-\alpha} - p_1 - p_{k-1}] A^{\alpha+(j-1)(k-1)}$$

$$-\frac{1}{\lambda(\lambda + 1)} \sum_{\beta=1}^{\lambda} [(\lambda + 1)p_k - \lambda(p_1 + p_{k-1})] A^{(k-1)(\lambda+1)+\beta}.$$

- λ odd:
  Now the ground state has $2\lambda(\lambda + 1)$ order, which changes the result in (6.38) to

$$= -\frac{1}{2(\lambda + 1)} \sum_{\alpha=2}^{k-2} \sum_{j=1}^{\lambda+1} [p_\alpha + p_{k-\alpha} - p_1 - p_{k-1}] A^{\alpha+(j-1)(k-1)}$$

(6.39)

$$-\frac{1}{2\lambda(\lambda+1)}\sum_{\beta=1}^{\lambda}[2(\lambda+1)p_k-\lambda(p_1+p_{k-1})]A^{(k-1)(\lambda+1)+\beta}.$$

6.3.6 Summary of calculations

We have compiled these results in Table G.1 in Appendix G. Each row corresponds to a family of SU(n) representations. The 'Min #' column counts the minimum number of $\mathbb{C}^n$ fields φ^α that have linear dispersion in the corresponding SU(n)/[U(1)]$^{n-1}$ sigma model. The larger, right hand column lists the conditions that the representation parameters p_α must satisfy in order for additional fields to acquire linear dispersion. Each condition is accompanied by a number in parentheses: this dictates how many fields φ^α become linearly dispersing when this condition is satisfied. For example, the second row of Table G.1 corresponds to representations with $n-1$ rows in their Young tableaux. These representations will always have at least two linearly dispersing fields in their sigma model. In order to have more linearly dispersing fields, we must start to satisfy conditions. When n is even, these conditions are $p_\alpha+p_{n-\alpha+1}=p_1$, for $\alpha=2,\ldots,\frac{n}{2}$. Each satisfied condition adds 2 more linearly dispersing fields to the sigma model. It is amusing to note that when all of these conditions are satisfied, we obtain the set of self-conjugate representations of SU(n) (that don't have two rows of the same length).

It is important to note that there is some ambiguity in the number of linear vs. quadratic modes, which follows from the trace identity $\text{tr}[U^\dagger\partial_\tau U]=0$. This expression allows us to rewrite a partial sum $\sum_{\alpha\in A}\varphi^{*,\alpha}\cdot\partial_\tau\varphi^\alpha$ in terms of the φ^β that do not occur in the sum:

$$\sum_{\alpha\in A}\varphi^{*,\alpha}\cdot\partial_\tau\varphi^\alpha=-\sum_{\beta\notin A}\varphi^{*,\beta}\cdot\partial_\tau\varphi^\beta. \tag{6.40}$$

To be consistent, we will always choose to write the Berry phase contribution in terms of the least number of fields possible. However, of primary interest to us in this thesis are theories that only have linearly dispersing modes; in this case, the counting becomes uniquely defined.

6.4 Topological Angles

In addition to the dispersion relations, we may also extract the topological angle content from the Berry phase terms. This requires taking into account the spatial variation of the fields φ^α in each of the terms found in the previous section.

As we have already seen, each field is associated with some condition on the Young tableaux parameters p_α. When determining the set of topological angles, it will be important to keep track of these conditions; ultimately, this will lead to a list of angles for each of the conditions appearing in Table G.1. Our motivation for this bookkeeping is so that we can understand which topological angles correspond to linearly dispersing fields. Since quadratic modes correspond to ferromagnetic order parameters, it is conceivable that by 'turning on' a subset of the p_α conditions, we may be able to effectively reduce the symmetry of our sigma model from SU(n)/[U(1)]$^{n-1}$ to SU(n')/[U(n')]$^{n'-1}$

for some $n' < n$. It will be essential to keep track of which topological angles survive in the smaller theory.

To begin, we recall (6.13):

$$\mathcal{L}_{\text{Berry}} = -\frac{1}{d} \sum_{j=1}^{d} \sum_{\alpha=1}^{k} p_\alpha \boldsymbol{\phi}^{\alpha,*}(j) \cdot \partial_\tau \boldsymbol{\phi}^\alpha(j) \tag{6.41}$$

where d is the unit cell length. The lowest-order terms were analyzed in the previous section, which amounted to replacing $\boldsymbol{\phi}^\alpha$ with $\boldsymbol{\varphi}^\alpha$. Now, we take into account spatial fluctuations of the $\boldsymbol{\phi}^\alpha$. Again, the non-uniform fluctuations $L_{\alpha\beta}$ do not contribute at this order, so in this case, we may write the leading order correction to (6.41) as

$$\mathcal{L}_{\text{Berry}} = \cdots + \epsilon_{\mu\nu} \frac{1}{d} \sum_{j=1}^{d} (j-1) \sum_{\alpha=1}^{k} p_\alpha \partial_\mu \boldsymbol{\varphi}^{*,x(\alpha,j)} \cdot \partial_\nu \boldsymbol{\varphi}^{x(\alpha,j)} \quad + \text{H.O.}. \tag{6.42}$$

Here all of the terms are evaluated at the same lattice site, and $\cdots$ hides the terms from the previous section. The notation $x(\alpha, j)$ reminds us that for each field in the sum, we must consult the ground state structure (see Section 3.4), and use both the row (α) and column (j) to determine the index x. Using this, we may rewrite this contribution from the Berry phase term as

$$\mathcal{L}_{\text{Berry}} = \frac{1}{2\pi i} \sum_{\alpha=1}^{n} \theta_\alpha q_\alpha, \tag{6.43}$$

where

$$q_\alpha := \epsilon_{\mu\nu} \partial_\mu \boldsymbol{\varphi}^{*,\alpha} \cdot \partial_\nu \boldsymbol{\varphi}^\alpha \tag{6.44}$$

is a total derivative. From here, we are able to read off the topological angles, θ_α. We will carry out this procedure for each family of SU(n) representation listed in the previous section.

6.4.1 Representations with one row

In the case of one-row representations, the Berry phase term reduces to

$$\mathcal{L}_{\text{Berry}} = \epsilon_{\mu\nu} \frac{p_1}{n} \sum_{\alpha=1}^{n} (\alpha - 1) \partial_\mu \boldsymbol{\varphi}^{*,\alpha} \cdot \partial_\nu \boldsymbol{\varphi}^\alpha, \tag{6.45}$$

so that

$$\theta_\alpha = \frac{2\pi p_1}{n} (\alpha - 1). \tag{6.46}$$

Since there are no quadratically dispersing fields when $k = 1$, these angles do not correspond to a nontrivial condition on the p_α.

6.4.2   Representations with $n - 1$ rows

Now we consider representations with $k = n - 1$ rows. Starting from (6.42), it is clear that we only have to focus on a single column in the coloured ground state diagram:

$$\mathcal{L}_{\text{Berry}} = \cdots + \frac{1}{2}\epsilon_{\mu\nu} \sum_{\alpha=1}^{n-1} p_\alpha \partial_\mu \boldsymbol{\varphi}^{*,\alpha} \cdot \partial_\nu \boldsymbol{\varphi}^\alpha. \tag{6.47}$$

The topological angles are then

$$\theta_\alpha = \pi p_\alpha. \tag{6.48}$$

According to the conditions in Table G.1, two fields are always linearly dispersing, corresponding to $\theta_1 = p_1 \pi$ and $\theta_n = 0$. The remaining $n - 2$ angles correspond to fields that must satisfy conditions on the p_α. The exact relationship between angle and nontrivial condition is given below in Table 6.2, making use of (6.48):

Subcase	Condition	Angles	
n even	$p_\alpha + p_{n-\alpha+1} = p_1$	$\theta_\alpha, \theta_{n-\alpha+1}$	$\alpha = 2, \ldots, \frac{n}{2}$
n odd	$p_\alpha + p_{n-\alpha+1} = p_1$ $2p_{\frac{n+1}{2}} = p_1$	$\theta_\alpha, \theta_{n-\alpha+1}$ $\theta_{\frac{n+1}{2}}$	$\alpha = 2, \ldots, \frac{n-1}{2}$

Table 6.2: The relation between topological angles and condition on the p_α, for representations of SU(n) with $n - 1$ rows. For each condition, one or two fields $\boldsymbol{\varphi}^\alpha$ becomes linear dispersing, and has topological angle provided in the right-most column.

6.4.3   Representations with row number dividing n

Now we consider representations with k rows, with $\frac{n}{k} = \lambda \in \mathbb{Z}$. In this case, the correction to $\mathcal{L}_{\text{Berry}}$ is

$$\mathcal{L}_{\text{Berry}} = \frac{1}{2\lambda}\epsilon_{\mu\nu} \sum_{\alpha=1}^{k} \sum_{j=1}^{\lambda} \left[(j-1)p_\alpha + (\lambda + j - 1)p_{k+1-\alpha}\right] \partial_\mu \boldsymbol{\varphi}^{*,\alpha,j} \cdot \partial_\nu \boldsymbol{\varphi}^{\alpha,j}, \tag{6.49}$$

so that the topological angles are

$$\theta_{\alpha,j} = \frac{\pi}{\lambda}(p_\alpha + p_{k+1-\alpha})(j-1) + \pi p_{k+1-\alpha}. \tag{6.50}$$

114

The range of these indices can be read off from the sums in (6.49). Here we use two indices to enumerate the fields. Since 2λ of the fields always have linear dispersion, the angles $\theta_{1,j}$ and $\theta_{k,j}$ are always present. Meanwhile, the remaining $(k-2)\lambda$ angles are associated with certain conditions, according to the following table Table 6.3.

Subcase	Condition	Angles	
k even	$p_\alpha + p_{k+1-\alpha} = p_1 + p_k$	$\theta_{\alpha,j}, \theta_{k-\alpha+1,j}$	$\alpha = 2, \ldots, \frac{k}{2}; j = 1, \ldots, \lambda$
k odd	$p_\alpha + p_{k-\alpha+1} = p_1 + p_k$ $2p_{\frac{k+1}{2}} = p_1 + p_k$	$\theta_{\alpha,j}, \theta_{k-\alpha+1,j}$ $\theta_{\frac{k+1}{2},j}$	$\alpha = 2, \ldots, \frac{k-1}{2}, j = 1, \ldots, \lambda$

Table 6.3: The relation between topological angles and conditions on the p_α for representations with $k = \frac{n}{\lambda}$ rows in their Young tableaux.

6.4.4 Remaining representations

Representations of $SU(2\lambda + 1)$ with 2 rows

Suppose $n = 2\lambda + 1$, and consider representations with 2 rows. We again refer to Table G.1. From

$$\mathcal{L}_{\text{Berry}} = \epsilon_{\mu\nu} \frac{p_1}{\lambda(\lambda + 1)} \sum_{j=1}^{\lambda} \sum_{t=1}^{\lambda+1} (t - 1 + (j - 1)(\lambda + 1)) \partial_\mu \varphi^{*,t} \cdot \partial_\nu \varphi^t \qquad (6.51)$$

$$+ \epsilon_{\mu\nu} \frac{p_2}{\lambda(\lambda + 1)} \sum_{j=1}^{\lambda} \sum_{t=1}^{\lambda+1} (j - 1 + (t - 1)\lambda) \partial_\mu \varphi^{*,j+\lambda+1} \cdot \partial_\nu \varphi^{j+\lambda+1},$$

we see that there are two families of angles:

$$\theta_t = \frac{2\pi p_1}{(\lambda + 1)}(t - 1) + \pi p_1(\lambda - 1) \qquad (6.52)$$

for $t = 1, \ldots, \lambda + 1$, and

$$\tilde{\theta}_j = \frac{2\pi p_2}{\lambda}(j - 1) + \pi p_2 \lambda \qquad (6.53)$$

for $j = 1, \ldots, \lambda$. The θ_t angles correspond to fields that are always linearly dispersing. The remaining angles are associated to the single condition $\lambda p_1 = (\lambda + 1)p_2$.

Representations of SU($k\lambda + 1$) with $k > 2$.

The representations of SU(n), with $n = k\lambda + 1$, may be divided into two cases, according to the parity of λ:

- Case 1: λ even.
  Since the first row of the ground state has ($\lambda + 1$)-site order, and the unit cell order is $2\lambda(\lambda + 1)$, we may write $\mathcal{L}_{\text{Berry}}$ as two parts:

$$\mathcal{L}_{\text{Berry}} = \mathcal{L}^{(1)}_{\text{Berry}} + \mathcal{L}^{(2)}_{\text{Berry}}. \tag{6.54}$$

The first part is

$$\mathcal{L}^{(1)}_{\text{Berry}} = \epsilon_{\mu\nu} \frac{p_1}{2\lambda(\lambda + 1)} \sum_{t=1}^{\lambda+1} \sum_{j=1}^{2\lambda} (t - 1 + (j - 1)(\lambda + 1)) \partial_\mu \boldsymbol{\varphi}^{*,t} \cdot \partial_\nu \boldsymbol{\varphi}^t, \tag{6.55}$$

which gives rise to the following topological angles:

$$\theta_t = \frac{\pi p_1}{\lambda(\lambda + 1)} \sum_{j=1}^{2\lambda} (t - 1 + (j - 1)(\lambda + 1)) \tag{6.56}$$

for $t = 1, 2, \ldots, \lambda + 1$. These angles can be further simplified to

$$\theta_t = \frac{2\pi p_1}{(\lambda + 1)}(t - 1) + \pi p_1. \tag{6.57}$$

The second part of the Berry phase corresponds to the lower $k - 1$ rows of the classical ground state. It reads

$$\mathcal{L}^{(2)}_{\text{Berry}} = \frac{\epsilon_{\mu\nu}}{2\lambda(\lambda + 1)} \sum_{\alpha=2}^{k} \sum_{j=1}^{\lambda} \sum_{t=1}^{\lambda+1} \left[p_\alpha(j - 1 + (t - 1)2\lambda) \right. \tag{6.58}$$

$$\left. + p_{k+2-\alpha}(j - 1 + \lambda + (t - 1)2\lambda) \right] \partial_\mu \boldsymbol{\varphi}^{*,\alpha,j} \cdot \partial_\nu \boldsymbol{\varphi}^{\alpha,j}.$$

The associated topological angles are

$$\theta_{\alpha,j} = \frac{\pi}{\lambda(\lambda + 1)} \sum_{t=1}^{\lambda+1} \left[p_\alpha(j - 1 + 2\lambda(t - 1)) + p_{k+2-\alpha}(j - 1 + \lambda + (t - 1)2\lambda) \right] \tag{6.59}$$

for $\alpha = 2, \ldots, k$ and $j = 1, \ldots, \lambda$. Again, the angles simplify to

$$\theta_{\alpha,j} = \frac{\pi}{\lambda}(p_\alpha + p_{k+2-\alpha})(j - 1) + \pi p_\alpha, \tag{6.60}$$

where we used the fact that $\lambda \pi p_\alpha \equiv 0$ since λ is even. The correspondence between angle and condition on the p_α is provided in the following table, Table 6.4

Subcase	Condition	Angles	
k even	$p_\alpha + p_{k+2-\alpha} = p_2 + p_k$ $(\lambda + 1)(p_2 + p_k) = 2\lambda p_1$	$\theta_{\alpha,j}, \theta_{k+2-\alpha,j}$ θ_t	$\alpha = 3, \ldots, \dfrac{k+1}{2};$ $j = 1, \ldots, \lambda; \quad t = 1, \ldots, \lambda + 1$
k odd	$p_\alpha + p_{k+2-\alpha} = p_2 + p_k$ $2p_{\frac{k+2}{2}} = p_2 + p_k$ $(\lambda + 1)(p_2 + p_k) = 2\lambda p_1$	$\theta_{\alpha,j}, \theta_{k+2-\alpha,j}$ $\theta_{\frac{k+2}{2},j}$ θ_t	$\alpha = 3, \ldots, \dfrac{k}{2};$ $j = 1, \ldots, \lambda$ $t = 1, \ldots, \lambda + 1$

Table 6.4: The relation between topological angle and condition on p_α for representations of SU(n), with $n = k\lambda + 1$, with $k > 2$ and $\lambda > 1$ odd.

- Case 2: λ odd.

  Assume $\lambda > 1$ so that this case is distinct from the representations considered previously. Now that λ is odd, the order of the unit cell has changed to $\lambda(\lambda + 1)$. The two parts of $\mathcal{L}_{\text{Berry}}$ from the previous subsection are modified to

  $$\mathcal{L}_{\text{Berry}}^{(1)} = \epsilon_{\mu\nu} \frac{p_1}{\lambda(\lambda + 1)} \sum_{t=1}^{\lambda+1} \sum_{j=1}^{\lambda} (t - 1 + (j - 1)(\lambda + 1)) \partial_\mu \varphi^{*,t} \cdot \partial_\nu \varphi^t, \tag{6.61}$$

  and

  $$\mathcal{L}_{\text{Berry}}^{(2)} = \frac{\epsilon_{\mu\nu}}{\lambda(\lambda + 1)} \sum_{\alpha=2}^{k} \sum_{j=1}^{\lambda} \sum_{t=1}^{\frac{\lambda+1}{2}} \Big[p_\alpha(j - 1 + (t - 1)2\lambda) \tag{6.62}$$
  $$+ p_{k+2-\alpha}(j - 1 + \lambda + (t - 1)2\lambda) \Big] \partial_\mu \varphi^{*,\alpha,j} \cdot \partial_\nu \varphi^{\alpha,j}.$$

  The angles are then

  $$\theta_t = \frac{2\pi p_1}{(\lambda + 1)}(t - 1) \tag{6.63}$$

  and

  $$\theta_{\alpha,j} = \frac{\pi}{\lambda}(p_\alpha + p_{k+2-\alpha})\left(j - 1 + \frac{\lambda(\lambda - 1)}{2}\right) + \pi p_\alpha. \tag{6.64}$$

  The range of these indices can be read off from the sums in (6.62). The same correspondence between condition and angle found in the previous case applies here as well, so long as the slightly modified conditions for λ odd are used (which can be found in Table G.1).

117

Representations of SU($k\lambda + c$) with $c \neq 1, k-1$

Write $n = k\lambda + c$, for $c \neq 1, k-1$, and consider representations with k rows. In this case, the ground state order is $2\lambda(\lambda + 1)$. Again, we split the Berry phase contribution into two pieces. The first c rows contribute the following term:

$$\mathcal{L}^1_{\text{Berry}} = \frac{\epsilon_{\mu\nu}}{2\lambda(\lambda + 1)} \sum_{j=1}^{\lambda} \sum_{t=1}^{\lambda+1} \sum_{\alpha=1}^{c} \Big[p_\alpha(t - 1 + (j-1)2(\lambda + 1)) \tag{6.65}$$
$$= +p_{c-\alpha+1}(t - 1 + \lambda + 1 + (j-1)2(\lambda + 1))\Big]\partial_\mu \varphi^{*,\alpha,t} \cdot \partial_\nu \varphi^{\alpha,t},$$

which gives the topological angles

$$\theta_{\alpha,t} = \frac{\pi(p_\alpha + p_{c-\alpha+1})}{(\lambda + 1)}(t - 1) + \pi\lambda p_{c-\alpha+1} + \pi(\lambda - 1)p_\alpha. \tag{6.66}$$

The range of these indices can be read off from the sums in (6.65). Meanwhile, the remaining $k - c$ rows contribute the term

$$\mathcal{L}^2_{\text{Berry}} = \frac{\epsilon_{\mu\nu}}{2\lambda(\lambda + 1)} \sum_{j=1}^{\lambda} \sum_{t=1}^{\lambda+1} \sum_{\beta=c+1}^{k} \Big[p_\beta(j - 1 + (t-1)2\lambda) \tag{6.67}$$
$$+ p_{k-\beta+c+1}(j - 1 + (t-1)2\lambda + \lambda)\Big]\partial_\mu \tilde{\varphi}^{*,\beta,j} \cdot \partial_\nu \tilde{\varphi}^{\beta,j}$$

which gives the topological angles

$$\tilde{\theta}_{\beta,j} = \frac{\pi(p_\beta + p_{k-\beta+c+1})}{\lambda}(j - 1) + \pi(\lambda + 1)p_{k-\beta+c+1} + \pi\lambda p_\beta. \tag{6.68}$$

The range of these indices can be read off from the sums in (6.67). Here, $\tilde{\theta}$ and $\tilde{\varphi}$ have been used in order to differentiate the two families of fields and topological angles, so as to simplify our notation. The relationships between topological angle and condition on the p_α are given in Table 6.5.

Representations of SU($k\lambda + (k-1)$)

Finally, we must consider the representations with $n = k\lambda + (k-1)$, with k boxes. Here we also have two subcases, according to the parity of λ:

- Case 1: λ odd
  The ground state has $2\lambda(\lambda + 1)$-site order. The first $k - 1$ rows have the following Berry phase contribution:

$$\mathcal{L}^{(1)}_{\text{Berry}} = \frac{\epsilon_{\mu\nu}}{2\lambda(\lambda + 1)} \sum_{\alpha=1}^{k-1} \sum_{j=1}^{\lambda} \sum_{t=1}^{\lambda+1} \Big[p_\alpha(t - 1 + (j-1)2(\lambda + 1)) + \tag{6.69}$$
$$= p_{k-\alpha}(t - 1 + \lambda + 1 + (j-1)2(\lambda + 1))\Big]\partial_\mu \varphi^{*,\alpha,t} \cdot \partial_\nu \varphi^{\alpha,t}.$$

118

Subcase	Condition	Angles	
k, c even	$p_\alpha + p_{c+1-\alpha} = p_1 + p_c$ $(\lambda+1)(p_\beta + p_{k-\beta+c+1}) = \lambda(p_1 + p_c)$	$\theta_{\alpha,t}, \theta_{c-\alpha+1,t}$ $\tilde\theta_{\beta,j}, \tilde\theta_{k-\beta+c+1,j}$	$\alpha = 2,\dots,\dfrac{c}{2}; t = 1,\dots,\lambda+1$ $\beta - c = 1,\dots,\dfrac{k-c}{2}; j = 1,\dots,\lambda$
k odd c even	$p_\alpha + p_{c+1-\alpha} = p_1 + p_c$ $(\lambda+1)(p_\beta + p_{k-\beta+c+1}) = \lambda(p_1 + p_c)$ $2(\lambda+1)p_{\frac{k+c+1}{2}} = \lambda(p_1 + p_c)$	$\theta_{\alpha,t}, \theta_{c-\alpha+1,t}$ $\tilde\theta_{\beta,j}, \tilde\theta_{k-\beta+c+1,j}$ $\tilde\theta_{\frac{k+c+1}{2},j}$	$\alpha = 2,\dots,\dfrac{c}{2}; t = 1,\dots,\lambda+1$ $\beta - c = 1,\dots,\dfrac{k-c-1}{2}$ $j = 1,\dots,\lambda$
k, c odd	$p_\alpha + p_{c+1-\alpha} = p_1 + p_c$ $2p_{\frac{c+1}{2}} = p_1 + p_c$ $(\lambda+1)(p_\beta + p_{k-\beta+c+1}) = \lambda(p_1 + p_c)$	$\theta_{\alpha,t}, \theta_{c-\alpha+1,t}$ $\theta_{\frac{c+1}{2},t}$ $\tilde\theta_{\beta,j}, \tilde\theta_{k-\beta+c+1,j}$	$\alpha = 2,\dots,\dfrac{c-1}{2}; t = 1,\dots,\lambda+1$ $\beta - c = 1,\dots,\dfrac{k-c-1}{2}$ $j = 1,\dots,\lambda$
c odd k even	$p_\alpha + p_{c+1-\alpha} = p_1 + p_c$ $2p_{\frac{c+1}{2}} = p_1 + p_c$ $(\lambda+1)(p_\beta + p_{k-\beta+c+1}) = \lambda(p_1 + p_c)$ $2(\lambda+1)p_{\frac{k+c+1}{2}} = \lambda(p_1 + p_c)$	$\theta_{\alpha,t}, \theta_{c-\alpha+1,t}$ $\theta_{\frac{c+1}{2},t}$ $\tilde\theta_{\beta,j}, \tilde\theta_{k-\beta+c+1,j}$ $\tilde\theta_{\frac{k+c+1}{2},j}$	$\alpha = 2,\dots,\dfrac{c-1}{2}; t = 1,\dots,\lambda+1$ $\beta - c = 1,\dots,\dfrac{k-c-1}{2}$ $j = 1,\dots,\lambda$

Table 6.5: The relation between topological angle and condition on the p_α for representations of SU(n) with $n = k\lambda + c$, with $c \neq 1, k - 1$.

The corresponding topological angles are

$$\theta_{t,\alpha} = \frac{\pi(p_\alpha + p_{k-\alpha})}{(\lambda + 1)}(t - 1) + \pi p_{k-\alpha}. \tag{6.70}$$

As before, the range of α and t can be read off from the sums in (6.69). Meanwhile, the last row of the ground state contributes the term

$$\mathcal{L}_{\text{Berry}}^{(2)} = \frac{\epsilon_{\mu\nu}}{2\lambda(\lambda + 1)} p_k \sum_{j=1}^{\lambda} \sum_{t=1}^{2(\lambda+1)} [(j - 1) + (t - 1)\lambda] \, \partial_\mu \varphi^{*,j} \cdot \partial_\nu \varphi^j \tag{6.71}$$

giving rise to the angles

$$\theta_j = \frac{2\pi p_k}{\lambda}(j - 1) + p_k \pi, \tag{6.72}$$

for $j = 1, \dots, \lambda$. The correspondence between condition on the p_α and topological angle can be found in Table 6.6.

Subcase	Condition	Angles	
k odd	$p_\alpha + p_{k-\alpha} = p_1 + p_{k-1}$ $(\lambda+1)p_k = \lambda(p_1 + p_{k-1})$	$\theta_{\alpha,t}, \theta_{k-\alpha,t}$ θ_j	$\alpha = 2, \ldots, \dfrac{k-1}{2};$ $j = 1, \ldots, \lambda; \quad t = 1, \ldots, \lambda+1$
k even	$p_\alpha + p_{k-\alpha} = p_1 + p_{k-1}$ $2p_{\frac{k}{2}} = p_1 + p_{k-1}$ $(\lambda+1)p_k = \lambda(p_1 + p_{k-1})$	$\theta_{\alpha,t}, \theta_{k-\alpha,t}$ $\theta_{\frac{k}{2},t}$ θ_j	$\alpha = 2, \ldots, \dfrac{k-2}{2};$ $t = 1, \ldots, \lambda+1$ $j = 1, \ldots, \lambda$

Table 6.6: The relation between topological angle and condition on the p_α for representations of SU(n) with $n = k\lambda + (k-1)$, with k boxes.

- Case 2: λ even

  This is the final case. Now that λ is even, the order of the unit cell has changed to $\lambda(\lambda+1)$. The two parts of $\mathcal{L}_{\text{Berry}}$ are modified to

$$
\mathcal{L}_{\text{Berry}}^{(1)} = \frac{\epsilon_{\mu\nu}}{\lambda(\lambda+1)} \sum_{\alpha=1}^{k-1} \sum_{j=1}^{\frac{\lambda}{2}} \sum_{t=1}^{\lambda+1} \Big[p_\alpha(t-1 + (j-1)2(\lambda+1)) \tag{6.73}
$$
$$
+ p_{k-\alpha-2}(t-1+\lambda+1+(j-1)2(\lambda+1)) \Big] \partial_\mu \varphi^{*,\alpha,t} \cdot \partial_\nu \varphi^{\alpha,t}
$$

and

$$
\mathcal{L}_{\text{Berry}}^{(2)} = \frac{\epsilon_{\mu\nu}}{\lambda(\lambda+1)} p_k \sum_{j=1}^{\lambda} \sum_{t=1}^{(\lambda+1)} [(j-1) + (t-1)\lambda] \, \partial_\mu \varphi^{*,j} \cdot \partial_\nu \varphi^j, \tag{6.74}
$$

and the angles are modified to

$$
\theta_{\alpha,t} \to \frac{\pi(p_\alpha + p_{k-\alpha})}{(\lambda+1)}(t-1) + \pi p_{k-\alpha} + \frac{\pi(p_\alpha + p_{k-\alpha})}{2}(\lambda-2) \tag{6.75}
$$

and

$$
\theta_j \to \frac{2\pi p_k}{\lambda}(j-1). \tag{6.76}
$$

The correspondence between angles and conditions on the p_α follows the same pattern as the previous case, with a slight modification of the conditions themselves, according to Table G.1.

Summary of calculations

In Table G.2, found in Appendix G, we collect the results of this section, by listing all possible topological angles for each representation of SU(n). The relationships between angle and conditions on the p_α were provided explicitly in the various tables above.

6.5 A New Generalization of Haldane's Conjecture

The lengthy analysis of the previous sections makes clear the fact that most representations of SU(n) chains do not lead to linearly dispersing sigma models like those of the symmetric SU(n) chains considered in Chapters 2,4, and 5. This is already apparent in SU(3): Any representation that is neither self-conjugate nor completely symmetric has at least one (and at most two) $\mathbb{CP}^2$ fields φ^α with quadratic dispersion. In order to achieve a purely linearly dispersing theory, a series of constraints on the Young tableaux parameters p_α must be satisfied. In the special case of representations with all p_α nonzero and distinct, these constraints lead to the self-conjugate representations of SU(n).

Here, we restrict to representations of SU(n) that satisfy the various constraints listed in Table G.1. This ensures that the corresponding sigma models have linear dispersion only. Before proceeding further, we must reflect on what we are hoping to achieve with this classification. Ultimately, we are interested in the possible gapless phases in SU(n) chains, and how one might extend Haldane's conjecture to novel representations. Based on our understanding of the symmetric models, we know that this task can be recast in terms of 't Hooft anomaly matching. The recipe is as follows:

- Step 1: Map an SU(n) chain to a (linear-dispersing) flag manifold sigma model at low energies.

- Step 2: Identify the 't Hooft anomalies of the sigma model. When such an anomaly is present, we may conclude that the ground state either exhibits spontaneously broken symmetry, or gapless excitations.

As we've mentioned several times already, in [78] and [79] it was shown that an 't Hooft anomaly may occur in the SU(n)/[U(1)]$^{n-1}$ sigma model when an additional $\mathbb{Z}_n$ discrete symmetry is present. It is a mixed anomaly between the physical PSU(n) symmetry of the chain, and the discrete $\mathbb{Z}_n$ symmetry. Actually, in [78] it was shown that mixed anomalies occur between PSU(n) and $\mathbb{Z}_{n'}$ whenever n and n' have a nontrivial common divisor. However, in this latter case, the corresponding sigma model cannot be embedded into a WZW theory that flows to level $k = 1$. Therefore, here we focus on chains that have this $\mathbb{Z}_n$ symmetry only. Moreover, this symmetry must act on the n complex fields transitively according to

$$\mathbb{Z}_n : \varphi^\alpha \mapsto \varphi^{\alpha+1}. \tag{6.77}$$

In the following chapter, this gapless property of SU(n) chains with 't Hooft anomalies will be reinterpreted in terms of fractional instantons. We will show that in the SU(n)/[U(1)]$^{n-1}$ sigma

model, topological excitations exist that generate a finite energy gap above the ground state, much in the same way that vortices drive the familiar Kosterlitz-Thouless transition [90, 91]. For a certain set of topological angles $\{\theta_\alpha^{(\circ)}\}$, these excitations destructively interfere with each other and the mass-generating mechanism breaks down, thus leading to a gapless ground state. It turns out that when an 't Hooft anomaly is present, the topological angle content in the sigma model is precisely $\{\theta_\alpha^{(\circ)}\}$. Ultimately, this follows from the form of the action (6.77). Therefore, in addition to concerning ourselves with linear dispersion, we also restrict our focus to SU(n) representations whose translational symmetry group $\mathbb{Z}_d = \mathbb{Z}_n$, and acts transitively on the fields $\boldsymbol{\varphi}^\alpha$.

Of course, it is important to acknowledge this is by no means an exhaustive classification of gapless phases in SU(n) chains. We do not attempt to classify all possible 't Hooft anomalies in these models, and so we are limited to the current list of known anomalies, and apply this knowledge to our theories. Moreover, we must also remember that the absence of an anomaly teaches us nothing: we are unable to predict any ground state properties when this is the case. However, we do have the LSMA theorem (see Section 3.5.2), which predicts either a gapless ground state or spontaneously broken symmetry for an SU(n) chain whenever the sum $p := \sum_\alpha p_\alpha$ is not a multiple of n.

6.5.1 Representations that admit transitive $\mathbb{Z}_n$ actions

Having made these remarks, we are now in a position to seek out representations of SU(n) that may be amenable to a generalized Haldane conjecture. We assume that all of the constraints on the Young tableaux parameters p_α have been satisfied, so that all of the n fields $\boldsymbol{\varphi}^\alpha$ are linearly dispersing. For each class of representation occurring in Table 6.1, we record when it is possible for the translation group to equal $\mathbb{Z}_n$, and act transitively on the set of fields.

- Case 1: $k = 1$.
  Since $\mathbb{Z}_d = \mathbb{Z}_n$, this is possible for all n.

- Case 2: $k = n - 1$
  Since $\mathbb{Z}_d = \mathbb{Z}_2$, this is possible only in SU(2) (which reduces to Case 1).

- Case 3: $k = \frac{n}{\lambda}, \lambda < n$
  Since $d = 2\lambda$, and $\lambda \leq \frac{n}{2}$, this is possible only when $k = 2$. See the ground state below for an example in SU(4):

  In other words, when n is even, Young tableaux with two rows (of differing lengths) give rise to flag manifold sigma models with an additional $\mathbb{Z}_n$ symmetry. According to Table G.1, such representations are always linearly dispersing, so no other assumption on the row lengths p_α is required. Note that the angles in this case are (see Table G.2)

$$\theta_\alpha = \frac{2\pi}{n}(p_1 + p_2)(\alpha - 1) \qquad \alpha = 1, 2, \ldots, n, \tag{6.78}$$

122

where we have shifted each angle by the constant πp_1.

- Case 4: $n = 2\lambda + 1, k = 2$
  Since n cannot equal $d = \lambda(\lambda + 1)$, no such representations give rise to a $\mathbb{Z}_n$ symmetry.

- Case 5: $n = k\lambda + 1, k > 2, \lambda > 1$.
  In this case, the $\mathbb{Z}_d$ symmetry does not act transitively on the set of n fields: Some of the fields lie in an orbit of order $\lambda + 1$, while the remaining fields lie in orbits of size 2λ.

- Case 6: $n = k\lambda + c, c \neq 1, k - 1$.
  Similar to Case 5, the fields do not lie in a single orbit under the action of $\mathbb{Z}_d$. So while it is possible for $\mathbb{Z}_d = \mathbb{Z}_n$, the fields do not transform under the necessary action (6.77). The simplest example of this is SU(12) with $k = 5$ rows in a Young diagram. Under the $\mathbb{Z}_n$ action, the fields partition into three orbits of size 6,4 and 2, and the anomaly classification is no longer applicable.

- Case 7: $n = k\lambda + (k - 1)$.
  Similar to the previous two cases, the fields do not lie in a single orbit under the action of $\mathbb{Z}_d$.

In summary, we find only one new family of SU(n) representations that give rise to a linearly dispersing SU(n)/[U(1)]$^{n-1}$ flag manifold sigma model with the $\mathbb{Z}_n$ symmetry (6.77). It is the set of representations with two rows (of different lengths) in their Young tableaux, when n is even. The corresponding topological angles in this theory are

$$\theta_\alpha = \frac{2\pi}{n}(p_1 + p_2)\alpha \qquad \alpha = 1, 2, \ldots, n \qquad (6.79)$$

so that $p_1 + p_2$ plays the role of p_1 in the symmetric models. This means that an 't Hooft anomaly is present whenever $p_1 + p_2$ is not a multiple of n. This is also consistent with the LSMA theorem, mentioned above. Moreover, based on the classification of SU(n) WZW flows discussed in Section 5.5.2, we may further conclude that only when $(p_1 + p_2)$ is coprime with n is a stable gapless phase possible. Otherwise, if $p_1 + p_2$ shares a nontrivial common divisor with n, then the theory is necessarily gapped with spontaneously broken symmetry.

On the other hand, when $p_1 + p_2$ is a multiple of n (and the LSMA theorem does not apply), it should be possible to have a unique, translationally invariant ground state with a finite energy gap. This statement is supported by the fact that when $p_1 + p_2 = n$, it is straightforward to write down a translationally invariant AKLT state. This is explained in Section 3.5.3.

6.6 Conclusion

In this chapter, we have attempted to classify all SU(n) chains that admit a mapping to the SU(n)/[U(1)]$^{n-1}$ sigma model at low energies. Our motivation for doing so was the presence of mixed 't Hooft anomalies between the physical PSU(n) = SU(n)/$\mathbb{Z}_n$ symmetry of the sigma model, and a transitive $\mathbb{Z}_n$ action. Such anomalies are an indicator of nontrivial low energy physics, and so by establishing such mappings, we may uncover novel gapless phases in SU(n) chains.

We have found that unless two rows of the Young tableaux have the same length, it seems possible to realize such a mapping for any irreducible representation of SU(n). When two row lengths are degenerate, the SU(n) matrices S lie in a different (partial) flag manifold that can not easily be embedded into the (complete) flag manifold SU(n)/[U(1)]$^{n-1}$.

However, even when no row lengths are degenerate, we find that the corresponding sigma model will have complex fields with both quadratic and linear dispersion relations. One consequence of this is that Lorentz invariance is likely never to emerge at low energies, as it does for the symmetric SU(n) chains that possess only linearly dispersing fields. We have classified which representations lead to only linearly dispersing models, and have determined the topological angles in each case. Moreover, within this subset of representations, we have further classified which chains also admit a $\mathbb{Z}_n$ symmetry that acts transitively on the SU(n) fields, so that the possibility for an 't Hooft anomaly exists.

In the end, we have found that only the SU(n) representations with even n and two rows in their Young tableaux, with lengths $p_1 \neq p_2$, satisfy all of these properties (in addition to the symmetric representations considered previously). As a result, we have made the following modest extension of the SU(n) generalization of Haldane's conjecture for even n: when $p_1 + p_2$ is coprime with n, a gapless ground state is predicted; otherwise, a gapped ground state is expected, with spontaneously broken symmetry if $p_1 + p_2$ is not a multiple of n. The magnitude of the gap can be predicted in the same way as in Section 5.5.3, and should generally decrease exponentially as a function of $p_1 + p_2$. In Table 6.7, we summarize these findings by listing which representations of SU(n) we predict to have a gapless phase driven by topological terms.
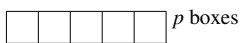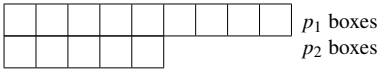
Representation	Condition
p boxes	$(p, n) = 1$
p_1 boxes p_2 boxes	$(p_1 + p_2, n) = 0$ and n even

Table 6.7: The set of SU(n) representations that exhibit a gapless phase at weak coupling.

Chapter 7

Fractional Instantons and the Haldane Gap in SU(n) Chains

7.1 Introduction

In the past few chapters, we have followed the program of extending Haldane's conjecture to more and more general SU(n) chains. In the end, we have come to the conclusion that a gapless phase should only occur for representations that admit a mapping to the SU(n)/[U(1)]$^{n-1}$ sigma model with $n-1$ nontrivial topological angles. Indeed, this statement summarizes our findings for SU(2) in Chapter 2, for SU(3) in Chapter 4, for the symmetric representations of SU(n) in Chapter 5, and finally for the most general representations of SU(n) in Chapter 6. Here, in this final chapter, we seek to develop an alternative argument that explains why these gapless phases arise. Instead of making use of formal 't Hooft anomaly matching arguments, we will establish a physical picture of Haldane's conjecture in terms of a gas of interacting fractional topological excitations.

This work generalizes an old result of Affleck that interpreted Haldane's original conjecture in terms of interacting merons, or 'half-instantons' [137]. Merons behave like planar vortices far from their centers, but lift out of the plane near their cores, and form finite action configurations when a collection of them has net vorticity zero. Remarkably, when the $\mathbb{CP}^1$ sigma model has a topological angle of π, corresponding to a half-odd integer spin chain, the merons that point up at their origin destructively interfere with the merons that point down at their origin (also known as anti-merons), and the mass generating mechanism of the model is no longer effective. While this isn't the full story, since larger-action configurations such as double-merons do not destructively interfere at $\theta = \pi$, it offers an intuitive picture in favour of Haldane's conjecture.

In Chapters 4, 5 and 6, we have generalized this paradigm of mapping spin chains to relativistic quantum field theories to SU(n) chains in various representations. When a transitive $\mathbb{Z}_n$ action is present, the corresponding sigma model has $n-1$ independent topological angles $\theta_\alpha = \frac{2\pi p}{n}\alpha$. Throughout, we will treat $p \in \mathbb{Z}_+$ as given, labelling a particular representation of SU(n) that admits such topological angle content. From the previous chapters, we know that there are two possibilities for p:

- Case 1: The SU(n) representation has one row, of length p, in its Young tableau.

- Case 2: The SU(n) representation has two rows, of lengths p_1 and p_2 in its Young tableau. Then $p = p_1 + p_2$. This case is possible only for even n.

According to our generalized Haldane conjectures, these SU(n) chains have a gapless ground

state whenever p and n are coprime: $\gcd(n, p) = 1$. This is in accordance with the LSMA theorem (see Section 3.5.2), which predicts either a gapless phase or spontaneously broken translation symmetry when p is not a multiple of n [80, 81]. A subtle feature of this result, which can only occur for $n \geq 4$, is that when p and n have a nontrivial divisor, and p is a not a multiple of n, translation symmetry is always spontaneously broken. This follows from an 't Hooft anomaly that forbids the flow of the above sigma model to $SU(n)_1$, the only stable $SU(n)$ fixed point [115, 116].

In this chapter, we will offer an intuitive explanation of this gap dependence on p and n, based on a mass generation mechanism due to fractionalized topological excitations. We begin by reviewing the Kosterlitz-Thouless transition in Section 7.2, and explain how it relates to the mass generation mechanism in $SU(2)$. In Section 7.3, we add anisotropic potentials to the $SU(n)$ chain that break the continuous global symmetry down to $U(1)$, and classify the topological excitations that have finite action. Next, in Section 7.4, we show how these excitations, so-called fractional instantons which have topological charge $\frac{1}{n}$, are responsible for generating a mass gap in the sigma model, in a similar fashion as the vortices in the Kosterlitz-Thouless transition [90, 91]. However, this mechanism is highly dependent on the topological angles of the model, which are determined by the representation p of $SU(n)$. This dependence is discussed in Section 7.5, where we ultimately conclude that mass generation by fractional instantons occurs except when p and n are coprime, in which case a gapless phase is possible.

7.2 Mass Generation in the O(3) Nonlinear Sigma Model

7.2.1 The Kosterlitz-Thouless transition

Since we hope to relate (the absence of) a finite energy gap in our sigma models to some form of topological excitation, let us begin by reviewing how a similar mechanism works in a very famous example. We are referring to the continuous phase transition in the 'XY model', which was described independently by Berezinskii in 1971 [90] and Kosterlitz and Thouless in 1973 [91]. This work contributed to Kosterlitz and Thouless sharing the Nobel prize with Haldane in 2016.

The XY model describes the physics of a classical spin restricted to a two-dimensional plane (which we can think of as corresponding to the 'X' and 'Y' directions in real space, hence the name). Explicitly, its Hamiltonian is

$$H = -J \sum_{\langle i,j \rangle} \vec{s}_i \cdot \vec{s}_j, \tag{7.1}$$

where $\sum_{\langle i,j \rangle}$ denotes summation over all nearest-neighbour sites in the two-dimensional lattice, and $\vec{s}_i \in \mathbb{R}^2$ is the classical spin vector at site $i \in \mathbb{Z}^2$. Note that the interaction is ferromagnetic, i.e. the prefactor of the spin-spin interaction is negative, unlike all of the $SU(n)$ chain Hamiltonians that we have considered thus far. If we write the spin vectors in polar coordinates according to $\vec{s}_i = s \cos(\rho_i)$, and rescale J by s^{-2}, we are left with

$$H = -J \sum_{\langle i,j \rangle} \cos(\rho_i - \rho_j). \tag{7.2}$$

In the continuum limit, the differences $\rho_i - \rho_j$ are replaced with partial derivatives, and we may Taylor expand the cosine, so long as we assume the classical spins vary smoothly from site to site. We end up with

$$H \approx E_0 + \frac{J}{2} \int d^2x (\nabla\rho)^2 \tag{7.3}$$

where $\vec{x} \in \mathbb{R}^2$, and $(\nabla\rho)^2 = (\partial_x\rho)^2 + (\partial_y\rho)^2$. The thermodynamics of this system is obtained from a partition function, which may be written as a path integral as follows

$$\mathcal{Z} = e^{-\beta E_0} \int \mathcal{D}[\rho] e^{-\beta\frac{J}{2} \int d^2x (\nabla\rho)^2}. \tag{7.4}$$

We may now identify the integrand in the exponent as a Lagrangian,

$$\mathcal{L}_{XY} = \frac{1}{2g} (\nabla\rho)^2. \tag{7.5}$$

with $g = \frac{1}{\beta J}$. This is the low temperature, or weak coupling, form of the XY model. To arrive at it, we had to assume that higher derivatives of ρ could be ignored in the expansion of the cosine in (7.2). Such terms do not reemerge upon renormalization, since it may be shown that all of the higher derivative terms are irrelevant.

This rewriting (7.5) will be useful later when we approach $\mathcal{L}_{XY}$ from our flag manifold sigma models through a limit of theories, which restrict the target space from $SU(n)/[U(1)]^2$ first down to $[U(1)]^{n-1}$, and then down to $U(1)$. At first glance, it appears that $\mathcal{L}_{XY}$ is simply a theory of a free boson, ρ, and will thus exhibit gapless excitations for all values of β. However, Kosterlitz and Thouless realized that this conclusion overlooks the crucial fact that ρ is a periodic variable. In other words, the target space of ρ is $U(1)$, which is equivalent to the circle S^1, and is topologically nontrivial. Accounting for this, they found that a finite mass will be generated for the boson ρ at sufficiently high temperatures (equivalently, at strong enough coupling), and that this mass generation can be explained in terms of topologically nontrivial field configurations.

To understand this mass generation, let us estimate $\mathcal{Z}$ using a saddle point approximation (which is exact in the zero temperature limit). This amounts to solving the Euler-Lagrange equations for $\mathcal{L}_{XY}$, and identifying extremal configurations, ρ_*, i.e. solving

$$\nabla^2 \rho_* = 0. \tag{7.6}$$

Of course, the most obvious solution to these saddle point equations is the trivial configuration, $\rho_* = $ const.. However, the story does not end here. Since ρ lives in $U(1) \cong S^1$, there also exist solutions ρ_κ that obey the following equation:

$$\oint_\Gamma dl \cdot \nabla\rho = 2\pi\kappa \qquad \kappa \in \mathbb{Z}. \tag{7.7}$$

Here Γ is a closed contour integral in the XY plane. For nonzero κ, this equation requires that ρ_κ has a singularity within the contour; consequently, it cannot be continuously deformed into the trivial

configuration, $\rho_* = $ const.. In other words, ρ_κ is a topologically distinct saddle point, and must also be included in the path integral over all field configurations in (7.4). The integer κ is called the topological charge of ρ_κ, and the simplest configurations ρ_1 and ρ_{-1} are called the vortex, and anti-vortex configuration, respectively.

Let us now determine the classical action of these configurations. Due to the U(1) symmetry of the problem, ρ_κ should only depend on the radius, r, so that by (7.7), $|\nabla\rho| = \frac{\kappa}{r}$. Then, we have

$$S[\rho_\kappa] = \frac{\kappa^2}{2g} \int d^2x \frac{1}{r^2}. \tag{7.8}$$

Unless $\kappa = 0$, we see that the action of ρ_κ exhibits both an infrared and an ultraviolet divergence. The ultraviolet divergence can be resolved by introducing a lattice spacing a, which we will discuss shortly, but the infrared divergence is problematic. If all topologically nontrivial configurations have infinite action, they will not enter the saddle point approximation, and will not be responsible for a mass generating mechanism, as predicted by KT. How then, do we proceed?

The resolution to this issue is found by considering configurations that are sums of vortices, with net topological charge zero. To see this more easily, define the dual field $\tilde{\rho}$ by

$$\epsilon_{\mu\nu}\partial_\nu\tilde{\rho} = \rho, \tag{7.9}$$

where $\epsilon_{\mu\nu}$ is the antisymmetric tensor with nonzero components $\epsilon_{01} = -\epsilon_{10} = 1$. Then the topological charge equation (7.7) can be rewritten as follows:

$$\int_\Sigma d^2x\nabla^2\tilde{\rho}_\kappa = -2\pi\kappa. \tag{7.10}$$

Here Σ is the oriented surface whose boundary is the contour Γ. This equation shows that the most general saddle point we can write down should obey the following Poisson equation:

$$\nabla^2\tilde{\rho} = -2\pi\sum_j\kappa_j\delta(\vec{x}-\vec{x}_j). \tag{7.11}$$

In other words, the Euler-Lagrange equation $\nabla^2\rho = 0$ is modified by singularities on the right hand side. Now, using $(\nabla\rho)^2 = (\nabla\tilde{\rho})^2$, one may show that the action remains finite so long as $\sum_j\kappa_j = 0$, i.e. the net topological charge vanishes. In particular, the least-action configurations that are topologically nontrivial consist of a vortex/anti-vortex pair, with separation distance R. Using (7.8), we see that

$$S[\rho_1 + \rho_{-1}] = \frac{1}{2g}\log\left(\frac{R}{a}\right) < \infty. \tag{7.12}$$

It is these configurations that KT used to explain the generation of a mass gap in $\mathcal{L}_{XY}$.

The simplest, and most famous explanation for this mass gap follows from energy and entropy considerations. It can readily be shown that below temperature $g_c = \pi/2$, the free energy for an individual vortex diverges, while above this temperature, it is favourable for individual vortices to

form.[37] Thus, we expect a phase transition to occur at this temperature, in which the vortex/anti-vortex pairs unbind, leading to so-called 'vortex proliferation'.

To see this mechanism at play more explicitly, one may derive an effective Lagrangian that describes fluctuations about the vortex/anti-vortex pairs in the low temperature phase. To this end, we write $\tilde{\rho} = \tilde{\rho}_c + \tilde{\rho}'$, where $\tilde{\rho}_c$ solves (7.11), and $\tilde{\rho}'$ are small deviations. The action for $\tilde{\rho}$ then reads

$$S[\tilde{\rho}] = \frac{1}{2g} \int d^2x \left((\nabla\tilde{\rho})^2 + 4\pi i \tilde{\rho} \sum_j \kappa_j \right), \tag{7.13}$$

where on the right hand side we've shifted $\tilde{\rho}' \to \tilde{\rho}$. Now, returning to (7.4), we must sum over all possible configurations of $\tilde{\rho}$, which amounts to summing over all choices of $\{\kappa_j\}$. It is here that we make the *dilute gas approximation*, allowing us to assume the individual vortices are far apart, and do not interact with each other. Then, we may write

$$e^{-S} = e^{-\frac{1}{2g} \int d^2x (\nabla\tilde{\rho})^2} \frac{1}{n!} \prod_{j=1}^{n} \int d^2x_j e^{-\frac{2\pi i}{g}\tilde{\rho}(\vec{x}_j)} \frac{1}{m!} \prod_{k=1}^{m} \int d^2x_k e^{\frac{2\pi i}{g}\tilde{\rho}(\vec{x}_k)}. \tag{7.14}$$

Here j and k label vortices and anti-vortices, respectively. Now, using the dilute gas approximation, we may sum over configurations *before* integrating over $\tilde{\rho}$. This yields

$$e^{-S} = e^{-\frac{1}{2g} \int d^2x (\nabla\tilde{\rho})^2} e^{\frac{\gamma}{2a} \int d^2x \left(e^{-\frac{2\pi i \tilde{\rho}}{g}} + e^{\frac{2\pi i \tilde{\rho}}{g}} \right)}, \tag{7.15}$$

for some constant γ, which depends on our choice of regularization. In the context of dilute instanton gases, γ is called the fugacity. This equation reveals that in the continuum limit, the XY model is characterized by the following Lagrangian, which is known as the sine-Gordon model:

$$\mathcal{L}_{SG} = \frac{1}{2g}(\nabla\tilde{\rho})^2 - \gamma a^2 \cos\left(\frac{2\pi\tilde{\rho}}{g}\right). \tag{7.16}$$

From here, the predictions of Kosterlitz and Thouless of a vortex unbiding phase transition are manifest. Indeed, at low temperatures, corresponding to $g \to 0$, the sine-Gordon model corresponds to a free boson, and gapless behaviour is predicted. We should think of the vortex/anti-vortex pairs as being tightly bound in this phase. Meanwhile, for large values of g, we may expand the interaction term to obtain (after rescaling $\tilde{\rho}$)

$$\mathcal{L}_{SG} = \frac{1}{2}(\nabla\tilde{\rho})^2 + \frac{2\pi^2 a^2 \gamma}{g}\tilde{\rho}^2 + O(g^{3/2}), \tag{7.17}$$

demonstrating that a boson mass $m_\rho := (2a\pi)^2 \gamma / g$ is generated. In this phase, the vortex/anti-vortex pairs are unbound, and unpaired vortices proliferate. A transition between these two phases will occur precisely when the scaling dimension of the interaction term turns relevant, which is known

---

[37]When discussing entropies, we set Boltzmann's constant, k_B, to 1.

in the sine-Gordon model to occur at $g_c = \pi/2$. This is the same temperature quoted above that followed from an energy vs. entropy argument.

As a final observation, we stress the fact that in the low temperature (weak coupling) regime, the XY model exhibits quasi-long range order. That is, correlation functions in the gapless phase exhibit power-low (i.e. algebraic) decay, and the U(1) symmetry is not spontaneously broken. This is the same kind of order that we predict for the topologically driven gapless phases of our SU(n) chains. Of course, true long-range order, which necessitates the spontaneous breaking of the (continuous) U(1) symmetry, would be in direct violation of Coleman's theorem.

7.2.2 Mass generation in the $\mathbb{CP}^1$ sigma model

Now that we've reviewed the explicit mass generating mechanism of the XY model, we are ready to relate this phenomenon to spin chains. Historically, this was first done by Affleck in the language of the O(3) nonlinear sigma model [137]. Here, we will repeat this derivation in $\mathbb{CP}^1$, as this will set the stage for our generalization to larger flag manifolds later on.

Our strategy is quite simple. Since the U(1) symmetry of the XY model can be embedded into the larger $\mathbb{CP}^1$ target space of the antiferromagnet, we will introduce a potential that restricts the fields $\varphi^\alpha \in \mathbb{C}^2$ to a U(1) subspace of $\mathbb{CP}^1$. In the limit where this potential is infinitely large, we have precisely the XY model, and we have an explicit mass generating mechanism at hand, namely vortex proliferation. Then, we will weaken this potential, and see how this mechanism persists through a family of models, all the way back to the isotropic theory of $\mathbb{CP}^1$.

Our starting point is

$$\mathcal{L} = \frac{1}{2g}\left(|\partial_\mu \boldsymbol{\varphi}|^2 - |\boldsymbol{\varphi}^* \cdot \partial_\mu \boldsymbol{\varphi}|^2\right) + \mathcal{L}_{\text{top}}. \tag{7.18}$$

with $g = 1/s$. For simplicity, we first consider the case of integer spin chains, so that we may neglect $\mathcal{L}_{\text{top}}$. In the following subsection, we will restore it, and see remarkably how it destroys the mass generating mechanism, and leads to the closing of the Haldane gap.

Next, let us add to (7.18) the following potential,

$$V = m(|\varphi_1|^2 - |\varphi_2|^2)^2. \tag{7.19}$$

In terms of the spin vectors $\vec{S} \in \mathbb{R}^3$, this corresponds to adding to the Heisenberg Hamiltonian the term $\sum_j S_z(j)S_z(j)$. Clearly, in the limit $m \to \infty$, this potential restricts $\vec{S}$ to lie in the XY plane. Or, to relate things to the O(3) nonlinear sigma model, parametrized by $\vec{n} \in S^2$, it forces the form

$$\vec{n} = \begin{pmatrix} \cos\rho & \sin\rho & 0 \end{pmatrix}^{\text{T}}, \tag{7.20}$$

which relates us back to (7.5). In the complex notation, we see that V restricts $\boldsymbol{\varphi}$ to lie in a U(1) subspace of $\mathbb{CP}^1$, parametrized by the angle σ:

$$\boldsymbol{\varphi} = \frac{1}{\sqrt{2}}\begin{pmatrix} 1 \\ e^{i\sigma} \end{pmatrix}. \tag{7.21}$$

In this form, we have explicitly chosen a gauge by setting the first component of $\boldsymbol{\varphi}$ to be real and positive. This reflects the fact that $\mathbb{C}P^1$ is a coset space, SU(2)/U(1).

Now, we know from the previous subsection that a mass is generated in this theory when $m \to \infty$, due to vortices. However, we stress that this argument necessitated the introduction of a UV cutoff, a^{-1}. In terms of a classical XY model on the lattice, a^{-1} naturally arises as the inverse lattice spacing. But here, in the continuum $\mathbb{C}P^1$ sigma model, a^{-1} must arise from somewhere else. It is perhaps not surprising that the UV cutoff now comes from m, the explicit (large) mass scale that we have inserted by hand, via V.

While this observation is satisfying, it does not help us relate back to the $\mathbb{C}P^1$ sigma model, which corresponds to $m = 0$. As we reduce m, how do we realize UV-finite vortex configurations? The answer to this question is that the vortices become nonplanar as we reduce m. In other words, since $\vec{S}$ is no longer restricted to the XY plane for finite m, it becomes energetically favourable for a vortex configuration in $\tilde{\rho}$ to lift off the plane and point in the $\pm\hat{z}$ direction at the vortex core. In the small-m limit, such configurations will have action

$$S[\tilde{\rho}] \to \frac{2\pi}{g} \log(mL),\tag{7.22}$$

where L is the system length. As before, the infrared divergence associated with $L \to \infty$ is remedied by considering configurations with net topological charge of zero.

Let us see what these nonplanar vortices look like in terms of the complex $\boldsymbol{\varphi}$. Far from its core, a configuration with topological charge +1 will have the form

$$\boldsymbol{\varphi} = \frac{1}{\sqrt{2}} \begin{pmatrix} 1 \\ e^{i\omega} \end{pmatrix}\tag{7.23}$$

where ω is the polar angle in the XY plane. In the infinite-m limit, such a configuration has a singularity in ω at the origin. However, for finite m, this singularity may be avoided by sending one of the two components of $\boldsymbol{\varphi}$ to zero (which corresponds to $n_3 \to \pm 1$ in the O(3) nonlinear sigma model):

$$\boldsymbol{\varphi} \to \begin{pmatrix} 1 \\ 0 \end{pmatrix} \qquad \text{or} \qquad \boldsymbol{\varphi} \to \begin{pmatrix} 0 \\ e^{i\omega} \end{pmatrix}.\tag{7.24}$$

The phase remains in the second case due to our gauge choice; however, at the configuration's core, it can be removed by a pure gauge transformation, and thus does not lead to a true UV singularity.

Such configurations are known as 'merons', or fractional instantons. Specifically, we will refer to the first as a meron, and to the second as an anti-meron. The word instanton makes reference to the fact that one of the two spatial dimensions in the $\mathbb{C}P^1$ theory is actually Euclidean time. Meron refers to the half-quantized charge of these configurations, which we now demonstrate.

Since the topological charge, Q, of $\boldsymbol{\varphi}$ is the integral of a total derivative, we may rewrite Q as the difference of two contour integrals, one around the origin and one around infinity:

$$Q = \frac{1}{2\pi i} \left[\oint_0 dx_\mu \boldsymbol{\varphi} \cdot \partial_\mu \boldsymbol{\varphi}^* - \oint_\infty dx_\mu \boldsymbol{\varphi} \cdot \partial_\mu \boldsymbol{\varphi}^* \right].\tag{7.25}$$

The contour is necessary to avoid any gauge singularity that may be present at the origin (see below). For both possibilities in (7.24), the contour about infinity contributes a charge of $\frac{1}{2}$. Meanwhile, the contribution from the contour about the origin is trivial in the first possibility, and -1 in the second, leading to $Q = \pm\frac{1}{2}$, which proves the half-quantized charge of the meron. At the end of this subsection, we will comment on the gauge invariance of this topological charge.

The arguments from the previous subsection carry over directly to these nonplanar topological configurations. As above, we may perform a dilute instanton gas summation, and arrive at a sine-Gordon Lagrangian. Before, the coupling constant g depended on the ultraviolet cutoff, a; now, it depends on the anisotropic parameter, m. And before, we realized the KT transition by increasing g at fixed a. However, we may equally well increase g at a fixed bare coupling constant, by lowering the energy scale, m. This follows from the asymptotic freedom of the parameter g, which is manifest in the following equation [137]

$$g_{\text{eff}} \simeq \frac{g}{1 + (g/2\pi)\log(ma)}. \tag{7.26}$$

Therefore, as we reduce m, we push the sine-Gordon model's temperature closer and closer to the transition temperature. Eventually, as m approaches zero, we will necessarily be above any critical value of bare g, and be in the gapped phase with condensed vortex configurations. Thus, we conclude that the $\mathbb{CP}^1$ sigma model, in the absence of any topological term, will be in a massive phase for any value of g, and that this mass is generated by topological excitations with half-integer charge.

Gauge Invariance of the Topological Charge

Before carrying on, let us reflect on the structure of (7.25). There, we rewrite the topological charge Q as a difference of two contour integrals. It is interesting to note that while their sum is necessarily invariant under the U(1) gauge symmetries $\varphi_\beta \to e^{i\vartheta_\beta}\varphi_\beta$, an individual contour integral is not. Indeed, under $\boldsymbol{\varphi} \mapsto e^{i\vartheta}\boldsymbol{\varphi}$,

$$\oint dx_\mu \boldsymbol{\varphi} \cdot \partial_\mu \boldsymbol{\varphi}^* \mapsto \oint dx_\mu \boldsymbol{\varphi} \cdot \partial_\mu \boldsymbol{\varphi}^* + i \oint dx_\mu \partial_\mu \vartheta. \tag{7.27}$$

The second term, which breaks the gauge invariance of the contour, is necessary in order to account for gauge transformations that alter the U(1) winding number of $\boldsymbol{\varphi}$ along the contour. This feature implies that it is not meaningful to ask where the topological charge of a configuration $\boldsymbol{\varphi}$ is localized. For instance, two gauge-equivalent versions of the SU(2) meron have the following behaviours at infinity:

$$\boldsymbol{\varphi} = \frac{1}{\sqrt{2}}\begin{pmatrix} 1 \\ e^{i\omega} \end{pmatrix} \qquad \boldsymbol{\varphi}' = \frac{1}{\sqrt{2}}\begin{pmatrix} e^{-i\omega} \\ 1 \end{pmatrix}. \tag{7.28}$$

Their behaviour at zero is given by the first possibility in (7.24). The contour around infinity in (7.25) equals $-\frac{1}{2}$ for the case of $\boldsymbol{\varphi}$, while it equals $+\frac{1}{2}$ for the case of $\boldsymbol{\varphi}'$. Meanwhile, the contour around zero is trivial in the case of $\boldsymbol{\varphi}$, and equals $+1$ for the case of $\boldsymbol{\varphi}'$. The full expression

in (7.25) yields $Q = \frac{1}{2}$ in both cases, as it must. Finally, we note that by choosing the gauge $\boldsymbol{\varphi}' = \frac{1}{\sqrt{2}}(e^{-i\omega/2}, e^{i\omega/2})^T$, the contour around infinity vanishes, which is what one finds in the O(3) version of the meron [137].

7.2.3 The breakdown of mass generation at $\theta = \pi$.

We are now in a position to interpret Haldane's conjecture in terms of fractional instantons in the $\mathbb{CP}^1$ sigma model. Let us restore the topological angle $\theta = \pi$, and study how the mass generating mechanism changes. For large m, we are in the U(1) model and the θ-term does not play a role; rather it is not well defined. However, as m is lowered towards zero, the fugacity in the sine-Gordon Lagrangian is modified as follows:

$$\gamma \to \gamma \cos(\theta/2). \tag{7.29}$$

This is because both vortices and anti-vortices are now weighted by the factor $e^{i\theta/2}$ if they correspond to merons, and by the factor $e^{-i\theta/2}$ if they correspond to anti-merons. Recall that we must sum over *all* possible saddle point configurations.

Thus, we see that γ vanishes at topological angle $\theta = \pi$, which corresponds to half-odd integer spin chains. This seems to suggest that the non-planar vortex/anti-vortex pairs will never unbind, and a massless phase will persist at all temperatures. However, this is not the whole story. Higher-order configurations, such as double vortices with $\kappa = \pm 2$ will have topological charge 0 or ± 1, and do not lead to a vanishing fugacity. Nonetheless, these configurations effectively raise the critical value of g, below which occurs a gapless phase. Thus, we may at least conclude that the critical value of m is smaller at $\theta = \pi$ than at $\theta = 0$. Based on the overwhelming evidence in favour of Haldane's conjecture, we expect that this critical value is driven all the way to $m = 0$, so that a gapless phase does indeed occur.

7.3 Reducing the Global Continuous Symmetry to U(1)

Now that we have reviewed in great detail how fractional instantons generate a mass gap in the $\mathbb{CP}^1$ sigma model, we are ready to study how this mechanism generalizes to flag manifold sigma models. Our strategy is the same: we break the symmetry of the flag manifold down to U(1), where a phase transition is well understood in terms of vortex proliferation. Our complete Lagrangian is (6.2), which we repeat here:

$$\mathcal{L} = \sum_{\alpha,\beta=1}^{n} \left[g_{\alpha\beta}\delta^{\mu\nu} + b_{\alpha\beta}\epsilon^{\mu\nu} \right] (\boldsymbol{\varphi}^{\alpha} \cdot \partial_{\mu}\boldsymbol{\varphi}^{*,\beta})(\boldsymbol{\varphi}_{\beta} \cdot \partial_{\nu}\boldsymbol{\varphi}^{*,\alpha}) + \mathcal{L}_{\text{top}}. \tag{7.30}$$

As in the previous section, we will for now neglect the topological Lagrangian. It will be restored later on, once we have established mass generation in the case of $\theta_\alpha = 0$. To this Lagrangian, we add an anisotropic potential V_1 that breaks the SU(n) symmetry down to $[U(1)]^{n-1}$, while preserving

the discrete $\mathbb{Z}_n$ symmetry and the $[U(1)]^{n-1}$ gauge structure:[38]

$$V_1 = m \sum_{\alpha=1}^{n} \sum_{\beta<\gamma} (|\varphi_\beta^\alpha|^2 - |\varphi_\gamma^\alpha|^2)^2. \tag{7.31}$$

This is the SU(n) generalization of adding the term $\sum_j S_z(j)S_z(j)$ to the SU(2) Hamiltonian. Indeed, for the symmetric SU(n) chains, it is straightforward to rewrite V_1 in terms of the SU(n) generators on the chain. We have

$$|\varphi_\beta^\alpha|^2 = \frac{1}{p} S_{\beta\beta}(j_\alpha), \tag{7.32}$$

so that

$$V_1 = \frac{m}{p^2} \sum_{\alpha=1}^{n} \sum_{\beta<\gamma} \left(S_{\beta\beta}(j_\alpha) - S_{\gamma\gamma}(j_\alpha)\right)^2. \tag{7.33}$$

To obtain the corresponding lattice terms, we simply multiply the right hand side of these expressions by n, and sum over j. It is interesting to note that in the case of SU(3), the potential V_1 is proportional to

$$\sum_{\alpha=1}^{3} [T_3(j_\alpha)T_3(j_\alpha) + T_8(j_\alpha)T_8(j_\alpha)], \tag{7.34}$$

where T_3 and T_8 are the two diagonal generators of SU(3) in the Gell-Mann basis. Now, in the limit $m \to \infty$, the potential V_1 restricts each of the φ^α to lie on an $n-1$ torus, parameterized by $n-1$ angles, $\varsigma_\beta = \varsigma_\beta(\alpha)$:

$$\varphi^\alpha = \frac{1}{\sqrt{n}} \left(e^{i\varsigma_1} \quad e^{i\varsigma_2} \quad \cdots \quad e^{i\varsigma_{n-1}} \quad e^{i\varsigma_n}\right)^{\mathrm{T}}. \tag{7.35}$$

Throughout, we fix a gauge by choosing φ_1^α to be real and positive, for all α. Since the number of free parameters equals the number of orthogonality constraints (both equal $n(n-1)/2$)), one might conclude that there is a unique configuration of the φ^α in this limit (up to permutations). However, the orthogonality constraints are invariant under the following transformations,

$$\varphi_\beta^\alpha \to e^{i\theta_\beta} \varphi_\beta^\alpha \qquad \forall \alpha, \beta, \tag{7.36}$$

which are true symmetries for each of the $n-1$ un-gauge-fixed directions, $\beta = 2, 3, \ldots, n$. Therefore, by introducing the potential (7.31), the continuous symmetry group of the sigma model has been broken down to $[U(1)]^{n-1}$. A typical configuration of the φ^α in this submanifold can be constructed from the nth root of unity, $\zeta := e^{i\frac{2\pi}{n}}$:

$$\varphi_\beta^\alpha = \frac{1}{\sqrt{n}} \zeta^{\alpha\beta} e^{i\sigma_\beta} \qquad \sigma_\beta \in [0, 2\pi]. \tag{7.37}$$

---

[38]Based on the previous chapters, we recognize how important the $\mathbb{Z}_n$ symmetry is to generalizing Haldane's conjecture. It would be a serious matter to break it explicitly now.

Indeed, orthonormality of these states follows from the identity $\sum_{\alpha=1}^{n} \zeta^{\rho\alpha} = 0$, which holds for all $\rho \neq 0 \mod n$. Since the Lagrangian (7.30) couples all of the $n-1$ copies of U(1) together, it will be useful to break the symmetry down further. To this end, we introduce a second potential V_2, given by

$$V_2 = -m \sum_{\alpha=1}^{n} \sum_{\beta=2}^{n-1} \left((\varphi_1^\alpha [\varphi_\beta^\alpha]^*)^n - ([\varphi_1^\alpha]^* \varphi_\beta^\alpha)^n \right)^2. \tag{7.38}$$

In terms of the SU(n) matrices, this potential takes the form

$$V_2 = -n \sum_{j} \frac{m}{p^2} \sum_{\alpha=1}^{n} \sum_{\beta=2}^{n-1} \left((S_{1\beta}(j_\alpha))^n - (S_{\beta 1}(j_\alpha))^n \right)^2. \tag{7.39}$$

The factors of n in the exponent are necessary in order to preserve the $\mathbb{Z}_n$ symmetry, which corresponds to translational invariance in the underlying lattice model.[39] Since V_2 is still minimized by the configurations (7.37), it can be rewritten in terms of the U(1) fields, σ_β, yielding

$$V_2 = 4m \sum_{\alpha=1}^{n} \sum_{\beta=2}^{n-1} \sin^2(n(\sigma_1 - \sigma_\beta)). \tag{7.40}$$

It is clear that the effect of V_2 is to equate all but one of the U(1) fields. In our fixed gauge, this amounts to setting $\sigma_\beta = 0$ for $\beta \neq n$, resulting in a theory that involves σ_n only. This is equivalent to the XY model. By inserting this restricted form of φ^α into (7.30), it is easy to show that the $b_{\alpha\beta}$ terms vanish, and the resulting O(2) coupling constant is g, defined by

$$g^{-1} = \sum_{\alpha,\beta} g_{\alpha\beta}^{-1}. \tag{7.41}$$

7.4 Mass Generation by Fractional Instantons

In this section, we would like to extend the discussion of non-planar vortices in the $\mathbb{CP}^1$ sigma model to the larger SU(n)/[U(1)]$^{n-1}$ sigma model. With any luck, we should find that a similar mass generating mechanism is at play here, and that it breaks down when particular topological angles are restored.

Recall that a non-planar vortex, (which we've already referred to as a meron or a fractional topological instanton) has the following form in terms of the $\mathbb{CP}^1$ field, φ. Far from its center, it reads

$$\varphi = \frac{1}{\sqrt{2}} \begin{pmatrix} 1 \\ e^{i\omega} \end{pmatrix}. \tag{7.42}$$

Meanwhile, near its center, it tends to either $(1,0)^{\mathrm{T}}$ or $(0, e^{i\omega})^{\mathrm{T}}$, in order to avoid an ultraviolet singularity.

---

[39] Since φ has dimension 0 in 1+1 dimensions, an operator with arbitrarily high powers of φ is still renormalizable.

Extending this calculation to SU(n) is straightforward. Now, the topological charge is a vector $\boldsymbol{Q} = (Q_1, Q_2, \ldots, Q_n)$, corresponding to the n fields $\boldsymbol{\varphi}^\alpha$. A configuration far from its core has $\varphi_n^\alpha = \frac{1}{\sqrt{n}} e^{i\omega}$ for all α, and receives a contribution to the topological charge of $\frac{1}{n}$ from the contour at infinity. Meanwhile, in order for the configuration to be UV finite at its core, the phase $e^{i\omega}$ in each of the nth components of the $\boldsymbol{\varphi}^\alpha$ must either vanish or become a pure gauge transformation. This leads to an n-fold family of topological excitations, distinguished by which one of the $\boldsymbol{\varphi}^\alpha$ tends to $(0, 0, 0, \ldots, e^{i\omega})^{\mathrm{T}}$. For that particular $\boldsymbol{\varphi}^\alpha$, a contribution of -1 is added to its topological charge from the contour about the origin in (7.25), while the remaining $n - 1$ fields receive no contribution, as they are topological trivially there. See the example below for an explicit solution in the case of $n = 3$. Thus, we obtain n species of topological configuration, with charges

$$\boldsymbol{Q}^\alpha = \frac{1}{n}(1, 1, \ldots, \overbrace{-(n-1)}^{\text{position } \alpha}, \ldots, 1). \tag{7.43}$$

And so for all n, we find fractionalized topological excitations, or fractional instantons, in our symmetry broken model.

7.4.1 Example: An explicit fractional instanton in SU(3)

Here, we prove the existence of a fractional instanton in SU(3), with topological charge $\boldsymbol{Q}^1 = (-\frac{2}{3}, \frac{1}{3}, \frac{1}{3})$. While the most general complex unit vector in $\mathbb{C}^3$ depends on five real parameters, we make a symmetric ansatz that reduces this number down to two, which is the minimum number of parameters necessary to construct a fractional instanton. For our three orthogonal vectors $\boldsymbol{\varphi}^\alpha$, we take:

$$\boldsymbol{\varphi}^1 = \frac{1}{\sqrt{2}}\begin{pmatrix} \sin\vartheta \\ \sin\vartheta \\ \sqrt{2}\cos\vartheta e^{i\omega} \end{pmatrix} \qquad \boldsymbol{\varphi}^2 = \frac{1}{2}\begin{pmatrix} \cos\vartheta + i \\ \cos\vartheta - i \\ -\sqrt{2}\sin\vartheta e^{i\omega} \end{pmatrix} \qquad \boldsymbol{\varphi}^3 = \frac{1}{2}\begin{pmatrix} \cos\vartheta - i \\ \cos\vartheta + i \\ -\sqrt{2}\sin\vartheta e^{i\omega} \end{pmatrix}. \tag{7.44}$$

Here ω is the polar angle coordinate, and $\vartheta \in [0, \pi/2]$ depends only on the radial coordinate: $\vartheta = \vartheta(r)$. Inserting this ansatz into the Lagrangian (7.30), one obtains

$$\mathcal{L} = \frac{1}{g}\left[(\partial_r\vartheta)^2 + \frac{1}{r^2}U_1(\vartheta) + mgU_2(\vartheta)\right], \tag{7.45}$$

where

$$U_1(\vartheta) = \sin^2\vartheta\cos^2\vartheta + \frac{1}{4}\sin^4\vartheta, \tag{7.46}$$

and

$$U_2(\vartheta) = \frac{5}{2}\left[\cos^2\vartheta - \frac{1}{2}\sin^2\vartheta\right]^2 + \frac{1}{128}\cos^2\vartheta(3\sin^4\vartheta - 4\cos^2\vartheta)^2. \tag{7.47}$$

Note that there is a unique coupling constant $g = g_{12} = g_{13} = g_{23}$ in the SU(3)/[U(1)]^2 sigma model, and the terms proportional to $b_{\alpha\beta}$ have vanished. This is the classical Lagrangian for a particle at position ϑ at time r, in a time-dependent effective potential

$$V_{\text{eff}} = -\frac{1}{r^2} U_1(\vartheta) - mgU_2(\vartheta). \tag{7.48}$$

Now, at radii r such that $r^2mg \ll 1$, V_{eff} is maximized by minimizing $U_1(\vartheta)$ on $[0, \pi/2]$, which is achieved with $\vartheta = 0$. On the other hand, for $r \to \infty$, the effective potential is maximized by minimizing $U_2(\vartheta)$, which is done with $\vartheta = \vartheta = \arccos(1/\sqrt{3})$. Since $\frac{d}{d\vartheta}U_1 \geq 0$ on $[0, \vartheta]$, and $\frac{d}{d\vartheta}U_2 \leq 0$ on the same interval, we may conclude that a solution exists with $\vartheta(r)$ increasing monotonically from 0 at $r = 0$ to ϑ at $r = \infty$. As expected, the vectors $\boldsymbol{\varphi}^\alpha$ in (7.44) tend to (7.37), up to a gauge transformation, as $r \to \infty$. Moreover, as $r \to 0$, the UV singularities $e^{i\omega}$ in $\boldsymbol{\varphi}^2$ and $\boldsymbol{\varphi}^3$ vanish, and $\boldsymbol{\varphi}^1 \to (0, 0, e^{i\omega})^{\text{T}}$. This completes the example.

7.4.2 Multiple copies of the sine-Gordon model

While the number of such topological configurations has increased, the original argument from $\mathbb{CP}^1$ for mass generation carries over to this more general case: for each species of topological excitation in this n-fold family, we have a species of particle in the Coulomb gas formalism [137]. That is, each particle has a partition function that is represented (at large distances) by its own sine-Gordon model,

$$\mathcal{L}_{SG} = \frac{1}{2}(\partial_\mu\sigma)^2 + \gamma\cos(\frac{2\pi}{g}\sigma), \tag{7.49}$$

which is identical for each of the n species. As above, γ represents the fugacity of the fractional instanton gas. Since all of the n species arise from the same action, each will have the same fugacity and critical g, so that the above model (7.49) is merely copied n times, and the SU(2) analysis from Section 7.2.2 can be applied directly. As m is lowered, the effective critical temperature is increased until the topological excitations condense and a mass gap is produced. Thus, we conclude that fractional instantons are responsible for generating a mass gap in the SU(n)/[U(1)]$^{n-1}$ sigma model (7.30), in the absence of topological angles.

7.5 Destructive Interference in the Presence of Topological Angles

We now restore the topological angles θ_α, and study how the mass generating mechanism changes. As before, when m is large, our theory reduces to the U(1) sigma model where the θ-terms do not play a role. However, as m is lowered towards zero, the fugacity γ in the sine-Gordon model is modified to

$$\gamma \sum_{\alpha=1}^{n} e^{i\theta \cdot Q^\alpha}, \tag{7.50}$$

where the sum is over the n species of fractional instanton, and $\theta_\alpha = \alpha\theta$, with $\theta = \frac{2\pi p}{n}$. Using (7.43), one easily finds that this sum equals $\gamma \sum_k \zeta^{pk}$. So long as p is not a multiple of n, this sum vanishes. In other words, for such values of p, the fugacity of the sine-Gordon model vanishes, suggesting that the Coulomb gas is always in its massless phase.

At first glance, this appears to be inconsistent with our results from the previous chapters, which also predict a gap when p is not a multiple of n, but has a nontrivial shared divisor with n. This discrepancy is resolved by considering higher-order topological excitations. Indeed, while objects that have winding number greater than ± 1 in ω have larger action, they too must be considered, and do not necessarily lead to a vanishing fugacity. A similar calculation shows that a configuration with winding number κ has charge $Q^{\alpha,\kappa}$, with

$$Q_\beta^{\alpha,\kappa} = \frac{\kappa}{n} - \kappa\delta_{\alpha,\beta}, \tag{7.51}$$

and modifies the fugacity to $\gamma \sum_k \zeta^{pk\kappa}$. If κ is a multiple of n, this will lead to a nonzero fugacity. This is also true in the case of SU(2): recall the double meron configurations discussed above. However, the conclusion arrived at before also applies here: since these higher winding objects have larger action, we can at least conclude that the critical value of m, above which occurs a gapless phase, is lower at $\theta = \frac{2\pi p}{n}$ than at $\theta = 0$.

Now, if $\gcd(n, p) \neq 1, n$, then not only do events with winding number n contribute to the fugacity, but so do events with winding number $d := n/\gcd(n, p)$. Since these contributions will have a much smaller action than the n-winding events, this shows that whenever p and n have a nontrivial common divisor, the critical value m is larger than at $\theta = \frac{2\pi}{n}$ (although still lower than at $\theta = 0$). Thus, it is possible to interpret our generalized Haldane conjecture in terms of these fractional topological excitations: When p and n are coprime, mass generation only starts to occur for configurations that have winding number $\pm n$. In SU(2), these events are not strong enough to open a gap at the isotropic point $m = 0$, and we predict that this holds for general n. In other words, we are claiming that the critical value of m is zero when p and n are coprime. When p and n have a nontrivial common divisor different from n, configurations that have much less action begin to contribute to mass generation, starting with objects that have winding number d. The simplest example of this is in SU(4), with $p = 2$. In this case, configurations that have winding number ± 2 successfully generate a mass gap, while for $p = 1$ these configurations destructively interfere, and a mass gap is not generated by the subleading configurations, with winding ± 4. Finally, when p is a multiple of n, the least-action configurations that have winding ± 1 produce a mass gap, just like the merons in SU(2).

While we haven't offered a rigorous argument as to why the critical value of m is indeed fixed at zero in the case of p and n coprime, we can make the following observation. According to the LSMA theorem, a finite energy gap above the ground state implies spontaneously broken $\mathbb{Z}_n$ symmetry whenever p is not a multiple of n. In the sine-Gordon model (7.49), this $\mathbb{Z}_n$ symmetry corresponds to the following transformation:

$$\sigma \mapsto \sigma - \frac{2\pi}{n}. \tag{7.52}$$

While this transformation acts nontrivially on most fractional instantons, it has no effect on configurations with winding number n, which are the elementary excitations in the sine-Gordon model when p and n are coprime. Thus, our prediction of a gapless phase in this case is perhaps not too unreasonable, since any finite gap would necessitate the spontaneous breaking of (7.52), which acts trivially on the Coulomb gas of n-winding events.

7.6 Conclusions

In this chapter, we have proposed a mass generating mechanism by fractional instantons in the complete flag manifold sigma models, with target space $\mathrm{SU}(n)/[\mathrm{U}(1)]^{n-1}$. These theories arise naturally from $\mathrm{SU}(n)$ chains in particular representations, as we have seen many times throughout this thesis. In particular, we have focused on theories with $n-1$ nontrivial topological angles, $\theta_\alpha = \frac{2\pi\alpha}{n}p$. These correspond to either the rank-p symmetric representations of $\mathrm{SU}(n)$, or the two-row representations for even n, with $p = p_1 + p_2$.

For p a multiple of n, we have shown that topological configurations with charge $\frac{1}{n}$ produce a finite gap above the ground state, much in the same way that vortices produce a gap in the Kosterlitz Thouless transition of the XY model. When p and n have a nontrivial common divisor different from n, we've shown that a mass gap is still produced, but now it is due to larger-action configurations that have charge $\frac{1}{\gcd(n,p)}$. Finally, when p and n are coprime, we have argued that no energy gap is produced by topological configurations. Together, these three results offer an intuitive explanation of the generalizations of the Haldane conjecture to $\mathrm{SU}(n)$ chains that have appeared in this thesis.

Chapter 8

Summary and Outlook

In this thesis, we have succeeded in achieving our original goal of extending Haldane's famous conjecture about antiferromagnetic chains to systems with $SU(n)$ symmetry. To summarize our main result succinctly, we have found that there are two families of $SU(n)$ chains that exhibit a gapless phase at low energies. The first family consists of those chains with a completely symmetric rank-p representation at each site, with p a positive integer whose greatest common divisor with n is 1. In the case of $n = 2$, these chains are precisely those with half-odd integer spin, i.e. the spin chains predicted by Haldane to be gapless. The second family of $SU(n)$ chains that we have identified are also labeled by a positive integer p satisfying the same coprime constraint with n, but are only gapless for even n. These representations are not completely symmetric: instead, they have two rows in their Young tableaux, of lengths p_1 and p_2 that sum to p. The simplest chain corresponding to this second family has $SU(4)$ symmetry, with the representation $(p_1 = 2, p_2 = 1)$ at each site.

While the above classification is elegant, and was the source of motivation for much of the work appearing in this thesis, it is by no means the only noteworthy result that has been obtained. Indeed, in our attempt to push the conceptual and technical limitations of Haldane's original calculations, we have made numerous discoveries that will have a lasting impact on the field of $SU(n)$ spin systems.

In Chapter 3, we learned early on that the nearest-neighbour Heisenberg model used by Haldane is inadequate for deriving a low energy field theory of chains with larger symmetry groups. This can be understood by considering how the Young tableau parameters p_α, which generalize the notion of spin in the antiferromagnet, determine the target space manifold of the chain's matrix degree of freedom, S. For $SU(2)$, this manifold is always $\mathbb{C}P^1$, and one may readily derive the familiar $\mathbb{C}P^1$ sigma model. But for $n > 2$, the space $\mathbb{C}P^1$ is promoted to a flag manifold, and further care must be taken when deriving a low energy description. Throughout Chapter 3, we developed a prescription for obtaining a well defined quantum theory, which amounted to adding longer-range interaction terms to the Hamiltonian. These interaction terms serve to restrict the target space of S to be an orthogonalized product of $\mathbb{C}P^{n-1}$ models. Then, by summing over the unit cell (which is determined by the classical ground state of the chain), we obtain n orthogonalized $\mathbb{C}P^{n-1}$ models, which together constitute a sigma model whose target space is the complete flag manifold, $SU(n)/[U(1)]^{n-1}$. As a result, we were able to answer in Chapter 3 the obvious question posed by many seeking to extend Haldane's conjecture beyond $SU(2)$: what is the appropriate generalization of the $\mathbb{C}P^1$ sigma model that describes the antiferromagnet at low energies? It turns out that $\mathbb{C}P^1$ should be promoted to the complete flag manifold of $SU(n)$. As a tangential development in

this chapter, we also extended the exact results of Lieb, Schultz, Mattis and Affleck (the LSMA theorem) to the longer-range Hamiltonians that we introduced.

In Chapter 4, in deriving an explicit expression for the sigma model of the SU(3) chain in the symmetric representation, we made three important realizations. First, unlike the $\mathbb{CP}^1$ Lagrangian that is characterized by a single parameter g, for $n > 2$ there is an additional λ parameter that corresponds to a two-derivative interaction term that couples the different $\mathbb{CP}^{n-1}$ sectors together. When we interpret the Lagrangian as a metric on the flag manifold target space, this parameter corresponds to a torsion, or antisymmetric tensor. Such terms were unanticipated, as torsion does not exist in the simpler case of $\mathbb{CP}^1$. Using the renormalization group, we were able to conclude that λ is a relevant parameter, and should be included in the low energy limit. The second realization we made concerned the topological angle content of these theories. Since flag manifolds may be embedded into a product of $\mathbb{CP}^{n-1}$ models, it is possible to define multiple topological charges, by pulling back the topological term from each $\mathbb{CP}^{n-1}$ sector. Mathematically, this is seen by noting that the second cohomology group of the flag manifold is $\mathbb{Z}^{n-1}$. In the symmetric SU(3) chains, we found that this led to two topological angles $\theta_1 = \frac{2\pi p}{3}$ and $\theta_2 = \frac{4\pi p}{3}$. Since 3 is prime, these angles both are nontrivial so long as p is not a multiple of 3; however, we began to speculate that for larger values of n, it might be possible for some, but not all of the topological angles to be trivial. How would Haldane's conjecture generalize in this case? Finally, the third realization we made in Chapter 4 arose from considering other (non-symmetric) representations. In spin chains, it was well understood that for translationally invariant systems, the classical model would always exhibit antiferromagnetic order for a positive interaction strength, J. However, for $n > 2$, we learned that it is possible to realize ferromagnetic and antiferromagnetic order simultaneously (in the classical limit). This led to the fascinating consequence of having Goldstone bosons with two types of dispersion relation: linear dispersion for those corresponding to antiferromagnetic order, and quadratic dispersion for those corresponding to ferromagnetic order. And all of these bosons arise from the same parent group, SU(n). We concluded this chapter by restricting to those representations with antiferromagnetic order only. In addition to the symmetric ones, this led also to the self-conjugate SU(3) chains. We found that these chains did not exhibit Lorentz invariance at low energies – a surprising feature, but one that would prove to ubiquitous in the remaining chapters of this thesis.

In Chapter 5, we were forced to confront the absence of Lorentz invariance head-on. Here, our goal was to extend our derivation of the flag manifold sigma model from the symmetric SU(3) chain to symmetric chains with generic SU(n) symmetry. Armed with our newfound understanding from the previous two chapters, we hoped to obtain a model with target space SU(n)/[U(1)]$^{n-1}$, that depended on two parameters g and λ. But yet again, we were confronted with the unexpected. Instead of a single g and a single λ, we instead found $\lfloor \frac{n}{2} \rfloor$ different coupling constants of each type. We now understand that this is consistent with the underlying symmetry of the model: the most generic metric and torsion tensors on the complete flag manifold sigma model of SU(n) each have $\lfloor \frac{n}{2} \rfloor$ free parameters. But more importantly, we also found that for $n > 3$, our theory was not characterized by a single velocity v (which corresponded to the velocity of spin-waves in the antiferromagnet). This feature of multiple velocities meant that for all values of $n > 3$, the

symmetric SU(n) chain seemed not to have a Lorentz invariant low energy description. It was at this point that we engaged in the arduous task of calculating the renormalization group flow of these distinct velocities. Our findings, which we believe are rather consequential to the study of SU(n) chains, were that at large length scales, these velocities all converge to a common value. As a result, we may write down a Lorentz invariant theory for the SU(n) chain after all. This observation was crucial in establishing an SU(n) version of Haldane's conjecture, which relies in part on 't Hooft anomaly matching arguments of Lorentz invariant quantum field theories. We concluded that the rank-p symmetric SU(n) chain corresponds to the relativistic complete flag manifold of SU(n), with topological angle content $\theta_\alpha = \frac{2\pi p \alpha}{n}$ for $\alpha = 1, 2, \ldots, n-1$. Moreover, we concluded that only when p and n share no common divisor, may this theory exhibit a gapless phase at weak coupling. As we alluded to above, only in this scenario are all $n-1$ topological angles nontrivial: if p and n have common divisor q, then $\theta_{n/q} \equiv 0$. This observation motivated our efforts in Chapter 7

Before investigating the consequence of a vanishing subset of topological angles, we saw it appropriate in Chapter 6 to classify all remaining (i.e. nonsymmetric) SU(n) chains. Having $n-1$ distinct topological angles seemed to be a necessary condition for realizing a gapless phase, and so we set out to list all representations that would map to a sigma model with this property. It was here that the phenomenon of linear vs. quadratic dispersion that appeared in SU(3) chains returned in full force. Throughout this chapter, we learned that linear dispersion is in fact quite a special property of SU(n) chains. For most choices of representation parameters p_α, there will at least be some corresponding Goldstone bosons with quadratic dispersion relations. In a series of tables, we were able to record exactly what relations must be satisfied between the p_α to guarantee that this does not occur. Having done this, we then turned to the classification of topological angle content for all of these purely linearly dispersing theories. Again, we were met with a surprising result: in addition to the symmetric chains, there is only one other type of SU(n) chain that has the appropriate dispersion relations and topological angles to allow for a mapping to the complete flag manifold of SU(n) with $\theta_\alpha = \frac{2\pi p \alpha}{n}$. This type of chain occurs only for even n, and has the representation with two rows of lengths p_1 and p_2 at each site, with $p = p_1 + p_2$ and $p_1 \neq p_2$. Using arguments similar to those presented in Chapter 5, we concluded that when p has no nontrivial common divisor with n, the corresponding SU(n) chain will be in a gapless phase at weak coupling.

Finally, in Chapter 7, we were able to provide a physical and intuitive argument as to why these flag manifold sigma models exhibit a gapless phase only when all $n-1$ topological angles are nontrivial. Arguably this chapter is one of most important of this thesis, as it recasts our generalized Haldane conjecture in the familiar Coulomb gas formalism, and explains why certain representations of SU(n) are so special. This work drew from an early result of Affleck that explained Haldane's original claims in terms of half-quantized topological excitations, or merons. Here, we generalized these notions to SU(n), and promoted the merons to excitations with topological charges $\pm\frac{1}{n}$. First, we showed that when $\theta_\alpha = 0$ for all α, the finite energy gap in the flag manifold sigma model can be understood as being generated by a proliferation of these topological objects. This is the same mechanism that drives a finite gap at the Kosterlitz Thouless phase transition in the XY model when vortex pairs unbind. Then, by turning on the θ_α, we were able to observe how inference effects come into play. In short, the fugacity in the Coulomb gas of topological excita-

tions is modified by the θ_α, and vanishes precisely when all $n-1$ values $\theta_\alpha = \frac{2\pi p\alpha}{n}$ are nonzero! With a vanishing fugacity, the mass-generating mechanism breaks down, so that a gapless phase occurs. Actually, what we observed is that the fugacity vanishes at lowest order for all values of $p \neq n$ (including those with a nontrivial common divisor), but when topological excitations with greater charge (and correspondingly greater action) are considered, only those with $\gcd(n, p) = 1$ lead to a gapless phase. That this Coulomb gas picture correctly describes our generalized Haldane conjecture is a very satisfying result.

Let us now close by commenting on future research directions. The most pressing issue left unsolved by the work in this thesis has to do with SU(n) chains that admit Goldstone modes with both linear and quadratic dispersion relations. This already occurs in SU(3) for any representation that is neither symmetric nor self-conjugate. How might one proceed in order to characterize such chains? One idea is that according to Coleman's theorem, quadratically dispersing Goldstone bosons are perfectly valid in one spatial dimension (at least at zero temperature). Therefore, it is conceivable that the subgroup of the SU(n) symmetry corresponding to ferromagnetic order might spontaneously order, leaving true quadratic Goldstone bosons coupled to a smaller theory. For instance, if only $m < n$ of the n copies of $\mathbb{CP}^{n-1}$ have linear dispersion, then perhaps the low energy theory of such a chain will be that of a complete SU(m) flag manifold sigma model, coupled to $n - m$ quadratically dispersing $\mathbb{CP}^{n-1}$ sectors. In anticipating such a possibility, already in Chapter 6 we have recorded which topological angles correspond to the linearly dispersing $\mathbb{CP}^{n-1}$ fields in such a scenario. If this description were true, then what we would have is a remarkable hierarchy of flag manifold sigma models: For each n, by altering the number of satisfied conditions on the p_α representation labels, we could realize a nested set of flag manifold sigma models of SU(m_1), ..., SU(m_k), with $m_1 < m_2 < \cdots < m_k = n$. Moreover, based on our topological Coulomb gas picture (and likewise the 't Hooft anomaly matching picture), an SU(n) chain with discrete $\mathbb{Z}_m$ symmetry (arising from an m-site classical unit cell), might now realize a gapless phase, characterized by an SU(m)$_1$ WZW point. Again, this scenario is only possible because quadratic Goldstone bosons are not forbidden by Coleman's theorem. This exciting possibility motivates our current research efforts into understanding these more general SU(n) chain systems.

In addition to this direct extension of our work, there are a variety of other research avenues that have now been opened up thanks to this thesis. In particular, it is now a major numerical challenge to verify our generalization of the Haldane conjecture. We expect that this task will spur the development of new techniques, just as the challenge of verifying Haldane's original conjecture led to great numerical progress, including the invention of the celebrated density matrix renormalization group. Already we have seen this occur in SU(3), with Gozel et. al. establishing the existence of a finite mass gap $\Delta/J \in (0.017, 0.044)$ in the symmetric SU(3) chain with $p = 3$ [77]. Antiferromagnetic SU(n) spin ladders have also been considered [139–141], as have two-dimensional SU(n) Heisenberg models [142–144].

Furthermore, our predictions about SU(n) chains also serve to challenge the experimental physics community. Over the past decade, cold atom physicists have continued to make advances in optical trapping technology, with the most recent publication being [66]. Our predicted finite energy gaps for particular representations should now be observable in such set-ups. For example,

the $p = 3$ representation of SU(3) should exhibit a nondegenerate ground state with a finite gap, and the $p = 2$ representation of SU(4) should exhibit a gap above two-fold degenerate ground states. Since $p > 1$ in these chains, one must devise a way to achieve multiple sets of n particle species at each site, either by trapping multiple atoms or by making use of an additional orbital degeneracy, such as the nearly degenerate clock states of alkaline Earth atoms. Of course, such experiments present a much greater challenge than those that originally measured the finite gap of the spin-1 chain, since in that case an actual quasi-one dimensional material was readily available.

Finally, a third research direction stemming from this thesis has to do with flag manifold sigma models in general. While these models have always been of interest to mathematical physicists, they have recently garnered more attention in the theoretical physics community thanks to their applicability to SU(n) spin chains. In particular, in [145] Bykov has since investigated integrable flag manifold sigma models, which generalize the older notions of integrability in the $\mathbb{CP}^1$ sigma model put forth by the Zamolodchikov brothers, among others. In fact, we will soon publish with Bykov and Affleck an extensive review article on flag manifold sigma models, which should further encourage cross-disciplinary research efforts from mathematicians and physicists alike [6]. We believe that this review, combined with our thesis, will inspire additional research efforts into the rich structure of flag manifolds themselves, ultimately bringing new insights into the SU(n) chains that we have focused on here.

Bibliography

[1] Miklós Lajkó, Kyle Wamer, Frédéric Mila, and Ian Affleck. Generalization of the Haldane conjecture to SU(3) chains. *Nuclear Physics B*, 924:508 – 577, 2017.

[2] Kyle Wamer, Francisco H. Kim, Miklós Lajkó, Frédéric Mila, and Ian Affleck. Self-conjugate representation SU(3) chains. *Phys. Rev. B*, 100:115114, 2019.

[3] Kyle Wamer, Miklós Lajkó, Frédéric Mila, and Ian Affleck. Generalization of the Haldane conjecture to SU(n) chains. *Nuclear Physics B*, 952:114932, 2020.

[4] Kyle Wamer and Ian Affleck. Mass generation by fractional instantons in SU(n) chains. *Phys. Rev. B.*, 101:245143, 2020.

[5] Kyle Wamer and Ian Affleck. Flag manifold sigma models from SU(n) chains. *Nuclear Physics B*, 959:115156, 2020.

[6] Ian Affleck, Dmitri Bykov, and Kyle Wamer. Flag manifold sigma models: spin chains and integrable theories. *arXiv*, 2101.11638, 2021.

[7] Ian Affleck. Field Theory Methods and Quantum Critical Phenomena. In *Les Houches Summer School in Theoretical Physics: Fields, Strings, Critical Phenomena Les Houches, France, June 28-August 5, 1988*, pages 0563–640, 1988.

[8] Sidney Coleman. There are no goldstone bosons in two dimensions. *Communications in Mathematical Physics*, 31(4):259–264, 1973.

[9] N. D. Mermin and H. Wagner. Absence of ferromagnetism or antiferromagnetism in one- or two-dimensional isotropic heisenberg models. *Phys. Rev. Lett.*, 17:1133–1136, Nov 1966.

[10] P. C. Hohenberg. Existence of long-range order in one and two dimensions. *Phys. Rev.*, 158:383–386, Jun 1967.

[11] W. Heisenberg. Zur theorie des ferromagnetismus. *Zeitschrift für Physik*, 49(9):619–636, 1928.

[12] H. Bethe. Zur theorie der metalle. *Zeitschrift für Physik*, 71(3):205–226, 1931.

[13] F.D.M. Haldane. Continuum dynamics of the 1-d heisenberg antiferromagnet: Identification with the O(3) nonlinear sigma model. *Physics Letters A*, 93(9):464 – 468, 1983.

[14] F. D. M. Haldane. Nonlinear field theory of large-spin heisenberg antiferromagnets: Semi-classically quantized solitons of the one-dimensional easy-axis néel state. *Phys. Rev. Lett.*, 50:1153–1156, Apr 1983.

[15] F. D. M. Haldane. Ground state properties of antiferromagnetic chains with unrestricted spin: Integer spin chains as realisations of the o(3) non-linear sigma model, 2016.

[16] F. Duncan M. Haldane. Nobel lecture: Topological quantum matter. *Rev. Mod. Phys.*, 89:040502, Oct 2017.

[17] Jacques des Cloizeaux and J. J. Pearson. Spin-wave spectrum of the antiferromagnetic linear chain. *Phys. Rev.*, 128:2131–2135, Dec 1962.

[18] Shmuel Elitzur. The applicability of perturbation expansion to two-dimensional goldstone systems. *Nuclear Physics B*, 212(3):501 – 518, 1983.

[19] Alexander B Zamolodchikov and Alexey B Zamolodchikov. Factorized s-matrices in two dimensions as the exact solutions of certain relativistic quantum field theory models. *Annals of Physics*, 120(2):253 – 291, 1979.

[20] G. Bhanot, E. Rabinovici, N. Seiberg, and P. Woit. Lattice θ vacua. *Nuclear Physics B*, 230(3):291 – 298, 1984.

[21] Gyan Bhanot, Roger Dashen, Nathan Seiberg, and Herbert Levine. Scaling and θ dependence in the O(3) σ model. *Phys. Rev. Lett.*, 53:519–522, Aug 1984.

[22] W. J. L Buyers, R. M. Morra, R. L. Armstrong, M. J. Hogan, P. Gerlach, and K. Hirakawa. Experimental evidence for the haldane gap in a spin-1 nearly isotropic, antiferromagnetic chain. *Phys. Rev. Lett.*, 56:371–374, Jan 1986.

[23] Jean-Pierre Renard, Louis-Pierre Regnault, and Michel Verdaguer. *Haldane Quantum Spin Chains*, pages 49–93. Wiley-VCH Verlag GmbH & Co. KGaA, 2003. and references therein.

[24] R. Botet, R. Jullien, and M. Kolb. Finite-size-scaling study of the spin-1 heisenberg-ising chain with uniaxial anisotropy. *Phys. Rev. B*, 28:3914–3921, Oct 1983.

[25] M. P. Nightingale and H. W. J. Blöte. Gap of the linear spin-1 heisenberg antiferromagnet: A monte carlo calculation. *Phys. Rev. B*, 33:659–661, Jan 1986.

[26] T Kennedy. Exact diagonalisations of open spin-1 chains. *Journal of Physics: Condensed Matter*, 2(26):5737, 1990.

[27] Steven R. White and David A. Huse. Numerical renormalization-group study of low-lying eigenstates of the antiferromagnetic S=1 heisenberg chain. *Phys. Rev. B*, 48:3844–3852, Aug 1993.

[28] Ulrich Schollwöck, Olivier Golinelli, and Thierry Jolicœur. $S = 2$ antiferromagnetic quantum spin chain. *Phys. Rev. B*, 54:4038–4051, Aug 1996.

[29] Synge Todo and Kiyoshi Kato. Cluster algorithms for general- S quantum spin systems. *Phys. Rev. Lett.*, 87:047203, Jul 2001.

[30] Synge Todo, Haruhiko Matsuo, and Hideyuki Shitara. Parallel loop cluster quantum monte carlo simulation of quantum magnets based on global union-find graph algorithm. *Computer Physics Communications*, 239:84 – 93, 2019.

[31] W. Bietenholz, A. Pochinsky, and U. J. Wiese. Meron-cluster simulation of the θ vacuum in the 2d o(3) model. *Phys. Rev. Lett.*, 75:4524–4527, Dec 1995.

[32] V. Azcoiti, G. Di Carlo, A. Galante, and V. Laliena. θ-vacuum systems via real action simulations. *Physics Letters B*, 563(1–2):117 – 122, 2003.

[33] B. Allés and A. Papa. Mass gap in the 2d O(3) nonlinear sigma model with a $\theta = \pi$ term. *Phys. Rev. D*, 77:056008, Mar 2008.

[34] Vicente Azcoiti, Giuseppe Di Carlo, Eduardo Follana, and Matteo Giordano. Critical behavior of the $O(3)$ nonlinear sigma model with topological term at $\theta=\pi$ from numerical simulations. *Phys. Rev. D*, 86:096009, Nov 2012.

[35] P. de Forcrand, M. Pepe, and U. J. Wiese. Walking near a conformal fixed point: The 2-d $O(3)$ model at $\theta\approx\pi$ as a test case. *Phys. Rev. D*, 86:075006, Oct 2012.

[36] B. Allés, M. Giordano, and A. Papa. Behavior near $\theta = \pi$ of the mass gap in the two-dimensional O(3) nonlinear sigma model. *Phys. Rev. B*, 90:184421, Nov 2014.

[37] A.B. Zamolodchikov and Al.B. Zamolodchikov. Massless factorized scattering and sigma models with topological terms. *Nuclear Physics B*, 379(3):602 – 623, 1992.

[38] Steven R. White. Density matrix formulation for quantum renormalization groups. *Phys. Rev. Lett.*, 69:2863–2866, Nov 1992.

[39] Steven R. White. Density-matrix algorithms for quantum renormalization groups. *Phys. Rev. B*, 48:10345–10356, Oct 1993.

[40] Stellan Östlund and Stefan Rommer. Thermodynamic limit of density matrix renormalization. *Phys. Rev. Lett.*, 75:3537–3540, Nov 1995.

[41] Guifré Vidal. Efficient classical simulation of slightly entangled quantum computations. *Phys. Rev. Lett.*, 91:147902, Oct 2003.

[42] J. Jordan, R. Orús, G. Vidal, F. Verstraete, and J. I. Cirac. Classical simulation of infinite-size quantum lattice systems in two spatial dimensions. *Phys. Rev. Lett.*, 101:250602, Dec 2008.

[43] G. Vidal. Class of quantum many-body states that can be efficiently simulated. *Phys. Rev. Lett.*, 101:110501, Sep 2008.

[44] Marcel den Nijs and Koos Rommelse. Preroughening transitions in crystal surfaces and valence-bond phases in quantum spin chains. *Phys. Rev. B*, 40:4709–4734, Sep 1989.

[45] M. Hagiwara, K. Katsumata, Ian Affleck, B. I. Halperin, and J. P. Renard. Observation of S=1/2 degrees of freedom in an s=1 linear-chain heisenberg antiferromagnet. *Phys. Rev. Lett.*, 65:3181–3184, Dec 1990.

[46] Frank Pollmann, Ari M. Turner, Erez Berg, and Masaki Oshikawa. Entanglement spectrum of a topological phase in one dimension. *Phys. Rev. B*, 81:064439, Feb 2010.

[47] Frank Pollmann, Erez Berg, Ari M. Turner, and Masaki Oshikawa. Symmetry protection of topological phases in one-dimensional quantum spin systems. *Phys. Rev. B*, 85:075125, Feb 2012.

[48] Ian Affleck. Exact critical exponents for quantum spin chains, non-linear σ-models at $\theta = \pi$ and the quantum hall effect. *Nuclear Physics B*, 265(3):409–447, 1986.

[49] Ian Affleck. The Quantum Hall Effect, σ Models at $\theta = \pi$ and Quantum Spin Chains. *Nucl. Phys. B*, 257:397–406, 1985.

[50] Ian Affleck. Critical behaviour of SU(n) quantum chains and topological non-linear -models. *Nuclear Physics B*, 305(4):582 – 596, 1988.

[51] N. Read and Subir Sachdev. Spin-peierls, valence-bond solid, and néel ground states of low-dimensional quantum antiferromagnets. *Phys. Rev. B*, 42:4568–4589, Sep 1990.

[52] Herbert Levine, Stephen B. Libby, and Adrianus M. M. Pruisken. Electron delocalization by a magnetic field in two dimensions. *Phys. Rev. Lett.*, 51:1915–1918, Nov 1983.

[53] Ferdinand Evers and Alexander D. Mirlin. Anderson transitions. *Rev. Mod. Phys.*, 80:1355–1417, Oct 2008.

[54] Congjun Wu, Jiang-ping Hu, and Shou-cheng Zhang. Exact SO(5) symmetry in the spin-3/2 fermionic system. *Phys. Rev. Lett.*, 91:186402, Oct 2003.

[55] Carsten Honerkamp and Walter Hofstetter. Ultracold fermions and the SU(N) hubbard model. *Phys. Rev. Lett.*, 92:170403, Apr 2004.

[56] M A Cazalilla, A F Ho, and M Ueda. Ultracold gases of ytterbium: ferromagnetism and mott states in an SU(6) fermi system. *New Journal of Physics*, 11(10):103033, oct 2009.

[57] A. V. Gorshkov, M. Hermele, V. Gurarie, C. Xu, P. S. Julienne, J. Ye, P. Zoller, E. Demler, M. D. Lukin, and A. M. Rey. Two-orbital SU(N) magnetism with ultracold alkaline-earth atoms. *Nature Physics*, 6:289–295, April 2010.

[58] Samuel Bieri, Maksym Serbyn, T. Senthil, and Patrick A. Lee. Paired chiral spin liquid with a fermi surface in $S = 1$ model on the triangular lattice. *Phys. Rev. B*, 86:224409, Dec 2012.

[59] F. Scazza, C. Hofrichter, M. Höfer, P. C. de Groot, I. Bloch, and S. Fölling. Observation of two-orbital spin-exchange interactions with ultracold SU(N)-symmetric fermions. *Nature Physics*, 10:779–784, Oct 2014.

[60] Shintaro Taie, Rekishu Yamazaki, Seiji Sugawa, and Yoshiro Takahashi. An SU(6) Mott insulator of an atomic Fermi gas realized by large-spin Pomeranchuk cooling. *Nature Physics*, 8(11):825–830, Nov 2012.

[61] H. Nonne, M. Moliner, S. Capponi, P. Lecheminant, and K. Totsuka. Symmetry-protected topological phases of alkaline-earth cold fermionic atoms in one dimension. *EPL (Europhysics Letters)*, 102(3):37008, may 2013.

[62] Guido Pagano, Marco Mancini, Giacomo Cappellini, Pietro Lombardi, Florian Schäfer, Hui Hu, Xia-Ji Liu, Jacopo Catani, Carlo Sias, and Massimo Inguscio. A one-dimensional liquid of fermions with tunable spin. *Nature Physics*, 10(3):198–201, Mar 2014.

[63] X. Zhang, M. Bishof, S. L. Bromley, C. V. Kraus, M. S. Safronova, P. Zoller, A. M. Rey, and J. Ye. Spectroscopic observation of SU(N)-symmetric interactions in sr orbital magnetism. *Science*, 345(6203):1467–1473, 2014.

[64] Miguel A Cazalilla and Ana Maria Rey. Ultracold fermi gases with emergent SU(n) symmetry. *Reports on Progress in Physics*, 77(12):124401, nov 2014.

[65] Christian Hofrichter, Luis Riegger, Francesco Scazza, Moritz Höfer, Diogo Rio Fernandes, Immanuel Bloch, and Simon Fölling. Direct probing of the mott crossover in the SU(N) fermi-hubbard model. *Phys. Rev. X*, 6:021030, Jun 2016.

[66] Hideki Ozawa, Shintaro Taie, Yosuke Takasu, and Yoshiro Takahashi. Antiferromagnetic spin correlation of SU($\mathcal{N}$) fermi gas in an optical superlattice. *Phys. Rev. Lett.*, 121:225303, Nov 2018.

[67] Martin Greiter and Stephan Rachel. Valence bond solids for SU(n) spin chains: Exact models, spinon confinement, and the haldane gap. *Phys. Rev. B*, 75:184441, May 2007.

[68] M. Führinger, S. Rachel, R. Thomale, M. Greiter, and P. Schmitteckert. Dmrg studies of critical SU(N) spin chains. *Annalen der Physik*, 17(12):922–936, 2008.

[69] Hosho Katsura, Takaaki Hirano, and Vladimir E Korepin. Entanglement in SU(n) valence-bond-solid state. *Journal of Physics A: Mathematical and Theoretical*, 41(13):135304, mar 2008.

[70] Stephan Rachel, Ronny Thomale, Max Führinger, Peter Schmitteckert, and Martin Greiter. Spinon confinement and the haldane gap in SU(n) spin chains. *Phys. Rev. B*, 80:180420, Nov 2009.

[71] Dmitri Bykov. Haldane limits via lagrangian embeddings. *Nuclear Physics B*, 855(1):100 – 127, 2012.

[72] Dmitri Bykov. The geometry of antiferromagnetic spin chains. *Communications in Mathematical Physics*, 322(3):807–834, 2013.

[73] Kasper Duivenvoorden and Thomas Quella. Topological phases of spin chains. *Phys. Rev. B.*, 87(12):125145, Mar 2013.

[74] Takahiro Morimoto, Hiroshi Ueda, Tsutomu Momoi, and Akira Furusaki. $\mathbb{Z}_3$ symmetry-protected topological phases in the SU(3) AKLT model. *Phys. Rev. B*, 90:235111, Dec 2014.

[75] Abhishek Roy and Thomas Quella. Chiral haldane phases of SU(N) quantum spin chains. *Physical Review B*, 97(15):155148, 2018.

[76] Samuel Gozel, Didier Poilblanc, Ian Affleck, and Frédéric Mila. Novel families of SU(N) AKLT states with arbitrary self-conjugate edge states. *Nuclear Physics B*, page 114663, 2019.

[77] Samuel Gozel, Pierre Nataf, and Frédéric Mila. Haldane gap of the three-box symmetric SU(3) chain. *Phys. Rev. Lett.*, 125:057202, Jul 2020.

[78] Yuya Tanizaki and Tin Sulejmanpasic. Anomaly and global inconsistency matching: θ-angles, SU(3)/$U(1)^2$ nonlinear sigma model, SU(3) chains and its generalizations. *Phys. Rev. B.*, 98(11):115126, 2018.

[79] Kantaro Ohmori, Nathan Seiberg, and Shu-Heng Shao. Sigma models on flags. *SciPost Physics*, 6(2):017, 2019.

[80] Elliott Lieb, Theodore Schultz, and Daniel Mattis. Two soluble models of an antiferromagnetic chain. *Annals of Physics*, 16(3):407 – 466, 1961.

[81] Ian Affleck and Elliott H. Lieb. A proof of part of haldane's conjecture on spin chains. *Letters in Mathematical Physics*, 12(1):57–69, 1986.

[82] Ian Affleck, Tom Kennedy, ElliottH. Lieb, and Hal Tasaki. Valence bond ground states in isotropic quantum antiferromagnets. *Communications in Mathematical Physics*, 115:477–528, 1988.

[83] S. Capponi, P. Lecheminant, and K. Totsuka. Phases of one-dimensional SU(N) cold atomic Fermi gases-From molecular Luttinger liquids to topological phases. *Annals of Physics*, 367:50–95, Apr 2016.

[84] Bill Sutherland. Model for a multicomponent quantum system. *Phys. Rev. B*, 12:3795–3805, Nov 1975.

[85] A.M. Tsvelick and P.B. Wiegmann. Exact results in the theory of magnetic alloys. *Advances in Physics*, 32(4):453–713, 1983.

[86] Ian Affleck and F. D. M. Haldane. Critical theory of quantum spin chains. *Phys. Rev. B*, 36:5291–5300, Oct 1987.

[87] Natan Andrei and Henrik Johannesson. Higher dimensional representations of the SU(N) heisenberg model. *Physics Letters A*, 104(6):370 – 374, 1984.

[88] H. Johannesson. The integrable SU(N) heisenberg model at finite temperature. *Physics Letters A*, 116(3):133 – 138, 1986.

[89] Henrik Johannesson. The structure of low-lying excitations in a new integrable quantum chain model. *Nuclear Physics B*, 270:235 – 272, 1986.

[90] V. L. Berezinskiĭ. Destruction of Long-range Order in One-dimensional and Two-dimensional Systems having a Continuous Symmetry Group I. Classical Systems. *Soviet Journal of Experimental and Theoretical Physics*, 32:493, January 1971.

[91] J. M. Kosterlitz and D. J. Thouless. Ordering, metastability and phase transitions in two-dimensional systems. *Journal of Physics C Solid State Physics*, 6(7):1181–1203, April 1973.

[92] Samuel Gozel, Frédéric Mila, and Ian Affleck. Asymptotic freedom and large spin antiferromagnetic chains. *Phys. Rev. Lett.*, 123:037202, Jul 2019.

[93] T. Holstein and H. Primakoff. Field dependence of the intrinsic domain magnetization of a ferromagnet. *Phys. Rev.*, 58:1098–1113, Dec 1940.

[94] J. Goldstone. Field theories with Superconductor solutions. *Il Nuovo Cimento*, 19(1):154–164, January 1961.

[95] Haruki Watanabe and Hitoshi Murayama. Unified description of nambu-goldstone bosons without lorentz invariance. *Physical Review Letters*, 108(25), Jun 2012.

[96] Haruki Watanabe and Hitoshi Murayama. Effective Lagrangian for Nonrelativistic Systems. *Phys. Rev. X*, 4(3):031057, 2014.

[97] Louk Rademaker, Aron Beekman, and Jasper van Wezel. Stability and absence of a tower of states in ferrimagnets. *Phys. Rev. Research*, 2:013304, Mar 2020.

[98] A. Altland and B.D. Simons. *Condensed Matter Field Theory*. Cambridge books online. Cambridge University Press, 2010.

[99] Manu Mathur and Indrakshi Raychowdhury. SU(N) coherent states and irreducible schwinger bosons. *Journal of Physics A: Mathematical and Theoretical*, 44(3):035203, dec 2010.

[100] Manu Mathur, Indrakshi Raychowdhury, and Ramesh Anishetty. SU(N) irreducible schwinger bosons. *Journal of Mathematical Physics*, 51(9):093504, 2010.

[101] J. Wess and B. Zumino. Consequences of anomalous ward identities. *Physics Letters B*, 37(1):95–97, November 1971.

[102] Edward Witten. Global aspects of current algebra. *Nuclear Physics B*, 223(2):422–432, August 1983.

[103] S. P. Novikov. The Hamiltonian formalism and a many-valued analogue of Morse theory. *Russian Mathematical Surveys*, 37(5):1–56, October 1982.

[104] Nathan Seiberg. Topology in strong coupling. *Phys. Rev. Lett.*, 53:637–640, Aug 1984.

[105] Jan C. Plefka and Stuart Samuel. Strong-coupling analysis of the lattice CP^{N-1} models in the presence of a θ term. *Phys. Rev. D*, 55:3966–3973, Apr 1997.

[106] Gerard 't Hooft. Naturalness, chiral symmetry, and spontaneous chiral symmetry breaking. *NATO Sci. Ser. B*, 59:135–157, 1980.

[107] Y. Frishman, A. Schwimmer, T. Banks, and S. Yankielowicz. The axial anomaly and the bound-state spectrum in confining theories. *Nuclear Physics B*, 177(1):157 – 171, 1981.

[108] H. Georgi. *Lie Algebras in Particle Physics: From Isospin to Unified Theories*, volume 54. CRC Press, 1982.

[109] Philippe Corboz, Miklós Lajkó, Andreas M. Läuchli, Karlo Penc, and Frédéric Mila. Spin-orbital quantum liquid on the honeycomb lattice. *Phys. Rev. X*, 2:041013, Nov 2012.

[110] N. Andrei, K. Furuya, and J. H. Lowenstein. Solution of the kondo problem. *Rev. Mod. Phys.*, 55:331–402, Apr 1983.

[111] F C Alcaraz and M J Martins. Conformal anomaly for the exactly integrable SU(N) magnets. *Journal of Physics A: Mathematical and General*, 22(18):L865–L870, sep 1989.

[112] L.A. Takhtajan. The picture of low-lying excitations in the isotropic heisenberg chain of arbitrary spins. *Physics Letters A*, 87(9):479 – 482, 1982.

[113] H.M. Babujian. Exact solution of the one-dimensional isotropic heisenberg chain with arbitrary spins s. *Physics Letters A*, 90(9):479 – 482, 1982.

[114] A. B. Zomolodchikov. "Irreversibility" of the flux of the renormalization group in a 2D field theory. *Soviet Journal of Experimental and Theoretical Physics Letters*, 43:730, June 1986.

[115] P. Lecheminant. Massless renormalization group flow in $SU(N)_k$ perturbed conformal field theory. *Nucl. Phys. B*, 901:510–525, 2015.

[116] Yuan Yao, Chang-Tse Hsieh, and Masaki Oshikawa. Anomaly matching and symmetry-protected critical phases in $SU(N)$ spin systems in $1 + 1$ dimensions. *Phys. Rev. Lett.*, 123:180201, Oct 2019.

[117] P. Fromholz and P. Lecheminant. Symmetry-protected topological phases in the SU(N) heisenberg spin chain: A majorana fermion approach. *Phys. Rev. B*, 102:094410, Sep 2020.

[118] Pierre Nataf and Frédéric Mila. Exact diagonalization of heisenberg SU(N) chains in the fully symmetric and antisymmetric representations. *Phys. Rev. B*, 93:155134, Apr 2016.

[119] Kianna Wan, Pierre Nataf, and Frédéric Mila. Exact diagonalization of SU(N) heisenberg and affleck-kennedy-lieb-tasaki chains using the full su(n) symmetry. *Phys. Rev. B*, 96:115159, Sep 2017.

[120] Pierre Nataf and Frédéric Mila. Density matrix renormalization group simulations of SU(N) heisenberg chains using standard young tableaus: Fundamental representation and comparison with a finite-size bethe ansatz. *Phys. Rev. B*, 97:134420, Apr 2018.

[121] N. Papanicolaou. Pseudospin approach for planar ferromagnets. *Nuclear Physics B*, 240(3):281 – 311, 1984.

[122] N. Papanicolaou. Unusual phases in quantum spin-1 systems. *Nuclear Physics B*, 305(3):367 – 395, 1988.

[123] Manu Mathur and Diptiman Sen. Coherent states for SU(3). *Journal of Mathematical Physics*, 42(9):4181–4196, 2001.

[124] Kyle Wamer. Renormalization group analysis of phase transitiions in the two dimensional Majorana-Hubbard model. Master's thesis, Univeristy of British Columbia, 2018.

[125] Kenneth G. Wilson. The renormalization group: Critical phenomena and the kondo problem. *Rev. Mod. Phys.*, 47:773–840, Oct 1975.

[126] Alexander M. Polyakov. Interaction of Goldstone Particles in Two-Dimensions. Applications to Ferromagnets and Massive Yang-Mills Fields. *Phys. Lett.*, B59:79–81, 1975.

[127] B. Berg and M. Lüscher. Definition and statistical distributions of a topological number in the lattice O(3) σ-model. *Nuclear Physics B*, 190(2):412 – 424, 1981.

[128] I Affleck. Exact results on the dimerisation transition in SU(n) antiferromagnetic chains. *Journal of Physics: Condensed Matter*, 2(2):405–415, jan 1990.

[129] Erik Schwartz Sørensen and A. Peter Young. Correlation length of the biquadratic spin-1 chain. *Phys. Rev. B*, 42:754–759, Jul 1990.

[130] Michael E. Peskin and Daniel V. Schroeder. *An Introduction to quantum field theory*. Addison-Wesley, Reading, USA, 1995.

[131] Xie Chen, Zheng-Cheng Gu, and Xiao-Gang Wen. Classification of gapped symmetric phases in one-dimensional spin systems. *Phys. Rev. B*, 83:035107, Jan 2011.

[132] Davide Gaiotto, Anton Kapustin, Zohar Komargodski, and Nathan Seiberg. Theta, time reversal and temperature. *Journal of High Energy Physics*, 2017(5):91, 2017.

[133] Sung-Sik Lee. Emergence of supersymmetry at a critical point of a lattice model. *Physical Review B*, 76(7):075103, 2007.

[134] Tarun Grover, DN Sheng, and Ashvin Vishwanath. Emergent space-time supersymmetry at the boundary of a topological phase. *Science*, 344(6181):280–283, 2014.

[135] Nikolai Zerf, Chien-Hung Lin, and Joseph Maciejko. Superconducting quantum criticality of topological surface states at three loops. *Phys. Rev. B*, 94:205106, Nov 2016.

[136] Joshua P Ellis. Tikz-feynman: Feynman diagrams with tikz. *Computer Physics Communications*, 210:103–123, 2017.

[137] Ian Affleck. Mass Generation by Merons in Quantum Spin Chains and the O(3) σ Model. *Phys. Rev. Lett.*, 56:408, 1986.

[138] Tomáš Brauner. Spontaneous symmetry breaking and nambugoldstone bosons in quantum many-body systems. *Symmetry*, 2(2):609657, Apr 2010.

[139] A. Weichselbaum, S. Capponi, P. Lecheminant, A. M. Tsvelik, and A. M. Läuchli. Unified phase diagram of antiferromagnetic SU(N) spin ladders. *Phys. Rev. B*, 98:085104, Aug 2018.

[140] S. Capponi, P. Fromholz, P. Lecheminant, and K. Totsuka. Symmetry-protected topological phases in a two-leg SU(N) spin ladder with unequal spins. *Phys. Rev. B*, 101:195121, May 2020.

[141] P. Lecheminant and A. M. Tsvelik. Two-leg SU($2n$) spin ladder: A low-energy effective field theory approach. *Phys. Rev. B*, 91:174407, May 2015.

[142] K. S. D. Beach, Fabien Alet, Matthieu Mambrini, and Sylvain Capponi. SU(N) heisenberg model on the square lattice: A continuous-N quantum monte carlo study. *Phys. Rev. B*, 80:184401, Nov 2009.

[143] Dietrich Roscher, Nico Gneist, Michael M. Scherer, Simon Trebst, and Sebastian Diehl. Cluster functional renormalization group and absence of a bilinear spin liquid in the J_1-J_2 heisenberg model. *Phys. Rev. B*, 100:125130, Sep 2019.

[144] Philippe Corboz, Karlo Penc, Frédéric Mila, and Andreas M. Läuchli. Simplex solids in SU(N) heisenberg models on the kagome and checkerboard lattices. *Phys. Rev. B*, 86:041106, Jul 2012.

[145] Dmitri Bykov. Complex structures and zero-curvature equations for σ-models. *Physics Letters B*, 760:341–344, 2016.

Appendix A

Proof of $\mathrm{tr}[U\partial U^\dagger] = 0$

In this appendix, we prove the identity $\mathrm{tr}[U\partial U^\dagger] = 0$ for an arbitrary unitary matrix U. We will make use of this identity frequently throughout this thesis. To begin, we write an arbitrary unitary matrix U as

$$U_{\alpha\beta} = \varphi_\beta^\alpha, \tag{A.1}$$

where the φ^α are the rows of U, and are orthonormal complex vectors: $\varphi^{*,\alpha} \cdot \varphi^\beta = \delta_{\alpha\beta}$. We can express the nth row-vector, φ^n, in terms of first $n-1$ rows using the antisymmetric unit tensor, as:

$$\varphi_{\alpha_n}^{*,n} = \epsilon_{\alpha_1,\alpha_2...\alpha_n}\varphi_{\alpha_1}^1\varphi_{\alpha_2}^2\cdots\varphi_{\alpha_{n-1}}^{n-1}. \tag{A.2}$$

This follows because

$$\varphi^{*,n} \cdot \varphi^\beta = \epsilon_{\alpha_1,\alpha_2\cdots\alpha_n}\varphi_{\alpha_1}^1\varphi_{\alpha_2}^2\cdots\varphi_{\alpha_{n-1}}^{n-1}\varphi_{\alpha_n}^\beta \tag{A.3}$$

and

$$\epsilon_{\alpha_1\alpha_2\cdots\alpha_n}\varphi_{\alpha_\beta}^\beta\varphi_{\alpha_n}^\beta = 0. \tag{A.4}$$

for $\beta = 1, 2, 3, \ldots, n-1$. Now, we use the identity

$$\epsilon_{\alpha_1\alpha_2,...\alpha_n}\epsilon_{\beta_1\beta_2...\beta_{n-1}\alpha_n} = \sum_{\{a_1,a_2,...a_{n-1}\}} \mathrm{sgn}\{a_1, a_2, \ldots a_{a_{n-1}}\}\delta_{\alpha_1\beta_{a_1}}\delta_{\alpha_2\beta_{a_2}}\cdots\delta_{\alpha_{n-1}\beta_{a_{n-1}}}. \tag{A.5}$$

Here the sum is over all permutations of $a_1, a_2, \ldots a_{n-1}$. Now, orthogonality and (A.5) imply

$$|\varphi^n|^2 = 1, \tag{A.6}$$

and

$$\varphi^n \cdot \partial\varphi^{*,n} = \epsilon_{\alpha_1\alpha_2\cdots\alpha_n}\varphi_{\alpha_1}^{*,1}\varphi_{\alpha_2}^{*,2}\cdots\varphi_{\alpha_{n-1}}^{*,n-1}\epsilon_{\beta_1\beta_2\cdots\beta_{n-1}\alpha_n}((\partial\varphi_{\beta_1}^1)\varphi_{\beta_2}^2\cdots\varphi_{\beta_{n-1}}^{n-1} + \cdots). \tag{A.7}$$

Here the $\cdots$ is a sum over derivatives of each factor. Now we use

$$\epsilon_{\alpha_1\alpha_2...\alpha_n}\varphi_{\alpha_1}^{*,1}\varphi_{\alpha_2}^{*,2}\cdots\varphi_{\alpha_{n-1}}^{*,n-1}\epsilon_{\beta_1\beta_2\cdots\beta_{n-1}\alpha_n}(\partial\varphi_{\beta_1}^1)\varphi_{\beta_2}^2\cdots\varphi_{\beta_{n-1}}^{n-1} = \varphi^{*,1} \cdot \partial\varphi^1, \tag{A.8}$$

which follows from orthogonality and (A.5). So

$$\varphi^n \cdot \partial\varphi^{*,n} = \sum_{\alpha=1}^{n-1}\varphi^{*,\alpha} \cdot \partial\varphi^\alpha, \tag{A.9}$$

which implies,

$$\sum_{\alpha=1}^{n}\partial\varphi^\alpha \cdot \varphi^{*,\alpha} = \mathrm{tr}[\partial U U^\dagger] = 0. \tag{A.10}$$

Appendix B

Low Energy Expansion of the Symmetric SU(n) Hamiltonian

In this appendix, we provide some details from the derivation of the low energy Hamiltonian of the SU(n) chain in the rank-p symmetric representation. These results are used both in Chapter 4 for the SU(3) chain, and more generally in Chapter 5 for the SU(n) chain. In particular, we simplify the following Heisenberg interaction term

$$\mathrm{tr}[S(j_\gamma)S(j_\eta)], \tag{B.1}$$

using (4.23). We write

$$\mathrm{tr}[S(j_\gamma)S(j_\eta)] = \sum_{i=1}^{2} X^i(\gamma, \eta) + \sum_{i=3}^{4}(X^i(\gamma, \eta) + X^i(\eta, \gamma)) + O(p^{-2}), \tag{B.2}$$

with

$$X^1(\gamma, \eta) := p^2\mathrm{tr}[U^\dagger(j_\gamma)\Lambda_\gamma U(j_\gamma)U^\dagger(j_\eta)\Lambda_\eta U(j_\eta)] \tag{B.3}$$

$$X^2(\gamma, \eta) := \mathrm{tr}[U^\dagger(j_\gamma)\{L(j_\gamma), \Lambda_\gamma\}U(j_\gamma)U^\dagger(j_\eta)\{L(j_\eta), \Lambda_\eta\}U(j_\eta)] \tag{B.4}$$

$$X^3(\gamma, \eta) := p\,\mathrm{tr}[U^\dagger(j_\gamma)\{L(j_\gamma), \Lambda_\gamma\}U(j_\gamma)U^\dagger(j_\eta)\Lambda_\eta U(j_\eta)] \tag{B.5}$$

$$X^4(\gamma, \eta) := \mathrm{tr}[U^\dagger(j_\gamma)\mathcal{L}(j_\gamma)U(j_\gamma)U^\dagger(j_\eta)\Lambda_\eta U(j_\eta)] \tag{B.6}$$

Since the matrices $U, L, \mathcal{L}$ are evaluated at different sites, we Taylor expand. For example,

$$U(j_\gamma) = U(nj + (\gamma - 1)) = U(j_\eta) + (\eta - \gamma)\partial_x U(j_\eta) + \frac{1}{2}(\eta - \gamma)^2\partial_x^2 U(j_\eta) + \cdots. \tag{B.7}$$

We assume the derivative is uniform, $\partial_x U(j_\eta) = \partial_x U(j'_\lambda)$, and consider each of the above terms separately. Since L characterizes a fluctuation, we treat it as the same order as ∂U. Finally, we suppress the argument j_γ of each matrix throughout. Then:

- Term 1:

$$X^1(\gamma, \eta) \approx p^2\mathrm{tr}[\Lambda_\gamma\Lambda_\eta + (\eta - \gamma)^2(U\partial_x U^\dagger\Lambda_\gamma\partial_x UU^\dagger\Lambda_\eta - \Lambda_\gamma\Lambda_\eta\partial_x U\partial_x U^\dagger)]. \tag{B.8}$$

Since $\Lambda_\gamma\Lambda_\eta = 0$ for $\gamma \neq \eta$, this simplifies to

$$X^1(\gamma, \eta) \approx p^2(\eta - \gamma)^2\mathrm{tr}[U\partial_x U^\dagger\Lambda_\gamma\partial_x UU^\dagger\Lambda_\eta]. \tag{B.9}$$

- Term 3:

$$X^3(\gamma, \eta) \approx p\mathrm{tr}[\{L, \Lambda_\eta\}\Lambda_\gamma] + (\eta - \gamma)p\mathrm{tr}[\{L, \Lambda_\eta\}U\partial_x U^\dagger \Lambda_\gamma] + (\eta - \gamma)\mathrm{tr}[\{L, \Lambda_\eta\}\Lambda_\gamma \partial_x U U^\dagger] \quad \text{(B.10)}$$

Since the first term is a product of a diagonal and an off-diagonal matrix, its trace vanishes. What remains is a commutator:

$$X^3(\gamma, \eta) = (\eta - \gamma)p\mathrm{tr}\left[[\{L, \Lambda_\eta\}, \Lambda_\gamma]\partial_x U U^\dagger\right], \quad \text{(B.11)}$$

which simplifies to

$$X^3(\gamma, \eta) = (\eta - \gamma)p\left(L_{\gamma\eta}[U\partial_x U^\dagger]_{\eta\gamma} + L_{\eta\gamma}[\partial_x U U^\dagger]_{\gamma\eta}\right). \quad \text{(B.12)}$$

Note that $X^3(\gamma, \eta) = X^3(\eta, \gamma)$.

- Term 4: Since $\mathcal{L}$ contains two powers of L, we only have to expand U to zeroth order. We find

$$X^4(\gamma, \eta) = |L_{\gamma\eta}|^2 = X^4(\eta, \gamma). \quad \text{(B.13)}$$

- Term 2: A similar calculation shows that

$$X^2(\gamma, \eta) = 2|L_{\gamma\eta}|^2 = X^2(\eta, \gamma). \quad \text{(B.14)}$$

Finally, combining the results of these five calculations, we find

$$\mathrm{tr}[S(j_\gamma)S(j_\eta)] = p^2(\eta - \gamma)^2 \mathrm{tr}[U\partial_x U^\dagger \Lambda_\gamma \partial_x U U^\dagger \Lambda_\eta] \quad \text{(B.15)}$$

$$+ 2(\eta - \gamma)p\left(L_{\eta\gamma}[\partial_x U U^\dagger]_{\gamma\eta} + L_{\gamma\eta}[U\partial_x U^\dagger]_{\eta\gamma}\right) + 4|L_{\eta\gamma}|^2 + \text{const.}$$

which proves (4.27).

Appendix C

Factorization of SU(*n*) Matrices

In this appendix, we prove a factorization identity for SU(*n*) matrices. Let Greek letters index the diagonal generators of SU(*n*), lowercase Latin letters index the off-diagonal generators of SU(*n*), and uppercase Latin letters index the full set of generators. That is,

$$\sum_A T_A = \sum_a T_a + \sum_\gamma T_\gamma. \tag{C.1}$$

Then, given $U = e^{i\omega_A T_A} \in \mathrm{SU}(n)$, we may factorize it as follows:

$$U = e^{i\omega_\gamma T_\gamma} e^{i\omega_a T_a}. \tag{C.2}$$

We will prove this identity to third order in the ω_γ and ω_a, but mention how the proof extends to every order in perturbation theory. Using the Baker-Campbell-Hausdorff formula,

$$\log(e^X e^Y) = X + Y + \frac{1}{2}[X, Y] + \frac{1}{12}\left([X, [X, Y]] - [Y, [X, Y]]\right) + \cdots, \tag{C.3}$$

we have

$$\log e^{i\omega_\gamma T_\gamma} e^{i\omega_a T_a} = i\omega_A T_A - \frac{1}{2}\omega_\gamma\omega_a[T_\gamma, T_a] - \frac{i}{12}\left(\omega_\gamma\omega_\beta\omega_a[T_\gamma, [T_\beta, T_a]] - \omega_\gamma\omega_a\omega_b[T_a, [T_\gamma, T_b]]\right) \tag{C.4}$$

to order $O(\omega^4)$, which equals

$$= i\left[\omega_a - \omega_\gamma\omega_b f_{\gamma bA} + \frac{1}{3}\left(\omega_\gamma\omega_\beta\omega_b f_{\beta bC} f_{\gamma CA} - \omega_\gamma\omega_d\omega_b f_{\gamma bC} f_{dCA}\right)\right]T_A + O(\omega^4). \tag{C.5}$$

The formula for the higher-order terms occurring in (C.3) and (C.4) are quite complicated, but always involve nested commutators. This important fact allows us to reduce every term in the expansion to one that is linear in the generators, T_A. A term that is $\sim \omega^n$ will involve $n - 1$ nested commutators, leading to a contribution that is proportional to a product of $n - 1$ structure factors f_{abc}, multiplied by a single SU(*n*) generator T_A. Therefore, order-by-order, we may construct a mapping between the ω_A and the ω_a:

$$\omega_A = \omega_a - \omega_\gamma\omega_b f_{\gamma bA} + \frac{1}{3}\left(\omega_\gamma\omega_\beta\omega_b f_{\beta bC} f_{\gamma CA} - \omega_\gamma\omega_d\omega_b f_{\gamma bC} f_{dCA}\right) + O(\omega^4). \tag{C.6}$$

To prove the factorization identity, we must be able to invert this formula. This is done by repeatedly inserting

$$\omega_a = \omega_A + \omega_\gamma \omega_b f_{\gamma b A} - \frac{1}{3}\left(\omega_\gamma \omega_\beta \omega_b f_{\beta b C} f_{\gamma C A} - \omega_\gamma \omega_d \omega_b f_{\gamma b C} f_{d C A}\right) + O(\omega^4). \qquad (C.7)$$

into each of the terms on its right hand side We find:

$$\omega_a = \omega_A + \omega_\gamma \omega_b f_{\gamma b A} + \frac{2}{3}\omega_\gamma \omega_\beta \omega_b f_{\beta b e} f_{\gamma e A} + \frac{1}{3}\omega_\gamma \omega_d \omega_b f_{\gamma b C} f_{d C A} + O(\omega^4). \qquad (C.8)$$

Thus, for any SU(*n*) matrix $U = e^{i\omega_A T_A}$, we may perform this transformation to obtain the factorized form occurring above.

Appendix D

Polyakov's Renormalization of the O(*n*) nonlinear Sigma Model

In this appendix, we review Polyakov's calculation of the beta function for the O(*n*) nonlinear sigma model [126]. In Section D.1, we use Polyakov's original notation. Then in Section D.2, we demonstrate how our calculations can equivalently be done in the SU(2)/U(1) sigma model language.

D.1 Renormalization in the Real-Space Vector Language

In this section, we start with the following Lagrangian

$$\mathcal{L} = \frac{1}{2g}|\partial_\mu \vec{n}|^2.$$ (D.1)

The idea is to construct a 'slow' unit vector $\vec{n}_s$ out of $\vec{n}$'s momentum modes below $b^{-1}\Lambda$, where Λ is a reduced cutoff, and $b \gtrsim 1$. The remaining modes of $\vec{n}$ can then be written in terms of an orthonormal basis $\{\vec{e}_a\}$, orthogonal to $\vec{n}_s$:

$$\vec{n} = \vec{n}_s(1 - \phi^2)^{1/2} + \sum_{i=1}^{n-1} \phi_i \vec{e}_i,$$ (D.2)

where $\phi^2 = \sum_{i=1}^{n-1} \phi_i^2$. The fields ϕ_i consist entirely of 'fast' modes, with momentum lying in the Wilson shell $[b^{-1}\Lambda, \Lambda)$. Integration over the shell is then equivalent to integrating out the fields ϕ_i. Inserting this expansion (D.2) into $\mathcal{L}$ gives (to quadratic order in ϕ_i)

$$2g\mathcal{L} = (\partial_\mu \vec{n}_s)^2(1 - \phi^2) + (\partial_\mu \phi_i)^2 + \phi_i \phi_j \partial_\mu \vec{e}_i \cdot \partial_\mu \vec{e}_j + 2\phi_i \partial_\mu \phi_j \partial_\mu \vec{e}_i \cdot \vec{e}_j - 2\phi_i \partial_\mu^2 \vec{n}_s \cdot \vec{e}_i .$$ (D.3)

A naive argument would claim that the term linear in ϕ_i can be neglected, since $\vec{n}_s$ and $\vec{e}_i$ contain slow modes only. However, their product will generically have modes lying in the Wilson shell; a better argument is presented in Section 4.5.2. Dropping linear terms, we are left to evaluate the Gaussian integral

$$\int \mathcal{D}[\phi] \exp\left(-\frac{1}{2g} \int d^2x \left((\partial_\mu \vec{n}_s)^2(1 - \phi^2) + (\partial_\mu \phi_i)^2 + \phi_i \phi_j \partial_\mu \vec{e}_i \cdot \partial_\mu \vec{e}_j + 2\phi_i \partial_\mu \phi_j \partial_\mu \vec{e}_i \cdot \vec{e}_j\right)\right).$$ (D.4)

Using

$$\int \mathcal{D}[\phi] = \int \prod_{b^{-1}\Lambda < k < \Lambda} \mathcal{D}\phi(k)\mathcal{D}\phi(-k), \tag{D.5}$$

the effective Lagrangian is

$$2g\mathcal{L}_{\text{eff}} = (\partial_\mu \vec{n}_s)^2 + g\,\text{tr}\left[\log\left(\delta_{ij} - G_{ij}\delta_{ij}(\partial_\mu \vec{n}_s)^2 + G_{ij}\partial_\mu \vec{e}_i \cdot \partial_\mu \vec{e}_j + 2\partial_\mu G_{ij}\partial_\mu \vec{e}_i \cdot \vec{e}_j\right)\right], \tag{D.6}$$

where $G_{ij}(x)$ is the Green's function of the fields ϕ_i. Since terms involving more than two derivatives of slow fields are irrelevant, we can expand the trace-logarithm:

$$\text{tr}\left[\log(\delta_{ij} - G_{ij}\delta_{ij}(\partial_\mu \vec{n}_s)^2 + G_{ij}\partial_\mu \vec{e}_i \cdot \partial_\mu \vec{e}_j + 2\partial_\mu G_{ij}\partial_\mu \vec{e}_i \cdot \vec{e}_j)\right] \tag{D.7}$$

$$= -\int d^2x\, G_{ij}(0)\delta_{ij}(\partial_\mu \vec{n}_s)^2 + \int d^2x\, G_{ij}(0)(\partial_\mu \vec{e}_i \cdot \partial_\mu \vec{e}_j) + 2\int d^2x\, \partial_\mu G_{ij}(0)\partial_\mu \vec{e}_i \cdot \vec{e}_j$$

$$-\frac{1}{2}4\int d^2x d^2y\, \partial_\mu G(x-y)[\partial_\mu \vec{e}_i \cdot \vec{e}_j](x),\, \partial_\nu G(y-x)[\partial_\nu \vec{e}_j \cdot \vec{e}_i](y) + \text{irrelevant},$$

where we defined $G(x)$ by $G_{ij}(x) = \delta_{ij}G(x)$.) The third term vanishes since

$$\partial_\mu G(0) = -i\int \frac{d^2k}{(2\pi)^2}\frac{k_\mu}{k^2} = 0. \tag{D.8}$$

Rewriting $G(0) = \int_{b^{-1}\Lambda < k < \Lambda} \frac{d^2k}{(2\pi)^2}\frac{\delta_{ij}}{k^2}$, the expansion in (D.7) reduces to

$$= \int_{b^{-1}\Lambda < k < \Lambda} \frac{d^2k}{(2\pi)^2}\frac{1}{k^2}\int d^2x\left(-(N-1)(\partial_\mu \vec{n}_s)^2 + (\partial_\mu \vec{e}_i \cdot \partial_\mu \vec{e}_i)\right) \tag{D.9}$$

$$-2\int \frac{d^2k d^2q}{(2\pi)^4}\frac{k_\mu}{k^2}\frac{(q+k)_\nu}{(q+k)^2}[\partial_\mu \vec{e}_i \cdot \vec{e}_j](q)[\partial_\nu \vec{e}_j \cdot \vec{e}_i](-q) + \text{irrelevant},$$

where we Fourier transformed the last term, and both $\vec{k}$ and $\vec{k}+\vec{q}$ lie in the Wilson shell $[b^{-1}\Lambda, \Lambda)$. Now we expand

$$\int_{b^{-1}\Lambda < |\vec{q}+\vec{k}| < \Lambda} \frac{(q+k)_\nu}{(q+k)^2} \tag{D.10}$$

in powers of q, and keep the zeroth order term only, since terms with more powers of q will correspond to irrelevant operators:

$$\int \frac{d^2k d^2q}{(2\pi)^4}\frac{k_\mu}{k^2}\frac{(q+k)_\nu}{(q+k)^2} = \int \frac{d^2k d^2q}{(2\pi)^4}\frac{k_\mu k_\nu}{k^4} + \text{irrelevant} = \frac{1}{2}\int \frac{d^2k d^2q}{(2\pi)^4}\frac{1}{k^2} + \text{irrelevant}. \tag{D.11}$$

Inserting this expansion into (D.9), and integrating over k, the effective Lagrangian becomes

$$2g\mathcal{L}_{\text{eff}} = (\partial_\mu n_s)^2 - \frac{g\log b}{\pi}\left[(n-1)(\partial_\mu \vec{n}_s)^2 - \partial_\mu \vec{e}_i \cdot \partial_\mu \vec{e}_i + (\partial_\mu \vec{e}_i \cdot \vec{e}_j)^2\right]. \tag{D.12}$$

162

Finally, we insert a complete set of states to obtain the identity

$$(\partial_\mu \vec{e}_i)^2 = (\partial_\mu \vec{e}_i \cdot \vec{e}_j)^2 + (\partial_\mu \vec{n}_s)^2 \tag{D.13}$$

since $\vec{n}_s \cdot \vec{e}_i = 0$. Thus,

$$\mathcal{L}_{\text{eff}} = \frac{1}{2g}(\partial_\mu \vec{n}_s)^2 \left[1 - g\frac{(n-2)}{2\pi} \log b \right]. \tag{D.14}$$

From this, we conclude

$$\beta(g) = \frac{dg}{d \log b} = \frac{(n-2)}{2\pi} g^2. \tag{D.15}$$

D.2 Renormalization in the Flag Manifold Language

In the previous section, the renormalization calculation relied on an expansion of the field $\vec{n}$ in terms of 'slow' and 'fast' components:

$$\vec{n} = \vec{n}_s(1 - \phi^2)^{1/2} + \sum_{i=1}^{2} \phi_i \vec{e}_i. \tag{D.16}$$

We would like to generalize this notion to matrix field theories, by writing

$$U = U_f U_s \tag{D.17}$$

for $U, U_f, U_s \in \text{SU}(2)$, where U_f contains the fast modes of U, and U_s the slow modes. Rewriting the O(3) nonlinear sigma model in terms of SU(2) matrices,

$$\vec{n} \cdot \vec{\sigma} = U^\dagger \sigma_z U \qquad U \in \text{SU}(2), \tag{D.18}$$

we prove that (D.17) is equivalent to (D.2) in the SU(2) case. We expand the fast matrix as

$$U_f = \mathbb{I} + i\omega_a \sigma_a - \omega_a \omega_b \sigma_a \sigma_b + O(\omega^3), \tag{D.19}$$

and only keep terms up to quadratic order in ω (higher-order terms will correspond to diagrams beyond one loop). Now

$$U^\dagger \sigma_z U = U_s^\dagger \left(\mathbb{I} - i\omega_a T_a - \frac{1}{2}\omega_a \omega_b T_a T_b \right) \sigma_z \left(\mathbb{I} + i\omega_a T_a - \frac{1}{2}\omega_a \omega_b T_a T_b \right) U_s \tag{D.20}$$

$$= U_s^\dagger \sigma_z U_s - \omega_a \omega_b U_s^\dagger \sigma_z T_a T_b U_s + i\omega_a U_s^\dagger [\sigma_z, T_a] U_s - \frac{1}{2}\omega_a \omega_b U_s^\dagger \{T_a T_b, \sigma_z\} U_s \tag{D.21}$$

$$= U_S^\dagger \sigma_z U_s(1 - 2\omega^2) + -2\omega_x U_s^\dagger \sigma_y U_s + 2\omega_y U_s^\dagger \sigma_x U_s. \tag{D.22}$$

Defining

$$\vec{e}_1 = \text{tr}\frac{1}{2}\vec{\sigma} U_s^\dagger \sigma_y U_s, \qquad \vec{e}_2 = \frac{1}{2}\text{tr}\vec{\sigma} U_s^\dagger \sigma_x U_s, \qquad (\phi_1, \phi_2) = (2\omega_y, -2\omega_x), \tag{D.23}$$

163

we find

$$\vec{\sigma} \cdot \vec{n} = \vec{\sigma} \cdot \vec{n}_s(1 - \frac{1}{2}\phi^2) + \phi_1 U_s^\dagger \sigma_y U_s + \phi_2 U_s^\dagger \sigma_x U_s. \tag{D.24}$$

To read off the components of $\vec{n}$, we use

$$n_i = \frac{1}{2}\text{tr}[\sigma_i \vec{\sigma} \cdot \vec{n}] = \frac{1}{2}\text{tr}[\sigma_i U^\dagger \sigma_z U]. \tag{D.25}$$

Applying $\frac{1}{2}\text{tr}[\sigma]$ to the above expression, we find

$$\vec{n} = \vec{n}_s(1 - \frac{1}{2}\phi^2) + \phi_1 \frac{1}{2}\text{tr}[\vec{\sigma} U_s^\dagger \sigma_y U_s] + \phi_2 \frac{1}{2}\text{tr}[\vec{\sigma} U_s^\dagger \sigma_x U_s] = \vec{n}_s(1 - \phi^2)^{1/2} + \phi_i \vec{e}_i + O(\phi^3). \tag{D.26}$$

Finally, we check that we've found an orthonormal basis:

$$\vec{e}_1 \cdot \vec{e}_2 = \frac{1}{2}\text{tr}[(\vec{e}_1 \cdot \vec{\sigma})(\vec{e}_2 \cdot \vec{\sigma})] = \frac{1}{2}\text{tr}[U_s^\dagger \sigma_y U_s U_s^\dagger \sigma_x U_s] = 0, \tag{D.27}$$

$$\vec{n}_s \cdot \vec{e}_i = \frac{1}{2}\text{tr}[(\sigma \cdot \vec{n}_s \vec{\sigma} \cdot \vec{e}_i)] = \frac{1}{2}\text{tr}[U_s^\dagger \sigma_z U_s U_s^\dagger \sigma_i U_s] = 0. \tag{D.28}$$

Therefore, our expansion (D.17) is equivalent to Polyakov's expansion (D.2).

Appendix E

Identities Involving f_{ABC} and T_A in SU(3)

In this appendix, we prove various identities involving the SU(3) generators T_A, and their structure factors f_{ABC}. We label the 8 generators of SU(3), the so-called Gell-Mann matrices, according to

$$T_1 = \begin{pmatrix} 0 & 1 & 0 \\ 1 & 0 & 0 \\ 0 & 0 & 0 \end{pmatrix} \quad T_2 = \begin{pmatrix} 0 & -i & 0 \\ i & 0 & 0 \\ 0 & 0 & 0 \end{pmatrix} \quad T_3 = \begin{pmatrix} 1 & 0 & 0 \\ 0 & -1 & 0 \\ 0 & 0 & 0 \end{pmatrix} \quad T_4 = \begin{pmatrix} 0 & 0 & 1 \\ 0 & 0 & 0 \\ 1 & 0 & 0 \end{pmatrix} \tag{E.1}$$

$$T_5 = \begin{pmatrix} 0 & 0 & -i \\ 0 & 0 & 0 \\ i & 0 & 0 \end{pmatrix} \quad T_6 = \begin{pmatrix} 0 & 0 & 0 \\ 0 & 0 & 1 \\ 0 & 1 & 0 \end{pmatrix} \quad T_7 = \begin{pmatrix} 0 & 0 & 0 \\ 0 & 0 & -i \\ 0 & i & 0 \end{pmatrix} \quad T_8 = \frac{1}{\sqrt{3}} \begin{pmatrix} 1 & 0 & 0 \\ 0 & 1 & 0 \\ 0 & 0 & -2 \end{pmatrix}$$

These matrices obey the $\mathfrak{su}(3)$ algebra

$$[T_A, T_B] = 2i f_{ABC} T_C \tag{E.2}$$

for completely antisymmetric f_{ABC}. Explicitly, the nontrivial values of f_{ABC} are

$$f_{123} = 1 \qquad f_{345} = f_{376} = f_{147} = f_{156} = f_{257} = \frac{1}{2} \qquad f_{458} = f_{678} = \frac{\sqrt{3}}{2}. \tag{E.3}$$

Throughout we use the following index notation: Lowercase Latin letters index the off-diagonal Gell-Mann matrices, lowercase Greek letters index the diagonal Gell-Mann matrices, uppercase Latin letters index all eight matrices, and repeated indices are summed over. By construction, the Gell-Mann matrices satisfy

$$\mathrm{tr}[T_A T_B] = 2\delta_{AB}, \tag{E.4}$$

as well as the completeness relation

$$[T_A]_{ij}[T_A]_{kl} = 2\delta_{il}\delta_{kj} - \frac{2}{3}\delta_{ij}\delta_{kl}. \tag{E.5}$$

E.1   Structure Factor Identities

In this section, we first prove two specific identities involving the f_{ABC} that we will require in our RG calculations in Chapter 4. Then we define the following composite objects, given a unitary matrix U:

$$M_A = U^\dagger T_A U \qquad N_\mu = \partial_\mu U U^\dagger. \tag{E.6}$$

With these new objects, we prove six additional identities.

E.1.1   Identity 1

Here we prove

$$f_{c\gamma a} f_{c\gamma b} = \delta_{ab}. \tag{E.7}$$

We first write

$$f_{c\gamma a} f_{c\gamma b} = f_{c3a} f_{c3b} + f_{c8a} f_{c8b}. \tag{E.8}$$

Then using the explicit values of f_{ABC} given in (E.3), we see the first term equals

$$f_{c3a} f_{c3b} = \delta_{a2}\delta_{b2} + \delta_{a1}\delta_{b1} + \frac{1}{4}\delta_{a5}\delta_{b5} + \frac{1}{4}\delta_{a4}\delta_{b4} + \frac{1}{4}\delta_{a6}\delta_{b6} + \frac{1}{4}\delta_{a7}\delta_{b7} \tag{E.9}$$

and the second term equals:

$$f_{c8a} f_{c8b} = \frac{3}{4} \left(\delta_{a5}\delta_{b5} + \delta_{a4}\delta_{b4} + \delta_{a6}\delta_{b6} + \delta_{a7}\delta_{b7} \right). \tag{E.10}$$

Adding (E.9) and (E.10) completes the proof.

E.1.2   Identity 2

Here we prove

$$f_{abC} f_{abD} = \begin{cases} \delta_{CD} & \text{if } C = c \text{ is off diagonal,} \\ 3\delta_{CD} & \text{if } C = \gamma \text{ is diagonal.} \end{cases} \tag{E.11}$$

First, we establish

$$f_{ABC} f_{ABD} = 3\delta_{CD}. \tag{E.12}$$

Using (E.4), we have

$$\text{tr}\Big[[T_A, T_B][T_A, T_C] \Big] = \text{tr}\Big[2T_A T_B T_A T_C - T_A^2 T_C T_B - T_A^2 T_B T_C \Big] = -8 f_{ABD} f_{ACD}. \tag{E.13}$$

Then using (E.5) on the middle term, this becomes

$$\begin{aligned}
\text{tr}\Big[2T_A T_B T_A T_C - T_A^2 T_C T_B - T_A^2 T_B T_C \Big] &= 2[T_A]_{ij}[T_B]_{jk}[T_A]_{kl}[T_C]_{li} - [T_A]_{ij}[T_A]_{jk}[T_C T_B + T_B T_C]_{ki} \\
&= -\frac{4}{3}\text{tr}[T_B T_C] - 6\text{tr}[T_C T_B + T_B T_C] + \frac{2}{3}\text{tr}[T_C T_B + T_B T_C] \\
&= -12\text{tr}[T_B T_C] \\
&= -24\delta_{BC}, \tag{E.14}
\end{aligned}$$

where in the last step we used (E.4). This proves (E.12). Now we expand it as follows:

$$3\delta_{CD} = f_{ABC} f_{ABD} = f_{abC} f_{abD} + 2 f_{\alpha\beta C} f_{\alpha\beta D}. \tag{E.15}$$

If $C = \gamma$ is a diagonal index, the second term vanishes, and the second case of (E.11) follows. If C is off-diagonal, the second term gives $2\delta_{CD}$ according to (E.7), which proves the first case of (E.11).

E.1.3 Identity 3

Here we prove

$$\sum_{A} \text{tr}[(\partial_\mu M_A)^2] = -6 \sum_{A} (\text{tr}[N_\mu T_A])^2. \tag{E.16}$$

Using (E.5), we have

$$[M_B]_{ij}[M_B]_{kl} = [U_s^\dagger]_{in}[T_B]_{nm}[U_s]_{mj}[U_s^\dagger]_{kp}[T_B]_{pq}[U_s]_{ql} \tag{E.17}$$

$$= [U_s^\dagger]_{in}[U_s]_{ql}[U_s]_{mj}[U_s^\dagger]_{kp}\left(2\delta_{nq}\delta_{pm} - \frac{2}{3}\delta_{nm}\delta_{pq}\right)$$

$$= 2\delta_{il}\delta_{kj} - \frac{2}{3}\delta_{ij}\delta_{kl}.$$

Also, using (4.92), we have

$$\text{tr}[M_B\partial_\mu M_A] = 2if_{BAC}\text{tr}[\partial_\mu U_s U_s^\dagger T_C]. \tag{E.18}$$

Now, we use these two expressions to simplify the following equation in two different ways. On one hand, we have

$$\sum_{A,B}(\text{tr}[M_B\partial_\mu M_A])^2 = \sum_{A,B}[M_B]_{ij}[\partial_\mu M_A]_{ji}[M_B]_{kl}[\partial_\mu M_A]_{lk} \tag{E.19}$$

$$= \sum_{A}[\partial_\mu M_A]_{ji}[\partial_\mu M_A]_{lk}\left(2\delta_{il}\delta_{kj} - \frac{2}{3}\delta_{ij}\delta_{kl}\right)$$

$$= 2\sum_{A}\text{tr}[(\partial_\mu M_A)^2] - \frac{2}{3}(\text{tr}[\partial_\mu M_A])^2$$

$$= 2\sum_{A}\text{tr}[(\partial_\mu M_A)^2]$$

since $\text{tr}[\partial_\mu M_a] = \partial_\mu\text{tr}[T_a] = 0$. On the other hand,

$$\sum_{A,B}(\text{tr}[M_B\partial_\mu M_A])^2 = -4\sum_{A,B,C,D} f_{BAC}f_{BAD}\text{tr}[N_\mu T_C]\text{tr}[N_\mu T_D] = -12\sum_{C}\text{tr}[(\partial_\mu U_s U_s^\dagger T_C)^2]. \tag{E.20}$$

This proves (E.16).

E.1.4 Identity 4

Here we prove

$$-2\sum_{c}(\text{tr}[N_\mu T_c])^2 = \sum_{\gamma}\text{tr}[(\partial_\mu M_\gamma)^2]. \tag{E.21}$$

We repeat the proof of (E.16), but reduce the summation over A to a summation over diagonal Gell-Mann matrices only. On the one hand,

$$\sum_{\gamma,B}(\text{tr}[M_B\partial_\mu M_\gamma])^2 = \sum_{\gamma,B}[M_B]^{ij}[\partial_\mu M_\gamma]_{ji}[M_B]_{kl}[\partial_\mu M_\gamma]_{lk} \tag{E.22}$$

$$= \sum_{\gamma}[\partial_\mu M_\gamma]_{ji}[\partial_\mu M_\gamma]_{lk}\left(2\delta_{il}\delta_{kj} - \frac{2}{3}\delta_{ij}\delta_{kl}\right) \tag{E.23}$$

$$= 2\sum_{A}\text{tr}[(\partial_\mu M_\gamma)^2] - \frac{2}{3}(\text{tr}[\partial_\mu M_\gamma])^2 = 2\sum_{\gamma}\text{tr}[(\partial_\mu M_\gamma)^2]. \tag{E.24}$$

On the other hand,

$$\sum_{\gamma,B}(\text{tr}[M_B\partial_\mu M_\gamma])^2 = -4\sum_{\gamma,B,C,D}f_{B\gamma c}f_{B\gamma d}\text{tr}[N_\mu T_c]\text{tr}[N_\mu T_d] = -4\sum_{c}(\text{tr}[\partial_\mu U_s U_s^\dagger T_c])^2 \tag{E.25}$$

where we used (E.7). This proves (E.21).

Identity 5

Here we prove

$$\text{tr}[N_\gamma T_a (T_3 T_b T_8 - T_8 T_b T_3)] = 2i\text{tr}[N_\gamma T_a (f_{3bc}T_c T_8 - f_{8bc}T_c T_3)]. \tag{E.26}$$

This follows directly from:

$$T_3 T_a T_8 = [T_3, T_a]T_8 + T_a T_3 T_8 = 2if_{3ac}T_c T_8 + \frac{1}{\sqrt{3}}T_a T_3. \tag{E.27}$$

Identity 6

Here we prove

$$f_{3bc}\text{tr}[N_\gamma(T_a T_c T_8 - T_8 T_a T_c)] + f_{8bc}\text{tr}[N_\gamma(T_3 T_a T_c - T_a T_c T_3)] \tag{E.28}$$
$$+ f_{3ac}\text{tr}[N_\gamma(T_8 T_b T_c - T_b T_c T_8)] + f_{8ac}\text{tr}[N_\gamma(T_b T_c T_3 - T_3 T_b T_c)]$$
$$= 2i\text{tr}[N_\gamma T_d T_c] (f_{3bc}f_{a8d} + f_{8bc}f_{3ad} + f_{3ac}f_{8bd} + f_{8ac}f_{b3d}) .$$

First, we rewrite the left hand side of (E.28) as

$$f_{3bc}\text{tr}\Big[N_\gamma[T_a T_c, T_8]\Big] + f_{8bc}\text{tr}\Big[N_\gamma[T_3, T_a T_c]\Big] + f_{3ac}\text{tr}\Big[N_\gamma[T_8, T_b T_c]\Big] + f_{8ac}\text{tr}\Big[N_\gamma[T_b T_c, T_3]\Big] \tag{E.29}$$

which can further be rewritten as

$$f_{3bc}\text{tr}\Big[N_\gamma (T_a[T_c, T_8] + [T_a, T_8]T_c)\Big] + f_{8bc}\text{tr}\Big[N_\gamma ([T_3, T_a]T_c + T_a[T_3, T_c])\Big] \tag{E.30}$$
$$+ f_{3ac}\text{tr}\Big[N_\gamma ([T_8, T_b]T_c + T_b[T_8, T_c])\Big] + f_{8ac}\text{tr}\Big[N_\gamma (T_b[T_c, T_3] + [T_b, T_3]T_c)\Big].$$

Replacing commutators with structure constants gives

$$2i\Big[f_{3bc}\text{tr}[N_\nu\,(T_a f_{c8d} T_d + f_{a8d} T_d T_c)] + f_{8bc}\text{tr}[N_\nu\,(f_{3ad} T_d T_c + T_a f_{3cd} T_d)] \tag{E.31}$$

$$+ f_{3ac}\text{tr}[N_\nu\,(f_{8bd} T_d T_c + T_b f_{8cd} T_d)] + f_{8ac}\text{tr}[N_\nu\,(T_b f_{c3d} T_d + f_{b3d} T_d T_c)]\Big],$$

which can be reorganized into

$$2i\Big[f_{3bc} f_{c8d}\text{tr}[N_\nu T_a T_d] + f_{3bc} f_{a8d}\text{tr}[N_\nu T_d T_c] + f_{8bc} f_{3ad}\text{tr}[N_\nu T_d T_c] + f_{8bc} f_{3cd}\text{tr}[N_\nu T_a T_d] \tag{E.32}$$

$$+ f_{3ac} f_{8bd}\text{tr}[N_\nu T_d T_c] + f_{3ac} f_{8cd}\text{tr}[N_\nu T_b T_d] + f_{8ac} f_{c3d}\text{tr}[N_\nu T_b T_d] + f_{8ac} f_{b3d}\text{tr}[N_\nu T_d T_c]\Big].$$

Now, terms of the form $f_{3bc} f_{c8d}$ vanish unless $b = d$. This means the first and fourth terms cancel. Likewise, the sixth and seventh terms cancel. What remains is

$$2i\Big[f_{3bc} f_{a8d}\text{tr}[N_\nu T_d T_c] + f_{8bc} f_{3ad}\text{tr}[N_\nu T_d T_c] + f_{3ac} f_{8bd}\text{tr}[N_\nu T_d T_c] + f_{8ac} f_{b3d}\text{tr}[N_\nu T_d T_c]\Big],$$

which proves (E.28).

Identity 7

Here we prove

$$\epsilon_{\mu\nu}\text{tr}[N_\nu T_d T_c]\Big(f_{abE}\text{tr}[N_\mu T_E] + f_{ab\gamma}\text{tr}[N_\mu T_\gamma]\Big)(f_{8bc} f_{3ad} + f_{3ac} f_{8bd}) \tag{E.33}$$

$$= -\epsilon_{\mu\nu}\,\sqrt{3}\Big(\text{tr}[N_\mu T_1]\text{tr}[N_\nu T_2] - \text{tr}[N_\mu T_4]\text{tr}[N_\nu T_5] + \text{tr}[N_\mu T_6]\text{tr}[N_\nu T_7]\Big). \tag{E.34}$$

To begin, we check explicitly that the term

$$f_{abE}\Big(f_{8bc} f_{3ad} + f_{3ac} f_{8bd}\Big) \tag{E.35}$$

vanishes unless E is diagonal. In fact, it is either zero or $\pm\frac{\sqrt{3}}{4}$. We find the left hand side of (E.33) equals

$$= \frac{\sqrt{3}}{4}\epsilon_{\mu\nu}\Big(\text{tr}[N_\mu T_1]\text{tr}[N_\nu(\{T_4, T_7\} - \{T_5, T_6\})] + \text{tr}[N_\mu T_2]\text{tr}[N_\nu(\{T_4, T_6\} + \{T_5, T_7\})] \tag{E.36}$$

$$+ \text{tr}[N_\mu T_4]\text{tr}[N_\nu(\{T_1, T_7\} + \{T_2, T_6\})] + \text{tr}[N_\mu T_5]\text{tr}[N_\nu(\{T_2, T_7\} - \{T_1, T_6\})]$$

$$+ \text{tr}[N_\mu T_6]\text{tr}[N_\nu(\{T_2, T_4\} - \{T_1, T_5\})] + \text{tr}[N_\mu T_7]\text{tr}[N_\nu(\{T_1, T_4\} + \{T_5, T_2\})]\Big).$$

Using

$$\{T_5, T_6\} = -\{T_4, T_7\} = T_2, \qquad \{T_4, T_6\} = \{T_5, T_7\} = T_1, \tag{E.37}$$

$$\{T_1, T_7\} = \{T_2, T_6\} = T_5, \qquad \{T_1, T_6\} = -\{T_2, T_7\} = T_4, \tag{E.38}$$

$$\{T_1, T_5\} = -\{T_2, T_4\} = T_7, \qquad \{T_1, T_4\} = \{T_5, T_2\} = T_6, \tag{E.39}$$

the left hand side of (E.33) becomes

$$
= \frac{\sqrt{3}}{2}\epsilon_{\mu\nu}\Big(-\operatorname{tr}[N_\mu T_1]\operatorname{tr}[N_\nu T_2] + \operatorname{tr}[N_\mu T_2]\operatorname{tr}[N_\nu T_1] + \operatorname{tr}[N_\mu T_4]\operatorname{tr}[N_\nu T_5] - \operatorname{tr}[N_\mu T_5]\operatorname{tr}[N_\nu T_4] \quad \text{(E.40)}
$$
$$
- \operatorname{tr}[N_\mu T_6]\operatorname{tr}[N_\nu T_7] + \operatorname{tr}[N_\mu T_7]\operatorname{tr}[N_\nu T_6]\Big).
$$

The $\epsilon_{\mu\nu}$ tensor allows us to combine these terms, proving (E.33).

Identity 8

Finally, we prove in this subsection that

$$
\epsilon_{\mu\nu}\Big(\operatorname{tr}[N_\mu T_1]\operatorname{tr}[N_\nu T_2] - \operatorname{tr}[N_\mu T_4]\operatorname{tr}[N_\nu T_5] + \operatorname{tr}[N_\mu T_6]\operatorname{tr}[N_\nu T_7]\Big) = -i\sqrt{3}\operatorname{tr}[N_\mu T_8 N_\nu T_3]. \quad \text{(E.41)}
$$

First note that

$$
\operatorname{tr}[N_\mu T_1] = [N_\mu]_{ij}[T_1]_{ji} = [N_\mu]_{21} + [N_\mu]_{12}, \tag{E.42}
$$
$$
\operatorname{tr}[N_\nu T_2] = [N_\nu]_{ij}[T_2]_{ji} = -i[N_\nu]_{21} + i[N_\nu]_{12}, \tag{E.43}
$$

so

$$
\epsilon_{\mu\nu}\operatorname{tr}[N_\mu T_1]\operatorname{tr}[N_\nu T_2] = i\epsilon_{\mu\nu}\Big[[N_\mu]_{21} + [N_\mu]_{12}\Big]\big[-[N_\nu]_{21} + [N_\nu]_{12}\big] \tag{E.44}
$$
$$
= i\epsilon_{\mu\nu}\Big([N_\mu]_{21}[N_\nu]_{12} - [N_\mu]_{21}[N_\nu]_{21} + [N_\mu]_{12}[N_\nu]_{12} - [N_\mu]_{12}[N_\nu]_{21}\Big) \tag{E.45}
$$
$$
= 2i\epsilon_{\mu\nu}[N_\mu]_{21}[N_\nu]_{12}. \tag{E.46}
$$

Similar results hold for T_4, T_5, T_6, T_7. Therefore the left hand side of (E.41) is

$$
2i\epsilon_{\mu\nu}\Big[[N_\mu]_{21}[N_\nu]_{12} - [N_\mu]_{31}[N_\nu]_{13} + [N_\mu]_{32}[N_\nu]_{23}\Big] = 2i\epsilon_{\mu\nu}\sum_{\alpha=1}^{3}\operatorname{tr}[N_\mu\Lambda_\alpha N_\nu\Lambda_{\alpha+1}]. \tag{E.47}
$$

Finally, using the results of Appendix E.2, we see that this equals

$$
-i\sqrt{3}\epsilon_{\mu\nu}\operatorname{tr}[N_\mu T_8 N_\nu T_3], \tag{E.48}
$$

which proves (E.41).

E.2 A Rewriting of the Sigma Model Lagrangian

In this section, we obtain an equivalent form of the $SU(3)/[U(1)]^2$ sigma model's Lagrangian. We rewrite Λ_α in terms of T_3, T_8 and $\mathbb{I}$, and expand each term occurring in (4.42) separately.

Real part:

We start with

$$\mathcal{L} = -\sum_{\alpha=1}^{3} \text{tr}[\partial_\mu U U^\dagger \Lambda_\alpha \partial_\mu U U^\dagger \Lambda_{\alpha+1}]. \tag{E.49}$$

This can be rewritten as

$$\mathcal{L} = -(1/2) \sum_{\alpha=1}^{3} \text{tr}[\partial_\mu (U^\dagger \Lambda_\alpha U) \partial_\mu (U^\dagger \Lambda_{\alpha+1} U)] \tag{E.50}$$

since $\text{tr}[\partial_\mu U \partial_\mu U^\dagger \Lambda_\alpha \Lambda_{\alpha+1}] = 0$. Note that

$$6\Lambda_1 = \sqrt{3}T_8 + 2\mathbb{I} + 3T_3, \tag{E.51}$$

$$6\Lambda_2 = \sqrt{3}T_8 + 2\mathbb{I} - 3T_3, \tag{E.52}$$

$$3\Lambda_3 = \mathbb{I} - \sqrt{3}T_8, \tag{E.53}$$

where I is the identity matrix. Substituting this into (E.50), we may drop the $\mathbb{I}$ terms since $\partial_\mu(U^\dagger U) = 0$. Thus

$$36\mathcal{L} = -(1/2)\text{tr}[\partial_\mu(U^\dagger(\sqrt{3}T_8 + 3T_3)U)\partial_\mu(U^\dagger(\sqrt{3}T_8 - 3T_3)U)] \tag{E.54}$$

$$- \text{tr}[\partial_\mu(U^\dagger(\sqrt{3}T_8 - 3T_3)U)\partial_\mu(U^\dagger(-\sqrt{3}T_8)U)] \tag{E.55}$$

$$- \text{tr}[\partial_\mu(U^\dagger(-\sqrt{3}T_8)U)\partial_\mu(U^\dagger(\sqrt{3}T_8 + 3T_3)U)]. \tag{E.56}$$

Collecting terms, we find

$$\mathcal{L} = (1/8)\text{tr}[\partial_\mu(U^\dagger T_\gamma U)\partial_\mu(U^\dagger T_\gamma U)]. \tag{E.57}$$

This result doesn't depend on how we choose the diagonal Gell-Mann matrices. Note that the diagonal matrix elements of the two diagonal Gell-Mann matrices together with $\sqrt{2/3}\mathbb{I}$ form a complete orthogonal set of real vectors with norm $\sqrt{2}$. Thus:

$$\sum_\gamma [T_\gamma]_{ii}[T_\gamma]_{jj} = 2\delta_{ij} - \frac{2}{3}, \tag{E.58}$$

and we may also write:

$$\mathcal{L} = (1/8)\partial_\mu([U^\dagger]_{ij}[U]_{jk})\partial_\mu([U^\dagger]_{kj}[U]_{ji}). \tag{E.59}$$

The 2/3 term can be dropped because it gives a term containing $\partial_\mu(U^\dagger U)$. The same result is obtained with any basis of diagonal Gell-Mann matrices which obey the same completeness condition and the same normalization.

Imaginary part:

We start with

$$-\epsilon_{\mu\nu} \sum_{\alpha=1}^{3} \text{tr}[\partial_\mu U U^\dagger \Lambda_\alpha \partial_\nu U U^\dagger \Lambda_{\alpha+1}] \tag{E.60}$$

and define $N_\mu := \partial_\mu U U^\dagger$. Then we have

$$36\text{tr}[N_\mu \Lambda_1 N_\nu \Lambda_2] = \text{tr}[N_\mu(\sqrt{3}T_8 + 2\mathbb{I} + 3T_3)N_\nu(\sqrt{3}T_8 + 2\mathbb{I} - 3T_3)] \tag{E.61}$$

$$= 2\sqrt{3}\text{tr}[N_\mu N_\nu T_8] + 3\sqrt{3}\text{tr}[N_\mu T_3 N_\nu T_8] + 2\sqrt{3}\text{tr}[N_\mu T_8 N_\nu] \tag{E.62}$$

$$+ 6\text{tr}[N_\mu T_3 N_\nu] - 3\sqrt{3}\text{tr}[N_\mu T_8 N_\nu T_3] - 6\text{tr}[N_\mu N_\nu T_3] \tag{E.63}$$

$$= -12\text{tr}[N_\mu N_\nu T_3] - 6\sqrt{3}\text{tr}[N_\mu T_8 N_\nu T_3] \tag{E.64}$$

and

$$36\text{tr}[N_\mu \Lambda_2 N_\nu \Lambda_3] = 2\text{tr}[N_\mu(\sqrt{3}T_8 + 2\mathbb{I} - 3T_3)N_\nu(\mathbb{I} - \sqrt{3}T_8)] \tag{E.65}$$

$$= 2\sqrt{3}\text{tr}[N_\mu T_8 N_\nu] - 6\text{tr}[N_\mu T_3 N_\nu] \tag{E.66}$$

$$- 4\sqrt{3}\text{tr}[N_\mu N_\nu T_8] + 6\sqrt{3}\text{tr}[N_\mu T_3 N_\nu T_8] \tag{E.67}$$

$$= 6\text{tr}[N_\mu N_\nu T_3] - 6\sqrt{3}\text{tr}[N_\mu N_\nu T_8] - 6\sqrt{3}\text{tr}[N_\mu T_8 N_\nu T_3] \tag{E.68}$$

and

$$36\text{tr}[N_\mu \Lambda_3 N_\nu \Lambda_1] = 2\text{tr}[N_\mu(\mathbb{I} - \sqrt{3}T_8)N_\nu(\sqrt{3}T_8 + 2\mathbb{I} + 3T_3)] \tag{E.69}$$

$$= 6\sqrt{3}\text{tr}[N_\mu N_\nu T_8] + 6\text{tr}[N_\mu N_\nu T_3] - 6\sqrt{3}\text{tr}[N_\mu T_8 N_\nu T_3]. \tag{E.70}$$

Taking the sum of all three, we find

$$36\epsilon_{\mu\nu} \sum_{\alpha=1}^{3} \text{tr}[\partial_\mu U U^\dagger \Lambda_\alpha \partial_\nu U U^\dagger \Lambda_{\alpha+1}] = -18\sqrt{3}\text{tr}[\partial_\mu U U^\dagger T_8 \partial_\mu U U^\dagger T_3]. \tag{E.71}$$

Appendix F

Two Identities Involving SU(n) Structure Factors

In this appendix, we prove two identities involving the SU(n) structure factors.

F.1 Identity 1

Here we prove

$$\frac{g_c h_e(\mu)}{g_e} f_{ace} f_{bce} = \delta_{ab} \sum_{\substack{i=1 \\ i \neq t}}^{n-1} \frac{h_i(\mu)}{g_i} g_{|t-i|} \tag{F.1}$$

where $t := |\alpha - \beta|\big|_{I_{\alpha\beta} \ni a}$ and $g_x := g_{x \bmod n}$ for $x > n$. Since a, c, e all correspond to off-diagonal generators, f_{ace} will vanish unless

$$I_a \neq I_c \neq I_e \neq I_a. \tag{F.2}$$

Moreover, for a and e fixed, there is a unique value of c such that $f_{ace} \neq 0$. Calling this value c_*, we then have

$$\frac{g_c h_e(\mu)}{g_e} f_{ace} f_{bce} = \frac{1}{4} \delta_{ab} \frac{g_{c_*} h_e(\mu)}{g_e} \quad \text{(no sum over } e) \tag{F.3}$$

since $f_{bc_* e} = 0$ unless $a = b$, and all purely off-diagonal structure factors in SU(n) have magnitude $\frac{1}{2}$. Moreover, one can verify explicitly that for $a \in I_{\alpha\beta}$ and $e \in I_{\gamma\delta}$, with $I_{\alpha\beta} \cap I_{\gamma\delta} = \emptyset$,

$$g_{c_*} = \delta_{\alpha\gamma} g_{|\beta-\delta|} + \delta_{\alpha\delta} g_{|\beta-\gamma|} + \delta_{\beta\gamma} g_{|\alpha-\delta|} + \delta_{\beta\delta} g_{|\alpha-\gamma|}. \tag{F.4}$$

Note that if $\{\alpha, \beta\} \cap = \{\gamma, \delta\} = \emptyset$, $[T_a, T_e] = 0$. Therefore, writing $\sum_e = \sum_{\gamma<\delta} \sum_{e \in I_{\gamma\delta}}$, the left hand side of (F.1) is

$$\frac{g_c h_e(\mu)}{g_e} f_{ace} f_{bce} = \frac{1}{4} \delta_{ab} \sum_{\gamma<\delta}^{n} \frac{h_e(\mu)}{g_e} \sum_{\substack{e \in I_{\gamma\delta} \\ e \notin I_{\alpha\beta}}} \left[\delta_{\alpha\gamma} g_{|\beta-\delta|} + \delta_{\alpha\delta} g_{|\beta-\gamma|} + \delta_{\beta\gamma} g_{|\alpha-\delta|} + \delta_{\beta\delta} g_{|\alpha-\gamma|} \right] \tag{F.5}$$

$$= \frac{\delta_{ab}}{2} \sum_{\substack{\gamma<\delta \\ I_{\gamma\delta} \neq I_{\alpha\beta}}}^{n} \frac{h_{|\delta-\gamma|}(\mu)}{g_{|\delta-\gamma|}} \left[\delta_{\alpha\gamma} g_{|\beta-\delta|} + \delta_{\alpha\delta} g_{|\beta-\gamma|} + \delta_{\beta\gamma} g_{|\alpha-\delta|} + \delta_{\beta\delta} g_{|\alpha-\gamma|} \right].$$

We simplify each of these four terms. Let $t := \beta - \alpha > 0$ (we assume without loss of generality that $\alpha < \beta$). Then:

- $$\sum_{\substack{\gamma<\delta \\ I_{\gamma\delta}\neq I_{\alpha\beta}}}^{n} \frac{h_{|\delta-\gamma|}(\mu)}{g_{|\delta-\gamma|}}\delta_{\alpha\gamma}g_{|\beta-\delta|} = \sum_{\substack{\delta=\alpha+1 \\ \delta\neq\beta}}^{n} \frac{h_{|\delta-\alpha|}(\mu)}{g_{|\delta-\alpha|}}g_{|\beta-\delta|} = \sum_{\substack{i=1 \\ i\neq t}}^{n-\alpha} \frac{h_i(\mu)}{g_i}g_{|t-i|} \tag{F.6}$$

- $$\sum_{\substack{\gamma<\delta \\ I_{\gamma\delta}\neq I_{\alpha\beta}}}^{n} \frac{h_{|\delta-\gamma|}(\mu)}{g_{|\delta-\gamma|}}\delta_{\alpha\delta}g_{|\beta-\gamma|} = \sum_{\gamma=1}^{\alpha-1} \frac{h_{|\alpha-\gamma|}(\mu)}{g_{|\alpha-\gamma|}}g_{|\beta-\gamma|} = \sum_{i=n-\alpha+1}^{n-1} \frac{h_i(\mu)}{g_i(\mu)}g_{|i-t|} \tag{F.7}$$

- $$\sum_{\substack{\gamma<\delta \\ I_{\gamma\delta}\neq I_{\alpha\beta}}}^{n} \frac{h_{|\delta-\gamma|}(\mu)}{g_{|\delta-\gamma|}}\delta_{\beta\gamma}g_{|\alpha-\delta|} = \sum_{\delta=\beta+1}^{n} \frac{h_{|\delta-\beta|}(\mu)}{g_{|\delta-\beta|}}g_{|\alpha-\delta|} = \sum_{i=1}^{n-\beta} \frac{h_i(\mu)}{g_i}g_{|t+i|} \tag{F.8}$$

- $$\sum_{\substack{\gamma<\delta \\ I_{\gamma\delta}\neq I_{\alpha\beta}}}^{n} \frac{h_{|\delta-\gamma|}(\mu)}{g_{|\delta-\gamma|}}\delta_{\beta\delta}g_{|\alpha-\gamma|} = \sum_{\substack{\gamma=1 \\ \gamma\neq\alpha}}^{\beta-1} \frac{h_{|\beta-\gamma|}(\mu)}{g_{|\beta-\gamma|}}g_{|\alpha-\gamma|} = \sum_{\substack{i=n-\beta+1 \\ i\neq n-t}}^{n-1} \frac{h_i(\mu)}{g_i}g_{|i+t|} \tag{F.9}$$

where it is understood that $g_x := g_{x \bmod n}$ for $x > n$. In (F.7) and (F.9), we used the fact that $g_i = g_{n-i}$ and $h_i = h_{n-i}$ in the last equations. Combining these results, we have

$$\frac{g_c h_e(\mu)}{g_e}f_{ace}f_{bce} = \frac{1}{2}\delta_{ab}\left[\sum_{\substack{i=1 \\ i\neq t}}^{n-1} \frac{h_i(\mu)}{g_i}g_{|t-i|} + \sum_{\substack{i=1 \\ i\neq n-t}}^{n-1} \frac{h_i(\mu)}{g_i}g_{|t+i|}\right]. \tag{F.10}$$

Finally, replacing $i \to n - i$ in the second sum, we see that these two terms are in fact equal. Therefore, we arrive at

$$\frac{g_c h_e(\mu)}{g_e}f_{ace}f_{bce} = \delta_{ab}\sum_{\substack{i=1 \\ i\neq t}}^{n-1} \frac{h_i(\mu)}{g_i}g_{|t-i|}, \tag{F.11}$$

which completes the proof.

F.2   Identity 2

Here we prove

$$g_c f_{bcE}f_{acE} = \frac{1}{2}\delta_{ab}\left[g_a + \frac{1}{2}\sum_c g_c\right]. \tag{F.12}$$

We first write

$$g_c f_{bcE} f_{acE} = \sum_{\gamma < \delta} \sum_{c \in I_{\gamma\delta}} g_c f_{bcE} f_{acE}. \tag{F.13}$$

If $c \in I_a$, then $f_{bcE} f_{acE}$ vanishes unless $b = a$, and in this case equals

$$\delta_{ab} \sum_E [f_{a\bar{a}E}]^2 = \delta_{ab}, \tag{F.14}$$

where $\bar{a}$ is the unique index satisfying $\bar{a} \in I_a$ with $\bar{a} \neq a$. Indeed, for $a, \bar{a} \in I_{\alpha\beta}$, we have

$$[T_a, \bar{T}_a] = \pm 2i(\Lambda_\alpha - \Lambda_\beta). \tag{F.15}$$

Since $\Lambda_\alpha - \Lambda_\beta$ generate the traceless diagonal Hermitian matrices, we may take them as the diagonal SU(n) generators. In this case, $f_{a\bar{a}E} = 0$ unless E corresponds to $(\Lambda_\alpha - \Lambda_\beta)$, where it equals 1. Now, if $c \notin I_a$, then f_{acE} will vanish except for a unique value e_*, with $e_* \notin I_a \cup I_c$. The term f_{bce} forces $a = b$, too. Since $|f_{abc}| = \frac{1}{2}$ for purely off-diagonal generators, we have

$$g_c f_{bcE} f_{acE} = \delta_{ab} g_a + \frac{1}{4} \delta_{ab} \sum_{c \notin I_a} g_c. \tag{F.16}$$

Finally, noting that

$$\frac{1}{2} g_a + \frac{1}{4} \sum_{c \notin I_a} g_c = \frac{1}{4} \sum_c g_c \tag{F.17}$$

completes the proof.

Appendix G

Dispersion Relations For SU(n) Chains

In this appendix, we record the results of Section 6.3 and Section 6.4 in two tables.

G.1 Dispersion Relations

The following table lists the possible dispersion relations for any SU(n) representation satisfying $p_\alpha \neq p_\beta$ for all nonzero p_α. The second column counts the minimum number of complex fields φ^α that will have linear dispersion in the corresponding sigma model. The third column lists conditions that the p_α must satisfy in order to achieve maximal linear dispersion (all n complex fields). Each condition is paired with a number in parentheses, (x), indicating how many fields become linear dispersing when that condition is satisfied. Additional comments are also included on the right hand side of the third column.

Representation	Min #	Conditions	
$k = 1$	n	none	
$k = n - 1$	2	$p_\alpha + p_{n-\alpha+1} = p_1$ (2)	n even; $\alpha = 2, \ldots, \frac{n}{2}$
		$p_\alpha + p_{n-\alpha+1} = p_1$ (2) $2p_{\frac{n+1}{2}} = p_1$ (1)	n odd; $\alpha = 2, \ldots, \frac{n-1}{2}$
$n = k\lambda$	2λ	$p_\alpha + p_{k+1-\alpha} = p_1 + p_k$ (2λ)	k even; $\alpha = 2, \ldots, \frac{k}{2}$
		$p_\alpha + p_{k+1-\alpha} = p_1 + p_k$ (2λ) $2p_{\frac{k+1}{2}} = p_1 + p_k$ (λ)	k odd; $\alpha = 2, \ldots, \frac{k-1}{2}$
$n = 2\lambda + 1, k = 2$	$\lambda + 1$	$\lambda p_1 = (\lambda + 1)p_2$ (λ)	

Continued on next page

$n = k\lambda + 1$ $\lambda = $ even$, k > 2$	2λ	$p_\alpha + p_{k+2-\alpha} = p_2 + p_k \quad (2\lambda)$ $(\lambda + 1)(p_2 + p_k) = 2\lambda p_1 \quad (\lambda + 1)$	k odd; $\alpha = 3, \ldots, \frac{k+1}{2}$
		$p_\alpha + p_{k+2-\alpha} = p_2 + p_k \quad (2\lambda)$ $2p_{\frac{k+2}{2}} = p_2 + p_k \quad (\lambda)$ $(\lambda + 1)(p_2 + p_k) = 2\lambda p_1 \quad (\lambda + 1)$	k even; $\alpha = 3, \ldots, \frac{k}{2}$
$n = k\lambda + 1$ $\lambda = $ odd$, k > 2$	2λ	$p_\alpha + p_{k+2-\alpha} = p_2 + p_k \quad (2\lambda)$ $(\lambda + 1)(p_2 + p_k) = 2\lambda p_1 \quad (\lambda + 1)$	k odd; $\alpha = 3, \ldots, \frac{k+1}{2}$
		$p_\alpha + p_{k+2-\alpha} = p_2 + p_k \quad (2\lambda)$ $2p_{\frac{k+2}{2}} = p_2 + p_k \quad (\lambda)$ $(\lambda + 1)(p_2 + p_k) = \lambda p_1 \quad (\lambda + 1)$	k even; $\alpha = 3, \ldots, \frac{k}{2}$
$n = k\lambda + c$ $c = $ even $c \neq k - 1$ $k > 1$	$2(\lambda + 1)$	$p_\alpha + p_{c+1-\alpha} = p_1 + p_c \quad (2(\lambda + 1))$ $(\lambda + 1)(p_\beta + p_{k-\beta+c+1}) = \lambda(p_1 + p_c) \quad (2\lambda)$ $2(\lambda + 1)p_{\frac{k+c+1}{2}} = \lambda(p_1 + p_c) \quad (\lambda)$	k odd $\alpha = 2, \ldots, \frac{c}{2}$ $\beta - c = 1, \ldots, \frac{k-c-1}{2}$
		$p_\alpha + p_{c+1-\alpha} = p_1 + p_c \quad (2(\lambda + 1))$ $(\lambda + 1)(p_\beta + p_{k-\beta+c+1}) = \lambda(p_1 + p_c) \quad (2\lambda)$	k even; $\alpha = 2, \ldots, \frac{c}{2}$ $\beta = c + 1, \ldots, c + \frac{k-c}{2}$

Continued on next page

$n = k\lambda + c$ $c =$ odd $c \neq k - 1$ $k > 1$	$2(\lambda + 1)$	$p_\alpha + p_{c+1-\alpha} = p_1 + p_c \quad (2(\lambda + 1))$ $2p_{\frac{c+1}{2}} = p_1 + p_c \quad (\lambda + 1)$ $(\lambda + 1)(p_\beta + p_{k-\beta+c+1}) = \lambda(p_1 + p_c) \quad (2\lambda)$ $2(\lambda + 1)p_{\frac{k+c+1}{2}} = \lambda(p_1 + p_c) \quad (\lambda)$	k even $\alpha = 2, \ldots, \dfrac{c - 1}{2}$ $\beta - c = 1, \ldots, \dfrac{k - c - 1}{2}$
		$p_\alpha + p_{c+1-\alpha} = p_1 + p_c \quad (2(\lambda + 1))$ $2p_{\frac{c+1}{2}} = p_1 + p_c \quad (\lambda + 1)$ $(\lambda + 1)(p_\beta + p_{k-\beta+c+1}) = \lambda(p_1 + p_c) \quad (2\lambda)$	k odd; $\alpha = 2, \ldots, \dfrac{c - 1}{2}$ $\beta = c + 1, \ldots, c + \dfrac{k - c}{2}$
$n = \lambda k + (k - 1)$ λ even	$2(\lambda + 1)$	$p_\alpha + p_{k-\alpha} = p_1 + p_{k-1} \quad (2(\lambda + 1))$ $(\lambda + 1)p_k = \lambda(p_1 + p_{k-1}) \quad (\lambda)$	k odd; $\alpha = 2, \ldots, \frac{k-1}{2}$
		$p_\alpha + p_{k-\alpha} = p_1 + p_{k-1} \quad (2(\lambda + 1))$ $(\lambda + 1)p_k = \lambda(p_1 + p_{k-1}) \quad (\lambda)$ $2p_{\frac{k}{2}} = p_1 + p_{k-1} \quad (\lambda + 1)$	k even; $\alpha = 2, \ldots, \frac{k-2}{2}$
$n = \lambda k + (k - 1)$ λ odd	$2(\lambda + 1)$	$p_\alpha + p_{k-\alpha} = p_1 + p_{k-1} \quad (2(\lambda + 1))$ $(\lambda + 1)p_k = \lambda(p_1 + p_{k-1}) \quad (\lambda)$	k odd; $\alpha = 2, \ldots, \frac{k-1}{2}$
		$p_\alpha + p_{k-\alpha} = p_1 + p_{k-1} \quad (2(\lambda + 1))$ $2(\lambda + 1)p_k = \lambda(p_1 + p_{k-1}) \quad (\lambda)$ $2p_{\frac{k}{2}} = p_1 + p_{k-1} \quad (\lambda + 1)$	k even; $\alpha = 2, \ldots, \frac{k-2}{2}$

G.2   Topological Angles

The following table lists the possible topological angles for various representations of SU(n) chains. The index j runs from 1 to λ and the index t runs from 1 to $\lambda + 1$. These angles can often be simplified by using the freedom of shifting each angle by the same constant. For the relationships between angle and conditions on the p_α, refer to Section 6.4 in the main text.

Representation	Topological Angles	
$k = 1$	$\theta_\alpha = \frac{2\pi p_1}{n}(\alpha - 1)$	$\alpha = 1, 2, \ldots, n$
$k = n - 1$	$\theta_\alpha = \pi p_\alpha$	$\alpha = 1, 2, \ldots, n$
$k = \frac{n}{\lambda}$	$\theta_{\alpha,j} = \frac{\pi(p_\alpha + p_{k+1-\alpha})}{\lambda}(j - 1) + \pi p_{k+1-\alpha}$	$\alpha = 1, \ldots, k$
$n = 2\lambda + 1, k = 2$	$\theta_t = \frac{2\pi p_1}{\lambda + 1}(t - 1) + \pi p_1(\lambda - 1)$ $$\tilde{\theta}_j = \frac{2\pi p_2}{\lambda}(j - 1) + \pi p_2 \lambda$$	
$n = k\lambda + 1, k > 2$ $\lambda = $ even$, \lambda > 1$	$\theta_{\alpha,j} = \frac{\pi(p_\alpha + p_{k+2-\alpha})}{\lambda}(j - 1) + \pi p_\alpha$ $$\theta_t = \frac{2\pi p_1}{\lambda + 1}(t - 1) + \pi p_1$$	$\alpha = 2, \ldots, k$
$n = k\lambda + 1, k > 2$ $\lambda = $ odd$, \lambda > 1$	$\theta_{\alpha,j} = \frac{\pi(p_\alpha + p_{k+2-\alpha})}{\lambda}(j - 1) + \pi p_\alpha + \frac{\pi(p_\alpha + p_{k+2-\alpha})}{2}(\lambda - 1)$ $$\theta_t = \frac{2\pi p_1}{\lambda + 1}(t - 1)$$	$\alpha = 2, \ldots, k$
$n = k\lambda + c, c \neq 1, k - 1$	$\theta_{\alpha,t} = \frac{\pi(p_\alpha + p_{c-\alpha+1})}{\lambda + 1}(t - 1) + \pi\lambda p_{c-\alpha+1} + \pi(\lambda - 1)p_\alpha$ $$\tilde{\theta}_{\beta,j} = \frac{\pi(p_\beta + p_{k-\beta+c+1})}{\lambda}(j - 1) + \pi(\lambda + 1)p_{k-\beta+c+1} + \pi\lambda p_\beta$$	$\alpha = 1, \ldots, c$ $\beta = c + 1, \ldots, k$
$n = k\lambda + (k - 1)$ $\lambda = $ odd	$\theta_{\alpha,t} = \frac{\pi(p_\alpha + p_{k-\alpha})}{\lambda + 1}(t - 1) + \pi p_{k-\alpha}$ $$\theta_j = \frac{2\pi p_k}{\lambda}(j - 1) + p_k \pi$$	$\alpha = 1, \ldots, k - 1$
$n = k\lambda + (k - 1)$ $\lambda = $ even	$\theta_{\alpha,t} = \frac{\pi(p_\alpha + p_{k-\alpha})}{\lambda + 1}(t - 1) + \pi p_{k-\alpha} + \frac{\pi(p_\alpha + p_{k-\alpha})}{2}(\lambda - 2)$ $$\theta_j = \frac{2\pi p_k}{\lambda}(j - 1)$$	$\alpha = 1, \ldots, k - 1$